The Design and Implementation of a 3D Bioprinter

Alexander D. Graham

New College
University of Oxford

A thesis submitted for the degree of
Doctor of Philosophy
Trinity 2015

Declaration

The work described in this thesis was carried out between October 2011 and October 2015 in the Chemistry Research Laboratory, University of Oxford, UK under the supervision of Professor Hagan Bayley. All the work described is entirely my work, unless where otherwise acknowledged in the text. No work in this thesis has been submitted previously for any other degree at the University of Oxford, or any other universities.

Alexander Graham

October, 2015

For my family

The Design and Implementation of a 3D Bioprinter

Alexander Graham
New College, University of Oxford
A thesis submitted for the degree of Doctor of Philosophy
Trinity 2015

Abstract

3D bioprinting is the additive manufacture of biological materials, such as cells, and has been implemented over the last two decades to print 3D constructs which can mature into functional tissues. Although there are many bioprinting techniques, there are few that are capable of simultaneously printing two or more cell types at high resolutions, high cell densities and high initial cell viabilities. These printing characteristics are required to pattern cells in tissue-like micro-architectures and to quickly mature physiologically relevant tissue. We developed a novel 3D bioprinter and bioprinting methodology, designed to pattern cells without compromising these printing characteristics. Initially a droplet-in-oil 3D printer was created, which assembled mm-scale aqueous droplet networks composed of thousands of picolitre volume micro-compartments. These networks were programmed to show emergent tissue-like properties, mimicking nervous tissue's rapid electrical communication or self-folding in a manner similar to muscle contractions. This printing process was then adapted to pattern HEK-293T cells within droplet networks at high droplet resolution (~50-150 μm), high initial cell viability (90±4%) and high droplet cell density (~30×10^6 cells/mL). Capillary-like and layered sheet cell architectures were formed with two printed fluorescent cell populations. These 3D printed constructs were transferred to culture medium with minimal loss in pattern fidelity using a novel phase transfer approach. Patterned HEK-293T cells developed into dense cell organisations which showed, high cell viabilities, high cell numbers (up to ~18,000) and mitotically active cells, when cultured over 7 days. Specialised tissues were also developed, here, patterned ovine mesenchymal stem cells were differentiated, after printing, into chondrogenic progenitor cells as affirmed by Sox9 expression.

Acknowledgements

I would like to thank the following people for their contribution to this work. Firstly, my close family and friends, for their continual support and encouragement throughout my DPhil.

Prof. Hagan Bayley, for his creative visions of the droplet network and cell printing projects and for enabling my development as a scientist. This work was achieved by his rigour in all details, from experimental conduct to the use of language in writings.

My collaborators, who were essential in progressing the projects. Dr Gabriel Villar who introduced me into the world of droplets and developed the custom electronics and software of the printer. Dr Sam Olof who provided insightful supervision and microscopy knowledge during the cell printing project. Madeline Burke and Dr James Armstrong for all their long journeys and endeavours during the stem cell research. James Nicholson for his many hours of immunostaining and discussion. Dr Adam Perriman for his creative input on the stem cell printing. Ellina Mikhailova for her caring maintenance of our Oxford cell-lines. Qiuhong Li for producing the alpha hemolysin used during network printing.

Members of the Chemistry Department's workshops for the development of printer parts. Kevin Valentine and Timothy Powell for replicating the piezo driver. Charles Evans and Howard Lambourne for creating a microscope gantry. Additionally, Alan Roper and the rest of the Chemistry Research Laboratory's facility team for their help setting up a workable lab area for cell printing.

Bayley group members past and present, especially the S4 group (Dr Sam Olof, Dr Michael Booth, Dr Linna Zhou, Dr Nobina Mukherjee, Dr Shaohua Ma and Vanessa Restrepo Schild) for their intellectual input during meetings and for making the lab a stimulating and enjoyable place to work. Anthony Watt's group members of 2012, particularly Dr Peter Judge, for my excellent DPhil rotation project and for their detailed tuition of membranes. Ben Davis group for the use of their confocal microscope. Mark Wallace group for intellectual discussion and for the use of their many instruments including the fabled CNC machine. Dr Sarah Wilkins and Dr Louise Walport for their immeasurable efforts in keeping the cell culture room in good working order.

Dr Wenmiao Shu and Prof. Francis Szele for dedicating their time to read my thesis and examine me. Dr Michael Booth, Dr Sam Olof, Dr James Armstrong and Prof. Bayley for reading my thesis drafts and helping the thesis progress rapidly.

I was supported by a Biotechnology and Biological Sciences Research Council Doctoral Training Programme in Molecular Biochemistry and Chemical Biology studentship. The work in Chapter 2 was published in Science in 2013[1].

Abbreviations

αHL	alpha hemolysin
2D	two dimensional
3D	three dimensional
ATP	adenosine triphosphate
CAM	calcein acetoxymethyl ester
CFP	cyan fluorescent protein
CLM	cell laden microfiber
CNC	computer numerical control
DHB	droplet hydrogel bilayer
DIB	droplet interface bilayer
DMEM	Dulbecco's modified Eagle's medium
DMEM-ITS	DMEM-insulin-transferrin-selenium (*see Chapter 6*)
DOPC	1,2-dioleoyl-*sn*-glycero-3-phosphocholine
DPhPC	1,2-diphytanoyl-sn-glycero-3-phosphocholine
DPhPE	1,2-diphytanoyl-sn-glycero-3-phosphoethanolamine
DR	CellTracker™ Deep Red
ECM	extracellular matrix
EDTA	ethylenediaminetetraacetic acid
FBS	fetal bovine serum
FGF	fibroblast growth factor
Fmoc	fluorenylmethyloxycarbonyl
Fmoc-FF	Fmoc-phenylalanine-phenylalanine
Fmoc-IG	Fmoc-isoleucine-glycine
Fmoc-XX	Fmoc-dipeptide mix
GAG	glycosaminoglycans

Abbreviations continued

HEK-293	human embryonic kidney 293
HEK-293T	human embryonic kidney 293 derivative containing SV40 T-antigen
HEPES	4-(2-hydroxyethyl)-1-piperazineethanesulfonic acid
hMSC	human MSC
HSF	human skin fibroblasts
HUVEC	human umbilical vein endothelial cells
LABP	laser assisted bioprinting
LIFT	light induced forward transfer
MEM	minimum essential medium
MEM-NEAA	MEM non-essential amino acid
MSC	mesenchymal stem cell
NBD	nitrobenzoxadiazol
oMSC	ovine mesenchymal stem cell
orange G	7-hydroxy-8-phenylazo-1,3-naphthalenedisulfonic acid disodium salt
PBS	phosphate buffer saline
PCL	polycaprolactone
PEG	polyethylene glycol
PenStrep	penicillin and streptomycin
PI	propidium iodide
PNIPAM	poly(*N*-isopropylacrylamide)
PSC	pluripotent stem cell
RC	CellTracker® Red CMPTX
SDS	sodium dodecyl sulfate
SR101	sulforhodamine 101
SS1-SS8	scaffold solution 1-8 (*see Chapter 6*)
SSXh	scaffold solution X for HEK-293T cells
SSXm	scaffold solution X for oMSC

Abbreviations continued

SVZ	subventricular zone
TEM	transmission electron microscopy
TGF-β3	transforming growth factor β3
TIRF	total internal reflection fluorescence
tris	2-amino-2-(hydroxymethyl)-1,3-propanediol
ULGT-agarose	ultra-low gelling temperature agarose
YFP	yellow fluorescent protein

Table of Contents

1 Introduction

Three dimensional (3D) printing, also known as additive manufacture, is a computer-aided manufacture process which assembles 3D objects additively based on digital 3D models. Over the last decade, 3D printing has become a widespread technology applied in industry[2], science[3,4] and commercially available for households[2]. It has enabled the rapid prototyping of complex 3D geometries from numerous materials including metals, ceramics, plastics and even food[5]. Since the first described 3D printing process i.e. stereolithography in 1986[6], many printing technologies have been developed but all follow the layer-by-layer assembly of the printing material .

The last two decades has seen the emergence and implementation of bioprinting[7], which is the additive manufacture of biological materials, such as cells, proteins, extracellular matrix components and biochemical factors[8]. Recent bioprinting advances have enabled the precise patterning of cells, biomaterials and supporting structures, and has attained 3D functional living tissues. Examples of printed tissues include inkjet printed skin[9], layered cartilage[10] and bone constructs[11], an extrusion printed aortic valve[12] and a cellularised skin construct produced by laser-assisted printing[13]. The ability to print functional tissues such as these is a promising prospect in the regenerative medicine field, as it may address the demand for tissues and organs suitable for transplantation[8,9,14]. However, the ability to produce functional tissues faces many challenges associated with the preservation of cellular activities and the ability to develop thick tissues which display natural processes[8,9,14]. Consequently, the attempt to generate tissues which recapitulate natural functions has seen the rise of various bioprinting techniques and alternative tissue generation strategies.

This introductory chapter summarises the various current methods of developing living tissues from cell populations, focusing on the current state of cell patterning by bioprinting. The techniques are then compared, scrutinising the advantages and

disadvantages of bioprinting cells. Finally a summary of the work presented in this thesis on the design and implementation of a novel 3D bioprinter is included.

1.1 Demand for Living Tissue

One of the major goals of tissue engineering is to generate transplantable tissues which can restore, maintain, or improve in vivo tissue function[15]. The requirements for suitable transplantable tissues is epitomised by organ shortages which have increased over time regardless of more willing organ donors[14]. For example from July 2000 to July 2001, 80,000 people awaited an organ transplanted in the United States however less than a third of these people received them[14].

The ability to generate miniature tissues is also of significant value, as long as the microtissues recapitulates natural tissue function[16]. These microtissues may serve as tissue models for high-throughput screening of reagents for drug discovery, toxicology or other research[9,16,17]. Alternatively, microtissues may prove as useful models, for host-pathogen interactions[18,19] or diseases such as cancer[20,21] or degenerative diseases[22]. Microtissues may also be used as building blocks to construct macro-sized tissues, for example constructs resembling blood vessels have self-assembled under a pulsatile flow of culture medium from microtissues composed of human artery derived fibroblasts and endothelial cells[23]. Examples of microtissues formed by cellular self-assembly include spheroids[24], which are spherical-shaped cellular aggregates and organoids which are microtissues that resemble organs[16]. However, other small tissues generated by the tissue bioprinting strategies should also be suitable as tissue models.

1.2 Biology of Tissues

To be able to generate tissues with intrinsic functions it is vital to reproduce or mimic natural tissue micro-architectures[8,9,14]. This is only possible by understanding the cellular organisation of tissues and the influences which affect the properties of tissues.

1.2.1 Cells, Tissues & Organs

Multicellular organisms are composed of different organisations of cells. Tissues are generally ensembles of similar cells which interact collectively to perform a specialised activity[25]. All higher biological organisms contain organs, which are structural units composed of collections of tissues that serve a common function[25]. In animals, tissues can be classified into four main types, connective, nervous, muscle and epithelial. Each of these tissues have unique spatial arrangements of specialised cells and their own extracellular matrix. For comparison, connective tissues are composed of cells separated with large intracellular spaces filled with fibrous ECM[25] while in epithelial tissues the cells are closely packed in continuous cellular sheets, present as either a single layer or multiple layers[25].

1.2.2 Extracellular Matrix

A substantial part of a tissue's volume is the extracellular space, which is predominantly filled by an organised mesh of macromolecules termed the extracellular matrix (ECM)[26]. The main classes of these macromolecules are fibrous proteins such as collagen and elastin, and glycosaminoglycan (GAG) polysaccharides which are typically covalently linked to proteoglycans[26]. However, many other macromolecules are present in the ECM. In mammals there are ~300 ECM proteins, and multiple ECM-modifying enzymes, ECM-binding growth factors and other ECM-associated proteins[27]. The proportion of these ECM macromolecules is tissue specific and result in varied structural properties, from high stiffness bones of vertebrates to mesoglea, the jelly-like substance in jellyfish[26]. Furthermore, the ECM regulates the behaviour of surrounding cells influencing their survival, development, migration, shape, proliferation and function[26,28]. Thus when designing an artificial living tissue it is important to understand the roles of the ECM.

As all human cells are anchorage dependent except blood cells, one of the main functions of the ECM is to a provide structural support for cells[29]. The ECM then provides a physical environment for the cells to attach, migrate, grow and respond to signals[29]. The structure of the ECM also provides the tissue its mechanical properties. Specifically the

ECM is resilient to compressive forces through a combination of the highly hydrated GAG and proteoglycan molecules, and certain fibrous proteins like elastin[26]. Additionally collagen fibres help strengthen the tissue structure, for example tendons which contain bundles of collagen type I, are highly resistant to stretching[29].

Apart from structural roles, the ECM also provides bioactive cues influencing cell behaviour. For example, cell-attachment to the ECM can be stimulated by the interaction of an arginine-glycine-aspartic acid (RGD) motif of fibronectins and other polypeptides with integrin. Furthermore the stiffness of the matrix influences both the extent of cell-matrix adhesion and the direction of differentiation from progenitor cells[30]. The ECM also acts as a reservoirs of growth factors and regulates their distribution, activation and presentation to cells[28]. Finally the ECM is also a degradable environment that can be remodelled by cells during times of development, tissue repair or neovascularisation[29].

1.3 Artificial Generation of Living Tissue

Physiological tissues cannot be produced using standard 2D cell culture methods, where cells are cultured as cell monolayers on a 2D substrate composed of glass or polymer. Although these 2D cellular monolayers are widely used for cellular biology research, they do not mimic the complex 3D physiological-architectures of in vivo tissues[31]. One issue is the polarity of cells are affected by 2D culture, as cells are restricted to spreading horizontally, forcing cells to polarise in a apical-basal manner, which is not ideal for all cell types[31]. Furthermore the mechanical forces generated between the cell and their surroundings is very different, as the 2D substrate is very stiff (in order of GPa) and thus orders of magnitude stiffer than natural tissue environments (in order of kPa)[31,32].

The artificial generation of tissue from living cells is more complex and follows two main strategies, either biomimicry of the tissue micro-environment or the autonomous self-assembly of cell populations[9]. The biomimicry approach involves patterning cells in tissue-like micro-architectures, typically within a scaffold, entrusting the patterned cells to proliferate, connect and mature into the desired tissue[8,9,14]. Whilst autonomous cellular self-assembly relies on the natural development processes of the

cells[16,24]. Cells are seeded either in a solution or a scaffold and then left to autonomously proliferate and organise into tissues[16,24]. These approaches face many challenges in forming functional living tissues and many considerations are necessary when selected the scaffold material and cell sources.

1.3.1 Challenges

The challenges of artificial tissue generation by biomimicry approaches, such as bioprinting, can be broadly split into three categories: successful patterning of functional living cells, the maturation of patterned cells and development of vascularised tissues.

Firstly, for cells to be successfully patterned, the cells need to be cytocompatible with the technique and patterned at sufficient resolution[8,9,14]. To be cytocompatible the process needs to avoid damaging the cells such that viability or healthy cellular activity is comprimised[8,9,14]. However, due to the mechanism of some approaches, such as extrusion bioprinting, the process is inherently damaging to a proportion of the patterned cells[33]. Consequently the challenge is limiting the extent of cell damage by modifying the process or materials. At the same time the multi-cellular patterning resolution of the technique needs to be at sufficient resolution to mimic micro-architecture of tissues[9]. Overall the cytocompatibility and patterning resolution of the technique dictate the types of tissues that can be fabricated by the process.

For the maturation of patterned cellular scaffolds into functional living tissues, the cells need to develop within optimal growth environments[31]. To achieve this, many approaches employ scaffolds which recapitulate many features of the tissue's ECM[29]. However, the choice of scaffold material is generally limited, as it needs to be compatible with the patterning process[8,9,14] and accommodate natural cellular development[29] (see *section 1.3.2*). Additionally, the speed which the tissue develops can also be aided by patterning cells at densities approximating or close to the end tissue i.e. 10^8-10^9 cells/mL[9]. At high cells densities the maturation speed of the artificial tissue would be much shorter than scaffolds seeded at lower densities, which rely on multiple doubling steps.

The major challenge for creating thick tissues or organs is vascularisation[14]. Without vascularisation tissues sized below the diffusion limit will have insufficient ingress of nutrients and oxygen, resulting in necrotic regions of cells[34,35] (*section 1.6*). Many techniques have attempted to grow vasculature alongside tissue-specific cells with some success[34,36] (*section 1.6*). The generation of larger tissues would also have to accommodate for mechanical integrity of the construct, possibly by including temporary structural supports or attaining accelerated tissue maturation to ensure self-support[14]. Even with current progress the ability to print vascularised organs is still a distant goal[9,14]. Due to the difficulties that arise from vascularising tissues, the majority of artificially generated living tissues are prepared with one dimension sized below the diffusion limit.

Comparably tissue generated by autonomous cellular self-assembly also have similar considerations to biomimicry approaches, excluding those of cell patterning. The self-assembling cells need to mature within an optimal growth environment and without the presence of vasculature will only form functioning tissues sized below the diffusion limit.

1.3.2 Scaffolds for Cells

The majority of artificial tissue generation strategies employ scaffolds, which provide a structural support for the cells to adhere and develop within[37]. Within tissues, cells are surrounded by a tissue-specific ECM, which accommodates for the requirements of cellular survival and contributes to the tissue's mechanical properties[27]. Thus the ultimate scaffold would be a tissue-specific ECM[29,37], however utilising ECM as a scaffold is not feasible in many cases. The process of ECM decellularisation is not always perfect and can lead to the ECM retaining detergent or residual dead cells[38]. Additionally decellularised ECM is not compatible with all bioprinting techniques, for example it is too viscous to be printed by inkjets bioprinters[9]. Consequently the role of the scaffold is to mimic some, if not all of the features of the tissue's ECM[29,37].

There are many key roles that a scaffold should fulfil. The scaffold should provide a structural support for the cells that is cytocompatible. The substrate should be porous

to allow the exchange of nutrients and waste product in the form of culture medium. Cells receiving nutrients should then be able to proliferate within the scaffold, ideally being able to remodel the scaffold where necessary. The scaffold should also be able to promote the relevant differentiation, by being the relevant stiffness and allowing the ingress of growth factors or other biological cues. For scaffolds to be implanted in vivo, it is especially important that the scaffold avoid rejection by the recipients immune system. Additionally, these scaffolds may need to biodegradable, in which case the degraded molecules need to be non-cytotoxic, this is more necessary for scaffolds which are designed to have cells invade or proliferate into their structure when implanted. Lastly, implanted scaffolds for vascularised tissues, such as muscular tissue, need to be remodelable by endogenous blood vessels to allow full integration with the host. However, this vascularisation is less pivotal for tissues which have little vasculature such as cartilage and bone.

Hence the material of the scaffold needs to accommodate for these key scaffold roles and also be compatible with the patterning technology. The majority of scaffolds are consequently either synthetic or biological hydrogels, due to their porous nature, tissue comparable stiffnesses and ease of being processed. Hydrogels typically utilised as scaffolds are either ECM-based, non-ECM related biological hydrogels or synthetic hydrogels[31]. ECM-based scaffolds are either decellularised version of the ECM, secreted matrix, or individual, or mixed ECM components such as collagen, laminin, fibronectin, gelatin and hyaluronic acid[31]. A commonly secreted matrix used is Matrigel® i.e. a solubilised ECM produced by Engelbreth-Holm-Swarm mouse sarcoma cells, due to its high laminin content. The advantage of using ECM-based scaffolds is that they, depending on their composition, directly reproduce some of the ECM features.

Other common scaffolds employed include natural polymers such as agarose, chitsosan and alginate, and synthetic polymers such as polyethylene glycol (PEG) and polyacrylamide[31]. Synthetic polymers can be designed to have specific mechanical properties, however, most synthetic polymers are without natural binding sites and thus rely on the cells having to form their own ECM. However, some semi-synthetic polymers,

which comprise of synthetic building blocks and natural ligands are a promising approach of tailoring gel properties whilst retaining biological activity[31]. For example, a multi-arm telechelic PEG was derivatised with terminal mono-cysteine peptide containing the integrin binding motif RGD (arginine-glycine-aspartic acid) and used as a scaffold to culture human dermal fibroblasts which displayed physiological polarisation[39,40].

Other research groups have tailored biocompatible hydrogels by synthesising biopolymers composed of only natural building blocks. For example, a polypeptide-DNA conjugate was printed alongside a DNA-linker, which upon mixing gelled within seconds due to DNA hybridisation, fabricating cell-laden constructs which were self-supporting and could be degraded by protease and nuclease digestion[41]. This approach enabled the cells to be printed from valve-based nozzles (*section 1.5.1.3*) as liquid suspensions avoiding nozzle clogging by gel formation (see below). The design also permitted rapid gelation of the scaffold without using harsh gelation methods that would be detrimental to cells (see below)[41]. While these synthesised polymers promise cell tailorable environments, they can also be very expensive, limiting their use.

The selection of the scaffold material is highly influenced by the hydrogel's gelation method, which also has to be compatible with the printing process. For example, thermoresponsive hydrogels are not very compatible with inkjet printing which involves the patterning of low viscosity liquids typically at room temperature[42]. If the gel transition temperature is below room temperature, then the scaffold would gel and clog the nozzle. Additionally the method of gelation could be detrimental or fatal to cells, limiting the choice of scaffold hydrogels[31]. For compatible thermoresponsive gels the gel transitions temperature would need to be within an bioamenable range. Whilst gels that involve photo-crosslinking need to be curable at low radiation energy to avoid phototoxicity. Finally hydrogels that gel by a change in pH are generally avoided as cells are pH sensitive, with mammalian cells cultured within a narrow range of pH 7.0-7.5.

1.3.3 Cell Sources

The choice of cells is vital for the generation of tissues which function correctly. One biomimicry approach is to pattern multiple primary cells in the micro-architectures faithful to the target tissues[9,14]. Alternative approaches use pluripotent stem cells (PSCs), which are cells capable of differentiating into multiple tissue-specific cells[8]. In their undifferentiated form, stem cells can divide into further PSCs i.e. they are self-renewable[8]. For tissue generation PSCs can be deposited with patterned biomolecules to induce differentiation post production[8]. Whilst with autonomous self-assembly methods, embryonic stem cells are commonly employed to develop the desired tissue by culturing the cells with the relevant biological cues[16].

Tissues developed for implantation will likely be rejected by the host immune system if composed of foreign cells. To overcome this issue, autologous primary cells could be obtained from biopsies and used unaltered or reprogrammed into induced pluripotent stem cells [43,44]. There is still a risk of the patient rejecting the tissue, but this significantly minimises the chances[14].

1.4 Autonomous Cellular Self-Assembly of Tissues

The autonomous self-assembly of tissues, entrusts unpatterned cells to develop naturally into to the desired tissue from a small cell population. It can be broadly split into spheroid production[24] and organoid production[16].

1.4.1 Spheroids

Spheroids are cellular aggregates cultured in an environment free of foreign materials[24]. They can be formed by multiple methods either hanging drop, spinner flasks, static liquid overlay techniques, centrifugation and more recently, with microfluidics devices[24]. The different methods all involve the cells aggregating in a culture medium leading to direct cell-cell contacts. Their culture under physiological conditions promotes ECM production and proliferation, and results in spheroids representative of physiological

tissues. As such, spheroids have been used as models for complex tissues such as, pancreatic tissue[45] and cardiac muscle[46].

Advances in microfluidic techniques has allowed the production of highly uniform spheroids, the size of which can be tuneable. This is advantageous, as spheroids can be produced with or without oxygen deficient cores attaining models for healthy or cancerous tissues[47]. Furthermore microfluidic techniques have been engineered to produce spheroids in high-throughput manners with up to 1,024 spheroid made within a single device[48]. The ability to perform tissue-based assays within these devices has the potential to allow the high-throughput screening of spheroids[47,48].

1.4.2 Organoids

Organoids are microtissues that resemble organs and are able to recapitulate some specific organ functions[16]. They are a collection of organ specific cells that have developed from organ progenitors or stem cells through self-organisation in a similar manner to processes observed in vivo[16]. During organoid development the cells produce their own ECM, form direct cellular contacts, sort into discrete cellular domains and exhibit spatially restricted lineage commitment[16]. Organoids are formed from PSC which are introduced to growth factors or growth promoting alternatives at different stages to develop the specific organoid. Utilizing this technique, human PSCs have produced gut[49], kidney[50], brain[22], retinal[51] and other organoids.

Organoids, due to their physiological relevance, have already been used as tissue models for various assays. Gut organoids have been used to study infectious diseases[18,19], tumour biology[20,21] and genetic conditions[52]. Whilst brain and liver organoids have been used as tissue models for microcephaly (a neurodegenerative disease)[22] and drug toxicity screening[17] respectively. Whilst organoids are useful tissue models, until the integration of vasculature they will be limited to be sized below the diffusion limit and will not be appropriate for many tissue replacement strategies.

1.5 Biomimicry Approaches of Tissue Generation

The biomimicry approach of artificial tissue generation is generally to pattern cells, typically within a scaffold, in tissue-like microarchitectures. The cells are then allowed to mature into tissues which are ideally faithful to their natural counterparts. The main strategies of biomimicry-base tissue generation are, bioprinting, scaffold seeding, cell-laden microfibers, assembly of cell-laden hydrogels and cell-sheets technology.

1.5.1 Bioprinting

Bioprinting strategies have been employed to print tissues as they can accurately place cells at high resolution forming defined sized constructs[8,9,14]. This offers great control to the user, who, with the right technique, can rapidly and reproducibly produce tissue constructs[8,9,14]. Such strategies have the potential to be scaled up, allowing the high-throughput fabrication of tissues[8,9,14].

Current tissue bioprinting strategies are classified by the technology employed to distribute cells, primarily the technologies are drop-on-demand, extrusion-based and laser-based. Drop-on-demand bioprinting ejects cell-laden liquid droplets onto a substrate in predefined locations, the solidification of these droplets allows 3D tissue constructs to be assembled. Whilst extrusion based bioprinting assemble tissues through the deposition of continuous beads/solid filaments of cell-laden hydrogels or cellular aggregates alone. Finally, laser assisted bioprinters pattern cells containing materials by laser induced forward transfer (LIFT). How 3D printers function and details of the different bioprinting techniques are now reviewed.

1.5.1.1 The 3D Printing Process

Although there are many 3D printing technologies the basic printing process is the same for all. Initially a computerised 3D model of the print item is designed and when interfaced with the manufacturing software is divided into thin 2D cross-sectional slices. The printer then distributes the print material in successive layers based on the cross-

sections. In some 3D printing approaches, structural supports are formed simultaneous to the model and need to be removed in a finishing step.

For bioprinting of tissues, the computerised model needs to represent the microarchitectures of the tissue[8,9,14]. The model would then be used to print multiple cell types with or without a scaffold. Most bioprinted cells have only been patterned in simple geometries roughly approximating tissue architectures. However, it is feasible to obtain precise structural information of tissues from medical imaging technologies such as computed tomography (CT) and magnetic resonance imaging (MRI)[9]. In the future these techniques may be combined with 3D bioprinting to form computerised print models of tissues with precise architectures.

1.5.1.2 Inkjet

Inkjet-based bioprinters are the classical drop-on-demand bioprinter. The "hacking" of commercial inkjet printers to pattern cells and biomaterials was pioneered in the early 2000s[53,54]. Here, the print cartridge was filled with a biological ink (bioink) which was dispensed through the nozzle of the print head. Early iterations of inkjet bioprinting involved patterning cells on a hydrogel support to create simple 2D patterns[54]. This technique was expanded to 3D, typically by dispensing a bioink composed of cells in a $CaCl_2$ solution, into a bath of alginate resulting in droplet gelation[10,11,42,55]. Within the bath would be a robotic stage that could move in the z-axis to allow the layering of alginate encapsulated cells.

Inkjets are classed as either thermal or acoustic, defined by the force used to generate droplets. In thermal printers the print solution is heated within the print head, with localised temperatures of 200-300 °C, producing pulses of pressure which generate droplets from the nozzle[42]. Due to the short heating applications the print solution shows an overall temperature rise of only 4-10 °C[56]. Whilst in acoustic printers a piezoelectric crystal in the print head expands generating an acoustic wave that breaks the liquid into droplets[57]. Both methods are capable of printing cells with minimal reduction of viability[54,57] (with cells typically remaining >85% viable[9]) or cellular functionality[54].

Additionally the resolution of ejected droplet volumes is high, with droplets capable of being formed between <1 pL to > 300 pL[9].

Despite advantageous print criteria, inkjet-based bioprinters are only able to eject droplets of low viscosity (range 3.5-12 mPa/s)[9], consequently bioinks are designed to be gelled after printing, for example one strategy is to print cell-laden $CaCl_2$ inks into an alginate solution[58]. Another limitation is that bioink cell densities are low (typically less than 5×10^6 cells/mL) to reduce sheer stress and avoid clogging issues[57].

Functional tissues have been fabricated in vitro using this technique. Notably a layered cartilage constructs which showed 80% viability and cartilaginous ECM was formed by inkjet and electrospinning techniques[55]. Here alternative layers of a chondrocytes in fibrin-collagen mix and a polycaprolactone support were deposited. Additionally simple bone tissues were matured from an inkjet printed constructs and were successfully implanted into mice to form highly mineralised tissues[11].

1.5.1.3 Valve-Based

An alternative drop-on-demand bioprinting technique to inkjet is valve-based bioprinting. Here droplets are ejected from a dispensing system composed of a nozzle attached to an electromechanically operated valve i.e. a solenoid valve[59,60]. The dispensing system is attached to a bioink reservoir which is pressurised at a tuneable pressure. The dispensing system and the printing stage are both motorised in the *z* and the *x*, *y* planes respectively. The deposition of droplets from one or multiple dispensing systems can be used to pattern individual droplets[59–61] or to form 3D tissue constructs[41,62,63].

The droplet formation of high viscosity solutions such as collagen[63], gelatin methacrylate[62] and a supramolecular polypeptide-DNA hydrogel[41], is made possible by the pressurised bioink reservoir. Although they can print a wider range of viscous materials than inkjets, their resolution is significantly lower. The bioprinter typical afford droplets sized ø 300-650 μm on the print substrate[62,63], but can generate droplets as small as 2 nL[60]. Additionally, cells dispensed from valve-based nozzles typically show normalised viabilities of >95%[60,63]. The technique has been employed to pattern single

cell-laden droplets for cell vitrification[59], creation of controllably sized human embryonic stem cell (ESC) spheroids[60] and RNA analysis of single mouse ESC[61]. Furthermore a 3D fibro-cartilage tissue model was formed by patterning human mesenchymal stem cells (hMSCs) in different growth factors as a multiphase interface[62]. This model showed an upregulation of both chondrogenesis and osteogenesis related genes after 36 days culture.

1.5.1.4 Acoustic

A nozzle-less version of drop-on-demand bioprinters are acoustic bioprinters[8,9]. Their droplet ejector comprises of periodically spaced interdigitated gold rings positioned at the base of an open liquid reservoir, which is filled with cell-laden ejector fluid[64]. Upon application of a microsecond length voltage pulse, ultrasonic acoustic waves are generated in the ejector fluid and form an acoustic focal point at the air-fluid interface, generating a cell-encapsulating droplet[64]. Droplet ejectors can been fashioned as arrays[64,65] and are positioned above or below a cell collecting substrate, with both or one of the components motorised[64–66]. This technique has the ability to generate uniform pL volume droplets (ø 10-500 μm) at rates up to 100,000 drops/s. Whilst the technique is not harmful to cells due to the low power of droplet generation, the author can only find examples of the technique being used to pattern, single cells[64] or cell populations in simple 2D patterns without generating tissue properties[66].

1.5.1.5 Extrusion

Extrusion bioprinters function by depositing continuous beads i.e. filaments of cell-laden hydrogels or cell spheroids onto a substrate layer by layer. All extrusion bioprinters comprise of a temperature controlled extrusion head and a printing stage, with one or both motorised, attaining the movement of components along three orthogonal axes[9]. The head contains the bioink and a dispensing mechanism of either pneumatic, piston or screw. Extrusion bioprinters are capable of handling a wide range of materials from 30 mPa/s to $>6\times10^7$ mPa/s viscosities[9]. However, the material has to be able flow through the nozzle; common approaches are to print, viscous liquids that can be gelled post print

or gels that can be partially melted within the nozzle. The extrusion method gives lower viabilities than drop-on-demand techniques, with cell survival being in the range of 40-85%[33]. It was found that lower pneumatic pressures (5 psi) and wider gauge nozzles (ø 400 μm) gave the highest survival rate[33]. The decreased viability is likely to be induced by shear stresses experiences by cells in high viscosity fluids, consequently another approach to maintain cell viability is the use shear thinning materials.

Extrusion based bioprinting has been employed to print various tissue constructs from cell-laden hydrogels. Recently decellularised ECM of specific tissues were printed alongside cells (tissue-specific or pluripotent) and a PCL structural support, to form constructs which differentiated or matured into either cardiac, cartilage or adipose tissue[38]. However, these constructs, like many others, generally contain low resolution features[36,38] due to their employment of wide gauge nozzles (ø 150-400 μm)[33]. Large, cm-scale constructs are easily achieved though, for example an aortic valve was printed with an anatomical architecture which mimicked a pig's valve root and leaflet[12]. Additionally, other materials can be printed alongside the cells for structural support or as interfacing electronics as exemplified by an extrusion printed bionic ear[67].

The other strategy employed is the deposition of cell spheroids (*section 1.4.1*) in 3D patterns to fabricate tissue constructs[68]. Here, the bioink is scaffold-free, comprising of only spheroids, yet the strategies still employ hydrogels either as the printer substrate or as structurally supporting rods[69,70]. After printing, the constructs are matured, typically in bioreactors, with the spheroids fusing into a singular solid tissue[69,70]. The advantage of this approach is that it avoids the use of scaffolds, eliminating problems of scaffold biocompatibility and degradation. Furthermore the spheroids lead to high cell density printed architectures reducing the necessary tissue maturation time relative to scaffold-based techniques.

Spheroid bioprinting has attained synchronously beating cardiac assemblies[70] and perfusable linear and branching vasculature structures composed of either, only human skin fibroblasts (HSFs) or both HSFs and human umbilical vein smooth muscle cells (HUVECs)[69]. Whilst these constructs are physiological relevant, their resolution was low

due to the patterning of wide spheroids and rods (both either 300 or 500 μm diameter). Consequently it was not possible to pattern vasculature with lumen smaller than 0.9 mm diameter[69].

1.5.1.6 Laser Based

Laser assisted bioprinting (LABP) is generally based on laser induced forward transfer (LIFT)[71]. The setup involves coplanar slides, comprising of a donor slide vertically above a collector side. This donor slide or ribbon comprises of an upper glass coverslip, a middle laser-energy-absorbing layer and a lower layer of cells suspended in hydrogel or solution[71]. Irradiation of the donor slide generates a high pressure air bubble within the cell-laden layer and propels the subjacent cell and hydrogel to the collector substrate[71]. The directing of the laser allows the precise placement of the cells on the collector substrate[71].

Microscale droplet resolutions are attainable using LABP, with droplet sizes reported down to 38 ± 3 μm[72]. LABP can also print a range of viscosities (1-300 mPa/s)[9], although rapid gelation of the propelled droplets on the collector substrate is necessary to retain shape fidelity[9]. This nozzle-less technique can also print mammalian cells with minimal deviations in their viability[73]. Due to the high cost of the system though, relatively few research groups are exploring the technique, and most research up until recently has been on patterning 2D cell constructs[71,73,74]. The notable exception found by the author is the 3D LABP of human fibroblasts and keratinocytes, which were patterned at high resolution in seven alternating layers. A simple dual layer of these cells was also patterned and matured to form a graft of simple skin tissue[13], these constructs were later implanted into mice, with blood vessels invading the constructs boundary[75].

1.5.2 Alternative Scaffold-Based Techniques

There are numerous non-bioprinting techniques to artificially generate tissue. The noteworthy approaches are, shaping cell-laden hydrogels, directed assembly of cell-laden

hydrogel building blocks, weaving of cell laden microfibers and seeding of commercial or fabricated scaffolds.

The most simple of these approaches is to suspend cells in a liquid hydrogel scaffold, gelate the scaffold in a thin shape and then culture the structure. Hydrogels can be shaped as droplets, spread on the surfaces of culture apparatus or shaped within moulds, which can be manufactured with high resolution horizontal features. The limitation to this approach is that cells within a hydrogel shape can at best be homogeneously distributed, but not patterned, restricting the type of tissues that can form.

The patterning of cell-laden hydrogel shapes can however be achieved randomly in constrained spaces or in a directed manner[76]. Directed assembly approaches guide the formation of a multiplicity of hydrogel building blocks into defined modulated structures[76]. In brief, these different hydrogel modules would either be structurally complimentary[77] (i.e. have lock-and-key designs) or have complimentary interfaces, through the coating of single stranded DNA[77,78] or other biomolecules[76]. These approaches however do not have the resolution of bioprinting strategies and so far are limited to simple patterns.

Fibres of cell-laden hydrogels have also been reeled and weaved into intricate 3D structures that display tissue properties and functionalities[79]. These cell-laden microfibers (CLMs) were formed using a microfluidic device under laminar flow, attaining core-shell hydrogels that contained a high-cell density core[80]. The maturation of tissue-specific CLMs gave rise to different tissue properties such as contracting cardiomyocyte fibres[80]. Furthermore, pancreatic cell-laden microfibers were implanted into diabetic mice and over two weeks were able to normalise the blood-glucose level by secreting insulin[80]. Whilst the core of these fibres were physiologically relevant, only fibrous 3D structures were constructible, restricting production of tissues to those with fibrous architectures.

Alternatively to assembly of cell-laden hydrogels, cells can be seeded into a preformed scaffold that is of the desired size and shape[81]. These preformed scaffolds can

either be bought or fabricated in-lab. BIOFELT® (*Biomedical Structures*) is an example of a commercial scaffold, it is a non-woven fibrous matrix composed of polyglycolic acid and can used to seed MSCs for cartilage development among other uses. Scaffolds can also be fabricated chemically or by 3D printing, the advantage of additive manufacture is the scaffold can be designed with precise architectures to tailor the porosity and mechanical strength of the structure[82]. The main challenge of using pre-formed scaffolds is to seed the structure evenly for tissue development and the complexity of cell micro-architectures is limited as they cannot be patterned within.

1.5.3 Alternative Scaffold-Free Techniques

Alternative non-bioprinting strategies to artificial tissue generation include scaffold-free approaches such as assembly of miniature tissues and cell sheet engineering. As described in spheroid printing (*section 1.5.1.5*), scaffold-free approaches circumvent the challenges of scaffold biocompatibility and degradability, with resulting structures forming more natural cell-cell and cell-matrix contacts.

Microtissues such as spheroids have been used as building blocks to create larger 3D tissue constructs[24]. For examples, thin disc-shaped and square tissues were formed with regions of vasculature, from the fusion and compaction of spheroids within agarose moulds[83]. Tissues have also be constructed by stacking cell monolayers referred to as sheets, which are held together through their own ECM and cell contacts[84]. These cell sheets are formed by culturing cells on a temperature responsive polymer, poly-N-isopropyl acrylamide (PNIPAM)[85]. Once confluent these sheets are liberated from the surface by cooling the vessel inducing the swelling of PNIPAM[85]. A notable example of cell sheet engineering was the formation of a cardiac tissue with perfusable endothelial vessels which was produced by stacking multiple tri-layer sheets onto a resected vascular bed[86]. Whilst this technique makes tissue with physiological architectures, it is only compatible with cells that secrete ECM and there is little control on how cells spatially arrange within the monolayer[79].

1.6 Vascularised Tissue Generation

The ability to vascularise engineered tissues is one of the most critical challenges in developing thick tissues and organs[14]. Without the integration of a vascular network, engineered three dimensionally thick tissues will have limited, nutrients ingress, gas exchange, and waste removal, all of which are essential for tissue maturation. This is a consequence of the small molecules being unable to diffuse across multiple layers of cells. Within vertebrates, which have closed circulatory systems, cells are located within the oxygen diffusion limit, i.e. approximately 100-200 μm from capillaries or other blood vessels[34]. Cells located beyond this experience low oxygen, i.e. hypoxic conditions and become necrotic, as observed in rapidly growing tumours[87]. Similarly to natural systems, cells of artificial tissues need to be spatial positioned within 100-200 μm of either vasculature, perfusable microchannels or a bulk phase of culture medium.

Vascularisation of artificial tissues has been tackled by numerous methods, however there are two main strategies involving 3D printing. The first strategy is to bioprint the vasculature alone and combine this with tissue specific cells at a later point. The most notable examples of printed vasculature are the linear and branched vasculatures formed from extruded spheroids[69] (as described in *section 1.5.1.5*). Here, vasculature could be printed as double layer tubes comprising inner HUVECs and outer HSFs attaining wide lumens (0.9-2.5 mm) that were perfusable[69]. However the vasculature was not integrated with tissue, as it was composed of wide vasculature walls (0.6-1.2 mm)[69] that were beyond the diffusion limit. Before vasculature structures can be incorporated into tissue, bioprinting methods need to be adapted to print higher resolution perfusable vasculature.

The second approach to is to fabricate a tissue with perfusable microchannels that can be seeded with endothelial cells. In such strategies, sacrificial templates shaped as channels have been 3D printed and then surrounded by cell-laden scaffolds. The embedded template is then dissolved and flushed away[35,36] or mechanically removed[88] leaving perfusable channels within the cell-laden scaffolds. This method has been used to attain vasculature tissue morphologies i.e. lumens along perfusable microchannels. In

one instance vasculature lined microchannels were formed from carbohydrate glass templates embedded in various hydrogel structures[35]. Perfusion of these structures sustained high viabilities for both the scaffold cells and the endothelial cells[35]. Another example employed a multi-material extrusion bioprinter that simultaneously printed channel templates (pluronic F127) and connecting cell-laden rods (fibroblasts in gelatin methacrylate)[36]. The final structure was perfused and supported cells viabilities of 60-80% over 7 days. In the future to fabricate vascularise functional tissues in this manner, fine templates would need to be precisely printed alongside tissue-specific cells, however to attain this the resolutions of current multi-material bioprinters needs to be significantly improved.

1.7 Summary of Techniques

The engineering of artificial living tissues which are physiologically comparable has been attempted by various techniques, but few examples of functional tissues, mm-scaled or larger have been produced. The autonomous self-assembly of miniature tissues such as cell aggregates and organoids, allows the production of tissues which have been used as physiological models. This approach however offers the researcher limited control of tissue size, with structures size-limited by the diffusion limit. Consequently this approach is not suitable for creating mm-scale or larger replacement tissues.

Biomimicry approaches, which involve patterning cells in scaffolds for tissue development, allows the fabrication of both miniature and larger tissues constructs. Bioprinting is a promising avenue compared to alternative biomimicry approaches, as it offers: precise spatial placement of cells, control of tissue size, rapid production times and the potential to be scaled up for high-throughput production. However, for the reproducible production of functional tissues, the resolution of many bioprinting techniques needs to be improved so that multiple cell types can be patterned in the fine micro-architectures representative of natural tissues. The other major challenge for bioprinting is the vascularisation of engineered tissues, without which, tissues will be limited to dimensions within the diffusion limit. The ability to bioprint sacrificial

channels templates alongside tissue specific cells may offer a solution, yet to mimic a capillary network in a grid form would require a high resolution multi-material bioprinter. Either improvements to current bioprinting methods or the creation of novel bioprinting approaches may overcome these challenges. This could lead to future bioprinters producing multiple tissue constructs, applied as tissue models for screening such as pharmacokinetics or implanted tissue constructs to restore, support or replace damaged endogenous tissue.

1.8 Summary of Thesis

This thesis reports the design and implementation of a novel bioprinting technique used to pattern cells at high resolution within droplet networks. It also describes the development of a method to culture these printed construct, such that their patterned cells matured into tissues.

The research is broken across three chapters. Chapter 2 narrates the creation of a droplet-in-oil 3D printer which could assemble thousands of picolitre volume droplets into self-standing networks which displayed tissue-like functionalities. Chapter 3 then explains how this printer was implemented to print cells at high resolutions within droplet networks. It also described the development of a method used to transfer networks to culture medium. In Chapter 4, the culture of cell containing printed constructs is described and focuses on the maturation of tissues within constructs over seven days. The potential applications of these printed droplet networks and cell patterned constructs is then described in Chapter 5. Details of the materials and methods employed throughout the research is reported in Chapter 6.

2 3D Printed Droplet Networks

2.1 Chapter Abstract

This chapter describes the development of a droplet-in-oil 3D printer that was used to fabricate networks containing thousands of picolitre volume droplets bound through lipid bilayers. These self-standing compartmentalised networks were of mm-scale and could be patterned with define architectures of down to 2-3 droplet width. The incorporation of membrane proteins or salt gradients into networks led to emergent behaviours demonstrating networks were functionally analogous to tissues. Specifically, networks were engineered either to be electrically conductive along a defined pathway, similar to nervous tissue, or to self fold mimicking muscle contraction.

2.2 Publications

The work described in this chapter was published in Science in 2013:

Villar, G., Graham, A. D. & Bayley, H. A tissue-like printed material. *Science* **340,** 48–52 (2013)[1]

2.3 Acknowledgement of Collaboration

The research in this chapter was performed in collaboration with **Dr Gabriel Villar**. The author and Dr Villar co-developed the 3D printer and performed all experiments together except in two instances. First, Dr Villar independently performed research on bulk aqueous printed networks which is briefly mentioned in this chapter. Second, the self-folding network experiments of this chapter were initially performed collaboratively, but were completed independently by Dr Villar. Additionally, Dr Villar wrote the printer software and performed modelling of the droplet networks.

2.4 Introduction

Networks composed of droplets joined through lipid bilayers form compartmentalised systems[89]. Communication between network droplets with each other or the bulk environment can be attained through the inclusion of membrane proteins which allow the translocation of small molecules[89,90]. Small networks of communicating droplets have demonstrated collective functions and have been engineered into functional electrical devices[91,92]. In the Bayley lab, it was envisioned that these droplet networks might be designed to be functional tissue mimics[89]. Structurally the networks are already very simple tissue mimics[93] and can be perceived as a collection of protocells[89]. To expand the system to also produce tissue activities the droplet networks would have to be pre-programmed to exhibit collective tissue-like functions.

Our primary goal was to develop droplet networks which mimicked tissue functionalities. To achieve this, networks needed to be high order 3D structures composed of heterogeneous droplets patterned such their cooperative interactions produced tissue-like functionality. At the time, there was no practical way to make such complex networks. Micro-pipetting could only form sub-microlitre droplets which would be impractical to assemble into complex networks[91,92]. Alternatively, microfluidic devices could produce networks composed of pL droplets, but there was no control of the network's architecture[94]. Thus to attain droplet networks which mimicked tissue functionalities we had to develop a new method of fabricating droplet networks. This took the form of a droplet-in-oil 3D printer. This chapter present the development of this printer and its implementation to create droplet networks which functionally mimicked tissues or displayed other emergent properties.

2.5 Background on Droplet Networks

A brief overview of droplet networks is now presented to surmise the current state of the field.

2.5.1 Droplet Interface Bilayers

Aqueous droplets made in a lipid-in-oil solution spontaneously become coated in a lipid monolayer[89,90] (**Figure 2.1 A**). If these lipid coated droplets are brought into contact they adhere by forming a lipid bilayer, referred to as a droplet interface bilayer (DIB)[89,90] (**Figure 2.1 A**). Droplets connected through DIBs make up networks, various sizes of which have been reported such as pairs[91,95] (**Figure 2.1 A**), simple networks (3 to ~25 droplets)[91,92] and high order networks (>100 droplets)[94]. Non-membrane permeable contents of the droplets remain compartmentalised unless the bilayer is functionalised with pores such as membrane proteins[91,95] or photopolymerisable lipids[96]. Functionalisation in this manner has allowed DIBs to be used for single molecule studies of membrane proteins[91,97] and development of functional droplet network devices[91,92].

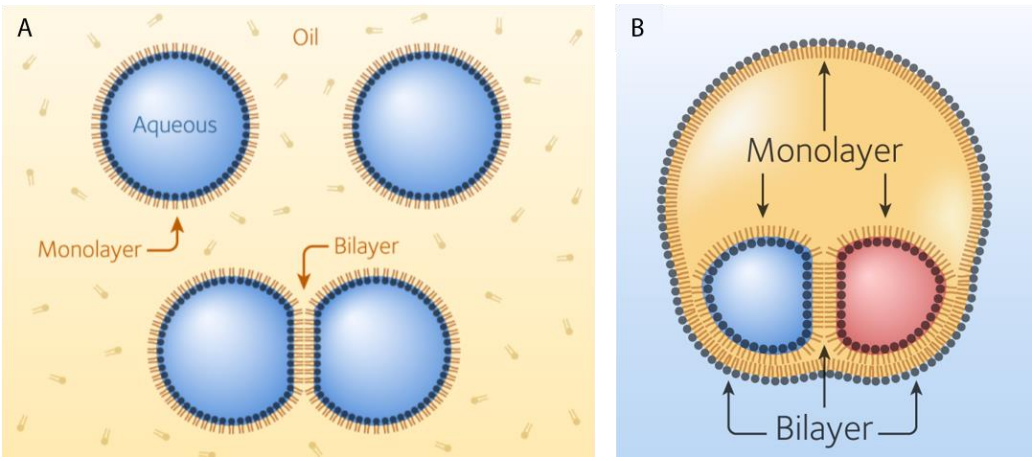

Figure 2.1 Illustrations of droplet interface bilayer formation. **A** Aqueous droplets in lipid-in-oil solution will become coated in a lipid monolayer. Lipid coated droplets can be joined through a lipid bilayer at their interface. **B** Aqueous droplets formed in a lipid-in-oil solution suspended in a bulk aqueous phase are called multisomes. Such networks contain internal droplet-droplet bilayers and external bilayers between droplets and the bulk phase. Permission to reprint the illustrations **A** and **B** from *Minimal Tissues*, DPhil thesis[98] was granted by Dr Gabriel Villar.

Droplet networks are typically made in oils consisting of a hydrocarbon, such as hexadecane[99], decane[95] or squalene[89]. Non-hydrocarbon based oils, such as silicone oils, have also been supplemented to density match the oil and aqueous phases[100,101] and to promote the formation of the lipid monolayer[100]. Stable DIBs which are electrically insulating and allow membrane protein insertion have been made from synthetic and

natural lipids, with the archaebacterial lipid 1,2-diphytanoyl-sn-glycero-3-phosphocholine (DPhPC) commonly incorporated[91,92,95,97,100,102]. Furthermore DIBs with asymmetric lipid leaflets have also been formed, here the lipid is incorporated into the aqueous phase as vesicles instead of the oil phase[102]. This approach has been used to study the behaviour of outer membrane protein G (OmpG, from *E. coli*) in different leaflet compositions as a function of charge[102].

2.5.2 DIBs for Single Molecule Studies

The behaviour of a single membrane protein inserted into a droplet interface bilayer can be monitored in the form of ionic current when a voltage is applied across the bilayer[89]. The behaviour of membrane proteins can be studied in this method by observing the modulation of current which indicate when the pore is open, gated or occupied[89]. This method has been used to study various membrane proteins including, the toxin pores anthrax toxin (from *B. anthracis*)[103] and alpha hemolysin (αHL, from *S. aureus*)[91], OmpG[102] and the proton pump bacteriorhodopsin (from *H. salinarum*)[91]. Furthermore this platform has been used as an array to screen the interaction of multiple analytes with a potassium channel from *Chlorella* virus PBCV-1 on a single molecule level[97].

2.5.3 Droplet Networks as Biodevices

Droplet networks containing multiple micro-compartments can communicate in a controlled way and display collective functions. These characteristics have be employed to form simple functional devices similar to electrical components. For example, a simple electrochemical battery was created from a network, which functioned by the production of voltage from the different rates of diffusion of anions and cations across network bilayers[91]. Another network which incorporated bacteriorhodopsin, was able to produce an ionic current upon illumination, creating a simple light sensor[91]. An effective ionic bridge rectifier circuit was also formed as a droplet network, which converted alternate phase current to a single phase current[92].

2.5.4 Droplet Networks in Bulk Water & Air

Droplet networks can also be formed in non-oil bulk phases, such as water[100] and in air[104], enabling the networks to interact with the bulk environment. Networks formed in an oil droplet suspended in bulk water are called multisomes[100]. Multisomes have both internal and external bilayers (**Figure 2.1 B**) and have been functionalised by different lipid bilayer compositions such that they can rupture with the bulk aqueous phase as a response to either a pH or temperature trigger[100]. Potentially, multisomes may be engineered to be drug-delivery agents that contain, water soluble prodrugs and their activators, which may be released by a physiologically triggered rupture[100].

Recently, networks have also been made in air, here droplets resting on a thin oil film were brought together to form simple 2D networks[104,105]. Subsequent electrical measurements of networks incorporating a single channel of alamethicin peptides demonstrated that they still functions like oil-bound networks[17]. These systems have the potential to sense airborne molecules, however, the networks are limited to basic 2D arrangements and need to be kept at the dew-point to prevent evaporation[104,105].

2.5.5 Hydrogel Interface Bilayer Systems

Interface bilayers have also been formed in lipid-in-oil solutions between aqueous droplets and planar hydrogels such as agarose or polyacrylamide[90,106]. These droplet-hydrogel bilayers (DHBs) have been commonly used for simultaneous optical and electrical recordings of various pore forming membrane proteins including αHL[107] and *M. smegmatis* porin A[108]. The optical measurements monitor fluorescent signals through the pore using total internal reflection fluorescence (TIRF) microscopy[89,90]. This setup was used to sequence DNA strands, with nucleotides discriminated by their modulation of the fluorescent and electrical signal[108]. Alternatively DHBs have been formed in a two phase system of oil above water, specifically between an agarose droplet and the lower aqueous phase. The composition of the lower aqueous phase could be exchanged at high flow speeds by a microfluidic device, allowing continuous electrical recordings of membrane proteins with different analytes[109].

Hydrogel-hydrogel interface bilayers have also been produced between pre-gelled agarose shapes[110]. Bilayers have also been formed between droplets containing photo-crosslinked polyethylene glycol dimethylacrylate attached before and after UV curing[111]. These interface bilayers could be inserted by membrane proteins[110,111] and were used to create functional agarose-based devices such as electrical circuits[110].

2.5.6 Fabrication of Droplet Networks

The fabrication of droplet networks was predominately by hand micropipetting, as exemplified by the functional droplet network devices[91,92], with networks only assembled into simple 2D structures of up to 24 droplets[99]. However, hand micropipetted droplets have also been assembled by external forces such as, mechanical manipulation[112], non-uniform electrical fields[113] and magnetic fields[114], but once again the network arrangements were either simple 2D or 3D geometries. Microfluidic approaches have offered rapid continuous flow production of droplets, which can be orders of magnitudes smaller than micropipetted droplets. This platform has enabled the production of simple 2D and 3D arranged droplet network, however, networks made by this approach so far have geometries restricted by the shape of the channels and architectures limited by the uncontrolled filling process[94,115–117].

2.6 3D Droplet Assembly

To develop a platform for the fabrication of high order 3D droplet networks, the manufacture process needed to generate lipid-coated droplets which could be spatially arranged into droplet networks. This restricted droplet production to bulk oil environments, with the assembly process designed around DIB formation. The process had to accommodate for the time required by droplets to form a lipid coating i.e. the droplet incubation time and the necessary time to form bilayers between droplets. To fulfil these requirements a custom printing technology was developed as conventional 3D printing approaches were typically performed in air and thus unsuitable. Additionally,

commercial printing heads were discounted as they would use volumes of print solution order of magnitudes larger than that required and would be wasteful for precious samples such as solutions containing purified protein.

2.6.1 Droplet Generation

The first development stage of the droplet network printer was the creation and testing of a novel droplet generator that could eject droplets rapidly, reproducibly and of a relevant size. To practically assemble 3D droplet networks, potentially containing thousands of droplets, the droplet volumes needed to be significantly smaller than micro-pipetted droplets and if possible approaching cell size to create a more faithful structural mimic of tissues.

We fabricated a piezo-actuated droplet generator to eject aqueous droplets into a bath containing lipid-in-oil solution (**Figure 2.2 A**). The droplet generator (**Figure 2.2 B**,**C**) was composed of a piezo-electric transducer that was sealed into an aqueous chamber, out of which protruded a custom made glass nozzle with a tapered end (*section 6.12.1.1* and *6.12.1.2*). Application of a voltage pulse to the piezo-electric transducer would result in a rapid expansion of the device. The subsequent acoustic wave generated in the aqueous chamber was expected to generate droplets from the nozzle.

To test the device we had to design a solution to eject (print solution) and an oil to print into (print oil). We designed our solutions around those employed in multisome formation as they produced networks which retained their structure over several weeks without any observed coalescence[100]. The **standard print oil** used for all prints of this chapter was a 50:50 v:v mix of hexadecane to silicone containing 0.2-0.6 mM DPhPC. The change in oil proportion (relative to multisome experiments) allowed the optimal sinking of droplets (see *section 2.6.3.1*). While the **standard print solution** was composed of 1 M KCl buffered with 25 mM Tris·HCl to pH 8.0. Here, the high concentration of KCl also contributed to optimal sinking (see *section 2.6.3.1*).

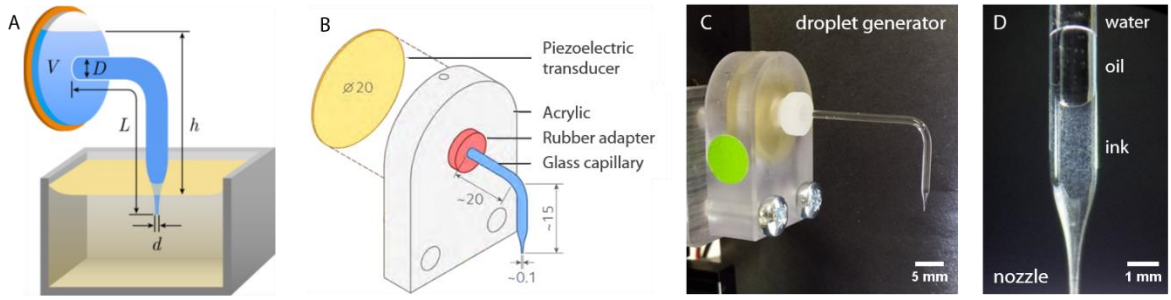

Figure 2.2 A piezo-actuated droplet generator. **A** Schematic of a droplet generator with its nozzle in an oil bath. Here the device comprises of an aqueous chamber backed by a piezo-electric transducer. From the aqueous chamber protrudes a capillary of length *L* that has an internal diameter of *d* at its tip and *D* at its base. The chamber is filled aqueous solution (blue) of volume *V*, and the distance between the aqueous level and the well's oil is *h*. **B** Blueprint of a droplet generator, depicting the different components and their dimensions. **C** Photograph of an unfilled droplet generator. **D** Micrograph of a printer nozzle loaded with a minimal volume of print solution a.k.a. ink. Here the ink is separated from the bulk water phase of the droplet generator by a small oil plug. Cartoon **A** and **B** was adapted from *A tissue-like printed material* (DOI: 10.1126/science.1229495)[1]. Reprinted with permission from AAAS.

Droplet production of the **standard print solution** was tested by submerging the nozzle in a bath containing **standard print oil** and activating the piezo element. This was by applying a square wave voltage pulses to the piezo-electric transducer, which subsequently expanded and contracted. This resulted in picolitre volume droplets forming below the nozzle tip that subsequently sank. It was observed that the application of a pulse initially caused a short-lived protrusion at the nozzle tip of the print solution into the oil phase ~50-150 μm long. This protrusion rapidly breaks up in <50 ms (i.e. it can at most only be seen in one frame of video recorded prints) to form either no droplet, a single droplet or multiple droplets (**Figure 2.3**).

The volume of these ejected droplets and their generation was subsequently assessed. Droplets could be produced at low volumes with diameters of 10-250 μm using the **standard print solution** in combination with the **standard print oil** (**Figure 2.3**). The type and size of droplet ejected depended on the pulse applied to the piezo-electric element (**Figure 2.3**). In general it was found that pulses with amplitudes ≤20 V would not produce droplets. Whereas pulses with amplitudes >20 V generally produced droplets. Increasing the amplitude of the voltage pulse under a constant pulse-width resulted in an increased droplet volume and an increased distance between the nozzle tip and the ejected droplet immediately after ejection, indicating a larger droplet protrusion was

formed. Varying the pulse-width of the applied pulse whilst keeping a constant amplitude, would vary the type of droplet formed, i.e. single droplets could transition to single droplets with multiple smaller satellite droplets. Droplet production was found to stay consistent upon application of a specific pulse (n = 10) and was latterly found to stay consistent across a print for a selected nozzle.

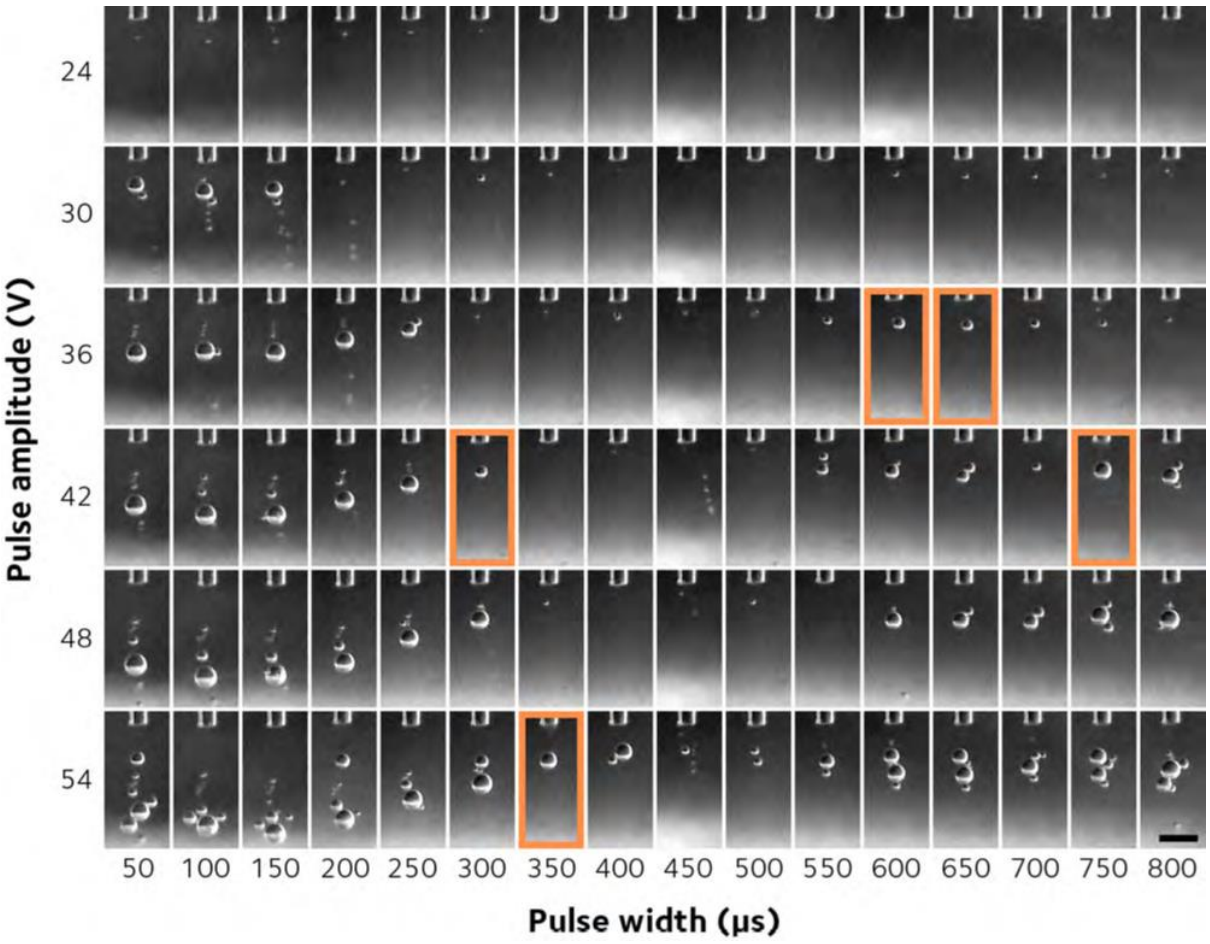

Figure 2.3 Piezo actuated droplet generation. Micrographs of droplet ejection by the droplet generator when applied with voltage pulses at different combinations of pulse width and pulse amplitude. The images were recorded immediately after droplet ejection. The droplet production remained consistent for each pulse combination (n = 10) for a given nozzle but varied from nozzle to nozzle. Conditions that gave single droplets of suitable print size (i.e. 40-100 µm diameter) have been highlighted. The scale bar is 200 µm. The figure was adapted from *A tissue-like printed material* (DOI: 10.1126/science.1229495)[1]. Reprinted with permission from AAAS.

Variations in nozzle dimensions gave rise to different characteristics of droplet production. The generator's nozzles were hand-made and non-identical, and consequently the overall droplet production varied from nozzle to nozzle. The nozzles

were made from glass capillaries with 1.0 mm internal dimeters (*D,* **Figure 2.2 A**), and were shaped to standardised dimension i.e. 3.5 mm in length (*L,* **Figure 2.2 A**) and tips with internal diameters of 122±23 μm ($\bar{d}$±s.d., n = 26, **Figure 2.2 A**). Nozzles produced with dimensions which deviated too far from the standard optimal dimensions were found to produce unreliable droplets. For example, making the tip too narrow (<80 μm) resulted in fewer conditions that gave ideal droplets compared with the standard nozzle size.

The filing of the droplet generator also affected droplet production. As the aqueous chamber of the droplet generator was elevated above the oil, it created hydrostatic pressure at the aqueous-oil interface. Consequently, the larger the distance between the oil and the aqueous reservoir (*h*, **Figure 2.2 A**) the larger the hydrostatic pressure at the nozzle and the less voltage was necessary to form droplets. The volume of the aqueous solution in the droplet generator (*V*, **Figure 2.2 A**) additionally affected how well the vibration from the piezo-electric transducer was coupled at the nozzle tip. In general it was observed that an almost-full droplet generator ejected droplets of sizes more readily controlled than when the generator was less full.

Additionally the lipid concentration in the oil affected droplet production. The amplitude of the voltage pulse to eject droplets of a specific size was lower at higher lipid concentrations. This is unsurprising as the adsorption of lipids at the nozzle's aqueous-oil interface decreases the interface's surface tension[118], hence, the energy needed to expand the interface, i.e. during droplet production, was lowered.

2.6.2 Printer Design

The piezoelectric droplet generator developed in *section 2.6.1* allowed us to reproducibly form pL volume droplets in lipid-in-oil solutions. We wanted to implement these droplet generators such that we could assemble their ejected droplets in 3D droplet networks. Our strategy was to place the lipid-in-oil bath on a motorised stage and position the ejected droplets in a layer-by-layer fashion.

The setup of our custom made droplet-in-oil 3D printer was as follows: two droplet generators containing different print solutions were aligned and have their nozzles submerged in a bath of lipid-in-oil solution (**Figure 2.4 A**). This bath rested on the arm of a motorised micro-manipulator [PatchStar 7000, *Scientifica*, UK] and computer software synchronised the droplet ejection with the manipulator motion. During a print, droplets would be ejected and sink until they rested on either the print substrate (typically glass) or the growing network. Droplets that come in contact would cohere through lipid bilayers and could be patterned layer-by-layer to form 3D networks (**Figure 2.4 B**). This printer could either eject one droplet type (one generator) or two droplet types (two generators with different print solutions). The motorised micromanipulator could move up to 20 mm in the *x*, *y* and *z* axes and travelled at a high resolution of 20 nm increments enabling droplet positioning to occur at a very high spatial resolution.

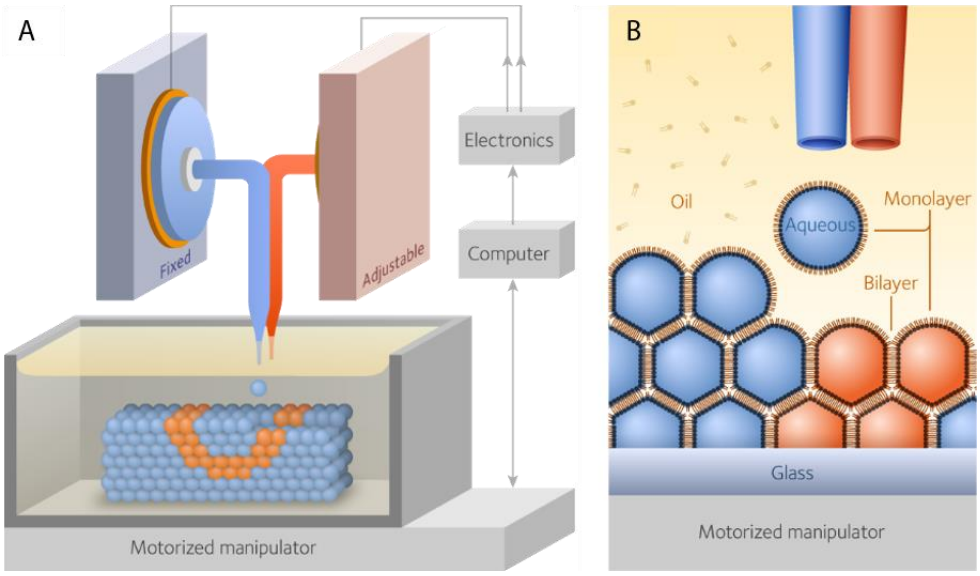

Figure 2.4 Illustration of the droplet-in-oil 3D printer. **A** Schematic of the droplet network 3D printer, which comprises of two static droplet generators, the nozzles of which are submerged in an oil bath which rests on a motorised stage. Droplet ejection is controlled by custom electronics which applies voltage pulses to the droplet generators. Computer software positions the motorised manipulator, and synchronises the ejection of droplets with manipulator's motion. Droplet networks are assembled by the layer-by-layer deposition of spatially assigned droplets. **B** Illustration of droplet network assembly by 3D printing. Droplets ejected in the lipid-in-oil solution become coated in a lipid monolayer as they sink and bind to other droplets through lipid bilayers. Well packed droplet networks assembled hexagonally distorting the droplet shape. Permission to reprint the illustrations **A** and **B** from *Minimal Tissues*, DPhil thesis[98] was granted by Dr Gabriel Villar.

The production of droplets or networks were controlled with custom-made software designed by Dr Gabriel Villar. A manual control software allowed the user to manually control the stage position and the ejection of droplets through a graphical user interface (*section 6.2.4*). This manual control software was used to find voltage pulse parameters (amplitude and pulse width) that produced reproducible singlet droplets for automated printing.

An automated printing software was also invented and can print, by automation, series of uploaded images, referred to as maps, which each represent a single horizontal network cross-section one droplet thick (**Figure 2.5 A**). The software constructs networks one horizontal layer at a time based on the maps, with the user defining the number of layers to print for each map. These maps are composed of three different coloured pixels, each of which represent a goal, i.e. a droplet ejection event at that location (with co-ordinates assigned to each pixel by the software). At the goal, depending on the pixel colour, either droplets will be formed from generator I (orange pixel) or generator II (blue pixel), or at empty goals (black pixel) no droplet ejection will occur.

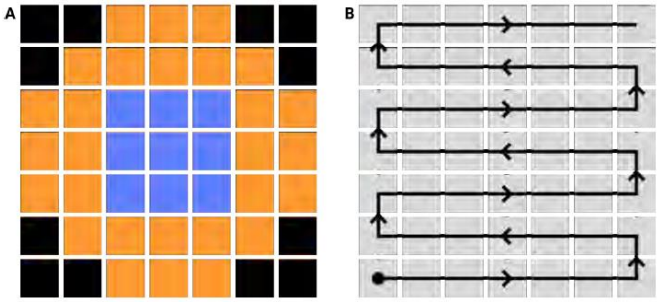

Figure 2.5 Printing pattern. **A** An example of a map of 49 pixels, including generator I (orange), generator II (blue) and empty (black) pixels. **B** Path taken by the printing nozzles across the map in each of the two passes, in the simplest variation of the printing algorithm. The figure is from *A tissue-like printed material* (DOI: 10.1126/science.1229495)[1] and reprinted with permission from AAAS.

Each layer of the network is printed in two passes, first generator I droplets are printed (pass one), followed by generator II droplets (pass two). During the printing of each pass the software instructs the nozzle to move and eject droplets along a specified path based on the uploaded map. The goals of the map are ordered such that nozzle moves in a raster

scan, i.e. prints the map in sequential rows. Specifically, the printing path starts at the bottom left pixel (minimum *x* and *y*), moves left to right (in *x*) for odd rows and from right to left (in *x*) for even rows. At the end of each row, the nozzle moves forward (in *y*) by one goal (**Figure 2.5 B**).

2.6.3 Preliminary Printing

With the ability to position ejected droplets, the assembly of simple droplet networks was attempted. This illuminated certain challenges to printing in an oil phase that needed to be resolved to pattern 3D networks.

2.6.3.1 Challenges of Printing in Oil

As droplets were being formed in an oil which had a dynamic viscosity ten times that of water there were several distinct consequences to droplet assembly that resulted in poor precision of placing droplets.

The viscous print oil slowed the descent of ejected droplets from the nozzle to their intended position in the network. As the nozzle formed an aqueous protrusion immediately prior to droplet formation, any object in its way deformed the protrusion and interrupted droplet ejection. As such droplets were ejected at 200-2000 μm from the network, sinking for 1-5 s before their placement. These sinking droplets could be displaced by viscous drag generated by the movement of nozzles in the oil phase and by the ejection of subsequent droplets. Consequently the desired patterned would no longer be printed accurately. Additionally once the ejected droplet came in contact with a network droplet, a bilayer would form after 1-3 s, presumably after the oil had thinned between the droplets. As this was not immediate, droplets resting on the network could also be displaced by further droplet ejection.

To limit droplet displacement, we optimised droplets to sink at an ideal rate by selecting solutions that ensured droplets were sufficiently dense compared to the oil phase. Some of the preliminary tests involved ejecting pure-water droplets and oils

containing different proportions of silicone oil. It was found that incorporating 1 M KCl into the print solution and using 50% v/v silicone oil allowed the droplets to sink at an ideal rate. Hence our standardised solutions for printing incorporated these properties. To further limit droplet displacement, only droplets above 30 μm diameter were printed. Below this volume the droplets suffered proportionately more viscous drag for their weight and had very slow sinking rates.

Delays between droplet ejection and movement of the nozzle were introduced to the printing process, allowing time for the droplet to sink to levels which don't experience high viscous drag. To ensure minimal droplet displacement by nozzle motion, the delay had to be 3-10 s. Employing these delay times significantly increased the time droplet networks were fabricated over. To minimise displacement whilst maintaining a high print speed, long delays at the end of printed droplet rows, of 2-10 s were used with short delays of 0.2 s between droplet ejections. This combination of delays displaced all the droplets of the row relatively evenly, and as such adjacent rows could be printed in a similar manner but employing a row offset to compensate for the overall displacement.

A strength of the system noticed during the adaptions was the decreased incubation time of droplets generated by piezo-electric actuation (~1 s) compared with previous hand micropipetted droplets (>15 min)[91]. For a given lipid concentration, smaller droplets incubate faster, this is a consequence of lipids adsorbing on the droplet interface creating a lipid deplete region around the droplet[119]. This depleted volume for smaller droplets is more accessible to replenishment by lipid diffusion.

2.6.3.2 Dual Nozzle Printing

Using the printer adaptions outlined in the previous section, the patterning of two droplet types was attempted as follows. For all single and dual nozzle prints of Chapter 2, either the droplet generator was entirely filled with print solution or a minimal volume of print solution (~5 μL) was suction loaded into the nozzle's tip below an oil plug (**Figure 2.2 C**). This allowed precious samples, such as the electrically conductive droplet solution which contained αHL (*section 2.7.1*) to be used with minimal waste. Additionally, printing was

typically performed with voltage pulses that produced single 50 μm diameter droplets. Lastly, voltage pulses that formed satellite droplets or multiple droplets were avoided where possible.

To print droplet networks containing two droplet type patterns, maps uploaded to the automated print software (*section 2.6.2*) would be printed layer-by-layer by two droplet generators. In this setup, the nozzles of the two generators were closely aligned. The nozzles were then lowered into the oil and voltage pulse parameters for the production of singlet droplets sized ~50 μm diameter were found for each generator using the manual control software (*section 6.2.4*). This voltage pulse parameters along with values for droplet spacing, delay times, starting position and positioning offsets were assigned in the automated print software (*section 6.2.6*). For dual nozzle printing, the most important offset was the nozzle offset as this accounted for the distance between the nozzles and allowed the accurate placement of the two droplet types.

It was also discovered that if a nozzle was left idle for >40 s, that it may leak into the lipid-in-oil bath. Leakage would occur initially as a slow growing hemispherical protrusion of the aqueous solution from the nozzle tip. Once the protrusion grew beyond the diameter of the nozzle it would rapidly grow as a spherical shape, that left unattended would fill the oil chamber. During dual nozzle printing, one nozzle would be left idle during a pass of the layer and could easily leak and destroy networks within the bath. This was avoided by applying a high frequency, low amplitude voltage pulse to the idle piezo at regular intervals during the print. Application of this pulse during the initial stage of leaking would reset the nozzle's aqueous-oil interface.

2.6.3.3 Preliminary Patterned Networks

Employing the dual nozzle printing process described in the previous section, droplet networks composed of two droplet types ($n > 50$), i.e. of orange and blue stained droplets, were successfully formed using the droplet-in-oil 3D printer at a rate of 1 drop/s. Cuboidal networks were printed with simple 2D and 3D patterns (**Figure 2.6 A,B**). Non-cuboidal

networks were also possible as epitomised by the hollow ring network and the cross network of **Figure 2.6 C**.

All the preliminary networks however, were initially patterned at low resolution or low accuracy. As seen in **Figure 2.6 A** there was an overlap of the blue and yellow pattern showing droplets were originally miss-aligned causing pattern inaccuracies. This emphasizes the necessity of accurately offsetting the capillaries prior to printing. With accurate offset values, patterning could be performed more precisely, as emphasized by the network containing a 3D diagonal pathway of blue droplets **Figure 2.6 B**. However, for most of these preliminary tall cuboidal networks (i.e. those >6 layers thick) sloped sides or domed tops were observed. This is a result of the droplets not immediately forming a bilayer as they contact the network, with border droplets becoming displaced down the sides of the network and rolling a significant distance down before being incorporated into the network. Consequently there was an excess of outermost droplets at the base of the network and depletion of outermost droplets in the upper layers.

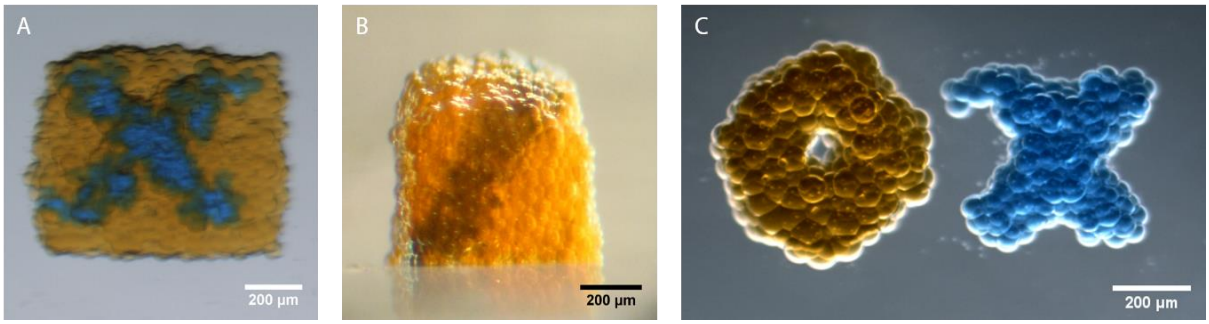

Figure 2.6 Preliminary 3D printing of patterned droplet networks. **A**-**C** Micrographs of droplet networks 3D printed using two droplet generators in parallel. **A** Nested diagonal cruciform network (approximately 12×12×12 droplets, $n = 1$) containing a misaligned cross pattern, with poor feature resolution. **B** Cuboidal network (9×9×21 droplets, $n = 1$) containing a pathway of droplets from the bottom front corner to the top back corner. Here it can be seen that the top slightly domes and the sides are slightly sloped. **C** Non cuboidal, hollow ring network (approximately 10×10×8 droplets. $n = 1$) and cross network (approximately 10×10×8 droplets, $n = 1$). These networks were printed accurately but with lower feature-resolution than the print map.

2.6.4 Optimised Printing

Printing accuracy was improved by using one of two methods. The first method was to print networks based on maps which had regions void of droplets, whilst the second method was to print as standard but deposit additional border droplets.

For networks containing a 2D pattern extended into the *z* dimension, such as the square ringed network ($n = 2$, **Figure 2.7 A,B**), networks could be accurately printed using special maps. These maps contained regions void of droplets between the pattern features of the two droplet types. During network printing the printed droplets would roll into these gaps ensuring defined regions of patterned droplets. Consequently the droplets gradually stacked across the whole network at a similar pace, without forming a domed surface or sloping sides (**Figure 2.7 B**). However, it was seen at the interfaces of the two droplet-types there was always an overlap of ~1 droplet thick. This is unavoidable due to both droplet types rolling into the void spaces, yet this type of patterning could be desirable for certain networks as a gradient of droplet types is present at the interface.

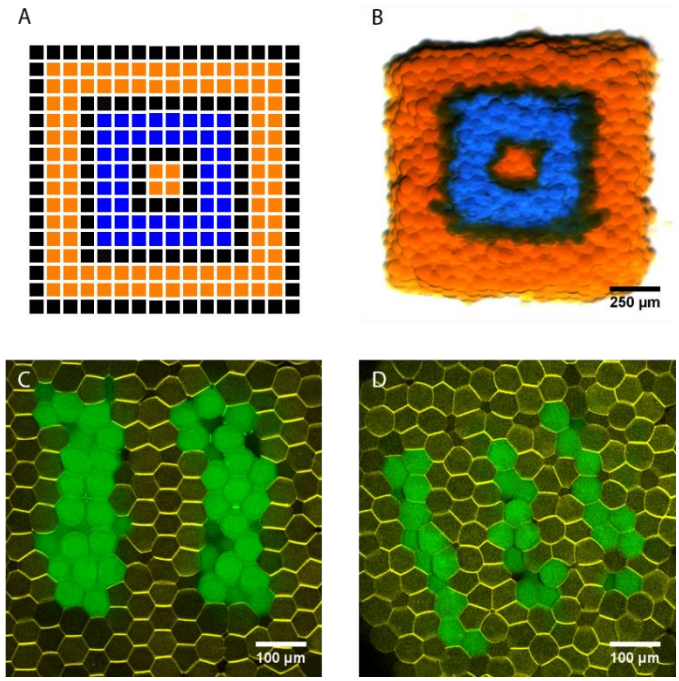

Figure 2.7 Optimised printing of patterned droplet networks. **A** Map of square ringed droplet network with 14×14 horizontal droplet dimensions. Each map feature, i.e. the two square rings and the centre, is separated by a droplet-void region of one droplet width. **B** Micrograph of a 3D printed square ring network (7 layers, $n = 2$) faithful to the map depicted in **A**. **C-D** Fluorescence confocal micrograph of printed networks containing internal narrow strips. The networks were printed 4 layers thick using 11×14 maps where the

stripes were either 2 droplets (**C**) or 1 droplet (**D**) wide. These networks comprised of fluorescent droplets containing either sulforhodamine-101 (SR101, yellow structural droplets) or fluorescein (green strip droplets). The images demonstrate that the droplets pack hexagonally and that the networks can be patterned with high resolution features, of 1-4 droplet width.

Using this method high resolution features could be patterned accurately down to two droplet widths. Networks patterned from maps with features two droplets wide, produced networks with architectures 2-4 droplets wide, as demonstrated by the yellow droplet network patterned with two internal green droplet strips (n = 1, **Figure 2.7 C**). This network contained continuous lines of connected green droplets and signifies features could be accurately patterned with droplets within one droplet width of their intended position. When the feature resolution of the map was increased to green strips only one droplet wide, it was found that printed networks contained narrow green droplet features 1-2 droplets wide however yellow structural droplets were present along the line (**Figure 2.7 D**, n = 1). Hence features could only be accurately be printed with maps where the patterned feature was ≥2 droplets wide.

Large networks composed of two droplet types could also be patterned accurately using a printing process which deposited additional border droplets each layer. Here the modification of the printing algorithm was used to eject 2-3 droplets in addition to normal ejection at each of the border goals. Consequently the border droplets stacked at the same rate as the network, rather than forming sloping edges. This prevented internal droplets from rolling out of their intended boundaries.

Using this border droplet print method 3D patterned networks composed of up to 35,000 droplets were formed (**Figure 2.8**). However, in the future, self-standing droplet networks could feasibly be fabricated to much larger dimensions.

Dr Gabriel Villar demonstrated networks could also be printed in bulk aqueous solution, attaining complex encapsulated networks (**Figure 2.9 D**, n > 10). These structures were fabricated in a similar manner to multisomes, here droplet ejection was performed in a lipid-in-oil drop suspended by a wire frame in a bulk aqueous phase. To prevent the printing solution flowing into the bulk aqueous phase during setup, an oil plug was suction loaded into the tip below the print solution. Upon lowering the nozzle

into the droplet, this oil plug would merge with the bulk oil phase, leaving the print solution at the nozzle's tip, thus enabling droplet ejection. After droplet networks were formed the oil would rest above the network, this was typically aspirated into the nozzle to leave encapsulated droplet networks (**Figure 2.9 D**).

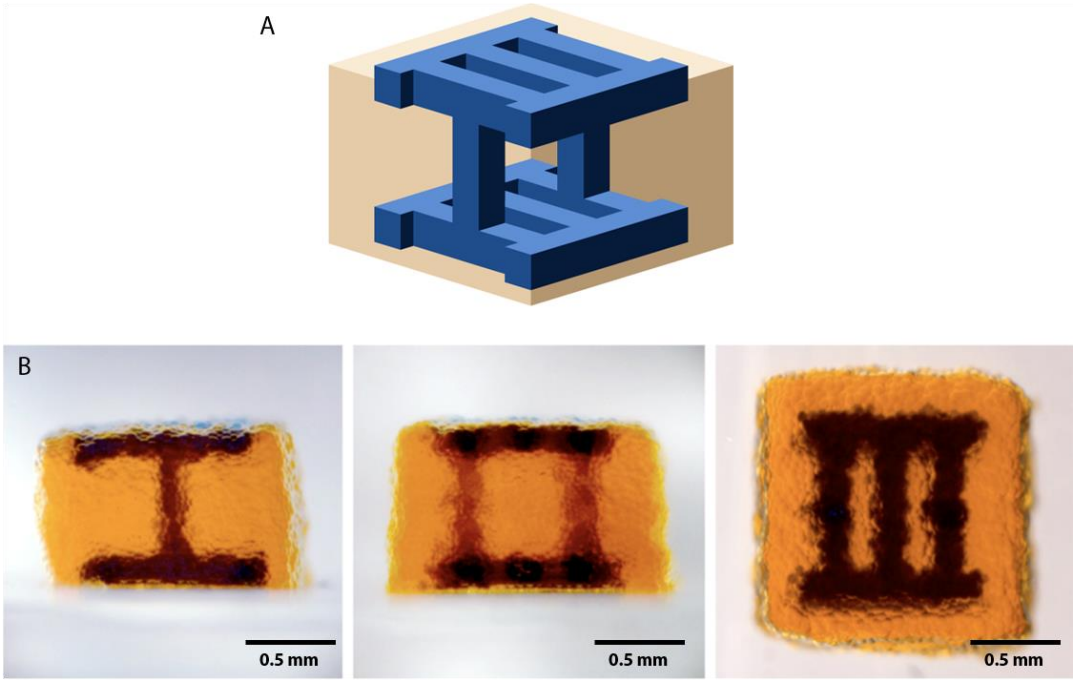

Figure 2.8 Printed droplet networks with 3D patterns. **A** 3D model of droplet network that consists of 28 layers of 24×24 droplets (n = 1). **B** Three orthogonal photographs of a network printed using the model of **A**. The figure was adapted from *A tissue-like printed material* (DOI: 10.1126/science.1229495)[1]. Reprinted with permission from AAAS.

Networks in bulk aqueous solutions were constructed with user directed placement of the droplets as automated printing was unsuitable. Ejected droplets would sink until they contacted the curved oil surface, at which point they would roll to the base of the droplet. Consequently, the automated printing of sequential parallel rows would result in non-defined spatial arrangements. Potentially in the future a printing algorithm may be adapted for bulk aqueous prints by patterning droplets as an outwardly expanding spiral. However, the structure won't remain static due to the less dense oil rising above the constructing network changing the overall geometry.

This method allowed the controlled fabrication of encapsulated networks in bulk water which showed structural retention over several weeks with no indication of inter-droplet coalescence or volume change. These encapsulated networks are analogous to multisomes, however, as they can be patterned with thousands of compartments, this should enable encapsulated networks to be engineered with more complex collective functionalities.

The droplet-in-oil 3D printer has enabled the rapid production of high-order networks that would be unattainable by hand micropipetting or current microfluidic methods. Furthermore our typical printed droplet is 65 pL which is thousands of times smaller than micropipetted droplets. The significant improvements in droplet resolution and network complexity is epitomised in **Figure 2.9** which displays the difference of syringe-made and printed networks. In the space of a syringe-made droplet pair thousands of droplets can be patterned, forming high-order 3D droplet networks.

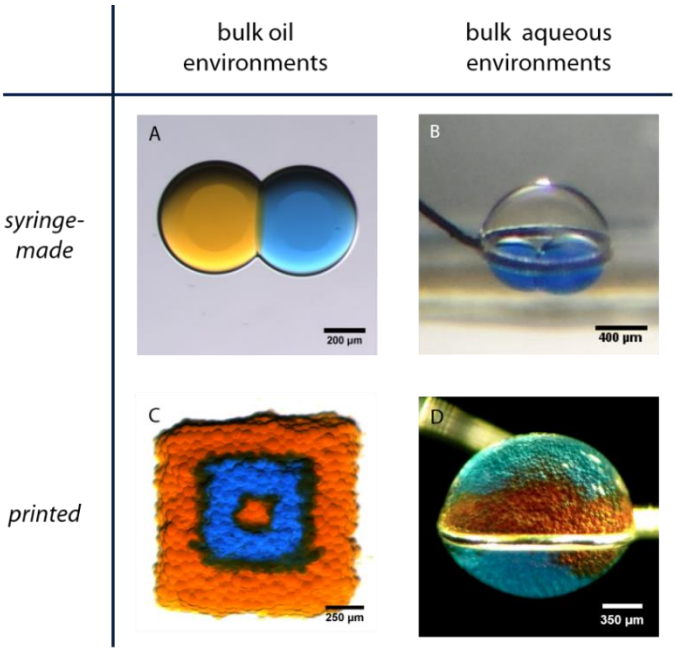

Figure 2.9 Comparison of droplet resolution in droplet systems that were syringed-made or printed. **A-D** Micrographs of droplet networks made by either a Hamilton syringe (**top row**) or a droplet-in-oil 3D printer (**bottom row**). Networks were made either in bulk oil environments (**left column**) or bulk aqueous environments (**right column**). In the space occupied by a pair of syringe made droplets (each 200 nL), thousands of droplets (~65 pL) can be assembled. Image **D** was adapted from *A tissue-like printed material* (DOI: 10.1126/science.1229495)[1]. Reprinted with permission from AAAS.

2.6.5 Network Modelling

Oil-bound printed networks were modelled by computer simulations designed and performed by Dr Gabriel Villar[1]. The network's resistance to deformation and ability to be self-supporting was assessed by modelling droplet pairs and linear droplet chains joined through bilayers. These simple models were suggested by scaling arguments[1] to give similar mechanical properties to three dimensional networks. The results obtained are now explained in brief.

It was determined that the lattice of bilayers allowed networks to retain their shape under gentle perturbation as each bilayer between connected droplets contributed an effective spring constant of ~4 mN m^{-1}. Consequently the energy required to separate a droplet pair, was determined as an ultimate tensile strength of ~25 Pa. Furthermore networks were estimated to have a Young's modulus of ~100-200 Pa, which is comparable to the elastic moduli of brain, fat and other soft tissues[32]. However, these estimated Young's modulus values need to be confirmed by empirical measurements, for example the elasticity of printed droplet networks may be analysed by atomic force microscopy[120]. Finally the conditions for network self-support were investigated as stacked droplets may exert enough pressure on lower droplets to separate them. It was estimated that it would take 1,300 layers (~20 cm) of connected droplets (sized 50 μm) to disjoin droplets on the lowest levels. Thus, self-supporting networks could feasibly be formed from several thousand layers if smaller volume droplets were used.

2.7 Functionalised 3D Printed Networks

With the ability to print high order 3D droplet networks, we designed constructs which functioned through the collective interactions of their droplets in attempt to make minimal tissue mimics. These networks were engineered to be either electrically conductive or to spontaneously fold into new geometries.

2.7.1 Electrically Conductive Network

To create a network that communicated in a directed manner we aimed to pattern a network that contained protein pores in specific bilayers. Such a network would allow the flow of measurable ionic current across the porous path upon the application of voltage. We selected staphylococcal αHL as the protein pore, due to its ability to readily insert into DPhPC bilayers as a heptameric pore[91,92], which is ionically conductive, weakly anion selective and weakly rectifying[121].

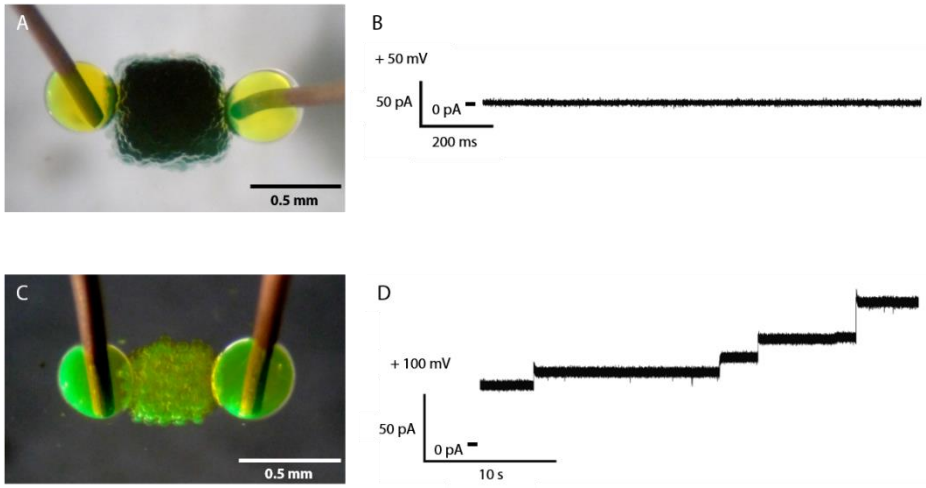

Figure 2.10 Electrical measurements of printed droplet networks with and without αHL. **A** Micrograph of a network (9×9×20 droplets, $n = 1$) which contained no αHL connected to two large droplets each impaled with an Ag/AgCl electrode. The network droplets comprised of **standard print solution** and no αHL, whilst the electrode-impaled droplets were composed of **standard print solution** with αHL. **B** Typical portion of a current measured at 50 mV for the arrangement seen in **A**. No transient spikes or steps were measured over 30 min. **C** Micrograph of an αHL containing network (9×9×20 droplets, $n = 1$) connected to electrodes. Here the network droplets and the electrode-impaled droplets comprised of the same solution as the electrode-impaled droplets of **A**. Current measurement at 150 mV of the configuration shown in **C**, immediately after the electrodes were placed on the network. Similar stepwise currents were recorded after twice removing and replacing the large droplets. The figure was adapted from *A tissue-like printed material* (DOI: 10.1126/science.1229495)[1]. Reprinted with permission from AAAS.

To perform electrical measurements on printed networks, two Ag/AgCl electrodes were attached to the networks to simultaneously apply a voltage potential and record current. To attach electrodes in a non-destructive way, their tips were each coated with a large buffer droplet containing αHL (**Figure 2.10**). To establish the difference between ionically conductive and insulating networks, electrical measurements were performed

on networks with and without αHL. A printed network (n = 1) without any protein pores only displayed negligible current over 30 min (**Figure 2.10 A**). Whereas when a network (n = 1) was composed entirely of droplets containing αHL, stepwise increments of currents were observed shortly after the attachment of the electrodes (**Figure 2.10 B**). This demonstrated the ~20 μg/mL αHL concentration was effective to attain printed networks which were ionically conductive.

To produce a network which had controlled electrical communication we printed αHL containing droplets along a defined pathway that was surrounded by insulating droplets (n = 1, **Figure 2.11 A**). When the electrodes were at either end of the pathway and a potential was applied, stepwise increments of ionic current were observed (**Figure 2.11 B,C**). The removal of one electrode from the pathway and its placement on a non-αHL containing region of the network gave electrical recordings displaying transient ionic current (**Figure 2.11 D,E**).

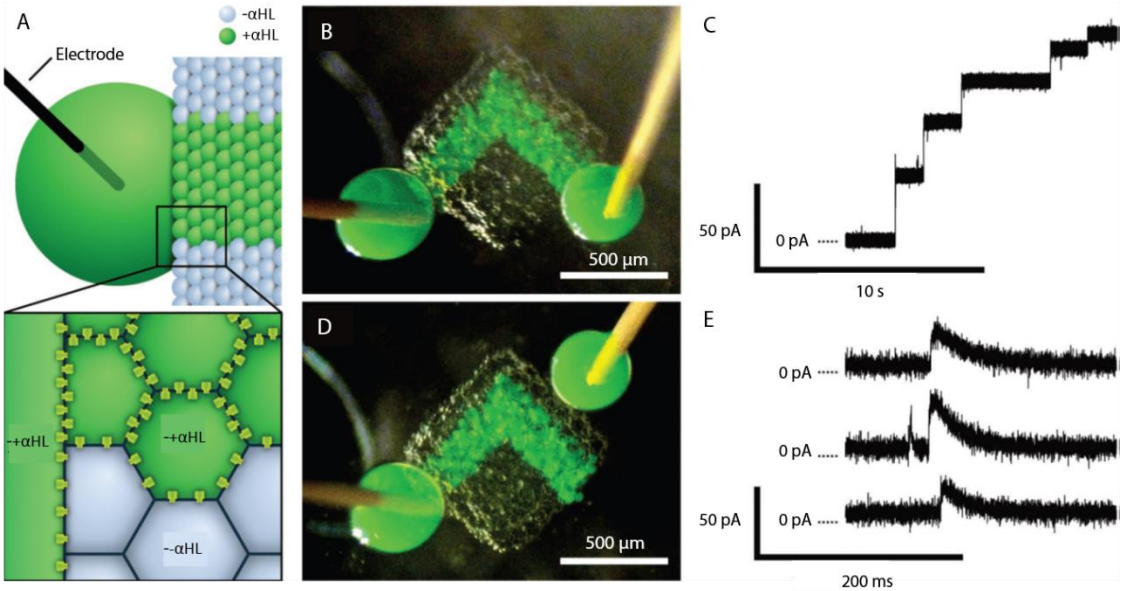

Figure 2.11 A droplet network printed with an electrically conductive pathway. **A** Schematic of a network (12×12 droplets printed for ~15 layers, n = 1) containing an ionically conductive pathway. Here, only the green printed droplets and large droplet contain αHL. A Ag/AgCl electrode is impaled in the large droplet to perform electrical measurements. **B** Micrograph of a printed network with an L-shape conductive pathway, with an electrode-impaled droplet attached to both the pathway ends. Printed droplets comprised of **standard print solution,** with pathway droplets (green) containing αHL whilst the other droplets (colourless) were protein free. **C** Current measurement at 50 mV of the configuration shown in **B**. **D** Micrograph of the network in **B** after one electrode-impaled droplet was repositioned away from the conductive pathway. **E** Selected portions of a current recording performed at 50 mV, for the configuration

depicted in **D** showing transient increases in ionic current. The figure was adapted from *A tissue-like printed material* (DOI: 10.1126/science.1229495)[1]. Reprinted with permission from AAAS.

The difference of measured ionic current across or away from the pathway indicates that only the pathway allowed the uninterrupted flow of current (**Figure 2.11**). As the network was printed over ~2 h, there was time prior to electrical measurements for αHL to insert into network bilayers. The stepwise increments of current measured across the pathway are thus likely to be pore insertions into bilayers between the border network droplets and the electrode droplet (**Figure 2.11 C**). This was also suggested by a consistent electrical model created by Dr Gabriel Villar, that computationally simulated the conductive pathway network in the different configurations used for electrical recording[1]. Here, the simulations assumed that each conductive pathway bilayer contained several pores and treated bilayers as capacitors and pores as resistors in parallel[1]. The model also suggested the transient currents observed away from the conductive pathway were a result of pore insertions into bilayers between the electrode droplet and insulating region of the network. Additionally the observed transient currents are capacitive and thus do not permit a steady resistive current.

Based on our findings we confirm that networks can be printed with protein pores in specific bilayers. Furthermore, the ionically conductive network is functionally analogous to a nerve axon in enabling electrical communication along a defined path but does not mimic the axon's mechanism of signal transduction.

2.7.2 Self-Folding Networks

The ability to deform the geometry of printed networks in a designed manner was explored. It was our goal to exploit osmotic water transfer between droplets to create self-folding i.e. short lived motile network. Self-folding network experimentation was initially performed by the author and Dr Gabriel Villar, however it was concluded independently by Dr Gabriel Villar. As such, only the main results for self-folding networks are discussed in brief.

A droplet pair joined through a lipid bilayer allows water transfer between the droplets through osmosis. When the pair is composed of a high osmolarity droplet and a low osmolarity droplet, the water transfer results in the droplets respectively swelling and shrinking until they are osmotically balanced (**Figure 2.12 A**). By expansion, if a network contained regions of high and low osmolarity droplets, the combined volume changes of the droplets should result in a network deformation (**Figure 2.12 B**).

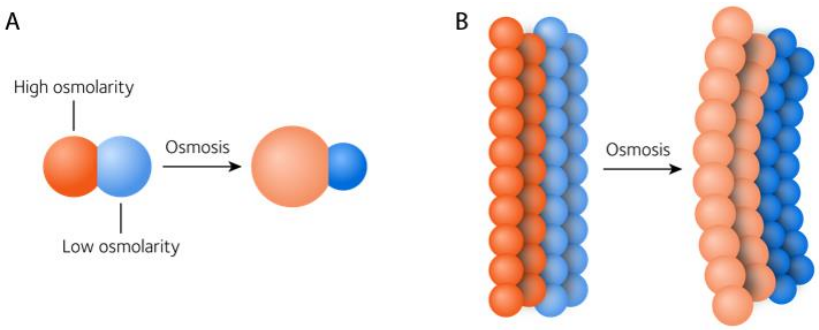

Figure 2.12 Osmotic volume changes in droplet networks. **A** Schematic of a droplet pair comprised of droplets of non-identical osmolarity. Water flows via osmosis across the lipid bilayer, causing the droplets to shrink or swell. **B** Schematic of a droplet network that comprises a dual strip of non-identical osmolarities. The water transfer results in deformation of the network. The figure was adapted from *A tissue-like printed material* (DOI: 10.1126/science.1229495)[1]. Reprinted with permission from AAAS.

Osmotic volume changes in droplet pairs were investigated to support the concept of osmotic water transfer and to determine the water permeability of the bilayer (**Figure 2.13**). Dr Gabriel Villar setup and monitored droplet pairs consisting of a 1 M KCl droplet bound to a 250 mM KCl droplet. Over a period of >2 h, the droplets swelled and shrank within the pair until they became osmotically balanced after ~120 min (**Figure 2.13**). The water permeability coefficient was calculated to be $P = 27 \pm 5$ μm s^{-1} ($\bar{P} \pm$ s.d., $n = 6$, *section 6.3.4.3*) and is consistent with other permeability measurements for DIB systems[122,123] and other lipid bilayer systems[124].

The observed permeability coefficient of droplets pairs indicated it would be feasible to design printed networks that could spontaneously self-fold through osmotic water transfer (**Figure 2.12 B**). To facilitate the fabrication of defined self-folding

networks, the printing process was adapted and the design of the network was optimised. For network motion to proceed across the printing substrate the network needed to avoid adhering to the surface. Consequently the typical printing substrate, which was glass, was unsuitable as droplet networks would partially wet to this substrate. Thus to avoid substrate adhesion, the printing substrate was changed to polymethyl methacrylate (PMMA) which displayed low wettability by printed droplets.

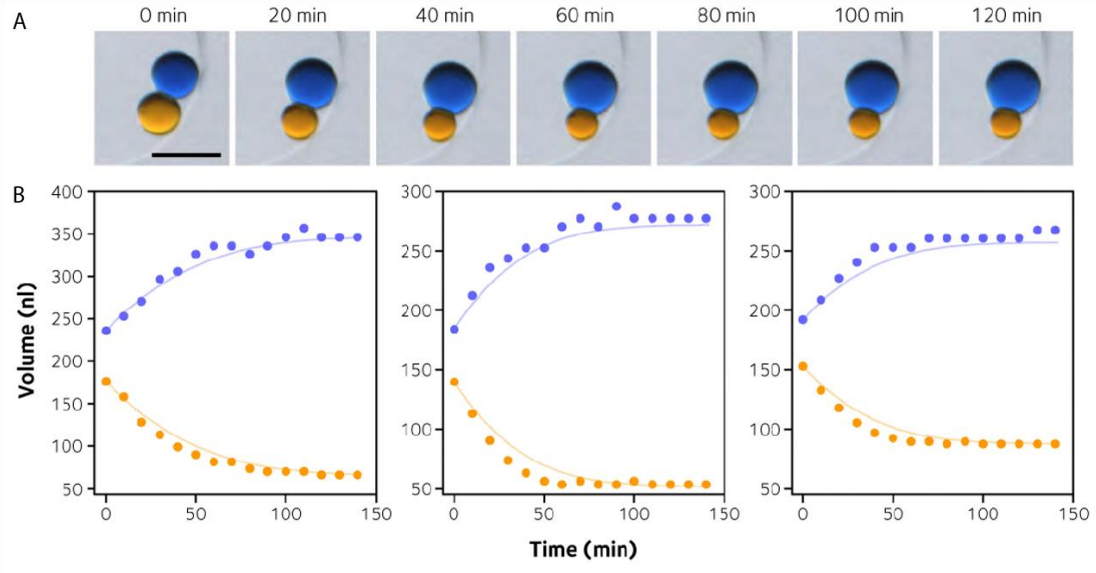

Figure 2.13 Osmotic volume changes within droplet pairs. **A** Micrographs of a single droplet pair changing shape by osmosis, with images recorded every 20 min post DIB formation. The blue droplet contained **standard print solution** (1 M KCl), whilst the orange droplet contained a diluted **standard print solution** (at 250 mM KCl). Scale bar, 200 μm. **B** Graphs of droplet volumes of three droplet pairs as exemplified in **A** over time (see *section 6.3.4.3* for volume calculation). The orange and blue circles represent the measured volumes of the orange and blue droplets respectively. The experiment and calculation were performed by Dr Gabriel Villar and the figure was adapted from *A tissue-like printed material* (DOI: 10.1126/science.1229495)[1]. Reprinted with permission from AAAS.

Networks would begin to spontaneously fold during print, which could lead to inaccurate patterning. To compensate for this, the printing time was decreased and the timescale the network deformed over was increased by varying the osmolarity of the print solution. The rate of water transfer between droplets is proportional to the difference between their osmolarities, whilst the extent of water transfer is determined by the ratio of the salt solutions. Thus, the folding process was slowed by using droplets with low salt

concentrations, which had a low osmolarity difference across the droplets but maintained a high ratio.

Self-folding printed networks were successfully programmed, by Dr Gabriel Villar, to fold in a controlled manner in and out of the horizontal plane (**Figure 2.14**). One network, composed of two strips of different osmolarities, folded over a 3 h period into a closed circle, with droplets at opposing strip ends eventually joining through DIB formation (**Figure 2.14 A**). This network was designed to avoid fracturing and consequently partially folding, by making the shrinking region significantly wider (in the horizontal plane) than the swelling region (**Figure 2.14 A**). A flower shaped printed network was also engineered to fold, but this time out of the horizontal plane (**Figure 2.14 B**). Here the network composed of four petals was patterned as two layers, with the lower layer being of higher osmolarity. The four petals of the network folded upwards and inwardly over 6 h, forming a self-supporting structure that approximated a hollow sphere (**Figure 2.14 B,D**). The observed motion was similar to a model network with similar initial parameters simulated by Dr Gabriel Villar (**Figure 2.14 C**). We estimated there was 1 μJ of available energy in this network from the osmotic water transfer, which is several orders of magnitude larger than energy needed to raise the droplets against gravity.

We have demonstrated that the cooperative behaviour of aqueous micro-compartments within printed networks can lead to emergent collective behaviour. In this manner the functioning of droplet networks is analogous to living tissues, the activities of which emerge from the combined interactions of their cells, distinguishing them from a collection of independently functioning units[125]. Furthermore, printed droplet networks have demonstrated that tissue-like behaviours can emerge in relatively simpler environments than living tissues. In networks the droplets can communicate across single lipid bilayers with the incorporation of membrane proteins. Whilst the cells of tissues have to communicate across two membranes and make use of specialised membrane proteins such as gap junction channels[126]. Thus we have managed to print

droplet networks which mimic collective behaviour of cells within tissues and also printed a network which acted as a functional nervous tissue mimic.

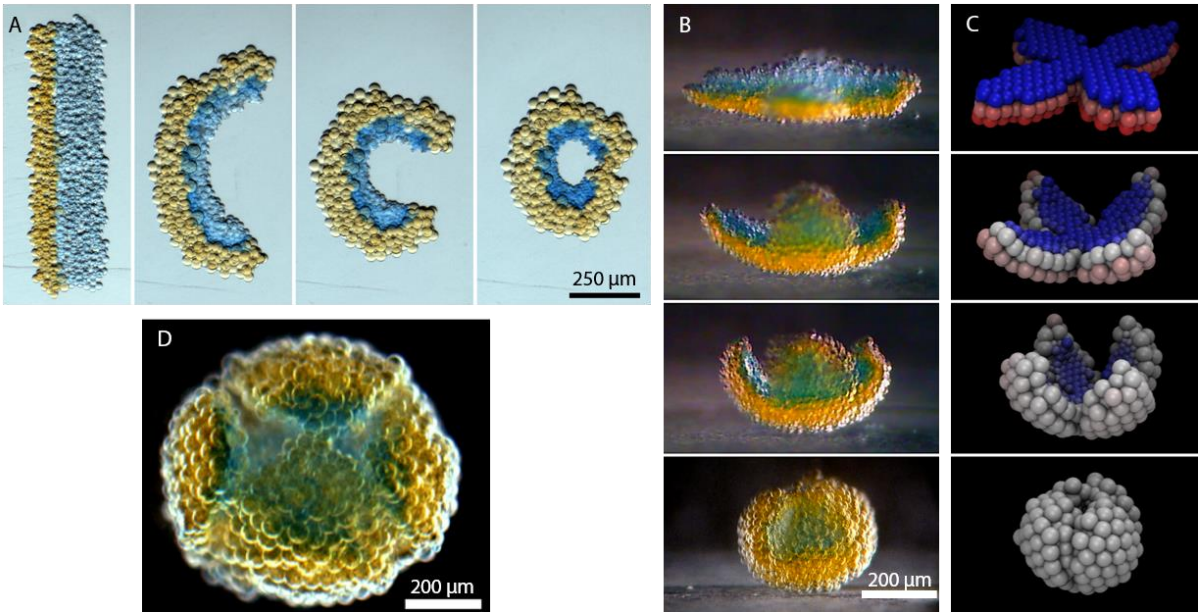

Figure 2.14 Self-folding droplet networks. **A** Micrographs of a rectangular network (19×9 droplets printed for ~5 layers, $n = 3$) that folded into a circle over ~3 h. The network comprised of two strips, with orange and blue droplets initially containing 250 mM and 16 mM KCl respectively. **B** Side-on micrographs of a flower-shaped network (25 droplets wide printed for ~8 layers, $n = 3$) folding into a hollow sphere over ~8 h. The network comprised of two stacked flower-shaped layers, with orange and blue droplets initially containing 80 mM and 8 mM KCl respectively. **C** Frames from a folding simulation (created by Dr Gabriel Villar), of a network with similar initial geometry to the network depicted in **B**. Spheres are coloured blue and red for high and low osmolarity respectively, while white signifies the average of the two. **D** Top-down Micrograph of the self-folded hollow sphere shown in **B**. The figure was adapted from *A tissue-like printed material* (DOI: 10.1126/science.1229495)[1]. Reprinted with permission from AAAS.

2.8 Conclusion

In order to construct large droplet networks with tissue-like properties we developed a novel droplet-in-oil 3D printer and analysed the emergent behaviours of printed droplet networks. Our approach was to assemble networks with droplets generated by piezo actuation in a lipid-in-oil phase. To attain accurate networks the printing process was optimised by varying droplet sinking rates and introducing droplet delays to prevent droplet displacement. Complex compartmentalised structures with 3D patterns were attained by assembling thousands of printed picolitre volume droplets in oil.

Encapsulated networks were also achieved by printing in a bulk aqueous phase giving structures, which retained their structure for week long durations. Thus we developed a printing process which could rapidly assemble defined large networks in high order architectures previously unattainable by other fabrication methods.

Furthermore, printed networks were engineered to present emergent behaviours. Rapid electrical communication across a defined pathway was achieved by incorporating αHL into specific bilayers. Such electrical communication is functionally analogous to a nerve axon's mechanism of signal transduction. Networks could also be programmed to self-fold by incorporating osmotic gradients, causing networks to fold by osmosis in and out of the horizontal plane. A petal shaped network was able to self-fold into a hollow sphere, which would be impossible to form by printing alone. Due to emergent behaviours arising from the collective functions of droplets within printed networks, these systems have demonstrated that they are functionally analogous to tissues.

3 Patterning Cells by 3D Printing

3.1 Chapter Abstract

This chapter describes the development of the methodology for the fabrication of 3D printed cell-laden droplet networks in oil and their subsequent transfer to culture medium. Printing was optimised to pattern cells at high densities and high viabilities. These networks could be solidified and transferred into culture medium whilst retaining their topology and cellular pattern. To demonstrate the high resolution patterning ability of this technology, phase transfer from oil was performed on droplet networks patterned with two cell populations in capillary-like and layered sheets architectures.

3.2 Publications

At the time of this thesis submission, our work on fabricating cell-patterned droplet networks for tissue development has been submitted for publication.

Provisional title: High-resolution patterned cell networks by 3D droplet printing.

3.3 Acknowledgement of Collaboration

All work included in this chapter was performed by the author unless specifically stated in the text. The author acknowledges the practical and intellectual input of **Dr Sam Olof** (University of Oxford) who supervised the work detailed in this section. Research on ovine mesenchymal stem cells (oMSCs) and their derivatives was performed in collaboration with **Madeline Burke** and **Dr James Armstrong** (both University of Bristol). They maintained the oMSCs prior to printing and provided practical assistance and intellectual input on the production of oMSC patterned droplet networks.

3.4 Introduction

The creation of cell patterned scaffolds which can develop into native tissue structures is a desired process for many research fields. Such tissue structures have the potential to be tissue replacements in regenerative medicine[15] or as tissue models for diseased or healthy tissues which potentially may be used in a high-throughput manner[16]. For cell patterned scaffolds to successfully develop intrinsic properties, multiple cell types need to be spatially organised at high resolution in native tissue architectures[9]. Subsequent proliferation of the cells to form functional tissues will then only proceed if cells are patterned in an optimal cellular growth environment[9]. Additionally, to develop tissues at high maturation rates, scaffolds should contain cells at high densities[14].

Bioprinting has offered a way of patterning multiple cell types at low to high resolution with low to high cell densities depending on the method. However, high resolution patterning is usual done at the expense of implementing materials with low cell density. Hence there is a demand for high resolution patterning of multiple cell lines at high-cell densities in tissue microarchitectures[9].

Chapter 2 described a droplet-in-oil 3D printer[1] which can assemble multi-compartment tissue-like structures. The individual compartments were typically of 65 pL. These structures were printed at high resolution with fine network features being patternable down to two droplet width i.e. ~100 μm. If cells could be incorporated within such a network, confined within each droplet by the lipid partitions, multiple cell types could be patterned at very high resolutions.

This chapter describes the adaption of the droplet-in-oil 3D printer to reproducibly fabricate cell-laden droplet networks in oil, along with the development of a method to phase transfer these networks to culture medium.

3.5 Cell Patterning by Droplet Printing

Our goal was to pattern cells as droplet networks by employing the droplet-in-oil 3D printer developed in Chapter 2. These networks would contain patterns of one or more cell types and act as an environment for the cells to proliferate to form tissues.

3.5.1 Overview of Cell Patterning

It was hypothesised that cells could be patterned by the droplet-in-oil 3D printer developed in Chapter 2, by incorporating cells into the print solution. This biological print solution, a.k.a. a bioink, would comprise of cells suspended in a scaffold solution containing culture medium to supply nutrients. Networks composed of cell-laden droplets could then be assembled, printed layer-by-layer, with droplets ejected in spatial-assigned locations based on digital printing maps (see *section 2.6.2*) (**Figure 3.1**). As such, an ideal print would have cells compartmentalised within each droplet (**Figure 3.1**). The resulting patterned cell network would then be maintained in a cell incubator to allow the cells to proliferate within the droplets. It was expected that the cells during their growth would break down the lipid partitions and develop into a tissue with the shape and tissue type dictated or at least influenced by the original printed pattern. As 3D printed droplet networks may provide an environment for cells to grow, cell-laden droplet networks can be thought of as and have been referred to as cell patterned scaffolds or cell containing scaffolds.

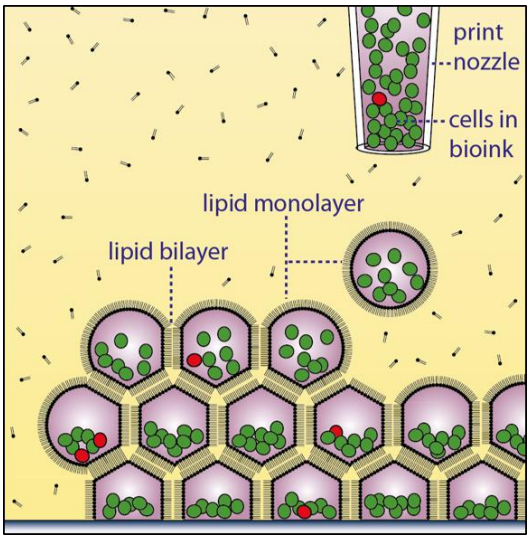

Figure 3.1 Schematic of cell-laden droplet network printing. A cell-laden bioink is printed in a lipid-in-oil bath as sequential layers of cell-laden droplets. Ejected cell-laden droplets are spontaneously coated in a lipid monolayer as they sink. These droplets are assembled into networks bound through bilayers, by the synchronised movement of the printing stage with droplet ejection. Within the network, cells are segregated within droplet compartments and are ideally present within every droplet.

3.5.2 Cell-Lines under Study

Throughout this chapter and Chapter 4 we have used human embryonic kidney (HEK) derived cell lines (**Figure 3.2 A**) and ovine mesenchymal stem cells (oMSCs, **Figure 3.2 B**) to produce patterned cell networks. The reason for their selection is described below, along with the method used for staining cells throughout this chapter and Chapter 4.

3.5.2.1 Human Embryonic Kidney (HEK)-293 Cell-Line Derivatives

HEK-293 is a well establish cell line that has been widely used as a host for recombinant protein expression[127]. The HEK-293T variant was derived from a standard HEK-293 to express the simian vacuolating virus (SV40) large T-antigen. It is commonly used to express various genes from retroviral vectors[128].

We choose HEK-293T due to its overall ease of culture and maintenance, its fast cell cycle (doubling time of ~20 h), its robust nature and its weak substrate adherence (**Figure 3.2 A**). Hence, a cell patterned scaffold containing HEK-293T could within a short time-frame be cultured into a tissue (see Chapter 4).

Fluorescent derivatives of HEK-293T were chosen to study cell patterning (see *section 3.9*). These were yellow fluorescent protein (YFP) and cyan fluorescent protein (CFP) expressing HEK-293. It was observed that HEK-293 had slightly different properties to the T variant; it was slightly more adherent to the culture substrate and had slower doubling time. Consequently HEK-293 cells were trypsinised before being processed into the bioink.

3.5.2.2 Ovine Mesenchymal Stem Cells

Ovine MSCs are multipotent stromal cells, which are capable of differentiating into mesenchymal tissues: bone, cartilage, muscle, ligament, tendon, and adipose[129]. Thus, multipotent oMSCs could be printed within a network and then differentiated into a specific lineage (see Chapter 4). Unlike the HEK-293T cell-line they have a high substrate adhesion and trypsinisation is a necessary step in cell harvesting. oMSCs are also slower to replicate and form highly polarised 2D cell cultures. This polarisation is fast, as depicted in **Figure 3.2 B,** which is an image of a plated oMSC after 30 min.

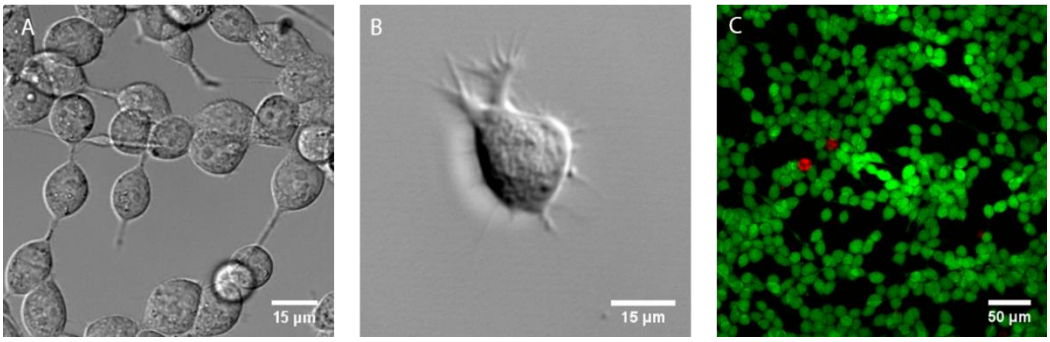

Figure 3.2 Cell-lines used. **A**-**C** confocal micrographs of cells on a glass substrate: **A** HEK-293T; **B** oMSC and; **C** live/dead stained HEK-293T. **A** & **B** are bright-field images whilst **C** is a fluorescence image. Cells imaged by **Dr Sam Olof**.

3.5.2.3 Live & Dead Staining

All cell-laden network viabilities were investigated by printing live/dead stained cells (*section 3.5-3.7*). Later, in phase transfer experiments, cell patterned scaffolds were stained after transfer into culture medium (*section 3.8 &* Chapter 4). Staining was

performed with the live cell dye calcein-AM (CAM) and the dead cell dye propidium iodide (PI) (**Figure 3.2C**). CAM is a cell membrane permeable dye that stains the cytoplasm of living cells green when its acetoxymethyl ester group is hydrolysed by intracellular esterases releasing the active fluorophore calcein (Em_{max} 515 nm)[130]. PI is an impermeant dye which can only pass into dead cells with degraded membranes. When PI is within a cell it stains the nucleus red (Em_{max} 617 nm) as it intercalates with double stranded DNA, enhancing its fluorescence 20-30 fold[131].

For the preliminary printing experiments in *section 3.6.3*, cells were stained and then washed, removing the dye molecules in the bioink solution. Consequently, cells that became necrotic post print would not be stained. To ensure that cell health could be monitored after printing, all other cell patterning optimisation experiments (*section 3.6.5* and *3.7*) had the live/dead dye in the print solution. This allowed the staining of cells that became necrotic after printing.

3.6 Preliminary Cell-Laden Droplet Networks

The compatibility of cells with the 3D printing process developed in Chapter 2 needed to be assessed. Specifically, cell-laden droplet ejection and the ability to form droplet interface bilayers in the presence of cells and culture medium were investigated.

3.6.1 Culture Medium-Only Scaffold Solutions

The solutions used to make cell-laden droplet networks have been referred to as scaffold solutions, as the droplet network can be thought as a 3D scaffold for tissue development. The initial scaffold solution was composed of cells suspended in minimum essential medium (MEM) with Glutamax® and with or without fetal bovine serum (FBS). This culture medium would provide a cytocompatible environment and the necessary nutrients needed for the cells to stay viable and proliferate within the network. Previously it was found that low viscosity salt solutions were printable (Chapter 2) and as such it was

predicted that a culture medium based bioink, which has a similar viscosity to the original salt solutions, would also be compatible with droplet generation.

MEM contains the essential cellular nutrients such as amino acids, vitamins and salts, to keep cells viable, but not able to proliferate[132]. It also provides a sustainable cytocompatible environment. Specifically, it is osmotically balanced with the cells (at 270-320 mOsm/kg) and buffered at physiological pH (i.e. pH 7.0-7.5). MEM is usually supplemented with animal serum, which provides reagents that are required for cell proliferation[132]. Specifically, the serum provides growth factors, but also buffers against perturbations and toxic effects such as: pH change, the presence of heavy metals, proteolytic activity and endotoxins[132].

For the first oMSC prints in *section 3.6.3*, cells were suspended at 0.1×10^6 to 4×10^6 cells/mL in either Dulbecco's modified Eagle's medium (DMEM) with 10% v/v fetal bovine serum (FBS) and 1% v/v GlutaMAX®, denoted as **MSC culture medium**. Here, DMEM with 10% v/v FBS was selected as it is the standard culture medium for oMSC expansion in 2D culture.

The subsequent preliminary cell prints (*section 3.6.4 and 3.6.5*) used alternative culture medium based solutions. The solutions were denoted as **scaffold solution 1m** or **1h** (**SS1m** or **SS1h**) for oMSC and HEK-293T containing networks respectively. These solutions had low or no serum content, because it was found the removal of FBS stabilised the network during the print (see *section 3.6.4)*,

SS1m and **SS1h** both comprised of culture medium with cell dyes CAM (5 μm) and PI (5 μm). The culture media were **DMEM-ITS** for **SS1m** and Opti-MEM® with 0.5% v/v FBS for **SS1h**. **DMEM-ITS** was selected for oMSCs as it is a serum free medium supplemented with insulin, transferrin and selenium. **DMEM-ITS** can also be combined with growth factors for oMSC differentiation experiments. Whereas Opti-MEM® can be used at low serum content to culture HEK-293T due to its supplementation with Glutamax® and growth factors.

3.6.2 Printer Setup

The **standard print oil** from Chapter 2 i.e. DPhPC in a 1:1 v:v mix of hexadecane with silicone oil AR20, had been shown to create networks that showed minimal coalescence and formed well packed structures. Therefore it was used for all preliminary cell prints in *section 3.6* and all optimising scaffold prints in *section 3.7*. The cell cargo might have perturb the lipid monolayer coating around the droplet during print leading to intra-network coalescences. Accordingly, the lipid concentration was increased to 1.2-2.4 mM to ensure droplets were coated with a lipid monolayer by the time they were forming DIBs (i.e. within 1 s).

Similarly to Chapter 2, printing was performed in two steps: manual tuning and automated printing. During the manual tuning stage, voltage pulses were tested until one which produced ideal droplets was found. For cell printing, ideal droplets were singlets containing cells of uniform size. The best possible voltage pulse would then be used for automated printing of an uploaded map. For *section 3.6* this was 9×11 horizontal droplets for 3 layers.

During the preliminary prints it was noticed that nozzles i.e. capillaries of the droplet generator stored in air for over a week had oil enter the tip during print, forcing the print solution to recede up the capillary. In such a state, droplets could not be ejected. Capillaries that were plasma cleaned prior to use rarely had oil enter the tip during printing, prolonging the usable lifetime of the nozzle. This observation indicates that the internal surface of the capillaries slowly becomes hydrophobic when left in air and with treatment of oxygen plasma becomes hydrophilic. Therefore oxygen plasma treatment of capillaries was performed on the day of use, prior to printing, for all prints described in this chapter and Chapter 4.

3.6.3 Cell-Laden Droplet Ejection

The ability to print cell-laden droplets was tested by printing a bioink comprising oMSCs in **MSC culture medium**. Preliminary tests (n = 4) revealed issues relating to nozzle leakage and cell clogging. Specifically, when the a nozzle loaded with bioink was lowered

into the oil the cells settled in the transparent tip, packing densely together (**Figure 3.3 A**). At this point the print solution was prone to leaking into the oil i.e. the bioink quickly expanded into the oil creating a large spherical protrusion at the nozzle tip (**Figure 3.3 B**). The leaking phenomenon is likely a result of the cells concentrating in the nozzle's tip and increasing the local buoyant density. This additional weight caused the nozzle's aqueous-oil interface to expand rapidly, due the surface tension of this interface being low in the high lipid presence[118] and needing little energy to expand. Further leaking could be stopped at this stage by raising the nozzle out of the oil, causing the budding droplet at the nozzle's tip to separate and sink as a single droplet in the oil (**Figure 3.3 C**). During the leaking stage no voltage pulses generated droplets and further leakage was only prevented by removing the nozzle's budding droplet.

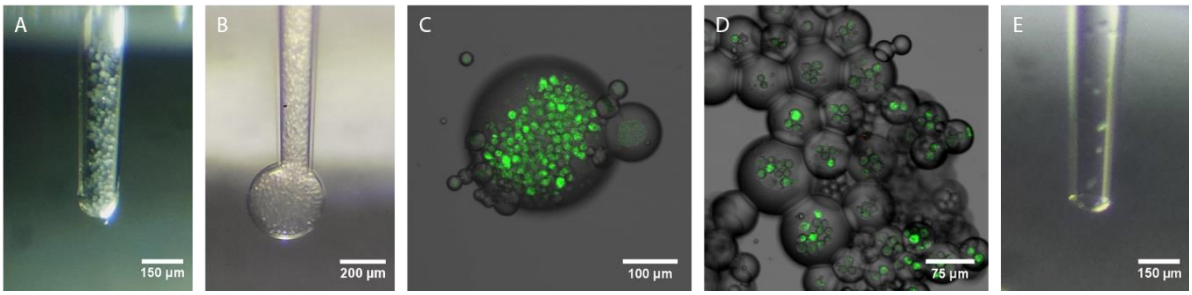

Figure 3.3 The preliminary print of oMSCs. **A-B** Images of the printer nozzle dense will cells: **A** prior to leaking and **B** while leaking into oil. **C-D** Composite bright-field and fluorescence confocal micrographs of printer dispensed cell-laden droplets: **C** a droplet which was budded from a leaking nozzle and; **D** a network of non-uniform droplets formed by manual printer control. **E** Image of the printer nozzle post leaking after ~20 min when cells have been mostly dispensed. Images **A**, **B** and **E** are bright-field micrographs.

After removing multiple budding droplets from the printer nozzle, the cell densities within the nozzle was reduced to a moderate concentration. At this point the leakage rate was also slowed and high voltage pulses could be used to eject droplets with or without cells. However, droplet production was not consistent during periods of moderate cell density in the tip. For a constant voltage pulse, droplets were generated non-uniformly sized and did not always contain cells. As no droplet generation parameters were consistent, automated printing was not successful, but networks composed of manually ejected droplets were formed (**Figure 3.3 D**). Within assembling networks it was observed

that droplets sized <50 μm diameter generally did not coalesce, whereas droplets >100 μm diameter frequently coalesced with neighbouring droplets.

Another issue observed during print was that cell-laden droplet ejection was generally short lived as the finite cell content of the bioink gradually deplenished through droplet ejection, resulting in a decrease in the average number of cells per droplet over time. When the bioink in the nozzle was at very low cell density (**Figure 3.3 E**) cell-laden droplet production was very infrequent as the cells were actuated vertically up within the nozzle for each applied pulse. Hence, cells had to sink to the nozzle's aqueous-oil interface for them to be ejected, which for successful printing would necessitate a long delay time between each droplet ejection.

Regardless of printing difficulties, the results proved cells could be ejected as droplets by the printer and suggested defined cell-laden constructs should be feasible with optimisation.

3.6.4 Refining the Base Culture Medium

The results shown in *section 3.6.3*, signified that viable cells could be manually printed as droplet networks. Furthermore with modifications to the printing procedure the method could feasibly be standardised to reproducibly make networks of defined structure so long as the network coalescence issue was resolved.

To better understand the coalescence and leakage issues, various culture media were printed as droplet networks, in order to find conditions that produced empty droplet networks without intra-network coalescences. DMEM with FBS (**MSC culture medium)**, DMEM only and Opti-MEM® with 0.5% v/v FBS, were each printed in **standard print oil** and imaged over 24 h (**Figure 3.4**). Networks (n = 1 per bioink) were printed as a 9×10 horizontal droplets for 7 layers and stored in hydration chambers.

The **MSC culture medium**, which contained 10% v/v FBS, was a far leakier print solution compared to DMEM only and Opti-MEM®. As such, it had to be printed quickly, i.e. with a short delay of ~0.4 s between each droplet ejection, to avoid nozzle leaking. Whereas DMEM only and Opti-MEM® with 0.5% v/v FBS would leak at a slower and

much more manageable rate. This indicated that the FBS decreased the surface tension of the interface between the print solution and the oil, allowing it to expand with less energy. This could arise due to amphiphilic serum molecules such as albumin coating the interface along with the lipid.

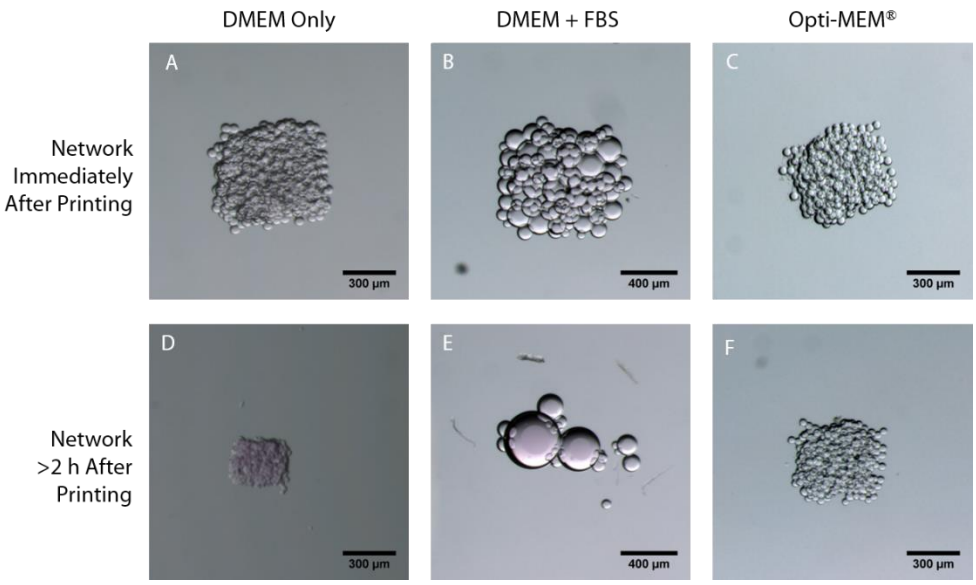

Figure 3.4 Printed networks containing culture medium only. **A**-**F** Bright-field micrographs of culture medium networks at different time-points: **A**-**C** straight after printing and; **D**-**F** the structures within 24 h after printing. Networks (n = 1 per bioink) were printed as 9×10 droplets for 7 layers, and were composed of: **A** 100% v/v DMEM; **B** 89:10:1 v:v:v DMEM : FBS : GlutaMAX® and; **C** 99.5:0.5 v:v Opti-MEM® : FBS. Networks **A**-**C** were left for 24 h, 14 h and 2 h respectively to give structures **D**-**F**. The networks with FBS were unstable over time.

During the print of the **MSC culture medium**, most droplets were involved in single or multiple coalescence events, resulting in a network with droplets of heterogeneous sizes (**Figure 3.4 B**). Within 14 h, the network was no longer square and had coalesced into ~10 droplets (**Figure 3.4 E**). In contrast, DMEM only and Opti-MEM® networks displayed relative few coalescence events during the print (~1-2 per network) and gave defined square sheet structures (**Figure 3.4 A,C**). These networks were found to be stable over 24 h, retaining their original structure, but they did shrink due to dehydration (**Figure 3.4 E,G**). It was concluded that the FBS was the main network destabilising component, potentially due to molecules such as albumin disrupting the lipid bilayer.

As FBS supplementation seemed to be the major issue for defined network printing, it was decided that oMSCs and HEK-293T would be suspended in **DMEM-ITS** and Opti-MEM® respectively.

3.6.5 Defined Cell-Laden Droplet Networks

By using bioinks composed of culture medium that omitted FBS, defined cell-laden networks were achieved for oMSCs and HEK-293T cell-lines. This bioink modification significantly reduced nozzle leaking and allowed droplets to be ejected more consistently. As such, cell laden networks were printed as 9×11 horizontal droplets for 3 layers, using bioinks with a range of cell densities 0.1×10^6 to 2×10^6 cells/mL. Resulting cell containing networks (n = 4) displayed square sheet structures with inhomogeneous distribution of cells (**Figure 3.5**).

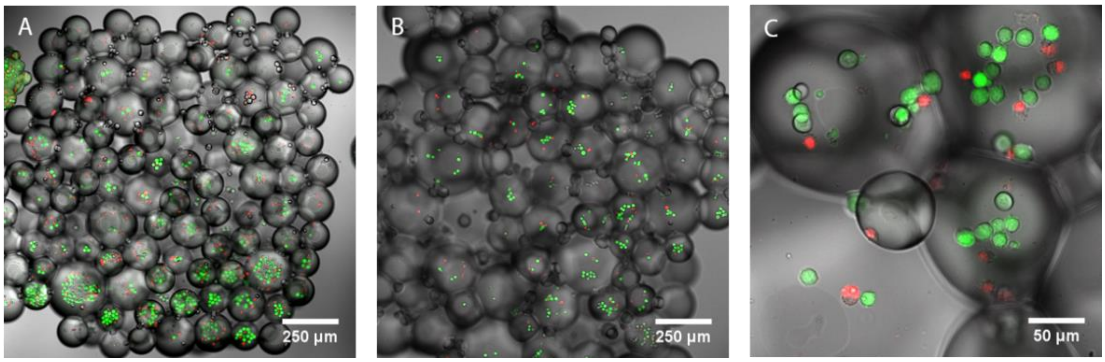

Figure 3.5 Printed cell-laden networks with defined structure. **A**-**C** Composite bright-field and fluorescence confocal micrographs of defined cell-laden networks. Networks were constructed with bioinks: **A** 2×10^6 oMSC/mL in **DMEM-ITS** and; **B** 2×10^6 HEK-293T/mL in Opti-MEM®. **C** Zoomed-in image of the network of **B**. Cells have been non-uniformly distributed and droplets are non-uniform in size due to coalescence events.

During the droplet tuning step only two type of droplets could be formed: those <50 µm diameter which did not contain cells or droplets >120 µm diameter which encapsulated cells. Hence pulses producing the larger droplets were used, giving inconsistently sized droplets of ~120-150 µm throughout the print. These large droplets displayed a moderate number of coalescence events, resulting in networks with a range of droplet volumes

(**Figure 3.5**). Interestingly, towards the end of the print, when the cell density became very low in the nozzle, droplet production was much more consistent, but cell ejection was infrequent. As such the first few printed rows of the networks were much denser with cells compared with the latterly ejected droplets.

oMSCs were printed at three different densities, 0.1×10^6, 1×10^6 and 2×10^6 cells/mL, giving defined square networks ($n = 1$ per bioink type, **Figure 3.6 A-C**). For the lowest cell density network only 3 cells were ejected and only one droplet, the cell-laden one, showed coalescence (**Figure 3.6 A**). Whereas for the other two oMSC containing bioinks, hundreds of cells were printed and over half the printed droplets were involved in at least one coalescence event. It was thus inferred that the cells destabilise the lipid bilayers, as low cell density and culture medium only bioinks display a minimal number of coalescence events.

3.6.6 Viabilities of Printed Cell-Laden Scaffolds

The total number and viability of the oMSC and HEK-293T cells within the printed networks were analysed (**Figure 3.6**). Counting was performed manually using a Cell Counter Plug-In[133] for ImageJ[134,135]. The determined number of live and dead cells was used to calculate the cell viability within the scaffold.

The total number of cells counted was in the order of hundreds for networks printed with 1×10^6 or 2×10^6 cells/mL bioinks (**Figure 3.6 B-D**), whilst the network from oMSCs printed at 0.1×10^6 cells/mL only contained 3 cells (**Figure 3.6 A**). It was observed that the two prints at 2×10^6 cells/mL dispensed a significantly different number of cells, with 590 oMSC and 339 HEK-293T counted within their scaffold. This supports the observations that bioinks containing $>1\times10^6$ cells/mL had their cells settle in the nozzle. Consequently there was varied cell densities of droplets throughout the print and lead to an inhomogeneous distribution of cells.

Viabilities were calculated to be 0%, 54% and 56% for the preliminary oMSC networks displayed in **A-C** of **Figure 3.6**, signifying that the printing process was not completely detrimental. Viabilities were improved to 76% with the preliminary HEK-

293T network (**Figure 3.6 D,E**), indicating that the process was may have been performed in a more cytocompatible way or the HEK-293T were more resistant to any detrimental piezo effects.

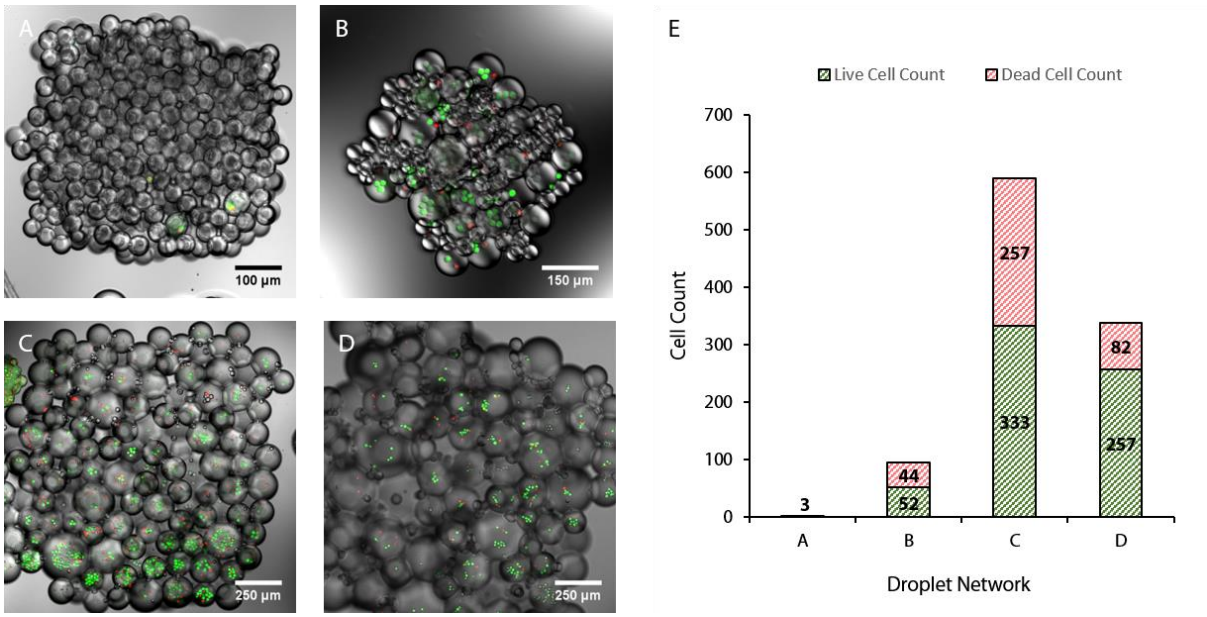

Figure 3.6 Preliminary cell patterned scaffolds and their viabilities. **A**-**D** Composite bright-field and fluorescence confocal micrographs of printed cellular networks straight after fabrication: **A**-**C** oMSC laden scaffold and **D** HEK-293T laden scaffold. Cells were printed using bioinks with cell densities of: **A** 0.1×10^6; **B** 1×10^6; **C** 2×10^6 and; **D** 2×10^6 cells/mL. **E** Stacked bar-chart of counted live and dead cells within networks of **A**-**D**. The total number of printed cells was in the order of hundreds for **C** and **D**.

3.6.7 Network Instabilities

The cell patterned droplet networks were studied over 48 h, in attempt to see if the cells would proliferate. It was quickly noticed that cell-laden structures were unstable and would either dehydrate, collapse or fully coalesce (**Figure 3.7**).

Two of the networks were visualised by time-lapse confocal microscopy, these either fully dehydrated into a salt crystal after showing multiple coalescence events (**Figure 3.7 B**), or fully coalesced into a single droplet as the network slowly dehydrated (**Figure 3.7 D**). The consequence of both was destabilisation of the bilayers and osmotic shock induced cell death.

The remaining two oMSC networks were left in humidified environments within custom made hydration chambers and imaged after 24 or 48 h. For the high cell density

network, containing 590 oMSCs, it was observed that the network collapsed into individual droplets with low droplet-droplet adhesion (**Figure 3.7 C**). All the cells were dead with a significant number of the cells located at the edge of the droplets, indicating they may have contributed to the decreased droplet cohesion. More interestingly, the low cell density network containing three dead cells retained its structure and showed no coalescence events (**Figure 3.7 A**). The difference in structure retention of networks with low or high cell densities, strongly suggests that cells were responsible for destabilising the network.

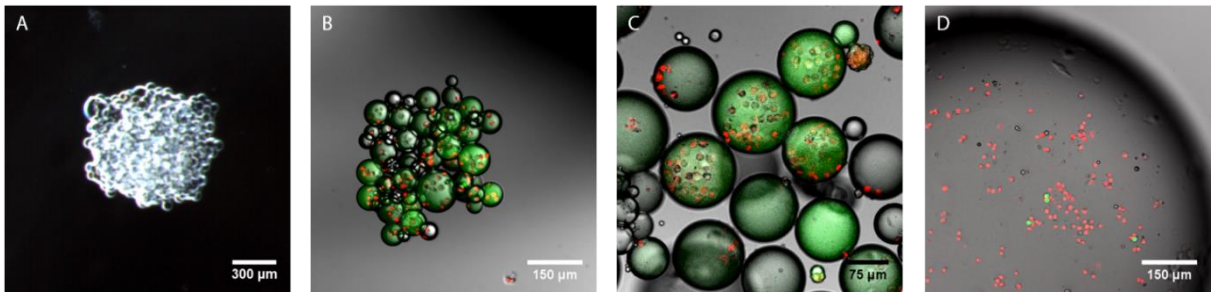

Figure 3.7 Stability of cell patterned droplet networks over time. **A**-**D** Micrographs of cell-laden droplet networks of *Figure 3.6 A-D* respectively within 48 h after print. **A** Dark-field micrograph of stable network at 48 h. **B**-**D** Composite bright-field and fluorescence confocal micrograph of: **B** dehydrated and high coalescence network at 6 h; **C** collapsed and coalesced network at 22 h and; **D** fully coalesced network at 3 h.

3.7 Optimisation of Cell Patterning

The preliminary experiments confirmed that cell-laden droplet networks could be used to create networks, however these were inaccurate version of their digital print maps. There were other additional drawbacks with the method at that point. The issue with the cell-laden networks were, lower than desired initial viabilities, low cell content, inhomogeneous cell distributions and poor structure retention. This section describes how these issues were resolved, by optimising the cell patterning procedure, resulting in the reproducible fabrication of high cell density droplet networks.

3.7.1 Obtaining Desired Print Criteria

Ideally droplet networks should be printed with, high resolution patterned cell features, high cell density and high cell viability, and retain the cell pattern overtime. When the cell-laden bioinks were preliminary printed certain printing issues were observed: nozzle cell clogging, non-uniform generated droplets, intra-network coalescence and low cell content of nozzle cell. The resulting scaffolds were moderately packed, with hundreds of heterogeneously distributed cells of 54-76% viability, and overtime would collapse. Hence, there were a lot of improvements to be made to the printing process if ideal scaffolds were to be fabricated. Strategies to improve the printing process are described below including **Table 3.1** which details idealised bioprinting criteria.

Table 3.1 List of desired bioprinting criteria. Alongside the criteria are feasible values that could be achieved with an optimised printing process, as wells as the best values in literature for a comparative valve-based droplet dispenser[41,60,62]. Problems which prevent the desired criteria from being reached are also listed, and adjacent are potential solutions to resolve these issues.

Desired Print Criteria	Printer's Potential	Valve-Based Printer	Current Problem	Potential Solution
high cell density	10×10^6 cells/mL	5×10^6 cells/mL[41]	low cell content during automated printing	increase bioink cell content
high droplet resolution	ø 50 μm	~ ø 160 μm / 2 nL[60]	ejected cell-laden droplets are large (ø ≥100 μm)	stick to low viscosity solutions
high feature resolution	two droplet width	~1 mm[41]	no patterned features possible within sheet structures	expand to alternative structures and printing ≥2 cell types
homogeneous cell distribution	uniform droplets with consistent cell content	uniform[41,62]	droplets ejected inconsistently with varied cell content	density match cells to bioink
high initial cell viability	90-95% viability	~95%[41]	printing process is slightly detrimental to cells	use low voltage pulses where possible
retention of pattern	N/A	N/A	intra-network coalescence and network collapse	incorporation of stabilising agents into bioink
retention of viability	N/A	N/A	network dehydration and no nutrient exchange	phase transfer structure to culture medium

3.7.1.1 Printing Process Modifications

In the preliminary experiments it was observed that cell viabilities were low post print, probably as a result of their handling and possible stress during droplet ejection. It was assumed that cells were in an unideal environment prior to printing when they were stored in a sealed microcentrifuge tube within a cell incubator. The environment caused cellular stress which subsequently decreased their viability. This stress arose from the cells not undergoing the ideal gas exchange whilst in the incubator and due to the fact they clumped at the base of the microcentrifuge tube. When the cells clumped into a

cellular mass, the structure became wider than the diffusion limit for nutrients and gas. Consequently the core cells of the mass were in a low nutrient and oxygen environment resulting in stress. To improve viability the time between bioink production and bioink printing was minimised, reducing the time the cells were stored in the sealed microcentrifuge tube. Specifically, a the cell processing time was significantly reduced by using an automated cell counter [Countess II FL, *Thermo Scientific*, USA] instead of performing cell counting manually, however, the counter only gave a rough estimate of cell density. The bioink processing procedure may be further improved in the future by incorporating flow cytometry, specifically fluorescence-activated cell sorting (FACS), to purify live cell samples[136].

It was observed that the cells were perturbed with each piezo pulse, and overtime this may have stressed the cells such that they became necrotic. Ergo, larger voltage pulses which are more powerful and dispense larger droplet volumes, would stress the cells more and potentially lower viability. Accordingly droplet generation was performed with the lowest voltage pulses possible.

3.7.1.2 Network Stabilisation

The preliminary scaffolds would lose their designed structures due to intra-network coalescence, hence patterned structures with high resolution features would not be attainable. Removal of these coalescence events would allow a more homogeneous distribution of cells throughout the network. As it appeared that the cells contributed to intra-network coalescences, a stabilising agent needed to be incorporated into the bioink. This stabilising agent should either act as a steric barrier between the cells and the lipid bilayer or strengthen the bilayers between the networks. *Section 3.7.2-3.7.4* describe how Fmoc-dipeptides were used to stabilise these structures.

3.7.1.3 Cell Density Matched Bioink

Cells were shown to be distributed heterogeneously across preliminary networks and were not present in every droplet. This was due to the effective cell density within the

nozzle changing overtime as the cells sank. The incorporation of a thickening agent into the bioink, which would density match the solution to the suspended cells, would allow the cells to be distributed homogeneously within the nozzle, producing ejected droplets with more regular cell numbers. The thickening agent would also allow a higher density of cells to be loaded into the bioink without clogging issues, allowing networks of high cell density to be attainable. *Section 3.7.2* and *3.7.4* explain how polyethylene glycol (PEG) was used to pattern cells homogeneously.

3.7.1.4 Transfer to Culture medium

A more long term problem was keeping the cells viable over an extended study. The scaffolds current form of cell patterned droplet networks in oil, would have limited nutrient resources and as cell waste metabolic products such as lactic acid accumulate, the environment becomes less cytocompatible[132]. Additionally, despite many efforts, an effective hydration chamber which worked at 37 ºC was hard to devise, meaning networks could not be kept at long durations in a cell incubator. Hence, a method of exchanging fresh nutrients and removing waste metabolic products with the cell was necessary.

Phase transfer of the scaffold from the print oil to culture medium was a desired process. It was thought the network could be phase transferred as either, a multi-compartment vesicle, with protein pores incorporated to allow nutrient exchange between the compartments, or as a solid scaffold with disrupted lipid bilayers that allows nutrient penetration. *Section 3.8* describes how we developed an agarose based bioink, which could convert droplet networks into solid phase transferrable scaffolds.

3.7.2 Designing a Bioink

To obtain ideal scaffolds with the desired print criteria outlined in *section 3.7.1* a bioink needs to satisfy a list of essential attributes (**Table 3.2**). The desired attributes of the bioink are that: it can form stable and strong DIBs, it is density matched to the cells and it can be triggered to gelate. Therefore new components, which could act as stabilising

agents, thickening agents or hydrogelators, were supplemented into the culture medium based solutions of *section 3.6.* (**SS1m** and **SS1h**) to give new scaffold solutions.

For these new components to be functional the resulting bioink needed to, remain cytocompatible, be printable, form well packed droplet networks and for the hydrogel, have a useful trigger for gelation. Additional considerations were that that the components were, non-reactive with other bioink components, easy to process and cost effective. With these considerations in mind Fmoc-dipeptides and PEG were selected and tested as stabilising and thickening agents respectively. Latterly agarose was also incorporated into the bioink acting as the base hydrogel, the reasons for its selection are described in *section 3.8.2.*

Table 3.2 List of desired bioink attribute and the components used to attain such features.

Desired Bioink Attribute	**Bioink Component(s) Used to Attain Attribute**
supply of nutrients	culture medium
cytocompatible	culture medium, **Fmoc-XX**, PEG, agarose
forms stable DIBs	**Fmoc-XX**
forms strongly adhesive DIBs	**Fmoc-XX**
density matched to cell	PEG, agarose
triggered gelation	agarose
fluorescent cells	cells, CAM & PI

3.7.2.1 Fmoc-dipeptides as Stabilising Agents

Fluorenyl-9-methoxycarbonyl (Fmoc) protected dipeptides have been shown to behave as low molecular weight hydrogelators, which in water can self-assemble into long fibrous structures[137]. The fibres form through the π-π stacking of the Fmoc groups and interactions between the amino acids including hydrogen bonding and electrostatic interactions namely salt bridges. These fibres can entangle to form 3D matrices which immobilise water[137]. Gelation can be triggered rapidly through acidification or temperature change, and then reversed to give the individual low weight molecules[137].

As Fmoc-dipeptide form soft fibrous hydrogels, it was hypothesised that their incorporation into cell-laden droplet networks could prevent lipid disruption by serum proteins or cells. Furthermore, the fibres would also increase the stiffness of the structure, providing further mechanical stability. Fmoc-dipeptides were also an attractive choice as many Fmoc-dipeptides have been used in the culture of 2D and 3D cell colonies[137–142].

Fmoc-phenylalanine-phenylalanine (Fmoc-FF) (**Figure 3.8 A**) is the most commonly used Fmoc-dipeptide for cell culture applications due to its physical properties. Unlike most of its dipeptide counter parts Fmoc-FF can gel at physiological pH[137]. This is attained due to Fmoc-FF having the highest recorded c-terminus pK_a (9.9). It has been used as an independent hydrogelator to successfully culture primary bovine chondrocytes in both 2D and 3D[138].

Fmoc-FF has also been mixed with Fmoc protected amino acids and dipeptides to form stiffer hydrogels with the additional chemical functionalities[138,139,142]. When co-gelled with Fmoc-serine it was employed to successfully culture, in 2D or 3D, bovine chondrocytes, human dermal fibroblasts and mouse embryo fibroblast cells[139]. The biological adhesion ligand, arginine-glycine-aspartate (RGD), which appears in fibrinogen and binds to cell integrins have also been successfully integrated into Fmoc-FF gels[142]. A co-gel of Fmoc-FF and Fmoc-RGD was used to 3D culture human dermal fibroblasts which polarised and spread along the fibres, and as the cells proliferated caused the gel to contract[142].

Hence Fmoc-FF was selected due to its ability to gel at physiological pH and for its cytocompatibility. However, Fmoc-FF based cell culture has usually been aided by an accompanying Fmoc-dipeptide. Similarly, we incorporated Fmoc-isoleucine-glycine (Fmoc-IG, **Figure 3.8 B**) with Fmoc-FF. It was thought that Fmoc-IG an analogue of Fmoc-leucine-glycine which has a lower c-terminus pK_a than Fmoc-FF, and a stiffness of ~200 kPa (at 14.62 mM, pH ~4)[143], would aid Fmoc-FF's gelation at physiological pH.

Before network printing of the Fmoc-dipeptides, the bulk solution was tested. As solution had to be printable, the Fmoc-dipeptides were prepared as low viscosity solutions, typically 10 mM stock solutions i.e. ~0.5% w/v. The dipeptides would be used as a mixed solution to obtain both of the desired properties. However, at the time their ability to co-gel and to gel under oil needed was uncertain and needed to be proved.

To test the gelation dipeptide solutions were prepared as 1:1 v:v mixtures of 10 mM Fmoc-FF with 10 mM Fmoc-IG, named 10 mM **Fmoc-XX**. Here the **Fmoc-XX** molarity is the total molarity of the two Fmoc-dipeptides in solution. Using this solution Dr Sam Olof independently investigated the fibre formation of the bulk phase using transmission electron microscopy (TEM), with gelation induced by dropwise addition of hydrochloric acid. Here, a mixture of thinner peptide protofibrils (ø 30-40 nm) and mature fibrils (ø 100 nm) were observed in the transmission electron micrograph of gelled **Fmoc-XX**. This verified that the dipeptides could be gelled in combination.

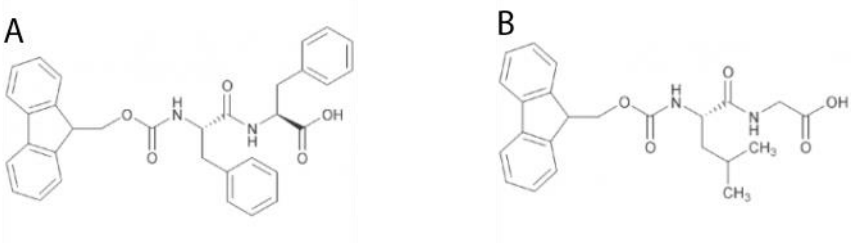

Figure 3.8 Structures of Fmoc-dipeptides. Molecular structure of **A** Fmoc-phenylalanine-phenylalanine and **B** Fmoc-isoleucine-glycine.

3.7.2.2 PEG as a Thickening Agent

The density of cells has been determined by density gradient centrifugation methods, in which cells and sub-cellular components can be centrifuge separated by sedimenting into bands within a solution containing a density gradient[144]. Mammalian cells have buoyant densities between 1.00-1.10 g/mL with skin fibroblasts being 1.03-1.05 g/mL[144], which we used as an approximate value for the density of our cells. Hence we wanted to add a supplement to our bioink which would raise the density from ~1.00 g/mL to this range, keeping the cells suspended within the nozzle.

Percoll® (a solution of colloidal silica particles) and sucrose have been used as the density gradient solutions and were candidates for testing, although sucrose would have to be used at high osmolarity for it to be effective. A more promising option was PEG which is water soluble, non-cytotoxic, and derivatised cross-linked polymers of which have been used in 3D cell cultures[31]. Generally the 3D culture used hydrogels composed of cross-linked PEG molecules conjugated to natural polymers or biological macromolecules[31]. These conjugates include hyaluronic acid[145], heparin[146,147], alginate[148] and lactone[149].

It was initially thought that unmodified low molecular weight PEG could be used at the appropriate buoyant density to optimise cell patterning. Later PEG could be substituted for a UV cross-linkable version, which could be gelled post print. However, it was realised, for some of the low molecular weight PEG solutions to be of the appropriate density they would have to be at cell hypertonic concentrations, and this consequently would lower cell viability post print. Hence, PEG was only to be used temporarily for printing density matched cells, and as it transpired we eventually moved away from PEG to an agarose based hydrogel method (*section 3.8*).

3.7.2.3 Bioink Compositions

For the cell patterning optimisation experiments (*section 3.7.3-3.7.6*), bioinks were prepared as scaffold solutions with suspended cells and containing the relevant supplements of either Fmoc-dipeptides, PEG, live/dead stain or a combination of these

supplements (see *section 6.5.1*). Here, the base culture medium was Opti-MEM® with 0.5% v/v FBS for HEK-293T scaffold solutions (**SSXh**), while oMSC scaffold solutions (**SSXm**) used **DMEM-ITS**. In brief the scaffold solutions used were as follows:

Scaffold Solution 2m and 2h (**SS2m** and **SS2h**) comprised of culture medium supplemented with Fmoc-dipeptides (1.0-1.2 mM **Fmoc-XX**) and live dead stain. It was used to test for enhanced network stability *(section 3.7.4.1*).

Scaffold Solution 3 (**SS3**) contained phosphate buffer saline (PBS) supplemented with PEG (0-20% w/v PEG 400) and bead solution. The bead solution composed of fluorescent polystyrene beads (ø 10 μm, *Life Technologies*) suspended in ultra-pure water. **SS3** was used to test bead ejection at different densities *(section 3.7.4.2*).

Scaffold Solution 4m and 4h (**SS4m and SS4h**) comprised of culture medium supplemented with PEG (0-20% w/v PEG 400), Fmoc-dipeptides (1.0-1.2 mM **Fmoc-XX**), and live/dead stain. This solution was optimised to print stable structures with homogenous cell distributions *(section 3.7.4.3*).

3.7.2.4 Printer Conditions

For printing new bioink composition, the same print procedure as outlined in (*section 3.6.2*) was used, except networks here were 11×14 horizontal droplets printed for 2-4 layers. **Standard print oil** at 1.2-2.4 mM DPhPC was used for all prints of *section 3.7*, except for the Fmoc-IG bead network (**Figure 3.9 A**). Here, a fluorescent print oil was then being trialled and was a 1:1 v:v mix of hexadecane and silicone oil containing 2.5 mM lipid mix. The lipid mix 8:2 mol:mol mix of DPhPC with cholesterol containing 0.1 mol% sulforhodamine-B bound DPPE. Cholesterol was added as it aided the incorporation of the fluorophore bound lipid, whilst allowing stable bilayer formation.

3.7.3 Stabilising Cell-Laden Networks

Fmoc-dipeptides were successfully incorporated into non-cell containing bioinks and allowed the production of well packed networks which did not coalesce as described below.

3.7.3.1 Fmoc-Dipeptides Networks with Cargo

The printability of Fmoc-dipeptide with a suspended cargo was initially tested. Here, fluorescent polystyrene beads (ø 5 µm, *Sigma-Aldrich*) were used as cell-sized particles. The preliminary Fmoc-dipeptide print (n = 1) was of a 12 mM Fmoc-IG in ultra-pure water solution containing 14×10^6 beads/mL (**Figure 3.9 A**). During print it was noticed that the beads were ejected homogenously and bilayers were formed with strong adhesion. For similar low osmolarity solutions, bilayer formation would be very weak with droplets keeping spherical morphologies. Whereas here the Fmoc-IG is interacting with the lipid such that the strength of the droplet cohesion has comparatively increased, giving large flat bilayers (**Figure 3.9 B**). As there were no observed coalescence events during the print, this was an encouraging result, showing the Fmoc-IG was compatible with printing and increased the relative network cohesion.

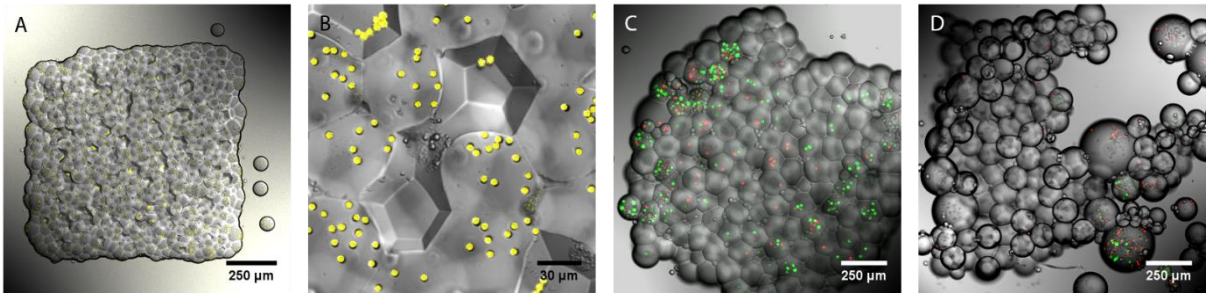

Figure 3.9 Initial Fmoc-IG networks with suspended cargo. **A-D** Composite bright-field and fluorescence confocal micrographs of printed networks comprised of Fmoc-IG additive and cargo. **A** A network (11×14×3 droplets) printed as a 12 mM Fmoc-IG in ultra-pure water solution containing ø 5 µm fluorescent polystyrene beads at a concentration of 14×10^6 beads/mL. **B** Zoomed-in section of network in **A**. **C** A printed network (11×14×2 droplets) containing a scaffold solution 2×10^6 oMSC/mL with 6.5 mM Fmoc-IG, 5 µm CAM and 5 µm PI containing 45% v/v **DMEM-ITS**, 10% v/v PBS, 45% v/v ultrapure water. **D** Coalescence of network in **C** after 24 h.

An oMSC laden print solution containing 6.5 mM Fmoc-IG was promptly tested (**Figure 3.9 C**) after this result. The network (n = 1) was successfully printed with only a few observed coalescence events and showed strong droplet cohesion. Cells were distributed heterogeneously and with a viability of 71% (**Figure 3.9 C**). However, there were still print issues of inconsistently ejected droplets of large volumes with low total cell content. Additionally, the stability of the network also was short lived as within 24 h the structure

had started to coalesce (**Figure 3.9 D**), but positively the network had not collapsed into individual droplets. oMSCs were also printed in a similar solution but containing Fmoc-FF instead of Fmoc-IG ($n = 1$), and showed similar print characteristics, but coalesced into a single droplet within 24 h. Hence, Fmoc-IG seemed to be the better stabiliser of the two.

3.7.3.2 **Fmoc-XX** Stabilised Culture medium Networks

Before attempting cellular networks again, the incorporation of Fmoc-IG and Fmoc-FF was optimised. It was thought that the preliminary Fmoc-IG and Fmoc-FF networks were printed with scaffold solutions composed at lower than calculated Fmoc-dipeptide concentration. This was because the Fmoc-dipeptide stock solutions were filtered through an ø 0.22 μm polyethersulfone membrane, which was thought to have partially retain the dipeptide amphiphile. As the coalescences observed in the previous networks may have been avoided if the concentration of these components was higher, culture medium was supplemented with unfiltered Fmoc-dipeptides in attempt to find a defined working Fmoc-dipeptide range.

Scaffold stability over 7 days was studied with printed scaffolds composed of 70% v/v Opti-MEM® containing between 0-3 mM **Fmoc-XX** tested at 0.6 mM increments ($n = 1$-2 scaffolds per composition, **Figure 3.10**). It was observed that during the print, the non **Fmoc-XX** solution was only moderately leaky and droplets could be ejected with a delay of up to 20 s between each droplet without causing the solution to leak into the oil. This delay decreased to ~5 s and ~1 s for 1.8 mM and 3 mM **Fmoc-XX** respectively as the solution became leakier. Demonstrating the presence of **Fmoc-XX** decreased the surface tension between the oil and print solution, increasing the nozzle's leaking rate. Even with the increased leaking, uniform singlet droplets (ø 50-60 μm) were printed as 11×14 horizontal droplets for 7 layers (**Figure 3.10 A-D**), and no coalescence events were observed for most prints, with only a few coalescence events observed for the 0.6 mM and 2.4 mM **Fmoc-XX** prints.

The networks printed were stored in hydration chambers at room temperature and imaged after 6 or 7 days depending on the sample (**Figure 3.10 E-H**). Each network was observed to have retained their shape and size, without coalescence, demonstrating **Fmoc-XX** could be present without destabilising the network.

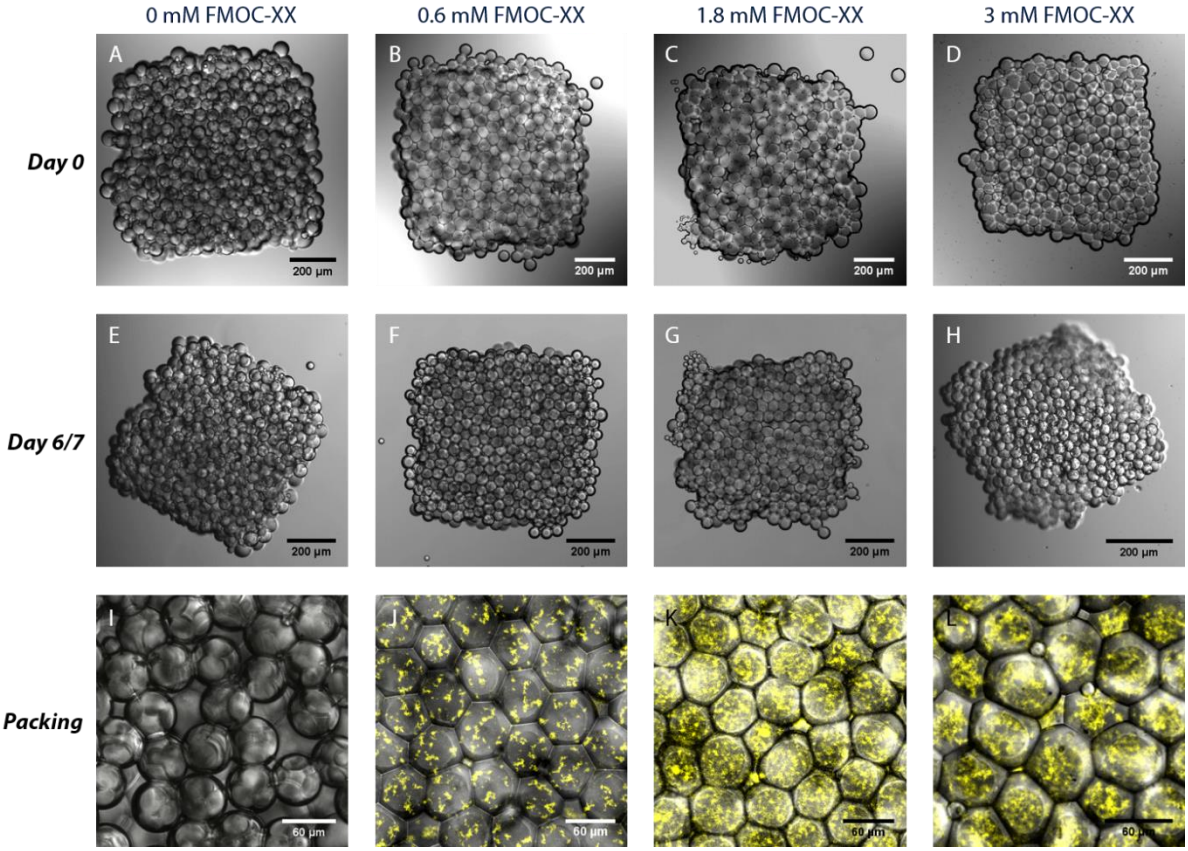

Figure 3.10 Fmoc-XX stabilised networks. **A-L** Confocal micrographs of printed networks (11×14×7 droplets) comprised of 69.6% v/v Opti-MEM®, 0.4% v/v FBS and 30% v/v 0-10 mM **Fmoc-XX** in ultra-pure water. **A-D** Bright-field micrographs taken immediately after print of networks containing a final **Fmoc-XX** concentration of **A** 0 mM; **B** 0.6 mM; **C** 1.8 mM and; **D** 3 mM. **E-H** Bright-field micrographs of networks displayed in **A-D** respectively after: **E** 6 days; **F** 7 days; **G** 7 days and; **H** 6 days. **I-L** Magnified composite bright-field and fluorescence micrographs of POPO-3 iodide stained **Fmoc-XX** fibres within networks displayed in **A-D** respectively. As shown in the figure, **Fmoc-XX** containing networks were stable for a week and had peptide fibres forming within each droplet of the structure.

To observe the fibre formation of **Fmoc-XX** within the networks, the print solutions also contained POPO-3 iodide. For the culture medium only print, no POPO-3 iodide signal was observed (**Figure 3.10 I**). As the molarity of the **Fmoc-XX** solution increased, so did the intensity of the POPO-3 iodide signal (**Figure 3.10 J-L**), indicative of increased fibre formation. As a consequence of this increased fibre formation the networks displayed

increased droplet cohesion and different packing morphologies. It can be seen that the 2D packing went from mainly connected distorted circles with large oil gaps (**Figure 3.10 I**) to hexagonal with few oil gaps (**Figure 3.10 J**). Raising the **Fmoc-XX** concentration further (of ≥1.8 mM), resulted in networks composed of highly connected droplets roughly hexagonally packed as rounded polygons, but displayed an increase in the number of oil gaps (**Figure 3.10 K-L**). The Fmoc-dipeptide mix had interacted with the lipid bilayer such that the average bilayer area increased, signifying that **Fmoc-XX** increased droplet-droplet adhesion. Networks such as **Figure 3.10 J** were better packed containing more droplet connections and consequently should be more mechanically stable, reaffirming that Fmoc-dipeptides are a good stabilising agent at low concentrations.

3.7.4 Reproducible Cell Patterning

It was decided that 1.0-1.2 mM **Fmoc-XX** would be a good supplementation concentration for a cell-laden bioink as it enhanced network packing and displayed practical printing characteristics. This was used to reproducibly pattern HEK-293T in **SS2h** and oMSC in PEG supplemented **SS4m**. The patterning of such networks is herein described, whilst, their cell viabilities and cell densities (*section 3.7.5)* and the scaffold's stability (*section 3.7.6)* are described in later sections.

3.7.4.1 Reproducible HEK-293T Networks (**SS2h**)

HEK-293T were reproducibly patterned as **SS2h** based networks (n = 3) which were initially stable i.e. showed no coalescence events during printing (**Figure 3.11**). Unlike the cell-laden **SS1h** and **SS1m** based networks, they contained high cell numbers and the cells were more homogenously distributed. During the print droplets were formed at a very high resolution, with droplets averaging ø 45-70 μm, they also contained cells at high cell densities, both of which were improvements over the **SS1h/SS1m** bioink prints. Almost all droplets contained cells and packed into strongly cohered networks without coalescing giving well defined square sheets (**Figure 3.11**). This signified that **Fmoc-XX**

supplemented cellular networks were stabilised towards cells throughout the print and imaging.

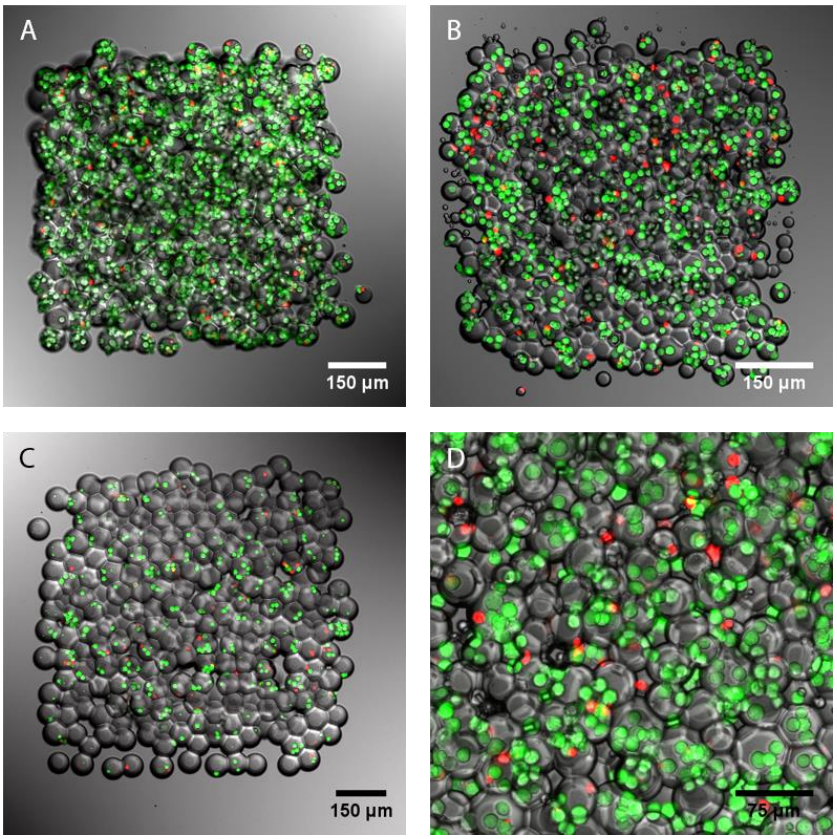

Figure 3.11 Reproducibly patterned HEK-293T cells using **SS2**. **A-C** Composite bright-field and fluorescence micrographs of independently printed HEK-293T networks (11×14×2 droplets, $n = 3$) imaged immediately after print. The bioinks printed were: **A-B** 2×10^6 HEK-293T cells/mL in **SS2h** and **C** 2×10^6 HEK-293T cells/mL in **SS2h** containing 22.5 mM HEPES buffer (64% v/v Opti-MEM® to 36% v/v ultra-pure water). **D** Magnified section of the network in **B**. The networks can be seen with high cell densities, high viabilities and homogeneous cell distributions.

To obtain these well-defined networks a specialised print procedure was developed. In each cell-laden **SS2h** bioink's case, cells needed to settle to the oil-aqueous interface of the nozzle for droplet encapsulation. Not only would each piezo pulse generate a droplet, it would also actuate the remaining cells upwards within the nozzle, consequently for cell-laden droplet ejection, the cells had to be left to sink back to the oil-aqueous interface. This meant long delays between droplet ejections (4-5 s) were used to print cell laden networks. However, within ~10 min of printing there was an accumulation of cells in the nozzle's tip, which appeared fully opaque with cells. This was due to cells settling into

clumps which were less affected by the piezo's pulse and would sink faster compared to individual cells. In this state droplet ejection was only possible when the voltage pulse was raised, typically by 5-10 V over the course of the print. With frequent manual amplifications of the pulse, singlet droplets were ejected sized 45±6 μm or 60±5 μm (diameter ± standard deviation) with occasional satellites (**Figure 3.11 A-B**). In the case of network **C** of **Figure 3.11**, cell density within the nozzle was low by the time of print, hence cells did not accumulate to the same extent and droplets were ejected with a constant voltage pulse, giving a slightly inhomogeneous distribution of cells.

As this was a significant improvement over the previous cell dispensing it proved that droplet networks could be patterned at a high droplet volume resolution with a cellular cargo. Hence, so long as the cells could be cultured within the network, the ability to develop functional microtissues within droplet-based scaffolds seemed feasible.

3.7.4.2 PEG as a Thickening Agent

As described in *section 3.7.2.2* PEG was selected as a temporary thickening agent to see if bioink cell distribution could be improved, and bioink cell density could be increased by density matching the bioink to the cells. As the PEG solutions would be more viscous than the previous bioinks, the printability of different weight PEGs was tested. It was found that PEG 400 could be printed between 0-40% w/v in PBS or ultra-pure water. Similarly, PEG 4,000 and PEG 20,000 could be printed at 0-20% w/v and 0-10% w/v respectively. It was noticed, as the viscosity of the print solution increased so did the energy needed to form droplets i.e. the amplitude of the voltage pulse. Above these PEG weight ranges, droplets could not be generated. It was also noticed that PEG dissolved in PBS would form networks of moderate cohesion whilst, if ultra-pure water was used as the solvent the network would shear into individual droplets due to low droplet cohesion.

With this in mind, PEG 400 was selected for further tests as it was practical to print and a 20% w/v solution in water has a viscosity of 65 mPa·s and density of 1.03 g/mL[150], which is the buoyant density observed for fibroblasts[144]. PBS containing PEG 400 at 0, 10 and 20% w/v i.e. **SS3** were used to test the ejection cell-sized particles (ø 10 μm

fluoresecent polystyrene beads, *Life Technologies*) (**Figure 3.12**). Unlike cells, these particles would sink through the oil-aqueous interface at the nozzle's tip for the 0% w/v print, and could sink out of the droplets for all weight fraction solutions, meaning the beads were not confined within the network (**Figure 3.12**). Regardless of the resulting scaffold, it was empirically noticed that as the weight fraction of the PEG increased, the rate that the beads sank decreased and fewer beads were ejected per network printed (**Figure 3.12**). Here networks (n = 1 per PEG weight fraction) were printed as an 11×14 horizontal droplet sheet for 1-2 layers and the ejected bead counts were 385, 84 and 47 for 0, 10 and 20% w/v solutions respectively. This verifies the empirical observation that the cell analogues were sinking much slower with increased PEG content.

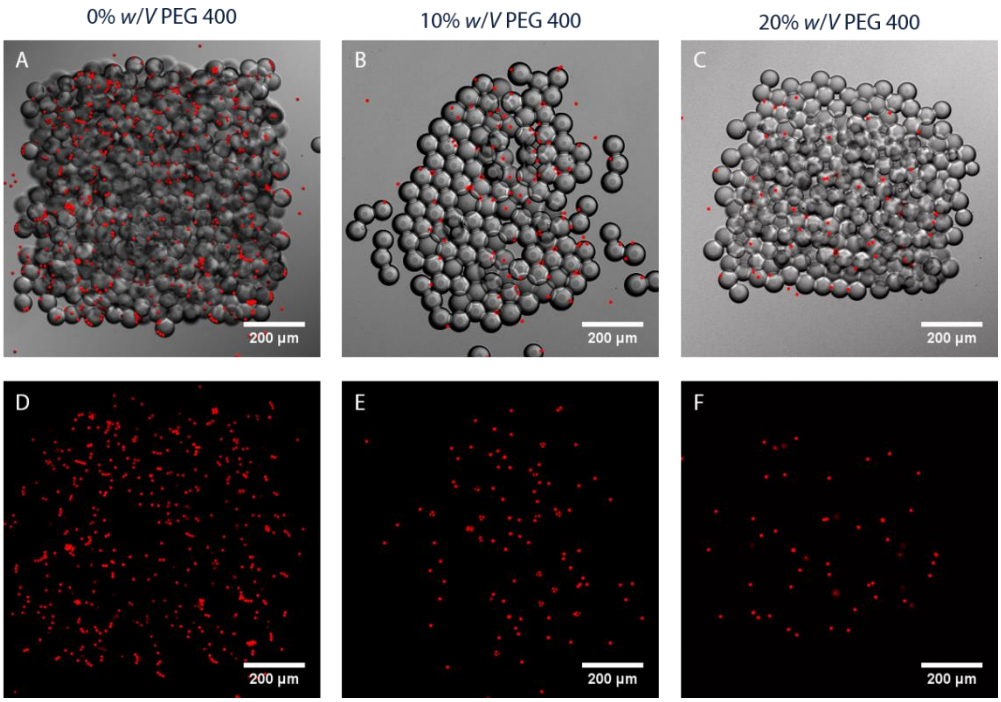

Figure 3.12 Density matching of cell-sized particles with PEG 400. **A-C** composite bright-field and fluorescence confocal micrographs of networks printed as 11×14 droplets for 1 to 2 layers and containing 10 µm polystyrene beads. The ink comprised of 1.8×10^6 beads/mL in different weight fractions of PEG 400: **A** 0% w/v; **B** 10% w/v and; **C** 20% w/v. **D-F** Fluorescence confocal micrographs of networks displayed in **A-C** respectively, showing the distribution of the beads from the print.

3.7.4.3 Reproducible oMSC Networks (**SS4m**)

With PEG demonstrated as an effective bioink thickening additive, PEG-400 was selected as a bioink additive. It was incorporated at 20% w/v since it was observed that cells were almost density matched at this fraction. Prints were tested with HEK-293T without the presence of **Fmoc-XX** and showed poor network cohesion, hence **SS4** was supplemented with both PEG-400 and **Fmoc-XX**, in attempt to both density match the cells and form strongly cohesive networks.

oMSCs were reproducibly patterned as **SS4m** based scaffolds (n = 3) which contained high cell numbers and homogenous cell distributions (**Figure 3.13**). Droplets were ejected at high droplet resolution (ø 80-100 μm), but this was a significant volume increase compared with the **SS2h** bioink prints which gave very high droplet resolution (down to ø 45 μm average). The increased viscosity meant that a larger voltage pulse was needed for droplet production (50-60 V average) and the minimum volume droplet that could be generated was increased to ø ~70 μm, lowering droplet resolution.

Unlike the HEK-293T in **SS2h** print, the cells within the nozzle were unperturbed by the piezo firing. As cells were continually present at the nozzle's oil-aqueous interface, this allowed cell-laden droplets to be ejected with a short delay between each pulse. The cells also sank very slowly in the nozzle compared to previous prints, meaning that the effective cell density within the nozzle's tip remained almost constant. Slow sinking was a result of the cells being almost density matched to the print solution. As a consequence networks could be printed relatively quickly, using constant voltage pulses, with almost every generated droplet containing cells, giving a homogeneous distribution of cells (**Figure 3.13 D**). Importantly these droplets also adhered well together without coalescence to give defined square sheets (**Figure 3.13 A-C**), showing that structures could be accurately patterned.

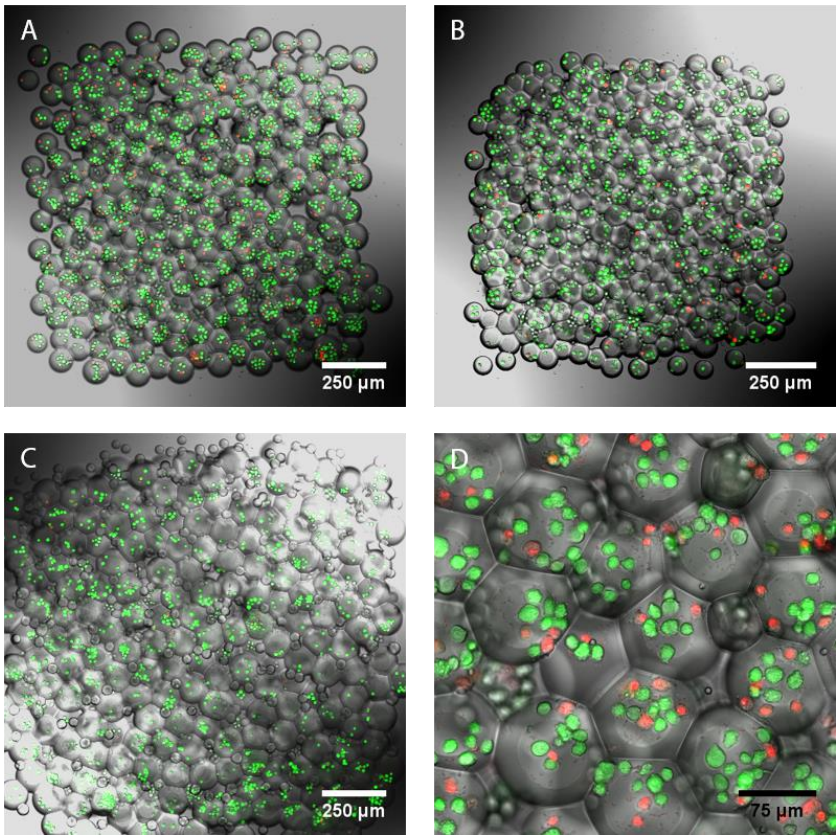

Figure 3.13 Reproducibly printed oMSCs suspended in **SS4m**. **A**-**D** Composite bright-field and fluorescence confocal micrographs of printed oMSC containing networks (11×14×4 droplets, $n = 3$) . **SS4m** solution was printed containing **A** 3×10^6 oMSCs/mL and; **B**-**C** 2×10^6 oMSCs/mL. **D** Magnified micrograph of the network displayed in **A**. oMSCs have been patterned reproducibly with homogeneous cell distribution, moderate cell density and at high droplet resolution.

3.7.5 Viabilities & Scaffold Cell Densities

The cells within the reproducibly printed scaffolds were counted, and showed total cell numbers between 324-1824 (see *section 6.11.6.2* / **Table 6.11**). Counting was performed manually, as before, with the Cell Counter Plug-In[133] for ImageJ[134,135]. This method gives an underestimation to the total number of cells in the high cell density networks, as they are counted in one plane of focus only. However, it gave a representation of the order of magnitude of scaffold cells and was be used to calculate accurate viabilities. Here, it was assumed cells in the lower layer would have the same viability as the upper layer cells, and thus the viability calculated from the cell count of the lower layer would be representative. The total number of cells within most networks were counted at levels of high hundreds to low thousands, with one oMSC laden scaffold composed of **SS4m**

containing 1824 cells. This is a significant improvement over the **SS1h** and **SS1m** bioink networks were the highest cell number was 590, of which greater than 40% of the cells were dead. Hence the **SS2h** and **SS4m** bioinks were employed to effectively print networks with high cell content.

Using the counted cell values the cell viabilities within scaffolds were calculated to be 78-93% (**Figure 3.14**). High average viabilities were determined for HEK-293T in **SS2h** based scaffolds (88±3%, $\bar{x}$±s.d., n = 3) and oMSCs in **SS4m** based scaffolds (87±7%, $\bar{x}$±s.d., n = 3). Demonstrating a viability improvement of 25% compared with the average cell viability of **SS1h** and **SS1m** based scaffolds (62±10%, $\bar{x}$±s.d., n = 3). With the high viabilities observed, cells would have a good chance of proliferating if placed in favourable culture conditions.

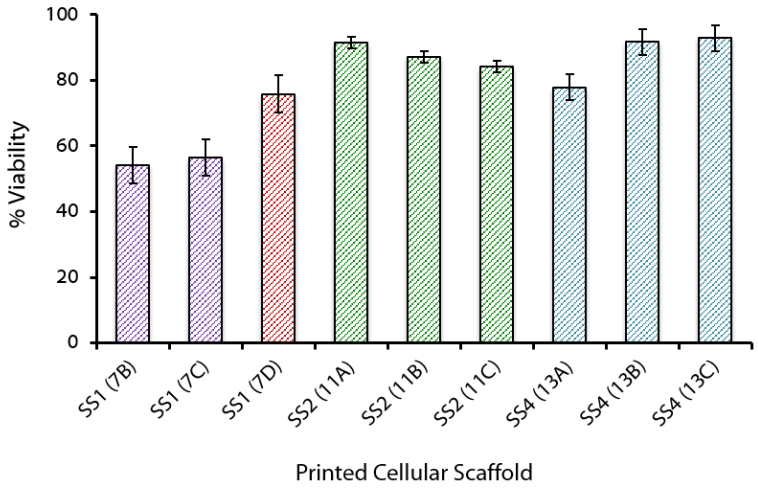

Figure 3.14 Viabilities of printed cell patterned scaffolds. The column chart displays the calculated cell viabilities from cells counted in scaffolds immediately after print. The scaffolds assessed were selected prints from the patterning optimisation: **purple column,** oMSCs in **SS1m** bioink (*Figure 3.6*, n = 2); **red column,** HEK-293T in **SS1h** bioink (*Figure 3.6*, n = 2); **green column,** HEK-293T in **SS2h** bioink (*Figure 3.11*, n = 3) and; **blue column,** oMSCs in **SS4m** bioink (*Figure 3.13*, n = 3). The printed cellular scaffold axis describes the bioink used and in brackets references the figure of the scaffold which the viability was calculated. As can be seen in the graph the average viability had increased from ~60% for **SS1h** and **SS1m** bioink prints to ~90% for **SS2h** and **SS4m** bioink prints. Error bars represent the standard error of the mean for the different bioink solutions: **SS1**, **SS2** and **SS4**.

This increased viability most likely arose due to two main factors. Firstly, the processing of the cell-laden bioink was conducted much faster in latter prints, limiting the time spent

by cells in unfavourable conditions. Secondly, the printing was better controlled and droplet ejection occurred at higher cell densities, meaning printed cells had more cell-cell contacts throughout the process and where likely in more favourable conditions (see *section 4.6.1*). It also transpired that for latter prints, the high voltage pulses (up to 60 V) used to form scaffolds did not reduce cell viability significantly, indicating the piezo pulse even at high amplitudes was not immediately detrimental to the cell. Surprisingly the cell viabilities only dropped a little within the PEG solution, whereas it was expected due to the high osmolarity of the solution, that the cells would be under osmotic stress and become necrotic during the print. Therefore, with the refinement of our technique we were able to reproducible attain high viabilities (**Figure 3.14**) showing the printing process is gentle on the cells.

Along with counting the cells, the number of droplets within the plane of view were recorded (**Table 3.3**). Using these values, the average number of cells per droplet was determined. For the HEK-293T laden scaffold composed of **SS2h** in **Figure 3.11 A**, an average of 4 cells per droplet was calculated (**Table 3.3**). While for the **SS4m** based oMSC laden scaffold in **Figure 3.13 A**, on average 9 cells were encapsulated per droplet ejected, however the droplet diameter is about 40 μm wider. This average cell number per droplet varies across all prints due to the distribution of droplet volumes across the print (**Table 3.3**), and due to the dynamic effective cell density within the nozzle.

Furthermore the effective cell density of the scaffold was determined by calculating the cell density of the average volume droplet containing the average number of cells (**Table 3.3**). This should produce an estimate to the network's total cell density. For two HEK-293T laden scaffold composed of **SS2h** seen in **Figure 3.11 A,B** the effective network's cell density was determined as 4×10^7 cells/mL, showing an apparent 20 fold concentrating of the bioink cell density (2×10^6 cells/mL). The oMSCs in **SS4m** bioink prints (**Figure 3.13 A-C**) also show a condensing of cells, but to a lesser degree, ~5 fold, giving scaffold cell densities of 1×10^7 to 2×10^7 cells/mL. Hence it can be seen that the **SS4m** bioink acted as a thickening agent, but at the concentration used, the scaffold solution did not match the buoyant density of cells.

Table 3.3 Summary of measured droplets within scaffold and effective scaffold cell density. The table list the bioink composition (cell type, solution and cell number density), measured droplet values (average diameter and total number) and calculated values: average no. of cells per droplet and effective cell density within scaffold. The networks which were analysed are displayed in previous figures which are referenced in the scaffold figure column. The droplet diameter column ($\bar{\varnothing}_{droplet}$) display the average measured droplet diameter ± the standard deviation of the population (n = 52). The average number of cells per droplet ($\bar{N}_{droplet\ cells}$) was calculated using the counted totals for the cells and droplets. Using the average of cells per droplet and the average droplet volume the effective cell density within the scaffold was determined.

Bioink	$n_{bioink\ cells}$ cells/mL	Scaffold Figure	$\bar{\varnothing}_{droplet}$ /µm	$N_{droplets}$	$\bar{N}_{droplet\ cells}$	$n_{scaffold\ cells}$ cells/mL	Viability (%)
HEK-293T in **SS2h**	2×10^6	11 A	57±5	228	4	40×10^6	92
HEK-293T in **SS2h**	2×10^6	11 B	45±6	302	2	41×10^6	87
HEK-293T in **SS2h**	2×10^6	11 C	71±4	227	1	5×10^6	84
oMSCs in **SS4m**	3×10^6	13 A	98±7	210	9	18×10^6	78
oMSCs in **SS4m**	2×10^6	13 B	83±6	255	3	10×10^6	92
oMSCs in **SS4m**	2×10^6	13 C	119±6	204	5	6×10^6	93

3.7.6 Cell Patterned Network Stability

The incorporation of the **Fmoc-XX** bioink additive allowed HEK-293T and oMSCs to be patterned as defined square cell-patterned sheets, whereas before they had coalesced during the print. These initially stabilised networks were maintained in hydration chambers which were stored in cell incubators. It was desired that these networks could remain stable so that the cells could be encouraged to proliferate into microtissues.

The cellular networks made from **SS2h** and **SS4m** bioinks were not stable over time, losing the original pattern and within 24 h the majority of the cells were dead (**Figure 3.15**). In all cases the networks would slowly dehydrate and if left long enough would form a smear of cellular debris on the glass (**Figure 3.15 A**). Not only did the networks dehydrate they showed multiple coalescence events and collapsed into distinct smaller droplet networks (**Figure 3.15 B,C**).

The dehydration issue arose from the water diffusing out of the droplets, through the oil and into the air. With a sufficiently humid environment this diffusion out could be

balanced with diffusion of water in i.e. water going from the air through the oil and into the droplet network. Designing a suitable hydration chamber was challenging as the structure needed to maintain a humid environment and prevent water from the air condensing as droplets on the lid, because these could fall into the oil and disrupt the printed network. Such a design was never achieved and consequently storing the networks within cell incubators set at 37 °C always resulted in network disintegration via dehydration.

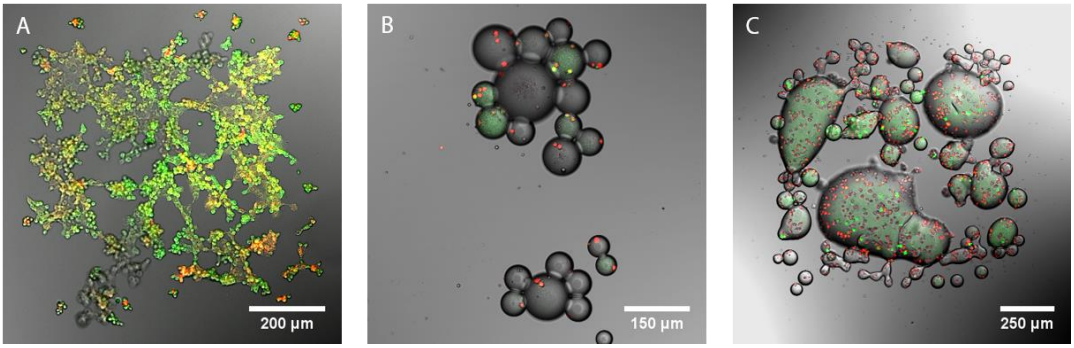

Figure 3.15 Stabilised scaffolds over time. **A**-**C** Composite bright-field and fluorescence confocal micrographs of printed cellular patterned networks left to incubate for days. **A**-**B** Printed HEK-293T in **SS2** bioink: **A** Network *A* of *Figure 3.11* after 4 days. **B** network *C* of *Figure 3.11* after 1 day. **C** Printed oMSC network in **SS4** bioink; network *B* of *Figure 3.13* after 1 day. All networks have either fully dehydrated (**A**) or partially dehydrated (**B**-**C**). Networks also showed multiple coalescence events resulting in cell pattern loss (**B**-**C**).

As dehydration has been previously noticed to shrink networks without loss of pattern, the coalescence events and networks collapse is to all appearances cell induced. When **SS2h** bioink was printed without cells, the networks were stored in hydration chambers (at room temperature) and were stable for a week. Hence the inclusion of cells, as previously inferred must destabilise and weaken the bilayers, causing the coalescences and eventual collapse over 24 h.

It was noticed that pattern cell scaffolds stored below the dew point at 4 °C, could prevent dehydration and delayed network coalescence events. As coalescence was precluded or slowed when the cells were cooled and thus inactive, it was concluded that the cells were the active component of network destabilisation. Cooling the networks for

cell culture however was not a viable option as the cells would essentially have arrested development.

3.7.7 Summary of Scaffold Solution Characteristics

The cell patterning was optimised by printing the scaffold solutions comprised of culture medium only (**SS1**) or culture medium with supplements of Fmoc-dipeptides (**SS2**) or Fmoc-dipeptides with PEG (**SS4**). Most of the desired print criteria (*section 3.7.1*) were achieved and a summary of the resulting printed scaffold properties can be seen in **Table 3.4**.

Table 3.4 Summary of scaffold properties for bioinks **SS1**, **SS2** and **SS4**. Listed are the average values for droplet resolution and effective cell density calculated from the best resolution scaffold. The average cell viability of scaffolds is displayed with standard deviation and was calculated from scaffolds (n = 3) immediately after printing. The other criteria describe scaffold observations: droplet uniformity, cell distribution and pattern retention over time.

Bioink	Droplet Resolution	Droplet Uniformity	Cell Distribution	Network Cell Density	Initial Cell Viability	Pattern Retention
SS1h and **SS1m**	~100 μm	inconsistent	most cells in beginning rows	2×10^6 cells/mL	62±10%	lost during print
SS2h	45±6 μm	slightly inconsistent	homogeneous	4×10^7 cells/mL	88±3%	<1 day
SS4m	83±6 μm	slightly inconsistent	homogeneous	2×10^7 cells/mL	87±7%	<1 day

The resolution of ejected cell-laden droplets was significantly improved using **SS2h** bioink compared with the **SS1** bioinks, with the generation of down to 35 μm diameter cell-laden droplets possible. The droplet ejection was also more uniform, utilising the **SS2h** and **SS4m** bioinks However, due to the dynamic distribution of cellular content within the nozzle, consistently sized droplets may be unattainable. Cells suspended in **SS2h** would settle within nozzle, and in this state high cell density droplets could be

ejected regularly unlike the **SS1** prints where cells could only be generated at low density due to clogging issues. **SS4m** was at a closer density to the cells (but still slightly less dense) and was found to be a much more practical ink with cells ejected homogeneously without the need of increasing the pulse amplitude (for the droplet generator) during the print. Hence using thickening agents like PEG, it should be feasible to raise the bioink cell density to the next order of magnitude. Overall droplets could be ejected at high resolution with high cell content but were generated slightly inconsistently.

The issue of intra-network coalescences during print observed implementing the **SS1** bioinks was resolved using the **SS2h** and **SS4m** bioinks, with the resulting cell patterned scaffolds showing almost no coalescence events. When these **SS2h** and **SS4m** based scaffolds were studied, they were found to have high average cell viabilities (88% and 87% respectively) and showed a viability elevation of 25% on the **SS1m** and **SS1h** bioink prints (from 62%). They also had enhanced cell densities compared with the **SS1** bioinks due cell settling in the nozzle, giving networks with up to 4×10^7 cells/mL for **SS2h** bioink and 2×10^7 cells/mL for the more viscous **SS4m** bioink. Thus optimised patterning can produce scaffolds accurately which contain cells at high viability and high cell density.

Overall, using optimised scaffold solutions and an optimised printing process, cell patterned droplet networks could be printed with desired attributes of uniform cell distribution, high droplet resolution, high initial cell viabilities, and high cell densities. These attributes are all necessary for cells to quickly mature within the droplet network into functional tissues.

3.8 Phase Transfer of Cell Patterned Scaffolds

Cell containing networks could be patterned at high density using culture medium-based bioinks, however, these scaffolds were prone to dehydrating and coalescing over 24 h, consequently their encased cells became disordered and necrotic. In order to retain the pattern of cells and cell viability a scaffold phase transfer method was necessary. By culturing the cell patterned scaffold in bulk culture medium the scaffold should remain hydrated and will have an abundant supply of fresh nutrients, facilitating cell proliferation. Conversely, even if a scaffold remained hydrated in bulk oil it would have finite nutrients and would only be able to keep cells viable for a limited period.

Initial phase transfer experiments focused on the transfer of liquid droplet networks in attempt to produce multi-compartment vesicle versions of printed networks. This was discontinued after it became apparent the structures frequently ruptured and coalesced with the bulk aqueous phase. Accordingly phase transfer of solidified droplet networks composed of an agarose hydrogel was adopted. This proved successful and was optimised to reproducibly phase transfer structures of defined shape. In this section the development steps of our phase transfer method are described, including the initial phase transfer attempts of liquid droplet networks through to the phase transfer of printed cell-laden scaffolds.

3.8.1 Phase Transfer of Droplet Networks

It has been previously demonstrated that lipid bilayer enveloped giant unilamellar vesicles and multi-compartment vesicles can be formed by phase transfer methodologies[151–159]. Specifically lipid monolayer coated droplets were passed through a planar lipid monolayer situated at the interface of an oil above aqueous column. Transfer was mediated either through centrifugal force[151,152,155,156] or gravity[153,154,157–159]. It was thought that the multi-compartment vesicle methodology could be adapted to phase transfer our printed structures into culture medium. For this transferred network to be compatible with cell culture, the network would have to be permeable to nutrients which may be possible through the incorporation of lipid bilayer pores. However, there would still be

limitations as diffusion through pores is slow and the pore's aperture would define the size of nutrient molecules able to translocate and could preclude protein transfer.

To adapt the process, it was key to understand the elements which promote phase transfer. In all phase transfer processes, emulsions of droplets or droplet networks are initially made in an lipid-in-oil solution[157]. When these droplets were placed in the column and the external force was applied, the droplets contact the planar lipid monolayer and form a lipid bilayer. Consequently the network was wrapped by the lipid monolayer, forming an external bilayer and sinking from the oil to the aqueous phase[157]. The multi-compartment version of this approach[158,159] is illustrated in **Figure 3.16**. Phase transfer is only possible within certain constraints, firstly the lower aqueous phase must be osmotically balanced with the droplet solution to avoid osmotic rupture of the vesicles. The choice of lipid to wrap the droplets is also key, as the energy needed to form the bilayer across the droplet will need to be low[157], consequently flexible tailed lipids are commonly used, such as DOPC[153–159] and POPC[151,152]. For successful gravity mediated transfer a.k.a. spontaneous transfer, the droplet needed to be denser than the bulk oil and ideally denser than the bulk culture medium. Accordingly, the oil mixes typically used gave buoyant densities of around 0.8 g/cm^3 allowing the droplet to sink to the interface[153,154,157–159]. In the multi-compartment vesicle approach, networks could be transferred due to their dense 0.5 M sucrose content, which allowed them to sink into the bulk pure water phase.

Due to the constraints mentioned, only two literature examples on the formation multi-compartment vesicles[158,159] were found by the author, both of which were from the Ces lab. However, analogous structures have also been produced by the Weitz lab, comprising of multi-compartment polymersomes formed from double emulsions using a volatile oil methodology[160].

To form multi-compartment vesicles the method involved transferring simple droplet networks, composed of 2-8 droplets, spontaneously through the interface of a two-phase column (**Figure 3.16**). Despite the success, there were limitations to the technique, firstly the phase transfer occurred without rupture only 43% or 80% of the

time (depending on the solution). The networks which did phase transfer were, large (droplet ø ≥500 μm) and composed of sucrose which would not be osmotically compatible with cells. The aqueous species were also short-lived, generally an hour, and could not be used as a long term scaffold.

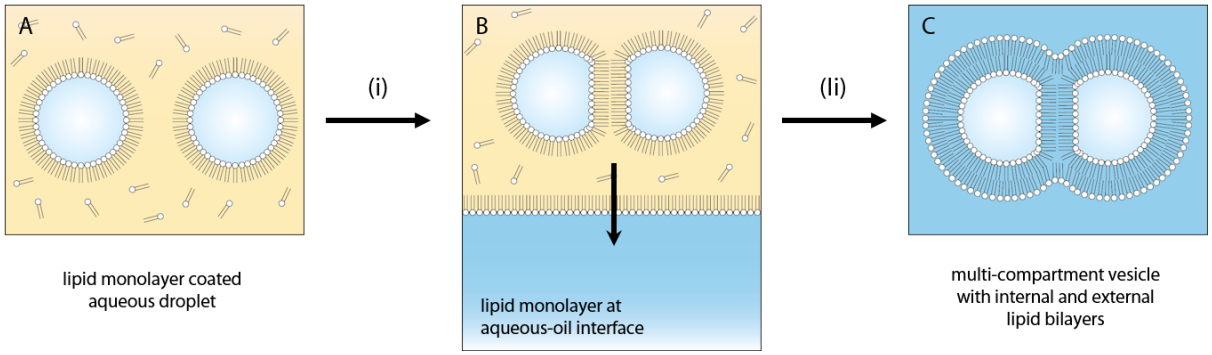

Figure 3.16 Droplet network phase transfer schematic. **A-C** Stages of droplet network phase transfer. **A** droplets in lipid-in-oil solution spontaneously form a monolayer coating. **B** Droplets brought together adhere through droplet interface bilayer to give networks, which can be phase transferred via gravity mediation through a planar lipid monolayer at the interface of bulk oil above bulk aqueous. **C** The droplet network gets wrapped by the interface lipid forming a multi-compartment vesicle with internal and external bilayers. Step (**i**) is the relocation of a droplet network (post formation) into the bulk oil of a two phase column. Step (**ii**) is the gravity mediated phase transfer of the droplet network.

Even with the current drawbacks of multi-compartment vesicle formation and the difficulties of nutrient delivery, it was still of interest to see whether we could phase transfer our droplet systems into aqueous environments. Previous work on multisomes i.e. droplet networks in oil suspended in bulk aqueous solution[100], showed that droplet networks could be stable in aqueous environments for week long periods. Hence it was thought by tweaking the phase transfer method, printed droplet networks could be phase transferred to an aqueous phase by a gravity mediated method and be stored for an extended study.

To recapitulate spontaneous phase transfer, micropipetted droplets were used to screen phase transfer conditions such as lipid choice and the solution composition of the droplet, bulk oil phase and bulk aqueous phase. Droplets would be pipetted into the upper oil phase of a transfer column similar to that depicted in **Figure 3.16 B** and would be left to transfer (**Figure 3.17 A**).

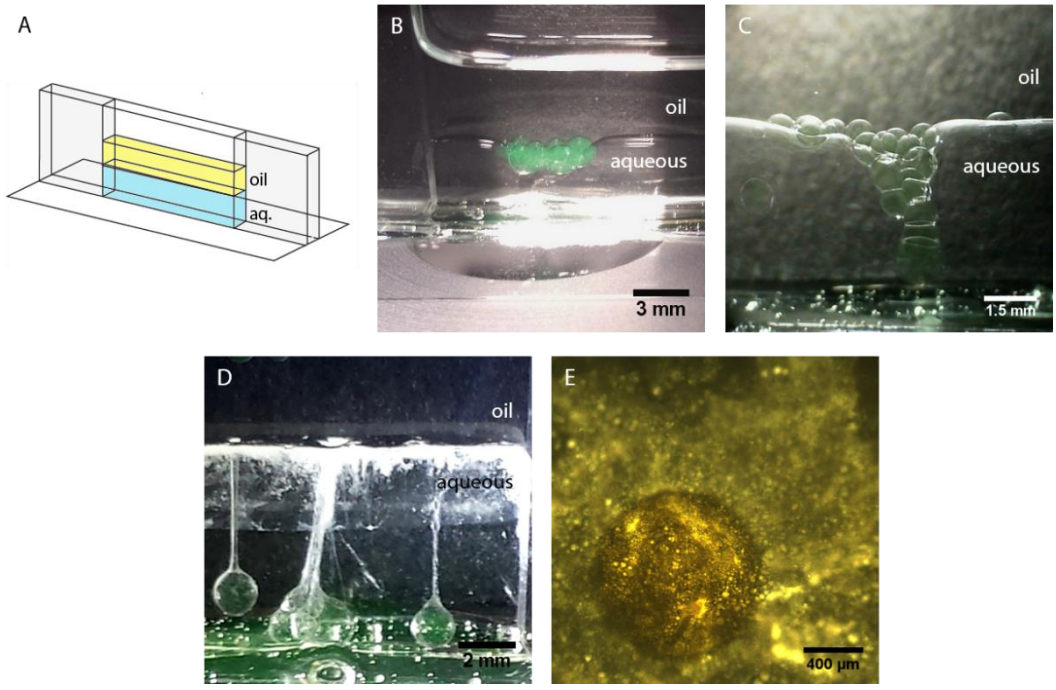

Figure 3.17 Initial attempts at µL droplet phase transfer. **A** Illustration of lab-made two phase column, with oil stacked above aqueous (aq.). Here the container was made of glass allowing phase transfer to be visualised side on or bottom up. **B-E** Images of attempted sucrose droplet phase transfer using a two phase column of 0.5 M glucose solution below: **B-C** 3:1 hexadecane: silicone oil containing lipid and; **D** mineral oil doped with lipid. **B** 6.0 mM DPhPC doped oil did not allow phase transfer, with multiple droplets resting at the interface. **A** 4.8 mM DOPC laced oil allowed phase transfer only when multiple droplets sank together, bending the interface. **D** Mineral containing 4.8 mM DOPC allowed phase transfer of short-lived aqueous droplets, which transferred with an oil tendril linking to the interface. **E** Wide-field transmission micrograph of orange-G stained 1 M KCl droplet resting on interface of 6.0 mM DOPC in mineral oil above 0.5 M glucose. **B-D** were captured with a camera, with **C** recorded down ocular of stereomicroscope.

In summary, multiple conditions (n > 10) were attempted but full phase transfer was only achieved in one instance, where the aqueous structures were short-lived (**Figure 3.17 B-D**). The main findings were that DPhPC was not a suitable lipid for phase transfer, the column's lipid monolayer only coated the lower part of sucrose droplets and the interface would not deform further (**Figure 3.17 B**). Conversely using the same two phase column but with DOPC lipid instead of DPhPC, it was found that sucrose droplets could partially phase transfer if stacked on top of each other. Here the droplets would deform the interface such that a tube of droplets surrounded by bulk aqueous was formed (**Figure 3.17 C**). Phase transfer was successful when using an upper phase of DOPC in mineral oil, here sucrose droplets would quickly sink through the interface, trailing a tube of oil back

to the upper interface (**Figure 3.17 D**). These phase transfer species were short-lived and typically lasted a couple of minutes. When the interface of DOPC in mineral oil above 0.5 M glucose solution was imaged by microscopy, it was observed that the interface was lined with tiny droplets (**Figure 3.17 E**). Hence it can be inferred that the phase transferred droplets, in **Figure 3.17 D**, were not necessarily coated by a lipid bilayer but instead by tiny lipid stabilised droplets.

Due to the continual rupture of aqueous bound droplets under the conditions tested, the phase transfer of droplet networks to give multi-compartment vesicles was discontinued. Instead a new approach of using a solidified droplet network was adopted.

3.8.2 A Hydrogel Based Bioink

For a reproducible phase transfer method that avoided scaffold coalescence with the bulk culture medium, the scaffold needed to be solid and non-soluble. As hydrogels have been widely used as scaffolds in 3D cell culture due to their tuneable stiffness, porous nature and degradability[31], it was decided that one should be blended into the bioink to provide the solid structure. Practically, a candidate bioink would need to be liquid at room temperature to be printable (using an unmodified printer), also its method of gelation needed to be non-detrimental to cells and avoid disrupting the bilayers. As the network is a compartmentalised system in oil, gelation cannot be triggered with reagent addition such as a pH change. Temperature and UV cross-linking mediated gelation seemed the only viable options, so long as the applied stimuli were for short durations. Thus the choice of materials was limited to thermoresponsive and cross-linkable hydrogelators.

Also of consideration was the working hydrogel concentration as this affects scaffold stiffness. The stiffness of the ECM influences cell adhesion, migration and differentiation, consequently the scaffold needs to be within a suitable range to mimic tissue environments[31]. Suitable ranges for different tissue types are: 0.1-1 kPA for neuronal tissues, 8–17 kPa for myogenic tissues, and 25–40 kPa for osteogenic tissues[32]. Additionally the environment ideally would also be degradable or remodelable by the cells, to allow intrinsic proliferation.

With these considerations in mind, an ultra-low gelling temperature agarose (ULGT-agarose) was selected due to its low gelling temperature and its wide-spread use in 3D cell culture of a range of cells[161–166], as elaborated in the section below. Whilst this hydrogel would not be easily degradable, we were primarily concerned with patterning cells as a stable scaffold which would then be transferred to culture medium.

3.8.2.1 Agarose

Agarose was supplemented into the bioink as it had many attractive properties, including cytocompatibility and the ability to form hydrogel-hydrogel bilayers. Additionally, networks composed of agarose should be able to gelate by cooling after printing. Agarose is a linear polysaccharide that acts as a thermoresponsive hydrogel, which can gelate through cooling, forming free standing materials. It is composed of chains of β-1,3 linked D-galactopyranose and α-1,4 linked 3,6-anhydro-αL-galactopyranose residues (**Figure 3.18 A**) and depending on the agarose source, may also contain traces of sulphate groups[167]. Upon cooling the agarose goes from random coils to double helixes, which entangle to form bundled double helices, with flexible chains[31,168]. Agarose hydrogels can be designed to have tuneable stiffness and porosity, by varying the concentration and agarose type. Gelled agarose tend to be isotropic and have an average porosity of 100-300 nm[165]. Whereas, elastic moduli of agarose networks have been recorded between ~1 kPa and few thousand kPa, complementary to the stiffness range of natural tissue[169]. These features have been exploited by using agarose as a 3D matrix to culture a range of cells[161–166,170], demonstrating agarose's suitability as a hydrogel bioink supplement.

Specifically, 3D agarose scaffolds have been seeded with chondrocytes for chondral tissue fabrication[163] and study of chondrogenic differentiation of adult stem cells[161]. Thus agarose scaffolds would be compatible patterned oMSCs. Additionally, ECM based peptides and proteins can be blended into the agarose[162,164–166] to enhance 3D cell culture, without the loss of gelation. These blended hydrogel cultures have been utilised with a variety of cells and show the proportion of agarose correlates to the cell function[165,166].

Collagen was added to agarose to study the migration of human glioma cells from spheroids in 3D[165]. Here, invading cells in low stiffness agarose (0.1 w/v%) were slowed compared to pure collagen, as the cells locomotion was dictated by the ability to squeeze through pre-existing agarose pores[165]. Peptides based on laminin have also been supplemented into agarose to culture a range of cells including human dermal fibroblasts, neurites and human submandibular gland cells[166]. It was found that the stiffer agarose hydrogels (≥0.5 w/v%) promoted cell attachment, and induced, capillary-like network formation for endothelial cells and neurite outgrowth[166]. Whereas the softer agarose hydrogels (0.1 w/v%) induced cells to from multicellular spheroids including acini-like morphologies[166]. Thus agarose supplementation would also allow the incorporation of biological adhesion sites, in the form of ECM proteins, potentially enhancing cellular proliferation.

Agarose has also been demonstrated to be compatible with interface lipid bilayer systems, such as hydrogel-hydrogel interface bilayers between agarose monoliths[114] and bilayer between droplets and planar hydrogels[89,90] (*section 2.5.5*). Therefore a droplet network, where each droplet is composed of agarose should be stable and could potentially be made permeable to small molecule nutrients by the incorporation of large membrane pores.

ULGT-agarose can be triggered to gel between 8-17 °C and was selected as it had the potential to be a practical print solution. At room temperature an ULGT-agarose based bioink would be liquid and printable without problems of gelation. Printed networks could then be induced to gel by cooling to low temperatures.

3.8.2.2 Designing an Agarose-Based Bioink

To make an ULGT-agarose based scaffold solution the agarose would initially have to be mixed with culture medium and it's gelation investigated. The gelation of ULGT-agarose in Opti-MEM® was tested at a range of concentrations (10, 20, 30 and 40 mg/mL), by gelling a small volume in a vial and inverting it (**Figure 3.18 B**). Below 10 mg/mL was not tested as ULGT-agarose has a minimum gelation concentration of 8 mg/mL. It was found that

agarose could gel at all tested concentrations, showing that the culture medium components did not inhibit gelation.

With the agarose concentration range of gelation known, the printability of the sol agarose was tested. Printing of solutions composed of 11 and 20 mg/mL ULGT-agarose dissolved in Opti-MEM® were attempted. The 11 mg/mL solution was printable (**Figure 3.18 C**) but the 20 mg/mL was not. The 20 mg/mL ULGT-agarose solution was found to be too viscous and no pulse settings could form any droplets. From further tests it was seen that ULGT-agarose may be printable up to 15 mg/mL, but printing difficulties such as droplet misfiring occurred as the concentration was increased.

The ULGT-agarose based scaffold solution used to perform the preliminary phase transfer and agarose print testing was **Scaffold Solution 5** (**SS5**) and composed of 10-13 mg/mL agarose in Opti-MEM®. The solution was either used unmodified, containing fluorescent polystyrene beads (ø 5 μm, *Sigma-Aldrich*, UK) or containing HEK 293T.

3.8.2.3 Print Settings for ULGT-Agarose

All ULGT-agarose based bioinks were printed like the previous cell-laden scaffold solution (*section 3.6.2*). Preliminary **SS5** bioink prints were still performed with **standard print oil** containing 1.5 mM DPhPC except for the bead-laden **SS5** print (**Figure 3.18 D**). Here the network was printed in 42:58 v:v mix of undecane: silicone oil containing 1.3 mM DPhPC (this was during the oil optimisation period, see *section 3.8.2.5*). All subsequent prints were in **bioink print oil** (see *section 3.8.2.5*). The **SS5** based networks were printed as 11x14 or 9x10 horizontal droplets for 3-5 layers.

3.8.2.4 Print Observations for ULGT-Agarose

When **SS5** was printed at 11 mg/mL ULGT-agarose (n = 1 print), it was quickly noticed that there was a low leakage rate compared to the previous culture medium and Fmoc-dipeptide based bioinks i.e. **SS1** and **SS2** respectively. Thus the ULGT-agarose solution was much more practical to use. It was also apparent that agarose droplets were

generated at very large volumes with diameters greater than 120 µm. Droplets of ø 140 µm were printed as almost uniform singlets to give a very large network of ~2×2 mm^2 which consequently could not fit within the standard field of view of the microscope (**Figure 3.18 C**). The generated droplet inconsistencies took the form of occasional misfires and slight variations in volume. Over the course of the print the misfires became more frequent, but could be prevented or minimised by the periodic raising of the amplitude of the piezo element's pulse in small increments of ~1 V.

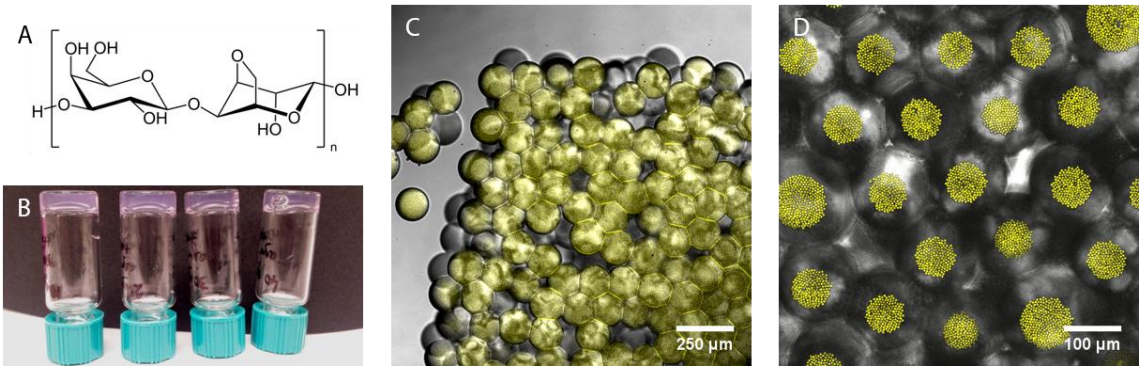

Figure 3.18 Agarose scaffold solution tests. **A** Molecular structure of agarose basic unit. **B** Inverted vials of free-standing agarose gels composed of ULGT-agarose dissolved in Opti-MEM® at 10, 20, 30 and 40 mg/mL concentration (from left to right respectively). **C**-**D** Composite bright-field and fluorescence confocal micrographs of printed agarose-based networks comprised of 11 or 13 mg/mL agarose in Opti-MEM® and also containing: **C** 1 µM SR101 and; **D** ø 5 µm polystyrene beads at 35×10^6 mL^{-1}. The droplet dimensions of the printed network were: **C** 11×14×7 and: **D** 11×14×5.

The **SS5** print solution was also supplemented with sulforhodamine 101 (SR101), which made the bulk print solution fluorescent but also inserted into the lipid bilayers at an enhanced fluorescent signal. The fluorescent network (**Figure 3.18 C**) clearly displayed moderate packing, with the droplets distorting little in shape and arranged hexagonally in places. However, there were frequent oil spaces along the base, signifying the packing could be improved.

Employing a **SS5** print solution containing ø 5 µm polystyrene beads at 35×10^6 mL^{-1} a cargo-laden agarose network was fabricated (n = 1, **Figure 3.18 D**). Bead-laden droplets were ejected uniformly, with similar printing characteristics to plain **SS5** print solution, affording a homogenous high bead content per droplet (**Figure 3.18 D**). Consequently the

network contained beads in every droplet (**Figure 3.18 D**). A HEK-293T laden **SS5** was also printed, showing similar printing traits, with 5-15 cells ejected per droplets (**Figure 3.19 A**). Thus the agarose print solution seemed to be compatible with a suspended cargo.

3.8.2.5 Optimising the Print oil

As the ULGT-agarose gelation required cooling the network down to the range of 8-17 °C, it was decided that initial networks would be cooled to 4 °C for 1 h to ensure gelation. As the **standard print oil** is 50% v/v hexadecane, which has a freezing temperature of 18 °C, it was found that the oil would freeze when performing the cooling steps. Post printing networks would have defined patterned structured in the **standard print oil** (**Figure 3.19 A**), but post gelation, i.e. when the oil thawed, there was a loss of patterned cargo in the network, which displayed multiple intra-network coalescence events (**Figure 3.19 B**).

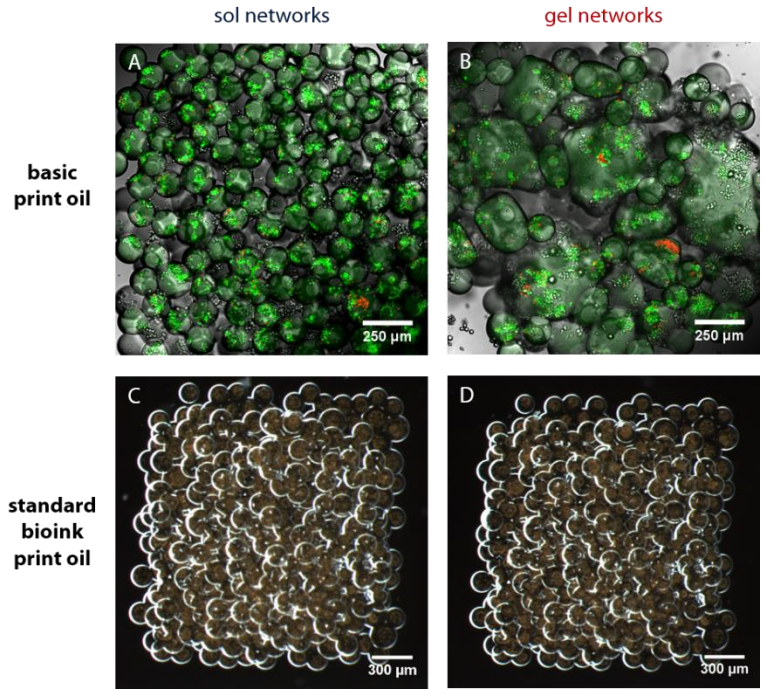

Figure 3.19 Optimised print oil for agarose scaffolds. **A**-**D** Micrographs of cargo laden **SS5** based networks (11×4×5 droplets) in different physical states: **A**, **C** liquid/sol networks imaged immediately after print and; **B**, **D** gelled networks imaged post network cooling step. **A**-**B** HEK-293T laden network (n = 2) printed in **basic print oil**, displayed a defined sol structure (**A**), which was lost upon gelation (**B**). **C**-**D** Bead-laden network (n = 2) were printed in **bioink print oil** and showed pattern retention post gelation. Images are **A**-**B** composite bright-field and fluorescence confocal micrographs and; **C**-**D** dark-field micrograph.

A modified print oil was designed, such that the gelation step was performed without oil freezing. Undecane a hydrocarbon similar in structure to hexadecane but with a melting point of -26 °C, was used to substitute the hexadecane component of the **standard print oil**. As the density of the undecane (0.74 g/cm^3) is lower than that of hexadecane (0.77 g/cm^3), it was found that a 1:1 v:v mix of undecane to silicone oil solution was unsuitable for printing. Here droplets sank much faster than normal and would be ejected far from the nozzles tip. If droplets sink quickly, they may have insufficient time to form a lipid coating, and thus could coalesce with network droplets. The long droplet ejection distance is also problematic as the printing height of the nozzle has to be raised, making the printing more impractical, less accurate with respect to patterning, and using a larger total volume of oil. Thus the ratio of undecane to silicone oil was modified.

Agarose networks were printed in undecane silicone oil mixtures in attempt to find an optimum ratio. The v:v ratios tested were: 50:50, 40:60, 35:65 and 30:70 undecane to silicone oil, with each print oil containing 1.2 mM DPhPC. It was found that the 35:65 v:v mix provided the best droplet sinking speed. At this ratio the mixture is slightly denser (0.91 g/cm^3) than the **standard print oil** (0.89 g/cm^3), but this helps compensate for the large agarose droplet which are slightly more dense than the salt solutions of Chapter 4 and previous bioinks of this chapter. Hence, a **bioink print oil** was formed and comprised of 35:65 v:v mix of undecane to silicone oil containing 1.5 mM DPhPC.

Bead-laden droplets could be generated in this **bioink print oil** and formed defined networks (**Figure 3.19 C**). When the network was gelled it retained its pattern (**Figure 3.19 D**), unlike the coalescence observed in hexadecane oil mixtures (**Figure 3.19 B**). The **bioink print oil** was used for all subsequent agarose based scaffolds, as it allowed, practical printing and networks to gel without loss in pattern fidelity.

3.8.3 Phase Transfer of Uncoated Gelled Networks

Phase transfer was reattempted using gelled micro-structures made in the optimised **bioink print oil** that comprised of ULGT-agarose based **SS5**. It was thought that these solidified scaffolds would not rupture when passed through the interface of the transfer

column into culture medium. At this stage of research, coating the scaffold in a lipid bilayer during transfer was still desired, because it was expected that the gelled droplet network would transfer as gelled versions of multi-compartment vesicles.

Initially μL gelled droplets were phase transferred to find the best conditions for phase transfer. With these conditions cargo-laden droplet networks were phase transferred as described.

3.8.3.1 Preliminary Phase Transfer of Gel Droplets

Phase transfer of gel droplets was performed similarly to the Ces method[158,159], by setting up a two phase column of bulk oil above bulk aqueous and then passing the gel droplets through the interface. The initial experiments were performed to find the ideal lipid-in-oil solution for the upper phase. It was necessary to screen this composition as previous droplet network phase transfer attempts had demonstrated many oil compositions would prevent droplet transfer or had a high rate of vesicle rupture (see *section 3.8.1*). To facilitate phase transfer centrifugal force was applied to the column, allowing the quick transfer of structures as shown by many research groups[151,152,155,156] and enabling us to screen conditions more efficiently.

With the ability to make numerous micropipetted droplets in parallel within a short amount of time comparatively to printed structures, multiple conditions were screened using the droplet analogue. For the preliminary tests gel droplet analogues were composed of **SS5** containing ~35×10^6 beads/mL. The bead content was to aid visualisation of the transparent hydrogel droplets within the aqueous environment and simultaneously test whether a cargo could be confined within the hydrogel.

Centrifugal force mediated phase transfer of gel droplets (n = 1 per column) was attempted in columns (n = 2 per condition) made of selected oil above PBS. Here the oil contained DOPC or POPC lipids in base oils of either, a 3:1 v:v mix of hexadecane with mineral oil, a 3:1 v:v mix of hexadecane with silicone oil or mineral oil alone. Using a gentle centrifugal force phase transfer of gel droplets were successful for the oil compositions 3:1 v:v mix of hexadecane with mineral oil and mineral oil alone. The 3:1 v:v

mix of hexadecane with silicone had the droplet remain stuck at the interface, so was disregarded as an oil candidate.

The upper phase transfer oil was selected to be 4.8 mM DOPC in 3:1 v:v mix of hexadecane with mineral oil, due to its empirical success and as this composition has been shown to be successful in the production of multi-compartment vesicles by Oscar Ces' research[158,159]. This upper oil phase was denoted as **initial scaffold phase transfer oil**.

3.8.3.2 Agarose-Based Droplet Network Transfer

With the success of transferring gel droplets using a transfer column comprised of **initial scaffold phase transfer oil** above PBS, gelled droplet networks (n = 2) were transferred using centrifugal force under the same conditions. This was to investigate whether these solid scaffolds could retain their printed pattern during the process. Bead-laden and cell-laden networks were printed with **SS5** bioink containing ø 5 μm polystyrene beads at ~18×10^6 /mL or 8×10^6 HEK-293T cells/mL, respectively. These defined square cuboid networks were gelled post print without pattern loss (**Figure 3.19 D**), and then were phase transferred (**Figure 3.20**).

The resulting structures showed that the network had sheared into individual printed droplets which still encapsulated most of the printed cargo (**Figure 3.20**). The individual printed droplets no longer contained their initial droplet-droplet connections, but retained their printed shape as seen by the flat edge droplets in **Figure 3.20 C**. Most of the cargo were retained in the sheared droplets (**Figure 3.20**), however, the cells were also present outside of the droplets, demonstrating that cells had presumably sheared off at the droplet edges (**Figure 3.20 D**). Whilst the networks had collapsed, cargo was mainly retained within the droplets at high cell viability. Thus as long as the network could retain its original structure we had the ability to relocate cell patterned scaffolds into an ideal culture environment.

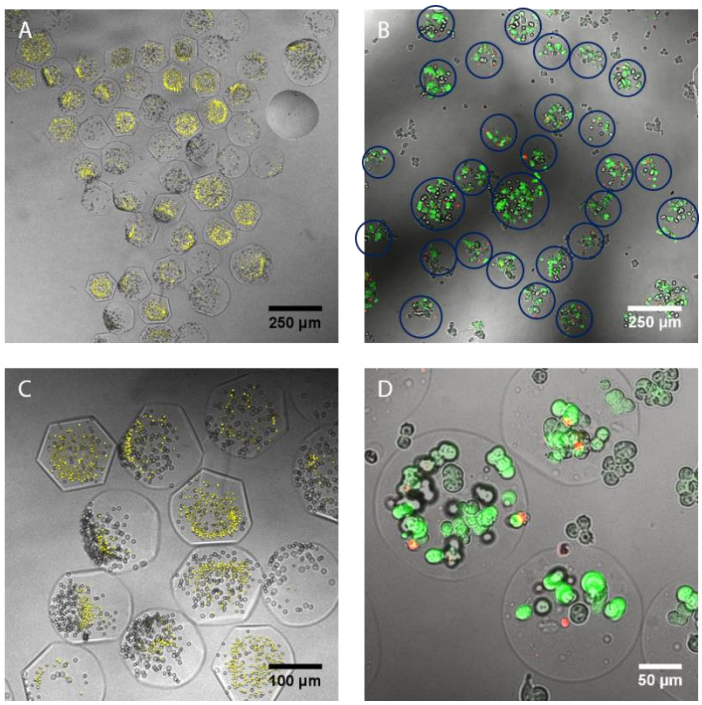

Figure 3.20 Phase transfer of uncoated agarose-based droplet networks. **A**-**D** Composite bright-field and fluorescence confocal micrographs of phase transferred cargo-laden networks. These networks (11×14×5 droplets, n = 2) did not have an additional supporting gel coating and sheared into the individual printed droplets. Networks were printed with a **SS5** based bioink containing: **A**,**C** ø 5 µm polystyrene beads at ~18×10^6 /mL (network *C* of *Figure 3.19*) and; **B**,**D** 8×10^6 HEK-293T/mL. **A**,**B** Low magnification micrographs of sheared networks showing droplet-droplet connections are no longer present. In **B** phase transferred droplets have been circled. **C**,**D** Magnified micrograph on a set of sheared individual printed droplets.

3.8.4 Phase Transfer of Coated Gelled Networks

To phase transfer cell-laden networks which retain their printed pattern, the printed network needed an additional supporting structure or a way to improve droplet-droplet adhesion in order to prevent the network from collapsing. After experimenting with different techniques a method of coating/wrapping the networks in a supporting gel was developed. Coated structures were successfully phase transferred as single structures containing either, patterned micropipetted droplets or a printed droplet network (**Figure 3.21**). The preliminary work of this technique is described, followed by an outline of how phase transfer was modified to give reproducible aqueous bound networks.

3.8.4.1 Preliminary Coating of Gelled Networks

It was thought that a gelled network could be wrapped in an exterior gel without significant changes to the patterned cargo. Such a structure could subsequently be phase transferred holding the patterned cargo in place and once in aqueous, cell patterned scaffolds could be cultured into microtissues. The initial coating experiments proved the concept using gelled micropipetted droplets (ULGT-agarose) coated with an exterior layer of further ULGT-agarose (**Figure 3.21 A**,**D**). The method was then adapted to printed networks (**Figure 3.21 B-C**).

The pilot coating experiment was with simple networks of gelled micropipetted droplet, specifically triplet (n = 1) and quartet (n = 1). As before, droplets were composed of **SS5** containing ø 5 μm polystyrene beads at ~35×10^6 /mL and were made as ~2 μL volumes in lipid-in oil solutions. After the droplet networks were gelled, a ~4 μL micropipetted droplet of liquid ULGT-agarose was brought in contact with the network to wet the network surface. Due to the presence of the lipid, the exterior gel droplet formed a droplet interface bilayer initially. Wetting was induced by repeated micropipette tip perturbation of the structure. The coated structure was gelled and subsequently phase transferred to PBS. It could be seen that the bead patterned droplet networks had retained their simple pattern and remained as triplet and quartet networks (**Figure 3.21 A**,**D**).

The pilot coating result signified that gelled droplet networks wrapped in a supporting ULGT-agarose can be transferred to aqueous solution as a single structure which encased the droplet network. Furthermore the internal gelled droplet network appeared to retain their initial geometry and could feasible retain a patterned cargo. Following this result, printed networks laden with either HEK-293T cells (at 8×10^6 mL^{-1}, n = 1) or ø 5 μm polystyrene beads (at ~18×10^6 mL^{-1}, n = 1) were formed and coated in a similar manner to perform phase transfer (**Figure 3.21 B-C**).

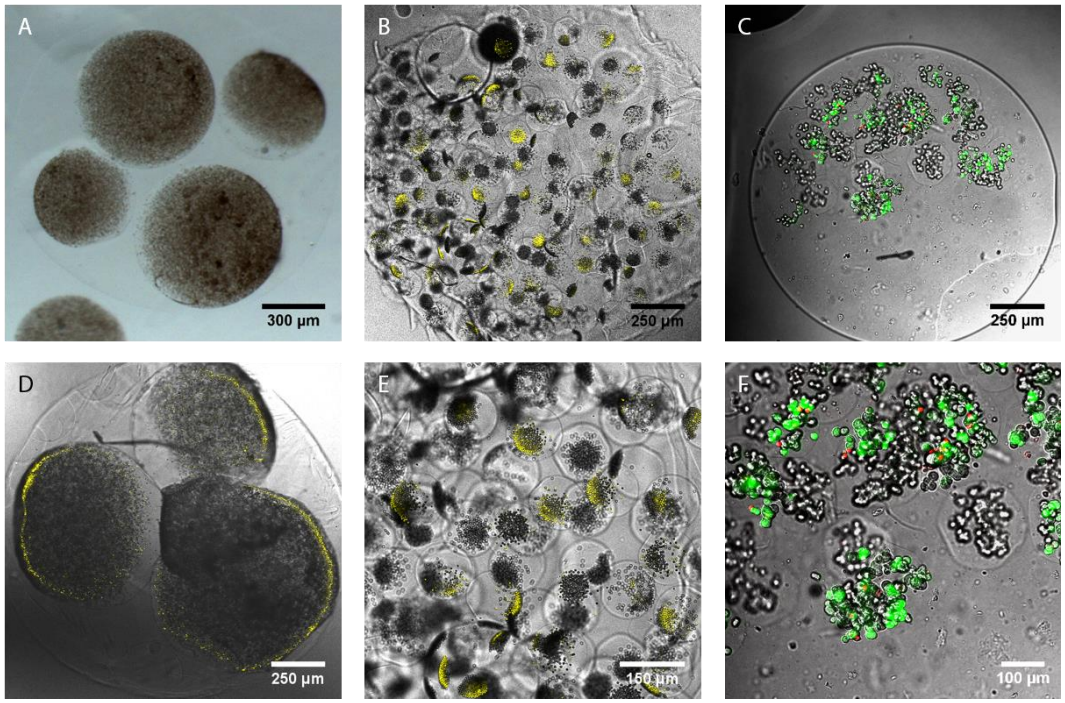

Figure 3.21 Preliminary phase-transfer of gelled scaffolds with exterior gel-coating. **A**-**F** Micrographs of gel-coated gelled scaffolds in PBS. **A**,**D** Conjoined micropipetted droplets laden with ø 5 µm polystyrene beads (at ~35×10^6 mL^{-1}), wrapped together in an agarose support. The networks retained their original topology after phase transfer. **B**,**C**,**E**,**F** Printed gelled droplet network wrapped in supporting agarose gel and containing printed cargo of: **B**,**E** ø 5 µm polystyrene beads at ~18×10^6 mL^{-1} or; **C**,**F** 8×10^6 HEK-293T/mL. **B**, **E**, Depicts network *C* of *Figure 3.19* after gel coating and phase transfer. **B**,**C** View of entire coated network showing the initial square sheet structure was lost through coating. **E**, **F** Magnified sections of coated networks, showing printed droplets have retained their shape but not their patterned droplet-droplet contacts. Images are: **A** an optical micrograph and; **B**-**F** composite bright-field and fluorescence confocal micrographs.

As with the gelled micropipetted droplets, the liquid exterior gel droplet formed a droplet interface bilayer with the gel network. When the network was perturbed by the micropipette tip, it was noticed that the liquid gel droplet would coalesce with individual droplets incrementally, rather than wetting the whole network. As such, the printed pattern was lost during the wrapping step. Regardless, the structures were gelled and phase transferred (**Figure 3.21 B-C**) to investigate how the printed droplets behaved during phase transfer.

On close inspection of the transferred coated scaffolds, it could be seen that the printed networks were confined within a single structure with the printed droplets retaining their original shape (**Figure 3.21 E-F**). These droplets were randomly distributed and had less droplet-droplet contacts than within the original printed

network. Cargo of the printed droplet were also mainly retained within the printed droplets, with a only a small quantity entering the void hydrogel coating. Suggesting that if that wrapping procedure was optimised the patterned cargo would initially, mainly remain in the printed structure.

The cellular pattern scaffold was successfully live-dead stained (see *section 3.5.2.3*) with CAM and PI post phase transfer (**Figure 3.21 C-F**). This demonstrated that the small dye molecules could cross the gelled scaffold and penetrate the cells. As such it can be inferred that other small molecules such as those of the culture medium can reach the cell in a similar manner. Hence the agarose-based scaffold should be porous enough for the exchange of small nutrient molecules essential to sustain cell viability.

3.8.5 Phase Transfer Methodology

Gel coating of scaffolds showed the potential for the conservation of the printed cellular pattern throughout the transfer process. However, in the preliminary form, gel coating resulted in the pattern being lost, as the printed network was coalesced incrementally as individual droplets rather than being wetted as one structure with the exterior gel droplet. Hence, the network coating step was optimised in an attempt to form cell pattern scaffolds which could reproducibly be phase transferred without loss of pattern fidelity. The coating step was made reproducible using a method of diluting out the lipid by washing the network multiple times with a lipid free oil (*Section 3.8.6.1*). Phase transfer was also adapted to a gravity mediated approach (rather than centrifugal), so that transfer could be performed directly into microscope chamber slides (*Section 3.8.6.1*).

3.8.5.1 Transfer of Cell Patterned Scaffolds to Culture Medium

The optimised method of transferring cell patterned scaffolds is as depicted in **Figure 3.22**. This method was adapted with experimentation, such adaptions are explained in s*ection 3.8.6.1.*

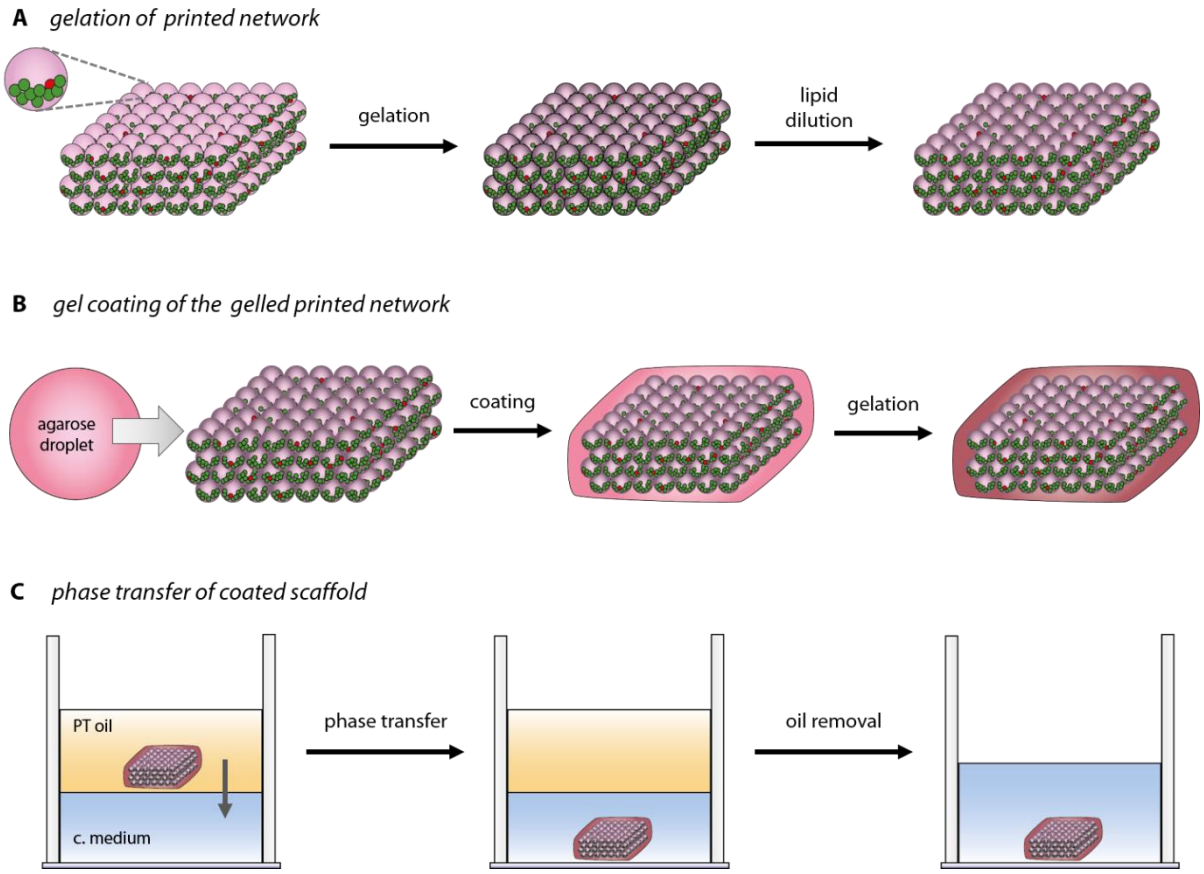

Figure 3.22 Schematic of the phase transfer steps of printed cell patterned scaffolds. **A** The cell-laden printed droplet network is initially gelled within the print oil by cooling. The lipid of the print oil is then diluted out, by repeated silicone oil washes, leaving the network free of an outer lipid coating. **B** The gelled network is coated by agarose by wetting the surface with a micro-pipetted agarose droplet. The agarose coated gelled network is then gelled again within the oil by cooling. **C** The gelled coated scaffold is relocated into the upper phase of a two phase column of oil above culture medium. The scaffold then spontaneously phase transfers by sinking across the interface. The oil is removed from the transferred scaffold container, topped up with extra culture medium and then stored in cell culture conditions.

The phase transfer process was split into three steps: the first step was the production of a gelled cell patterned printed network (**Figure 3.22 A**); specifically the network was printed in oil, then gelled (**Figure 3.23 A**) and subsequently washed with lipid free oil (**Figure 3.23 B**). The second step was the gel coating of the gelled cell patterned printed network (**Figure 3.22 B**), which involved coalescing the structure with a supporting ULGT-agarose solution and then gelling the scaffold (**Figure 3.23 C**). The final step was the transfer of the scaffold into culture medium (**Figure 3.22 C**). This involved transporting the network via micropipette tip into the upper phase of the transfer column i.e. oil above culture medium and then allowing the network to sink through the interface

(**Figure 3.23 D**). After phase transfer the upper oil phase was removed and the scaffold was cultured (see Chapter 4).

The state of the scaffold can be seen at the different stages of the optimised transfer process in **Figure 3.23**, here scaffolds in culture medium display no loss in pattern fidelity (*section 3.8.6.4*). The first step of gelling the network had consistently shown that cellular patterns were conserved (**Figure 3.23 A**). The poor pattern preservation in the preliminary gel coating experiments was likely due to lipid bilayer formation between printed structure and exterior gel droplet. Therefore we washed away the bulk lipid, with repeated washes of lipid-free oil to prevent this. After oil washes the network had retained its shape but the droplet boundaries, which usually appear black due to the lipid membrane thickness[171], are no longer defined indicative of internal lipid bilayers being distorted (**Figure 3.23 B**). The lipid disruption may not have resulted from the wash step alone, the gelation of agarose may have caused gel outgrowths which may have strained or broken the lipid bilayers.

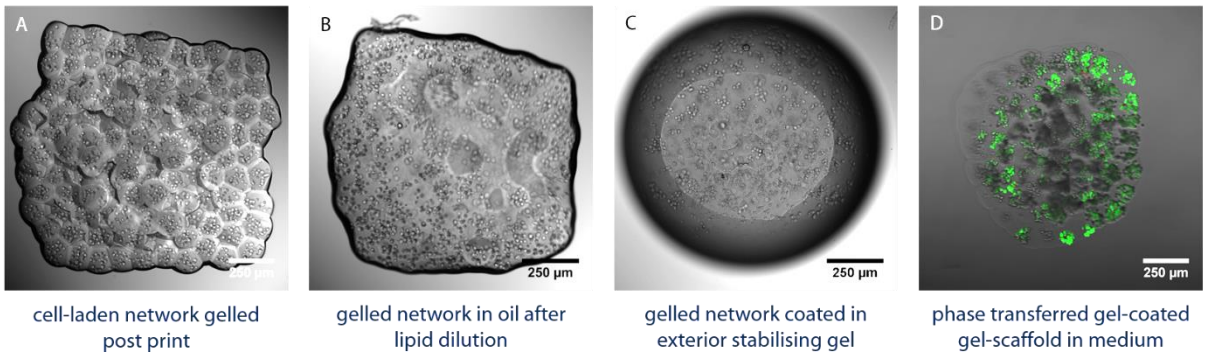

Figure 3.23 Cell scaffolds during the different stages of phase transfer. **A**-**D** Bright-field confocal micrographs of oMSC laden networks composed of **SS6** with 5×10^6 cells/mL at different points of the phase transfer process. **A** Gelled network immediately after gelation in bulk oil. **B** Network of **A** post dilution of lipid in bulk oil. **C** An ULGT-agarose coated network in bulk oil, here more exterior gel than necessary has coated the gelled network causing the structure to become spherical. **D** Phase transferred oMSC laden scaffold in bulk culture medium, showing a rounded square geometry. Image **D** is a composite image including the fluorescence channels. The images are of independent networks except **A** and **B** which are the same network.

With the gelled network in a very dilute lipid containing oil, networks displayed almost instantaneous wetting by the exterior ULGT-agarose solution. These structures gelled

and either kept the initial geometry or became spherical if too much exterior gel (~0.6 μL) was added (**Figure 3.23 C**). The spherical nature was due to the immiscible phases of the bulk oil and aqueous network minimising their interactions by decreasing the interface surface area. Whereas when very low volumes of exterior gel (~0.3 μL) were added to networks, they remained rigid, resisting changes in geometry .

The gel-coated gel networks/scaffolds, were successfully phase transferred with minimal changes in pattern or structural topology when sufficient gel coating was present (**Figure 3.23 D**). The process involved micropipette transporting the scaffold into a two phase column, at which point the scaffold sank to the interface and spontaneously phase transferred. The sinking networks would land in different orientations and appeared as rounded squares. The curved corners were the result of the network flexing during the phase transfer process. Phase transfer allowed the total exclusion of oil around the scaffold as seen visually (**Figure 3.23 D**). Additionally cells appeared at high viabilities, with a 91% average viability observed for oMSC patterned scaffolds (*section 4.7.4*) inferring the scaffold solution and process was non detrimental to cell health.

Overall the method attained gelled scaffolds in medium that conserved their printed cellular pattern. Furthermore, as seen in the preliminary scaffold transfer experiments and in **Figure 3.23 D**, scaffolds could be stained once in bulk culture medium by dye molecules indicating that the structure is permeable to small molecules. Hence the culture of patterned cellular scaffolds became accessible through this process (see Chapter 4).

3.8.6 Optimising Scaffold Phase Transfer

Without reproducible pattern conservation, high order cellular architecture would not be attainable, limiting the scope of producible cellular scaffolds. Therefore phase transfer was optimised to reproducibly conserve the printed cellular pattern, i.e. using the method described in *section 3.8.5.1*. This section outlines the multiple optimisation steps performed to achieve reproducible scaffold transfer to culture medium, including supplementing the bioink with **Fmoc-XX** to improved droplet cohesion.

3.8.6.1 Standardisation of Phase Transfer

The process of phase transfer was continually altered throughout the attempts to produce culture medium bound cell patterned scaffolds. Through experimentation this method was standardised (see *section 6.8*). The most important modifications in making the process standardised were as follows.

Shortened gelation time. The time spent at 4 °C for ULGT-agarose gelation was reduced to 20 min as this was sufficient time to gel the scaffold and reduced the time the cells spent in non-optimal conditions.

Silicone wash oil. Preliminary network washing steps were performed with hexadecane, but, upon changing to silicone oil it was found fewer wash steps were needed and the exterior gel solution wet the network much easier.

Low exterior gel volume. The initial volume of exterior gel added to a 3-4 layer cell patterned droplet network was about 0.8 μL, which caused the scaffolds to become spherical in nature. When the gel coating volume was reduced to 0.2-0.4 μL, the networks kept their original structure and were enveloped by a thinner layer of ULGT-agarose.

Silver wired aided wetting. It was observed post lipid dilution that a small proportion of networks could not be wet by the exterior ULGT-agarose solution and instead formed a weak contact. In these circumstances, a sterilised silver wire was used to induce wetting of the network surface. Specifically, the ULGT-agarose droplet could be directed by the silver wire's tip onto the network resulting in coating or in some circumstances placing the silver wire in the oil was enough to induce the liquid agarose droplet to wet the exterior of the networks. It was likely there could be some static interference between the network and exterior gel droplet which prevented wetting[172]. By using the highly conductive silver wire the static could be discharged mediating wetting.

Lipid free two phase column. Initially scaffolds were being treated as droplet networks, which needed to be enveloped in external lipid so that the system could phase transfer as a multi-compartmentalised vesicle. As the gel coated scaffolds being phase transferred no longer contained internal lipid bilayers, there was longer the need to coat the network in this peripheral lipid. Consequently the two phase column was stripped of lipid such that the upper phase used was just a 3:1 v:v mix of hexadecane to mineral oil mix. This solution was entitled **standard scaffold phase-transfer oil** and was equally as efficient at phase transfer as its lipid containing predecessor.

Gravity mediated phase transfer. The centrifugation phase transfer method was exchanged for a gravity mediated one. This allowed scaffolds to be directly phase transferred to a microscope chamber slide, which was the standard culture vessel for cell patterned scaffold. Prior to this, centrifuged transferred scaffolds would have to be relocated from the microcentrifuge tube into the chamber slide. This process provided an additional step in which the scaffolds structure could be damaged. Gravity mediated transfer proved just as productive as centrifuge transfer, with scaffolds being transferred at 100% success rate using the standardised method.

3.8.6.2 Modified Bioink

The packing of agarose networks may have been enhanced to omit oil gaps, improving the likelihood that the networks maintain their structure during the gel coating. As the Fmoc-dipeptides where shown to increase droplet-droplet adhesion in *section 3.7.3.2*, they were selected to supplement the agarose-based **SS5**. The resulting solution was called, **scaffold solution 6** (**SS6**) and comprised of 11-13 mg/mL agarose with 1 mM **Fmoc-XX** in culture medium. Here the culture medium was Opti-MEM® for test and HEK-293T scaffolds (**SS6h**) and **DMEM-ITS** for oMSC scaffolds (**SS6m**).

A print solution of **SS6** was utilised to fabricate a network ($n = 1$) of 9×11 horizontal droplets for 5 layers. The solution printed similarly to **SS5**, giving uniform singlet droplets

with the occasional misfire. The only noticeable printing difference was the solution displayed slightly more leakage from the nozzle.

Droplet networks composed of either salt solution only (n = 2), **SS5h** (n = 2) and **SS6h** (n = 2) were printed for packing comparison by SR101 droplet staining (**Figure 3.24 A-C**). The aqueous soluble SR101 dye was found to concentrate in the lipid bilayers of droplet networks composed of salt solutions and was used to clearly display droplet packing (**Figure 3.24 D-F**). The salt solution was physiologically isotonic (i.e. 145 mM KCl) and is analogous to culture medium. The salt solution only network (**Figure 3.24 A**) showed moderate droplet network cohesion, but did not cohere tightly, giving rise to many gaps (**Figure 3.24 D**). Whereas the **SS5** based network (**Figure 3.24 B**) demonstrated that by adding agarose to the culture medium the droplet cohesion is enhanced to give hexagonally packed droplet networks with some oil gaps (**Figure 3.24 E**). When **Fmoc-XX** is also supplemented along with agarose (i.e. **SS6h**) the resulting network is highly cohesive but still showed oil gaps (**Figure 3.24 C**). Upon closer inspection the droplets have become quite deformed from previous packed circles or hexagons (when viewed in a 2D plane) and adhere as non-uniform polygons with large bilayers (**Figure 3.24 F**). Additionally it appeared that the presence of **Fmoc-XX** interferes with the SR101 binding to the lipid bilayer. In **SS6h** solutions the SR101 instead was homogenously distributed across the bulk droplet phase, presumably binding to the bulk **Fmoc-XX** (**Figure 3.24 F**).

To ensure that the networks were cohered strongly prior to exterior gel coating, **SS6** based bioinks were selected over **SS5**. It was thought that as the **SS6** based droplets deformed to form larger bilayers, that the final structure was more tightly adhered. Furthermore it was hypothesised that the upper layers would contain less oil gaps, as **SS6** droplets spread within gaps during print. As such all subsequent cell laden networks were printed with the presence of **Fmoc-XX**. Ejection of HEK-293T cells was tested using **SS6h**. It was found that droplet production remained similar to the cell-laden **SS5** prints of *section 3.8.2.4*, i.e. homogeneous dispensing of cells across a print.

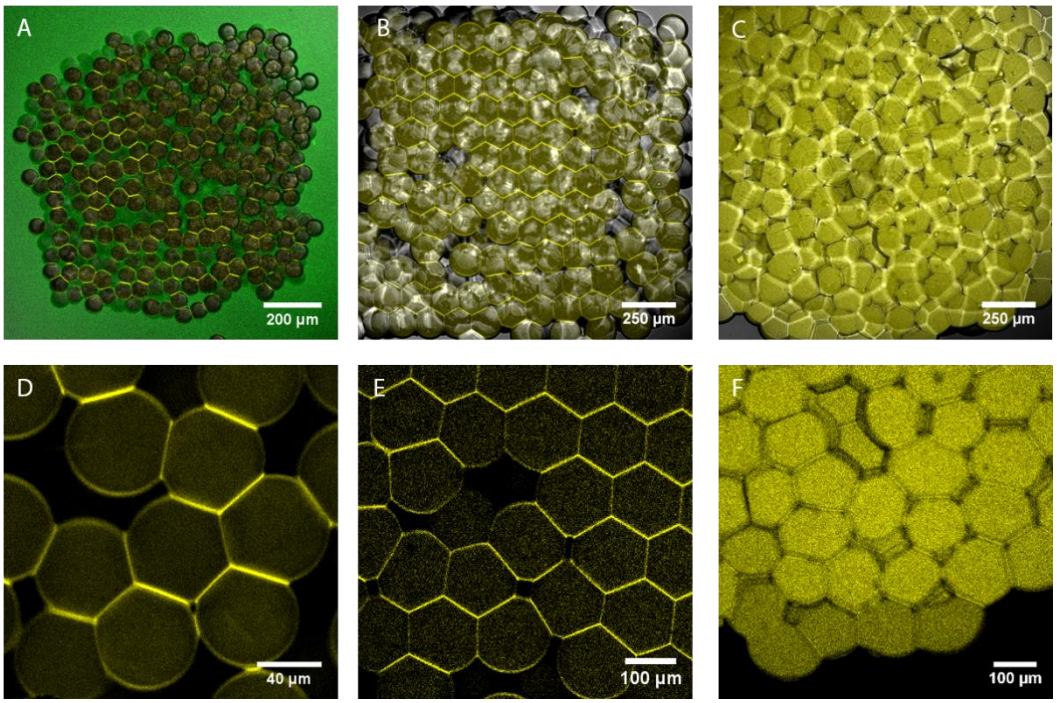

Figure 3.24 Packing of agarose-based printed networks. **A**-**C** Composite bright-field and fluorescence confocal micrographs of printed networks (9×11×5 droplets) composed of: **A** 145 mM KCl; **B** gelled **SS5h** and; **C** gelled **SS6h**. **D**-**F** Fluorescence confocal micrographs at high magnification of networks displayed in **A**-**C** respectively showing the packing of the network by yellow SR101 staining. **D** The physiologically isotonic network displayed moderate droplet-droplet adhesion, but with numerous gaps. **E** The incorporation of agarose into the print solution enhanced the droplet cohesion, giving mainly hexagonally packed structures but with some gaps. **F** Further print solution supplementation with **Fmoc-XX** gives structures with high droplet-droplet adhesion, causing the droplets to distort into non-uniform polygons with large bilayers. Network **A** was printed in **standard print oil** containing DPhPC doped with green NBD-DPhPE at 0.1 mol%.

3.8.6.3 Optimised Phase Transfer

Using the standardised phase transfer method (**Figure 3.22**), cell patterned scaffolds could be transferred retaining their structural configuration and printed cellular pattern (**Figure 3.25**). As an example, one of the first phase transferred scaffolds with defined geometries is shown in **Figure 3.25 B**. The network was printed with **SS6h** containing 8×10^6 HEK-293T/mL as an accurate square sheet (**Figure 3.25 A**). This network was coated in a small volume of agarose, gelled and phase transferred, giving a conserved square sheet (**Figure 3.25 B**). The dimensions of the scaffolds are similar in oil (horizontal: ~1.0×1.0 mm^2) and culture medium (horizontal: ~1.0×1.1 mm^2). There is a slight increase in the phase transferred volume due to the exterior gel coating inserting around droplets. The patterned cells within the phase transferred structure were also conserved. When

the cells are displayed as a 3D projection they are fairly homogenously distributed and have a square profile (**Figure 3.25 C**).

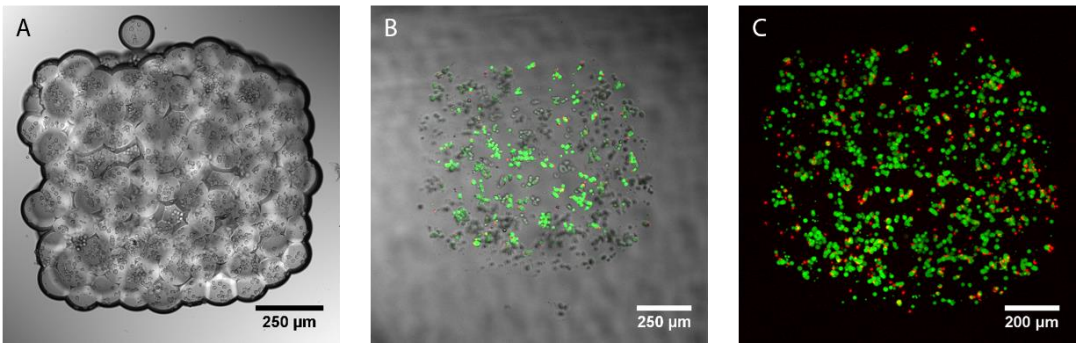

Figure 3.25 Optimised phase transfer of a cell patterned scaffold with square sheet geometry. **A**-**B** Bright-field confocal micrograph of a gelled HEK-293T laden network (7×9×4 droplets) in: **A** bulk oil and; **B** bulk culture medium. Image **B** is a composite which also displays the fluorescence channel. The scaffold was composed of **SS6** with 8×10^6 HEK-293T/mL and shows that the defined square sheet geometry was maintained. **C** 3D projection of the cells in the scaffold displayed in **B**, showing the cells are homogenously distributed in an approximately square geometry.

3.8.6.4 Reproducible Phase Transfer

By implementing a standardised phase transfer method, it was possible to reproducibly fabricate cell-laden square cuboid scaffolds. This method was employed to transfer greater than a hundred cell-laden scaffolds with latter structures showing very high structure and pattern conservation. An example of how reproducible phase transfer became is in **Figure 3.26**, which depicts triplicate transferred cell patterned scaffolds with square cuboid topologies and square-body patterned cargo. The horizontal dimensions of the example square phase transfer networks were either ~1.2×1.2 mm^2 (**Figure 3.26 A**,**C**) or ~1.2×1.1 mm^2 (**Figure 3.26 B**).

Using this phase transfer technique developed, cell patterned scaffolds were cultured into tissues (Chapter 4) and were transferred with heterogeneous cells patterned as high resolution architectures (see *section 3.9*).

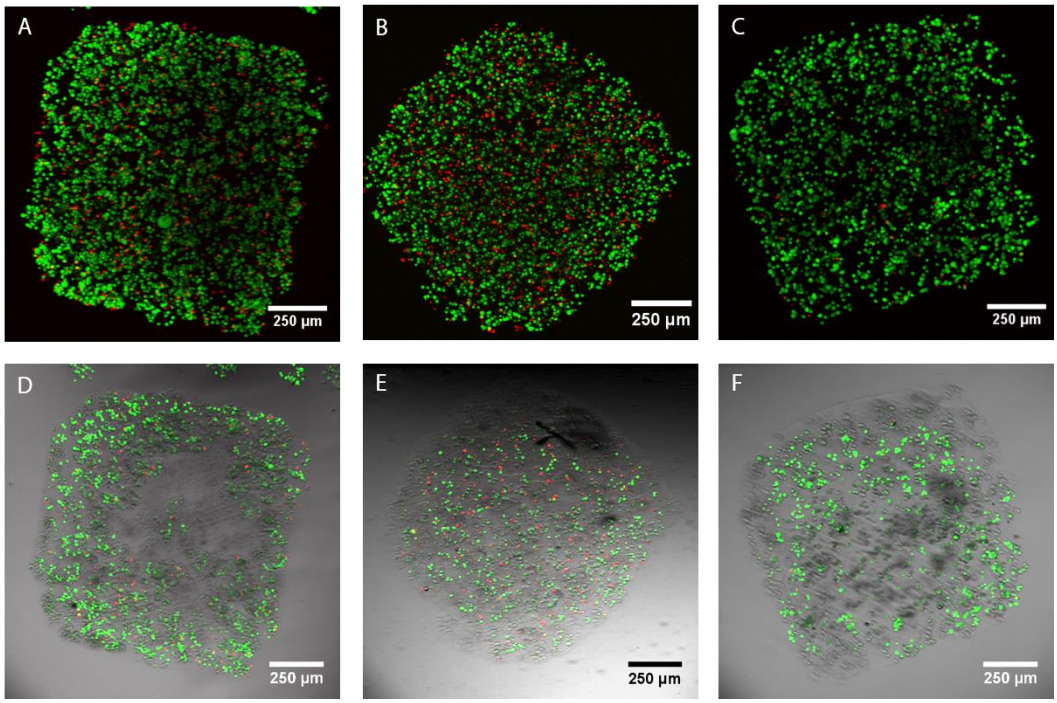

Figure 3.26 Cell patterned scaffolds with defined square sheet geometries in culture medium. **A-C** Bottom-up 3D projections of culture medium bound cell patterned scaffolds, comprised of **SS8** (see Chapter 4) and printed as 7×9×4 droplets. The printed bioink also contain 15 µg/mL collagen I and either: **A-B** HEK-293T at 15×10^6 cells/mL or; **C** oMSC at 8×10^6 cells/mL. **D-F** Composite bright-field and fluorescence confocal micrographs of scaffolds shown in **A-C** respectively. All networks showed an accurate square profile that was conserved through phase transfer.

3.9 Two Cell-Type Scaffolds

Almost all tissues involve the interaction of various cell types, as such, spatially patterning hierarchies of multiple cell-types is key in generating cell patterned scaffolds which can develop into physiological tissue. Therefore, we demonstrated the patterning ability of our 3D bioprinting technique by manufacturing cell patterned scaffolds with tissue-like architectures and high feature resolutions. Here we employed the ability to pattern cells as cell-dense droplets at high droplet volume resolution and high spatial resolution to pattern capillary-like structures and layered sheets including a native bone-cartilage junction made of chimeric sheep and mouse cells.

3.9.1 Patterning Overview

The patterned droplet networks of Chapter 2 had high resolution features, which ideally we wanted to recapitulate using our cell patterning technique. In Chapter 2, two printing solutions were dispensed alternatively using two droplet generators whose nozzles remained in the print oil throughout the print. This technique could not be repeated at all using the optimised agarose bioinks composed of either **SS6**, **SS7** or **SS8** (see Chapter 4).

The main problem is the leakage of bioink during the print. All the cell-laden bioinks are initially very leaky, this high initial leakage rate can only be reduced by raising the capillary out of the oil and forming a large droplet (*section 3.6.3*). After lowering the nozzle back into the oil, the leakage rate is only moderate but still requires frequent droplet generation to prevent the print solution leaking into the oil. Therefore it takes all the printer user's efforts to setup automated printing for a single nozzle. There are also additional considerations of dual nozzle printing. With these bioinks, the piezo's voltage pulse had to be continually amplified over the print due to agarose slowly gelling and becoming more viscous. Whilst this is feasible with one generator, two would almost be unmanageable. Additionally these bioinks are dynamic due to the suspended cells, which slowly sink when idle. As discovered with dual nozzle prints of ø 5 μm polystyrene beads (data not shown), the cells can clog in the idle nozzle whilst the other is continually generating droplets. With these considerations in mind a single droplet generator printing approach was implemented.

For printing two cell-types, the cells were patterned sequentially using a single droplet generator. Specifically this was by initially loading the selected generator's nozzle with the bioink of cell-type 1 and then printing the desired structure, after which the bioink of cell-type 2 was loaded and the remaining structure was printed. Using this technique, 3D scaffolds with 2D and 3D cell patterns such as branching pathways and stacked layers architectures were printed.

3.9.1.1 Discerning Patterned Cells

In order to discern the location of patterned cell populations a combination of fluorescent cells were utilised. The fluorescent cells were either HEK-293 derivatives which expressed fluorescent proteins (either CFP or YFP) or CellTracker™ stained HEK-293T cell-lines. The CellTracker™ fluorescent probes are dyes that freely pass through the cell membrane and once inside are converted into cell-impermeant fluorophores. In this form the fluorophore is retained within the living cell for several generations, with the probe passed to daughter cells. As the CellTracker™ fluorophore will display fluorescence for at least 72 h, the cellular location can easily be monitored immediately after the print or after a few days of culture. We selected Deep Red (DR) (Em_{max} = 660 nm) and Red CMPTX (RC) (Em_{max} = 602 nm) CellTracker™ probes, which can be viewed alongside each other with minimal fluorescent emission crossover and could also be used in combination with calcein-AM or CFP.

3.9.2 Capillary-Like Structures

Numerous tissues contain arborised architectures, such as, tube-like passageways for blood (capillaries) and air (bronchi), and communication pathways of the peripheral nervous systems. To replicate such tissue would need high resolution patterning of at least two cell types, with scaffolds containing pathways of cells that bifurcate at specific points. As such we fabricated scaffolds with arborised cell architectures i.e. consisting of a fine pathway which split at a node into two or three further paths (**Figure 3.27**).

Scaffolds with these architectures were printed as followed, the pathway structure was printed first, followed by structural droplets within the plane of the path and then additional layers of structural droplets on top of the structure. Using this technique, scaffolds (n = 3) containing a bifurcated pathway of RC stained HEK-293T droplets surrounded by structural droplets containing DR stained HEK-293T was fabricated (**Figure 3.27 A**,**B**).

The arborised cell pathway under oil displayed distinguishable cell populations with a fine branching pathway (**Figure 3.27 A**,**B**). The pathway was between 1 and 3

droplets wide, with an average width of 180±60 μm ($\overline{w}$ ± s.d., for 14 measurements). It was also noticed that at its narrowest point the pathway was a single droplet with a width of 80 μm. Using this printed network as a model print, we can assume that future prints can be reproducibly performed to produce scaffolds with horizontal features of down to 150 μm resolution.

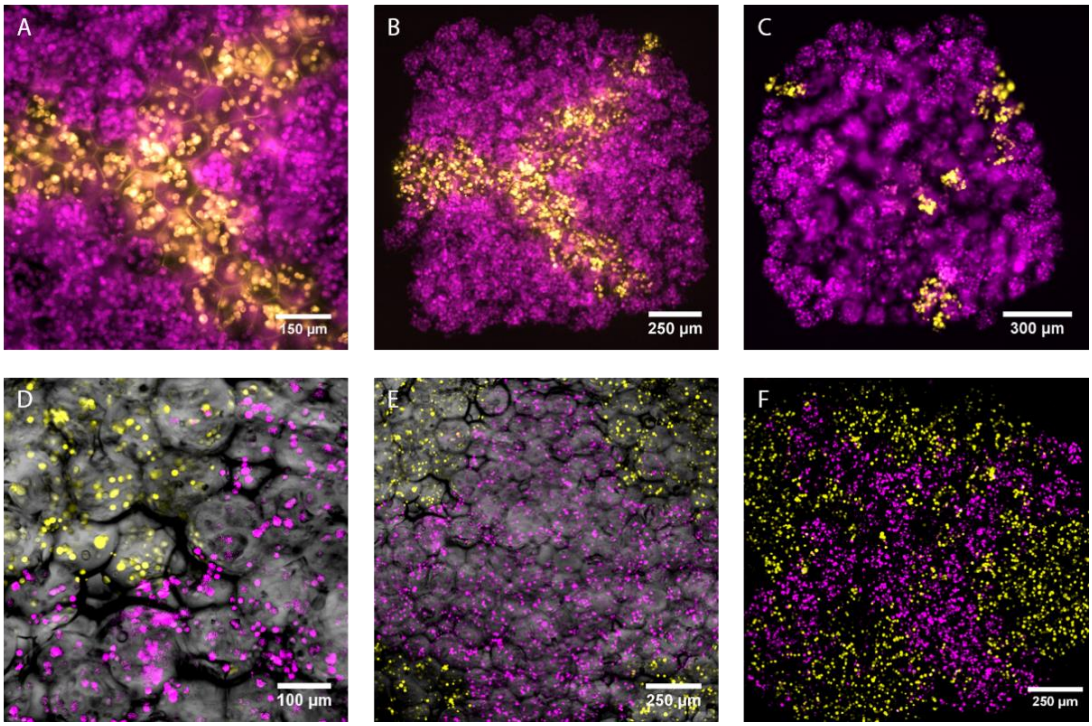

Figure 3.27 Capillary-like and cruciform cellular patterns. **A**-**C** Composite fluorescence wide-field micrographs of a network (8×9×4 droplets, n = 3) containing an arborised/bifurcated pathway of cells in: **A**,**B** oil after gelation and; **C** culture medium after phase transfer. **A** Magnified section of scaffold showing pathway node with distinguishable cell populations of RC stained HEK-293T (pathway, yellow) and DR stained HEK-293T (structure, purple). **B** Gelled scaffold showing fine branching pathway across structure. **C** Phase transferred scaffold shows loss of fine patterned pathway. **D**-**F** Images of a network (13×13×5 droplets, n = 2) containing a cruciform cell pattern in: **D**,**E** oil after gelation and; **F** culture medium after phase transfer. **D**-**E** Composite bright-field and fluorescence micrographs of the scaffold's cross showing discernible cell populations of DR stained HEK-293/CFP (pathway, purple) and HEK-293/YFP (structure, yellow). **F** 3D projection of phase transferred scaffold shows retention of the cross path with a slight relaxation of pattern fidelity.

When the arborised scaffold was transferred to culture medium the pathway cell population was lost to shear forces experienced during phase transfer (**Figure 3.27 C**). This is indicative of an insufficient gel coating of the scaffold, meaning the under layer structure became delaminated (**Figure 3.27 C**). However, pattern conservation was

demonstrated for lower resolution cruciform scaffolds (n = 2) i.e. a nested cross scaffold (**Figure 3.27 D,E**). This network was found to have retained its cross topology when viewed in bulk culture medium (**Figure 3.27 F**). The cruciform patterned scaffold in bulk oil clearly showed four isolated HEK-293/YFP populations, separated by a cross of droplets containing DR stained HEK-293/CFP cells, which had an average width of 338±33 μm ($\overline{w}$ ± s.d., for 12 measurements). When phase transferred the scaffold did not become flush with the microscope chamber's base and was imaged slanted. The 3D projection of the scaffold showed that the cross was retained but was slightly wider with the average pathway width increasing to 425±73 μm ($\overline{w}$ ± s.d., for 12 measurements). The gel coating step was likely the cause of this minor distortion, as peripheral network droplets could move slightly into the void gel.

These fabricated cell-patterned scaffolds showed that complex tissue architecture such as arborised topologies were printable at high resolution, with narrow cellular pathways of 180±60 μm ($\overline{w}$ ± s.d., for 14 measurements). However, the phase transfer process needed to be further optimised to ensure the retention of these very fine features. Yet, successful phase transfer was still demonstrated for fine patterned structures such as the nested cross (425±73 μm pathway), which demonstrated pattern conservation during the phase transfer process This signified that cells could be grown from patterned tissue-like architectures, potentially encouraging intrinsic tissue development.

3.9.3 Layered Sheets

Many tissues are composed of layered thin sheets of different cell types, such as the retina which comprises of seven layered cell types and skin which is composed of, an external epidermis, a separatory basement membrane and a lower dermis. Consequently, for many fabricated tissues to recapitulate native function, cells need to be grown as connecting cell sheets. To recreate these laminar architectures cell patterned scaffolds were produced as layered sheets.

Layered sheet networks (n = 5) were printed as a lower square cuboid (3-4 droplets thick) of cell-type 1 followed by an upper square cuboid (2-4 droplets thick) of cell-type 2 (**Figure 3.28 C**). This technique was employed to create a high resolution layered sheets scaffold of HEK-293/YFP cells below DR stained HEK-293/CFP cells (**Figure 3.28**). After gelation the cell patterned scaffold was found to comprise of distinct cellular layers (**Figure 3.28 A**,**B**) with average layer thicknesses of ~220 μm (lower) and ~130 μm (upper). When the structure was phase transferred the cells remained isolated as connected layers (**Figure 3.28 D**,**E**), with layer thickness of ~150-300 μm (lower) and ~140-210 μm (upper).

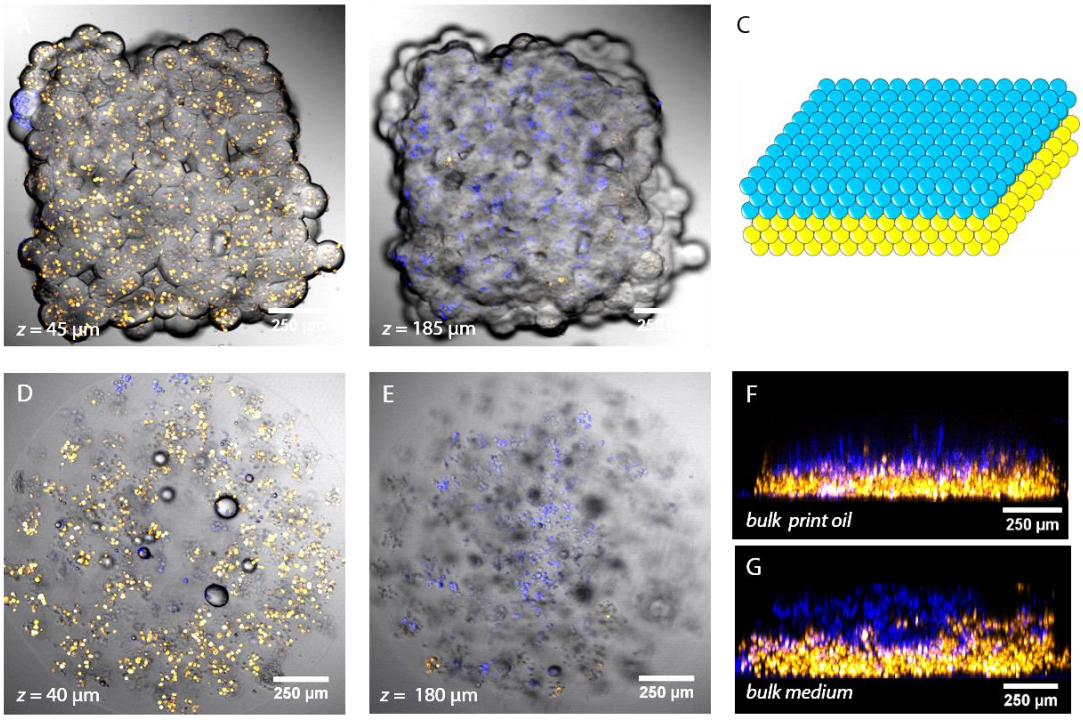

Figure 3.28 Fluorescent HEK-293 cells printed in lamellar architectures. **A**-**B** Composite bright-field and fluorescence micrographs of layered cell sheets (lower: 7×9×3 droplets; upper: 6×7×4 droplets) composed of HEK-293/YFP (yellow) below DR stained HEK-293/CFP (blue). Scaffolds were imaged immediately after gelation at heights of: **A** 45 μm and; **B** 185 μm. **C** Illustration of cellular layered sheet, here, the lower yellow droplets would contain HEK-293/YFP whilst the upper blue droplets would contain DR stained HEK-293/CFP. **D**-**E** Composite bright-field and fluorescence micrographs of the layered cell sheet in aqueous, imaged at heights of **D** 40 μm and; **E** 180 μm, showing conserved layers. **F**-**G** Side on 3D projections of the layer cell sheets in: **F** print oil and; **G** culture medium, demonstrating layered cellular patterning is conserved through phase transfer.

The 3D projections of the layered sheets scaffold in oil showed that these layers were fairly even (**Figure 3.28 F**). Once in culture medium, the layers were less uniform with the

lower layer appearing stretched at the right hand side of **Figure 3.28 G**. This signified that the basic printed pattern was mainly conserved, with only a slight loss in fidelity. It should also be noted that the scaffolds in medium should appear as clear images. This was due to the refractive index of the gel and the bulk phase being similar and the loss of internal lipid bilayers which cause droplets to act like lenses. Consequently more cells in the upper layer of the layered sheets were visible in scaffolds within culture medium than when they were in oil (**Figure 3.28 F,G**).

With the ability to print layered cellular sheets at high resolution (i.e. with layers 150-200 μm thick) we printed a bone-cartilage junction (n = 5) out of pre-differentiated chimeric sheep and mouse cells (**Figure 3.29**). Such architectures are found in joints, here, articular cartilage coats the bone and acts as a cushion between the two bones allowing them to move. DR stained murine chondrocytes were printed below RC stained ovine osteoblasts (**Figure 3.29 A,B**). Once again cells were printed at high vertical resolutions (**Figure 3.29 C**), with layer thicknesses of 120 μm (lower) and 176 μm (upper). When this scaffold was phase transferred the network flexed, but still managed to retain the topology of chondrocytes laminated to osteoblasts (**Figure 3.29 C**). However, layered cell sheets can be transferred with better pattern retention as demonstrated in **Figure 3.28 G**, as such the bone-cartilage junction needs to be repeated to improve the interface.

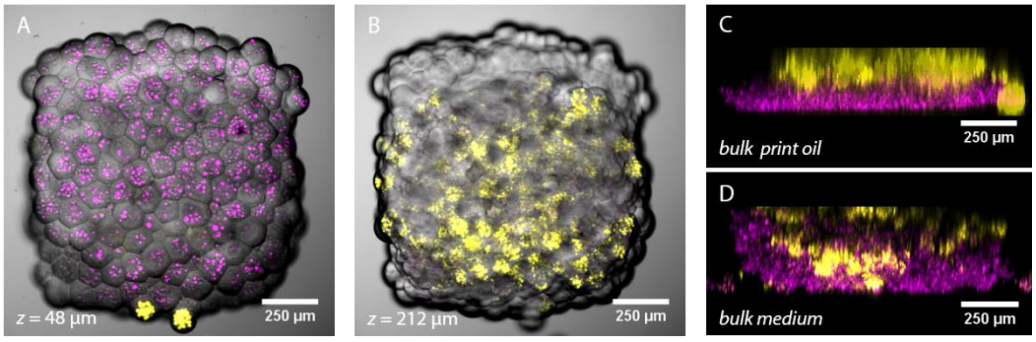

Figure 3.29 Printed scaffold with bone-cartilage junction architecture. **A**-**B** Composite bright-field and fluorescence micrographs of printed bone-cartilage junction (lower: 7×9×4 droplets; upper: 6×7×4 droplets, n = 5) composed of DR stained murine chondrocytes (purple) below RC stained ovine osteoblasts (yellow). Scaffolds were imaged post gelation at heights of **A** 48 μm and; **B** 212 μm and showed distinct cell-laden layers. **C**-**D** Side on 3D projections of the cell patterned scaffold in: **C** bulk print oil and; **D** bulk culture medium, demonstrating that the murine osteoblasts remained laminated on the ovine osteoblasts.

These layered sheet scaffolds demonstrate the high resolution patterning of cells in the vertical axis, with layers as thin as 150 μm. With this technique a native bone-cartilage architecture representative of articular tissue was printed. Thus this technique can be employed to pattern two cell-types in native tissue architectures. These architectures can also be printed with cell types that would not naturally come together, to create tissue chimeras composed of cell populations that originated from different organisms.

3.10 Conclusions

This chapter described the adaption of the droplet-in-oil 3D printer developed in Chapter 2 into a 3D bioprinter of cell patterned scaffolds. It was conceived that cell-laden droplet networks could be utilised as scaffolds for tissue development as there was the potential to pattern cells within droplet compartments at high spatial resolution. Preliminary tests proved cells could be ejected as cell-laden droplets and assembled to form droplet networks with compartmentalised cells. However, the resulting networks had non-uniformly distributed cells and were prone to intra-network coalescence over time.

As such cell patterning was optimised; cell-laden networks were first stabilised towards coalescence by excluding FBS from and incorporating Fmoc-dipeptides into the bioink. PEG 400 was also added to the bioink as a thickening agent, causing the cells to be suspended more homogeneously within the nozzle and demonstrating viscous solutions could enable high density cell printing. PEG supplementation also allowed cells to be patterned more homogeneously as nozzle leakage was significantly reduced. These optimised printed cell patterned scaffolds contained hundreds or thousands of cells at high initial cell viabilities (88%). The print resolution was found to be very high for the Fmoc-dipeptide supplement bioink, giving 40-60 μm diameter droplets containing an average of 3-4 cells. During print, cells were observed to concentrate in the nozzle's tip giving scaffolds with up to 20-fold increased densities (relative to overall bioink concentration), with cells present in the printed network at high densities of 2×10^7 to 4×10^7 cells/mL. Thus these printing characteristics signified that our 3D bioprinting

technique had the potential to fabricate cell patterned scaffolds with viable cells, patterned such that they could proliferate into a functional tissue.

The optimised cell patterned scaffolds were still prone to intra-network coalescence over time and also displayed dehydration, resulting in pattern loss and cell death. A phase transfer method was then developed to relocate the cell patterned scaffolds into a culture medium, promoting culture conditions. An ULGT agarose based bioink was developed that allowed the high droplet resolution (ø 120-150 μm) printing of cellular containing scaffolds, which retained their cellular pattern post gelation. To ensure that the structure of the printed droplet networks and thus the cellular pattern was retained throughout transfer, it was necessary to coat the gelled network with an exterior stabilising gel to prevent the structure from collapsing. Phase transfer standardisation allowed the transfer of gel coated scaffolds predominantly without loss of the printed cellular pattern or reduction in cell viability. As a consequent of our technique the internal lipid bilayers of the scaffolds were disrupted, allowing small dye molecules to penetrate the structure and enter the cells. Therefore transferred cell-patterned scaffolds were likely to be permeable to small nutrient molecules of culture medium, enabling the culture of patterned cells (Chapter 4)

To exemplify the capability of this new technique, two fluorescent cell populations were patterned with tissue-like architecture at high feature resolution. A capillary styled scaffold was printed with a bifurcating cellular pathway, which had an average width of 180±60 μm. This demonstrated that bioprinting can be performed at a horizontal feature resolution of 2-3 droplets wide. Layered cell sheets composed of two cell populations were also printed, with high resolution layers of 130-220 μm height. These patterned features can also be conserved throughout transfer if sufficiently gel coated as demonstrated by the layered sheets and the cruciform patterned scaffolds. However, phase transfer was unsuccessful for the arborised structure which was not coated sufficiently, indicating further optimisation of the process is necessary. Lastly it was demonstrated that native tissue architectures were also patternable as epitomised by the fabricated bone cartilage junction made as a chimera of sheep and mouse cells.

Overall a high resolution 3D bioprinting technique was developed that was used to fabricate patterned cell scaffolds with tissue-like architectures. The ability to grow functional tissues from the internal cells was subsequently investigated and described in Chapter 4.

4 Biological Assessment of Patterned Cells

4.1 Chapter Abstract

This chapter describes the culture of patterned cells within printed scaffolds fabricated using the printing and phase transfer techniques of Chapter 3. Biological characteristics, specifically life and proliferation, of patterned cells after culture were subsequently investigated. Furthermore the ability to grow cells from patterns of two cell populations was explored within printed constructs composed of layered cell sheets over 5 days culture. Finally chondrogenesis was induced in ovine mesenchymal stem cells (oMSCs) patterned within printed constructs as demonstrated by Sox-9 expression.

4.2 Publications

At the time of this thesis submission, our work on fabricating cell-patterned droplet networks for tissue development has been submitted for publication.

Provisional title: High-resolution patterned cell networks by 3D droplet printing.

4.3 Acknowledgment of Collaboration

All work included in this chapter was performed by the author unless specifically stated in the text. The author would like to acknowledge the practical and intellectual input of **Dr Sam Olof** (University of Oxford) who supervised the work. Research on oMSCs and their derivatives was conducted in collaboration with **Madeline Burke** and **Dr James Armstrong** (both University of Bristol) who maintained the cells prior to printing and performed digital PCR analysis of oMSC patterned scaffolds. The proliferation study of cell-patterned scaffolds was aided by **James Nicholson** (University of Oxford) and Dr Sam Olof who immunostained 3D cultured HEK-293T and oMSC patterned scaffolds.

4.4 Introduction

The culture of 3D cell patterned scaffolds is a process that could produce cellular structures which exhibit tissue properties. This method maybe adapted to fabricate tissues in vitro for tissue replacement of damaged organs, or to produce microtissues which could be used as healthy or diseased tissue models, potentially to screen reagents in a high throughput manner.

For the development of functional living tissue from cell patterned constructs, cells need to be able to proliferate into native tissue morphologies[9]. The development of cellular organisations/tissue within the construct will be influenced by the original cellular pattern. In a printed cell containing construct, the cells are patterned within a material i.e. scaffold, which is typically hydrogel based. Consequently their culture invites additional considerations compared to standard 2D cell culture methodologies. These considerations include overcoming the nutrient diffusion limit and providing an optimal environment for proliferation and differentiation, and the ability for the environment that can be remodelled by the growing cells[29].

The nominal diffusion limit is based on vascularised tissue, where cells are typically found 100–200 μm from the nearest capillary. Cells within this region can effectively exchange nutrients, gases and waste products with the blood[173]. It has been shown that large tissues grown without vasculature become hypoxic, and subsequently form necrotic regions, as epitomised by necrotic cores of tumour tissues and spheroids[87]. To prevent necrotic regions developing within the growing tissue, the cell patterned construct needs to be fabricated either within the diffusion limit (200 μm) or containing perfusable microchannels[35,36].

To create an optimal growth environment the material of the cell patterned construct needs to be tailored for the cell type that is patterned. In addition to being non cytotoxic, the material needs to be porous to allow nutrient exchange and ideally should present cell adhesion sites to encourage cell polarisation, migration and proliferation[29]. Bioprinted cell patterned constructs are frequently prepared using a blend of extracellular matrix (ECM) proteins or biological ligands based on ECM proteins to

encourage cell adhesion within the scaffold[9]. The stiffness of the hydrogel also affects cell adhesion along with migration and differentiation. Therefore the material of the bioink are usually selected or tuned to be within a suitable stiffness range to mimic tissue environments[31].

Lastly, it should be possible for proliferating cells to remodel the construct, otherwise the construct would impede or prevent full tissue development. Ultimately for cell patterned scaffolds intended for regenerative medicine applications, such as in vivo implants, the cell-laden construct needs to be able to degrade at a similar rate to host ECM production[29]. Thus if all these criteria are fulfilled then cells within tissue engineering scaffolds should be able to proliferate into tissue structures.

In Chapter 3 we developed a method for fabricating cell patterned constructs with high cell densities and high feature resolution. Subsequently, in this chapter, we have developed a method to culture these cell patterned scaffolds accounting for the considerations described. The biological characteristics of 3D patterned cells after culture were studied, specifically life and proliferation. To investigate the feasibility of developing complex tissues from patterns of two-cell populations, cellular layered sheets were cultured over 5 days. Finally the ability to print multipotent oMSCs within a construct and induce their differentiation was investigated.

4.5 Culture of 3D Cell Patterned Scaffolds

The ability to phase transfer cell patterned scaffolds, fabricated by the 3D droplet printing technique outlined in Chapter 3, enabled the culture of patterned cells over an extended period of time. It was our goal to culture patterned cells within constructs such they grew into structures exhibiting desirable tissue properties. The tissue properties to be investigated were the ability of the cells to, sustain viability, and proliferate into tissue-like densities and respond to growth factors i.e. be induced to differentiate.

Employing typical 2D cell culture methods on our printed constructs would have resulted in the cell-laden scaffold being lost. Specifically, the scaffold would be aspirated into the micropipette tip during culture medium exchanges, due to the inability of the

printed construct to adhere to the culture vessel's substrate. Consequently, we designed a 3D culture method based around the non-substrate-fixed printed constructs and employed it to study the cellular development of preliminary printed and control cell constructs.

4.5.1 3D Culture Methodology

Throughout this chapter the patterned cells studied were fabricated using the printing and phase transfer techniques outlined in Chapter 3. These cell patterned scaffolds were composed of patterned cells in **scaffold solution 6** (**SS6**) i.e. an ultra-low gelling temperature agarose (ULGT-agarose) and **Fmoc-XX** hydrogel. Agarose fulfils the requirements of 3D cell-laden scaffold culture, i.e. it is, non-cytotoxic, porous and in the stiffness range of tissues (see *section 3.8.2.1*). It does not however contain biological ligands which act as cell adhesion sites, thus ECM proteins were latterly blended into the scaffold solution (see *section 4.6.2*). Scaffolds were also fabricated to be within or close to the diffusion limit, with structures being typically 1.1×1.1×0.4 mm^3, thus the internal cells were never more than 200 μm away from the nutrient supply.

A demonstration of the porosity of the printed construct was the observation that when calcein-AM (CAM) and propidium iodide (PI) could be incorporated from the bulk culture medium into the bound cells (previously described in *section 3.8.5*). It was thus inferred that other small molecules could traverse the construct and could be exchanged with the cell, but potentially not larger molecules like proteins. Thus the cells should be able to exchange some of necessary nutrient and waste molecules for culture, and more importantly allow the exchange of O_2.

Cell patterned scaffolds were cultured within microscope chamber slides (**Figure 4.1 A**), which could hold an approximate volume of 1 mL per well. The patterned cells were typically grown in 300-600 μL of culture medium, with the chamber left in an ideal culture environment i.e. a cell incubator set to 37 ºC and 5% CO_2. The culture medium would be exchanged every 2-3 days (**Figure 4.1 B**). Here, due to the lack of adhesion to the substrate of the chamber, the printed construct could easily be aspirated by the

micropipette if the chambers volume became too low. Therefore the culture medium exchange involved the repeated, removal of old/mixed culture medium and addition of fresh culture medium, with the well's volume never falling below 300 µL (**Figure 4.1 B**).

The printed constructs were imaged within these containers, allowing the study of tissue development (**Figure 4.1 A**). It was expected that the patterned cells would grow from individual single cells into clusters of cells, which would, further proliferate, connecting with neighbouring cell clusters forming dense cellular masses.

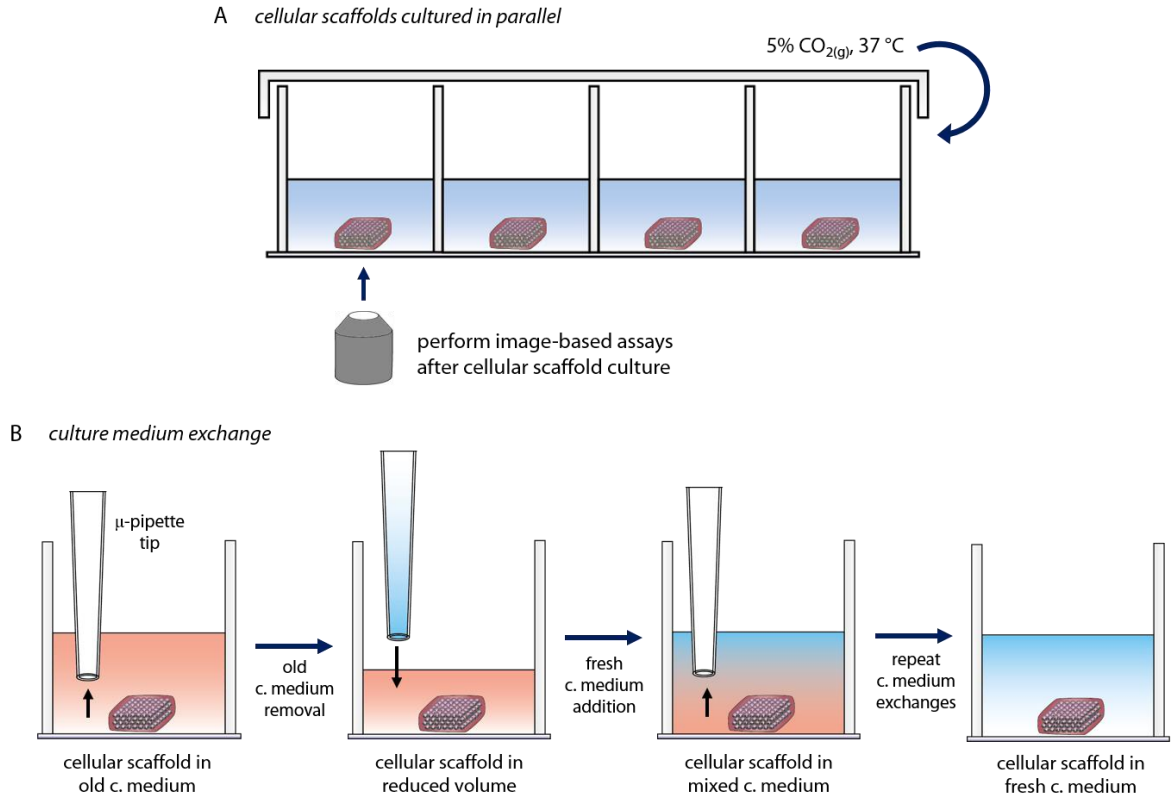

Figure 4.1 Schematic of the 3D culture of cell patterned constructs. **A** Cell patterned constructs were cultured within a multi-well microscope chamber slide at 37 °C with 5% CO_2. The base of the chamber was glass and allowed bottom-up visualisation of scaffolds by microscopy enabling the study of tissue development. **B** Culture medium exchanges for cell patterned constructs were performed every 2-3 days as illustrated. Old and mixed culture medium is partially removed from the well and replenished with fresh culture medium. This is repeated until the culture medium is predominantly fresh medium.

Initially, cells were cultured in culture medium containing foetal bovine serum and GlutaMAX™ (**initial cell scaffold culture medium**), as this was standard culture medium for HEK-293T cells. However, additional supplements were latterly added to ensure cells

would have optimised growth. The **standard cell scaffold culture medium** was additionally supplemented with antibiotics (penicillin and streptomycin), buffering agent (HEPES) and additional nutrients (non-essential amino acids). These extra supplements, prevented bacterial infection and pH drifting, and additionally accelerated the initial cell proliferation.

Due to their small size, printed constructs were easily perturbed by fluidic flow created by micropipette action. Consequently it was possible to break the printed construct if too much flow was generated. However, with correct handling, cell patterned scaffolds retained their structure throughout the culture duration.

4.5.2 Preliminary Culture of Printed Constructs

To investigate if cells patterned within printed constructs could proliferate, preliminary HEK-293T ($n = 2$) and oMSC ($n = 4$) patterned constructs were cultured and imaged over a week (**Figure 4.2**). Here phase transferred constructs (**Figure 4.2 A**,**E**) were cultured in **initial cell scaffold culture medium**, and the same printed construct was live/dead assayed over the culture duration.

The preliminary results showed viable cell signals throughout the cellular pattern on day 0 (**Figure 4.2 B**,**F**). After 5 days HEK-293T scaffold showed mostly dead cell signals (**Figure 4.2 C**), and viable signals fell further by day 7 (**Figure 4.2 D**). Similarly the oMSC scaffold also showed a decline in viability over the week (**Figure 4.2 G,H**), however, here some of the viable signals were coming from objects sized 35-45 um wide, indicating that patterned cells either migrated together or proliferated. For both scaffolds the hydrogel structure was retained over culture, with the cells remaining in roughly their original pattern.

Scaffolds viability were analysed for live/dead assays by counting cells in ImageJ[134,135], using the plug-in *3D Object Counter*[174,175], which counts discrete objects within a *z*-stack image. This software was used to count the number of live and dead objects within a scaffold (**Figure 4.3 A**) and each object was treated as a single cell. The counted values were subsequently used to calculate a scaffold viability (**Figure 4.3 B**).

The preliminary scaffolds on day 0 displayed 358 HEK-293T cells and 370 oMSC cells (**Figure 4.3 A**). The initial viabilities were calculated to be 65% (HEK-293T) and 78% (oMSC) (**Figure 4.3 B**). Over the culture duration the HEK-293T scaffold displayed a decline in the number of living cells and a rise in dead cells (**Figure 4.3 A**). As there was an overlap of live and dead signals for the HEK-293T scaffolds on day 3 and 6, the number of counted living cells here was probably an over estimate. Thus the HEK-293T viability was probably lower than the calculated value i.e. lower than 38% by day 7 (**Figure 4.3 B**). With oMSC patterned constructs the oMSC's viability also dropped over time, falling to 32% on day 6 (**Figure 4.3 B**).

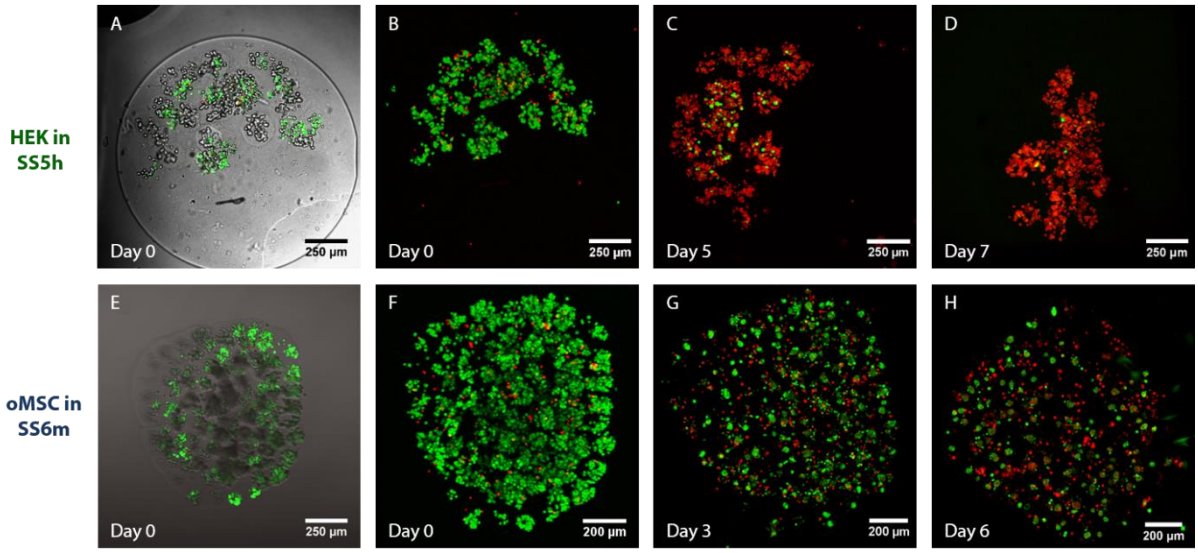

Figure 4.2 Preliminary culture of printed cell patterned scaffolds over 7 days. **A**-**H** Live/dead stained cell patterned scaffolds composed of: **A**-**D** HEK-293T at 8×10^6 cells/mL in **SS5h**; and **E**-**H** 5×10^6 oMSC/mL in **SS6m**. **A**,**E** Composite bright-field and fluorescence confocal micrograph of scaffolds in culture medium post phase transfer. **B**-**D**,**F**-**H** 3D projections of live/dead channels over a week's culture at time points: **B** day 0; **C** day 5; **D** day 7; **F** day 0; **G** day 3 and; **H** day 6. Over the culture duration the live signal declines whilst the dead signal increases.

In the 3D projections of the scaffolds (**Figure 4.2**) it can be seen that the live cell count was likely underestimated for the day 0 counts and the oMSC counts. This was a consequence of the living cells being initially joined or growing as small clusters (oMSC day 3 and 6), and resultantly these clusters were counted as a single object rather than individual cells. Due to the object count being unable to resolve connected live cells, there

was the inclusion of viability error bars which represent viabilities determined with twice and half as many live cells as counted. This gave positive and negative error bars of ~15% viability.

Even though the viability dropped, the fact that viable oMSC aggregates formed by day 6 indicated that scaffolds potentially showed some, albeit limited, proliferation. Alternatively, scaffold cells may have either migrated into aggregates or fused together to form syncytia i.e. cells with ≥2 nuclei. Consequently, printed scaffolds could feasibly be cultured so long as the culture process was optimised.

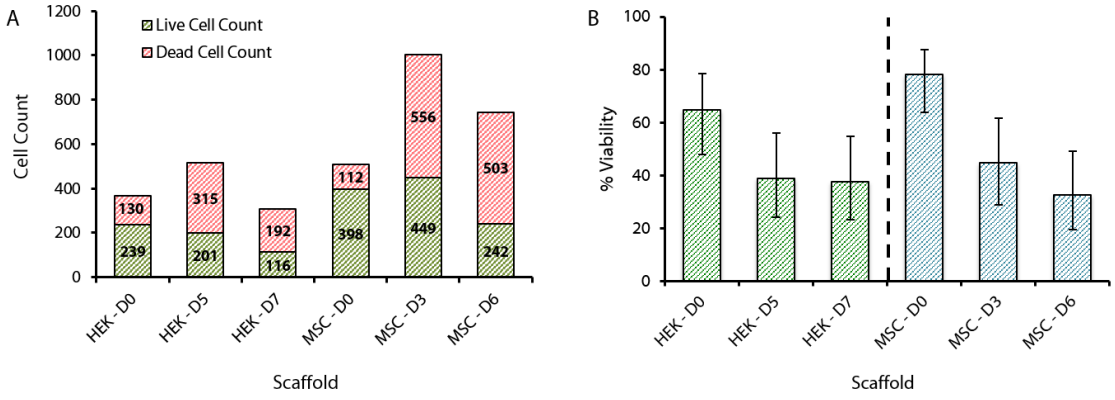

Figure 4.3 Viabilities of preliminary 3D cultured scaffolds. **A** Stacked column chart of automatedly counted live (**green**) and dead (**red**) cells of preliminary HEK-293T and oMSC scaffolds depicted in *Figure 4.2*. **B** Column chart of calculated viabilities for HEK-293T (**green**) and oMSC (**blue**) preliminary scaffolds using live/dead count of **A**. Over a week's culture there was a decline in the scaffolds viabilities.

4.5.3 Culture of Control Constructs

It was uncertain whether the viability decay of preliminary scaffolds was due to the scaffold solution or the culture methodology. To investigate the cytocompatibility of the scaffold solution, non-printed HEK-293T scaffold controls were cultured. Hydrogel-block controls were made to study the ability of HEK-293T to proliferate in the scaffold solution as a bulk hydrogel phase. Whilst hydrogel-sphere scaffolds, made as droplets under oil and phase transferred to medium, were performed to investigate the effects of the oil and phase transfer process on cellular proliferation within printed constructs.

4.5.3.1 HEK-293T Culture in Hydrogel Blocks

To investigate the effects of the components of the scaffold solution on cellular proliferation, control hydrogel blocks were cultured in parallel for four days (**Figure 4.4**). Here the control "hydrogel-blocks" were composed of the scaffold solution gelled on the surface of the culture chamber and thus were never in contact with any oil. The scaffolds solutions under study were **SS6h** and **SS5h**, i.e. ULGT-agarose with or without **Fmoc-XX** respectively. This was to elucidate whether the presence of **Fmoc-XX** influenced cell proliferation.

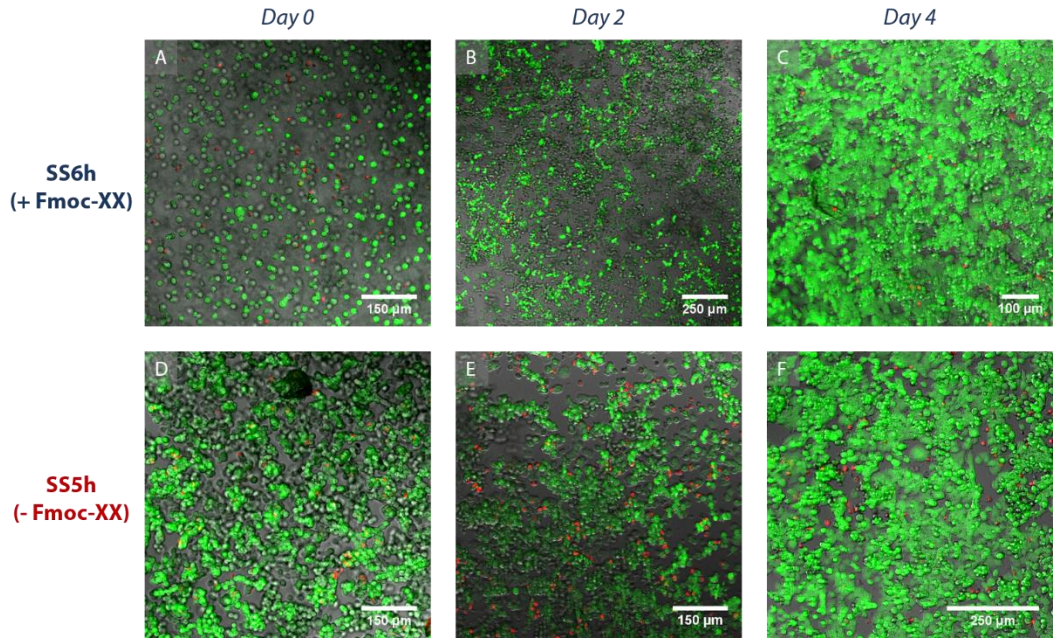

Figure 4.4 Control 3D culture of HEK-293T in hydrogel blocks. **A**-**F** Composite bright-field and fluorescence confocal micrographs of HEK-293T blocks scaffolds live/dead assayed over 4 days culture. The blocks were composed of 5×10^6 cells/mL in **A**-**C** ULGT agarose with **Fmoc-XX** (**SS6**) and **D**-**F** ULGT-agarose only (**SS5h**). Scaffolds ($n = 3$ per time-point) were imaged on: **A**,**D** day 0; **B**,**E** day 2 and; **C**,**F** day 4 Over the 4 days there was an increase in cellular density for both scaffold solutions.

The viability of HEK-293T within the hydrogel-blocks was assessed by live/dead staining the scaffold on day 0, 2, and 4 (**Figure 4.4**), using a separate blocks ($n = 3$) for each time point. On day 0 HEK-293T cells displayed low dead cell signals (**Figure 4.4 A**) and appeared as either single cells or small cell clusters (**Figure 4.4 D**). Over a 4 day period

most cells appeared viable, with increased cell density (**Figure 4.4 C,F**). As the density of cells was significantly higher by day 4, with the viable signal appearing confluent in certain areas, it was inferred that the cells were proliferating within the scaffold and the control study was stopped. Due to a lack of increasing dead signal with respect to time, it was established that the scaffold components did not inhibit growth and were therefore unlikely to be cytotoxic.

As there was a low dead cell signal throughout the culture, it was assumed that the scaffold solutions were not cytotoxic. Furthermore the live cell signal increased to confluency in places, indicating the scaffold environment was ideal for growth. The cellular viability and proliferation in the **SS6h** and **SS5h** samples were also similar indicating that the **Fmoc-XX** had a low influence of cellular proliferation. Thus the decline in viabilities in the preliminary experiments was unlikely due to the composition of the scaffold solution and was likely another factor.

4.5.3.2 HEK-293T Culture in Hydrogel Spheres

It was possible that the oil and the phase transfer process could have contributed to the declining viabilities, to elucidate this, HEK-293T were cultured in control hydrogel spheres. The spheres were made in a similar manner to printed scaffolds, i.e. hydrogel droplets were made under oil, gel coated and then phase transferred. Thus, the live/dead assay of sphere controls would reveal whether the oils were detrimental to subsequent cell culture.

Cell-laden droplets were made between 0.15 to 0.20 μL volumes resulting in droplets with diameters of ~600-700 μm, i.e. producing structures larger than the tissue diffusion limit. Similarly to previously discussed hydrogel block controls, the scaffolds were composed of either **SS6h** or **SS5h**. These control scaffolds ($n = 3$ per time-point) were cultured over 4 days and a scaffold previously unimaged was imaged on days 0, 2, and 4 (**Figure 4.5**). Over the course of culture, both scaffold formulations showed high viable cell signals and increased cellular mass as a likely result of proliferation, but could also in part be a result of cell migration (**Figure 4.5**).

It could be seen for the **SS6h** spherical scaffolds, that rounded cells of ø ~15 µm were distributed as discrete units (**Figure 4.6 A**). Within 2 days these grew into small circular morphologies sized between ~24 and ~33 µm diameter (**Figure 4.6 B**), and after further growth, these connected forming large clusters with widths of up to 77 µm (**Figure 4.6 C**). Whereas for the Fmoc-dipeptide free scaffolds, the HEK-293T formed clusters of cells which connected together by day 2 (**Figure 4.5 E**) and by day 4 these cells had outgrown from the scaffold and onto the chamber's surface (**Figure 4.5 F**).

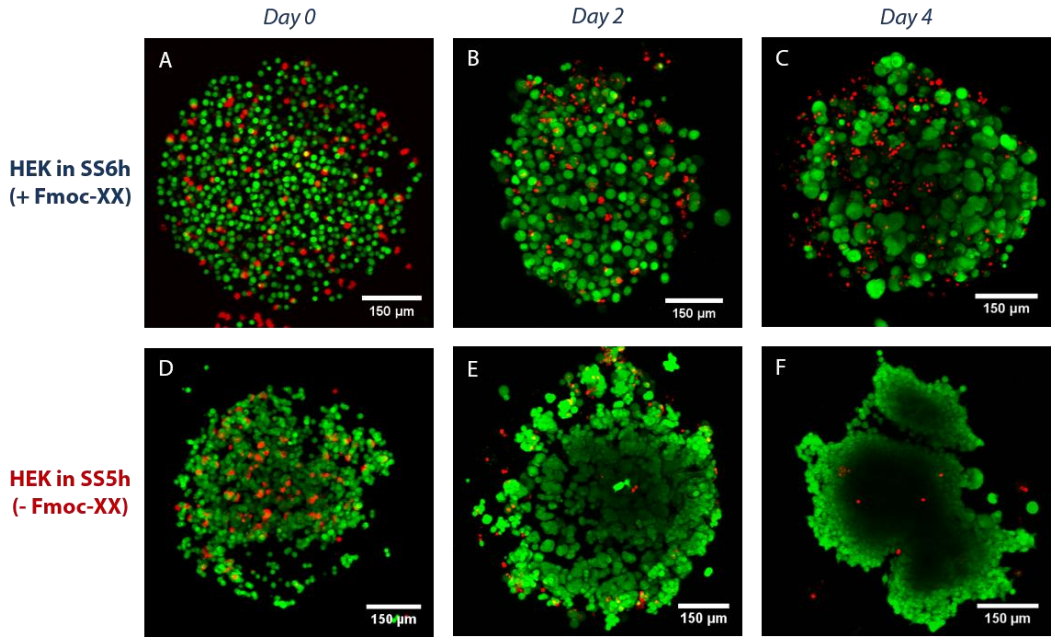

Figure 4.5 Control 3D culture of HEK-293T in spheres. **A**-**F** 3D projections of live/dead cell stained HEK-293T spherical scaffolds over 4 days culture. The spheres were composed of 5×10^6 cells/mL in **A**-**C** ULGT agarose with **Fmoc-XX** (**SS6h**) and **D**-**F** ULGT-agarose only (**SS5**). Scaffolds were imaged on: **A**,**D** day 0; **B**,**E** day 2 and; **C**,**F** day 4. Over the 4 days the majority of cells proliferated into dense cellular masses but also showed cell death owing to un-optimised handling techniques.

The number of live and dead cells was determined for scaffolds by automated object counting (**Figure 4.6 D**). Once again a diminishing viability was observed, with the **SS6h** sphere declining from 71% to 30% viability (**Figure 4.6 E**). Here, throughout the culture there were always >100 counted dead cells, as a result of un-optimised culture. Additionally the number of counted live cells decreased (**Figure 4.6 D**), even though there was observed proliferation (**Figure 4.6 A-C**). This underestimated live cell count was due

to cell aggregates being counted as 1 cell by the automated object counter. In reality the volume of the aggregates where the size of multiple cells, with the volume of day 2 cell clusters equivalent to 2-3 cells and day 6 aggregates were the equivalent volume of 5-6 cells. With this taken into account, corrected viabilities should be around 80% for day 2 and 4 in the **SS6h** based scaffolds. With the **SS5h** scaffolds the calculated viabilities showed a viability rise for day 6, due to very few dead cells being present. However, even this was an underestimate as only 45 live cells were counted for a structure that clearly contained hundreds of cells.

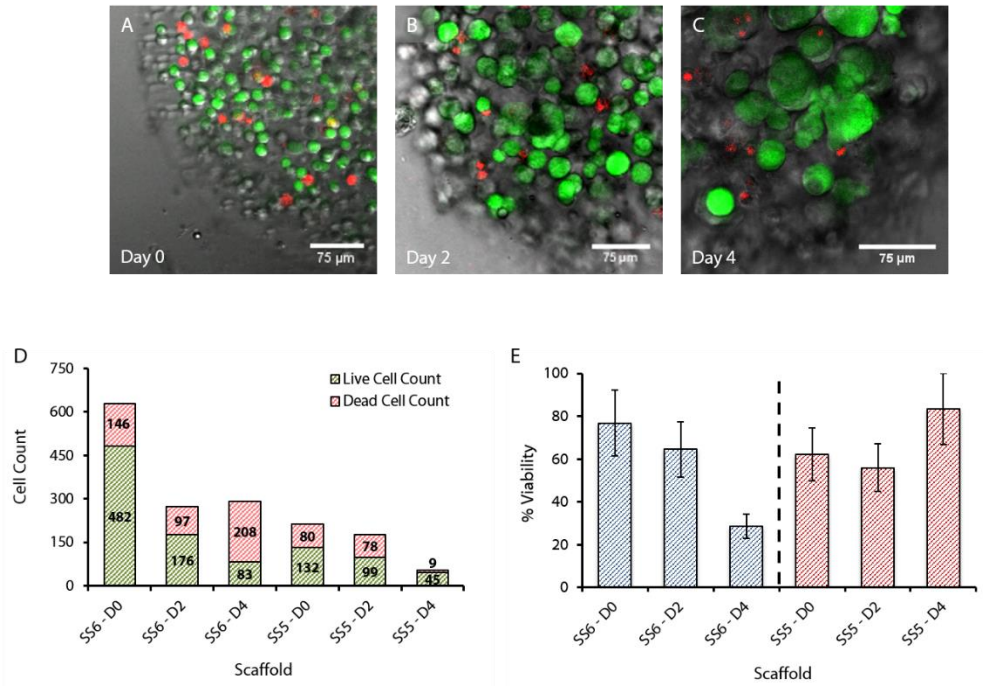

Figure 4.6 Cell morphologies & viabilities of HEK-293T in control sphere scaffolds. **A**-**C** Composite bright-field and fluorescence confocal micrographs of HEK-293T cellular morphologies within live/dead stained spherical scaffolds on: **A** day 0; **B** day 2 and; **C** day 4. Here, **A**-**C** are the same scaffolds as depicted in *A*-*C* of *Figure 4.5*. **D** Stacked column chart of live (**green**) and dead (**red**) cells automated counted for control HEK-293T scaffolds displayed in *Figure 4.5*. **E** Column chart of calculated viabilities for HEK-293T spheres composed of either **SS6h** (**blue**) or **SS5h** (**red**) using live/dead count of **D**. Over 4 days of culture there was a calculated decline in the viabilities, even though cellular proliferation was observed.

Overall the controls showed internal cellular proliferation over a 4 day period, reaffirming the scaffolds is an optimal growth environment and also the phase transfer process is non detrimental. Thus the reason for declining viabilities in the preliminary

controls was attributed to either piezo induced necrosis, poor cell handling or time away from ideal culture conditions.

4.5.3.3 Culture of Piezo Dispensed HEK-293T Cells

The final culture control investigated whether piezo dispensed cells were damaged during the droplet ejection process leading to cell death. As such HEK-293T suspended in **SS6h** and **SS5h** were loaded into the droplet generator and ejected as droplets through air into culture medium (n = 1 print per bioink, data not shown). These cells showed high initial viabilities (~84%) which were maintained after two days, with cells polarising onto the chamber slides surface. It was inferred that the generation of droplets was not detrimental to cells. As such it was concluded that the reason for the viability decline in the culture of preliminary printed scaffolds was down to poor culture techniques, poor cell handling or time away from ideal culture conditions.

4.6 3D Culture Optimisation

To be able to reproducibly culture cell patterned scaffolds such that their patterned cells proliferated, the culture process was optimised. The optimisation involved adapting the scaffold solution through increasing the cell density and the introduction of biological cell adhesion sites in the form of blended ECM proteins. Additionally, the culture methodology was adapted, including how cells were cultured in parallel.

4.6.1 Bioink Cell Density

In healthy tissues, cells are cohered through tight junctions and can also communicate to each other through gap junctions. It was hypothesised that if more cells were initially in contact within a scaffold, the more cell-cell interactions would be present initially and the faster a tissue would mature. As such, over the course of experimentation, the scaffold solution's cell density was raised from 5×10^6 to 15×10^6 cells/mL, with 15×10^6 cells/mL becoming the standard concentration. It was empirically discovered that as the bioink's

cell density increased, more cells were contained per printed droplet and the more initial cell-to-cell contacts were present.

To characterise the number of cells encapsulated per printed droplet, HEK-293T scaffolds (n = 2 per condition) were printed at different cell densities: 1×10^6, 5×10^6, 10×10^6 and 15×10^6 cells/mL (**Figure 4.7 A-D**). It was observed that for bioinks of $\geq5\times10^6$ cells/mL, the cells sank within the nozzle and concentrated in the tip within 10 min. Consequently high number of cells were manually counted (generally >20) within each droplets of the resultant networks. Using 25 droplet measurements, an average number of cells per droplet was determined (**Figure 4.7 E)**. It was found that average number per droplet showed a roughly linear increase from 1×10^6 to 10×10^6 cells/mL prints, which then levelled out for 10×10^6 to 15×10^6 cells/mL prints. For the highest density print (15×10^6 cells/mL), scaffold droplets contained an average of 38±8 cells ($\bar{n}$ ± s.d., n = 25 network droplets) and had an average size of 135 μm diameter.

The scaffold density was calculated as a function of the average number of cells per average volume of printed droplets, and was plotted against bioink cell density (**Figure 4.7 F**). Here it can be seen that the initial bioink cell density was concentrated in the nozzle's tip 2-4 fold, resulting in high cell density droplets. Except in the case of the 1×10^6 cells/mL print where the cells were ejected at roughly the density of the bioink. This was due to the cells being sparsely distributed within the bioink as discrete items and as they did not clump, they were unable to sink fast enough to concentrate. Whereas with the higher bioink cell density prints the total scaffold concentration plateaued at ~30×10^6 cells/mL, demonstrating the cells concentrated to a maximum density within the nozzle's tip. As such bioinks more cell dense than 10×10^6 cells/mL, won't display an increase in scaffold cell density, however, the abundancy of cells to print will increase.

Within the droplets made from high cell density bioinks, i.e. those containing 5 to 10×10^6 cells/mL, it was found that most encapsulated cells were adjoined to one or multiple neighbouring cells forming clumps (**Figure 4.7 D**). These droplets contained cells at densities at the same order of magnitude as some soft tissues including certain mammalian brain tissues[176]. At these initial scaffold densities (30×10^6 cells/mL) it would

only take cells two to three doubling events to reach 10^8 cells/mL i.e. the density range for cardiac tissue[177]. Additionally the final number of cultured scaffold cells can be estimated. For example, a scaffold composed of 224 droplets (of ø 130 µm) containing cells at 15×10^6 cells/mL, would, after 3 doubling events, proliferate from the 3,865 printed cells to 30,920 cultured cells.

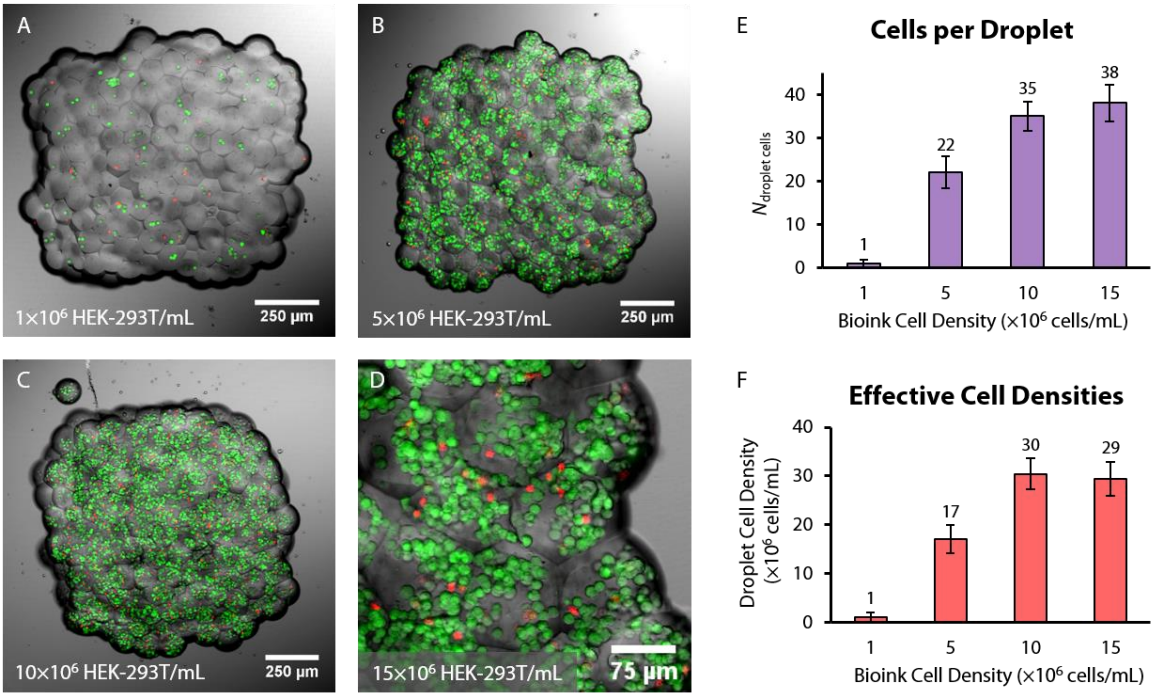

Figure 4.7 Optimisation of bioink cell density. **A**-**D** Composite bright-field and fluorescence confocal micrographs of HEK-293T scaffolds printed at different bioink cells densities: **A** 1×10^6; **B** 5×10^6; **C** 10×10^6 and; **D** 15×10^6 cells/mL. Scaffolds were composed of **SS7h** containing live/dead dyes and were imaged post print whist in bulk oil. Images are magnified to view: **A**-**C** whole scaffold or **D** compartmentalised cells within droplets. **E** Column chart of average cell number per droplet for scaffolds **A**-**D** calculated from manual counts, here the average droplet sizes were: **A** 120; **B** 135; **C** 130 and; **D** 135 µm diameter. **F** Column chart of effective cell densities for scaffolds **A**-**D** calculated as the cell density of the average cell-laden droplet. Error bars represent standard deviation of cell count (**E**) and compound error of count deviation and droplet volume deviation (**F**).

4.6.2 ECM Supplementation

4.6.2.1 ECM Protein Supplemented Scaffold Solution

To provide biological ligands within the scaffold for the cells to adhere to, the scaffold solution was supplemented with either collagen type I, laminin or fibronectin. These are

common ECM proteins that have been shown to bind to integrins, mediating cellular polarisation and proliferation. Collagen, a fibrous protein, was selected as it is the most abundant protein in the ECM and has been commonly used as cellular scaffolds[38]. Laminin, the major component of the basal lamina, is a high molecular weight protein, and was selected due to its extensive culture of a variety of cells including neuronal stem cells[178]. Finally fibronectin a high-molecular weight glycoprotein containing the integrin binding RGD motif was chosen as it is a common cell culture substratum shown to promote the attachment and subsequent spreading of many cells.

The ECM proteins were blended into ULGT-agarose and Fmoc-dipeptide containing **SS6** at low concentrations. These scaffold solutions were tested to see if they could co-gel and whether droplet generation was affected compared to **SS6**. Scaffold solutions were prepared either as control solutions that omitted ECM proteins (**Scaffold Solution 7** (**SS7**)) or ECM protein blended solutions (**Scaffold Solution 8** (**SS8**)). Here, **SS7** and **SS8** were composed of 10.4-12.0 mg/mL agarose, i.e. at a diluted agarose concentration compared to **SS6**. Once cell culture was standardised, **SS8** was always supplemented with 15 μg/mL collagen type I. As before, the base culture medium of these scaffold solutions was Opti-MEM® for HEK-293T scaffolds (**SS7h** and **SS8h**) and **DMEM-ITS** for oMSCs scaffolds (**SS7m** and **SS8m**).

4.6.2.2 Gelation of ECM Protein Supplemented Scaffold Solution

To test if the ECM protein blended **SS8** could co-gel, inverted vial tests were performed on gelled **SS8h** solutions comprised of a range of ECM concentrations, which were intentionally very low (**Figure 4.8 B**). This was to avoid a large volume of ECM gel forming within the scaffold solution and disrupting the agarose gelation. It was hypothesised that cell proliferation would still be aided at very low concentrations, as there would be a small proportion of ECM with which the cells could bind to, and subsequently begin synthesis of their own ECM.

The ECM concentrations employed were, similar to or below, the lowest gelation concentration of the supplemented ECM. Specifically collagen's lowest concentration for

gelation was 0.3 mg/mL, whilst laminin and fibronectin are used as cell culture substrates, plated at 0.5-50 μg/mL. Thus the tested concentration ranges for co-gelation were 15-300 μg/mL for collagen type I and 0.5-10 μg/mL for laminin and fibronectin.

The inverted vial tests on the different **SS8h** blends demonstrated that the solution co-gelled across the ranges studied (**Figure 4.8 B**). However, it appeared that the ECM protein supplemented gels were slightly softer (as they deformed more in the tubes) than the un-supplemented control (i.e. **SS7h**). Thus it was concluded that the supplemented ECM proteins minimally affected the gelation of ULGT-agarose.

4.6.2.3 Printability of ECM Protein Supplemented Scaffold Solution

To investigate the printability of **SS8h**, a blend of each ECM protein was printed in **bioink print oil** and then gelled (**Figure 4.8 A-C**). The scaffold solution was supplemented at either 300 μg/mL collagen type I, 10 μg/mL laminin or 10 μg/mL fibronectin, i.e. the highest ECM concentrations tested in the preceding section. It was found that all the scaffold solutions printed well and could form tightly packed networks (n = 2-3 per bioink, **Figure 4.8 A-C**).

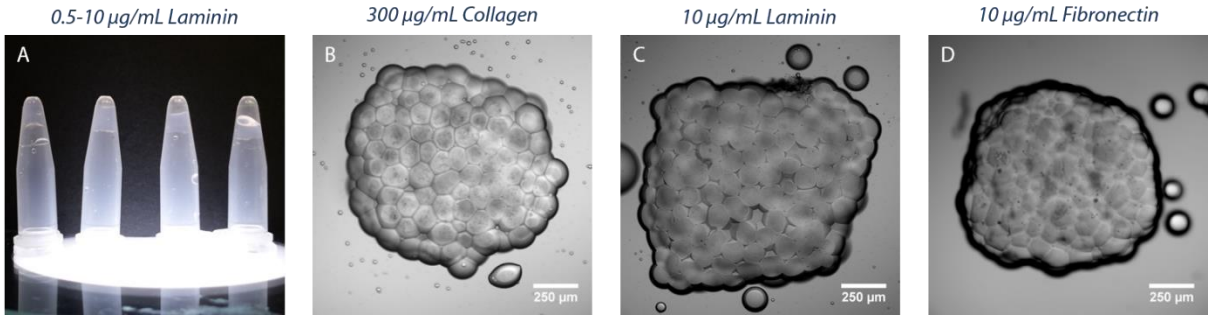

Figure 4.8 ECM protein supplemented bioink tests. **A** Photograph of inverted vial test for laminin at concentrations: 10, 2, 1 and 0.5 μg/mL (from left to right). **B**-**D** Bright-field confocal micrographs of droplet networks composed of **SS8h** supplemented with either: **B** 300 μg/mL collagen type I; **C** 10 μg/mL laminin and **D** 10 μg/mL fibronectin. As depicted, ECM proteins supplemented scaffold solutions co-gelled and were compatible with the printing process.

4.6.2.4 Culture of HEK-293T Scaffolds Containing Collagen

To investigate whether collagen type I supplementation could improve the viability and proliferation of printed HEK-293T cells, HEK-293T patterned scaffolds were produced and live/dead assayed after culture. Here, scaffolds (n = 2) was assembled by printing 10×10^6 cells/mL in 300 μg/mL collagen type I supplemented **SS8h** and then cultured over 6 days (**Figure 4.9**).

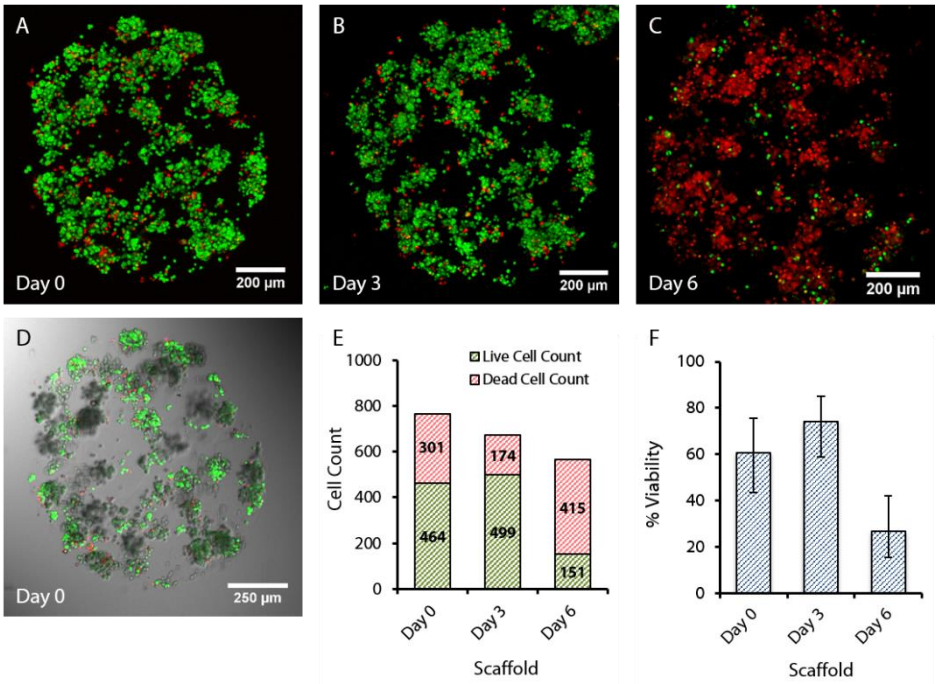

Figure 4.9 Live/dead assay of collagen supplemented HEK-293T scaffold. **A**-**C** 3D projections of live/dead cell stained HEK-293T scaffolds supplemented with 300 μg/mL collagen type I over 6 days of culture. The scaffold was imaged on: **A** day 0; **B** day 3 and; **C** day 6. **D** Composite bright-field and fluorescence confocal micrograph of HEK-293T scaffold post phase transfer; here the scaffold contains non-uniformly patterned cells. **E** Stacked column chart of automatedly counted live (**green**) and dead (**red**) cells of collagen supplemented HEK-293T scaffolds (displayed in **A**-**C**). **F** Column chart of calculated viabilities for HEK-293T scaffolds using live/dead count of **E**. It was observed that the viability slightly rose after 3 days and then fell by day 6.

During the scaffold print, the nozzle's tip alternated between either being full of cells and containing no cells. Essentially the nozzle's bioink composed of bands of dense cell aggregates and cell free scaffold solution. During the cell aggregate bands, high voltage pulses (≥59 V) were necessary to form droplets, which were densely packed with cells (**Figure 4.10 A**). When cells were not present the voltage had to be reduced to ~40 V, as

very large volume droplets (ø >160 μm) were formed. To ensure that printed scaffold composed of mainly cell laden droplets, when the non-cellular band began in the nozzle's tip, the cell-free solution was removed; this was by raising the capillary out of the oil and absorbing the solution into a medical wipe.

As a consequent to the presence of non-cellular bands, the network had regions of non-cell containing droplets and was not uniformly patterned (**Figure 4.9 A,D**). Within the scaffold, spherical cell aggregates were observed and corresponded to dense cell-laden droplets ejected during the print (**Figure 4.10 A**).

Viability was found to be retained in the collagen supplemented scaffold after 3 days of culture (**Figure 4.9 B**), with the scaffold looking almost identical to how it did in day 0. However, by day 6 the scaffold had showed high necrosis (**Figure 4.9 C**), with the viability calculated to be 27% (**Figure 4.9 F**). The automated object count recorded 765 counted cells post phase transfer on day 0 (**Figure 4.9 E**) giving a viability of 61% (**Figure 4.9 F**). The viability rose to 74% on day 3 (**Figure 4.9 F**) due to a slight increase in the number of live cells and a large decrease in the number of counted dead cells. In reality, the day 3 viability is probably similar to day 0 as seen visually in **Figure 4.9 A-C**. Here, the apparent increase in counted live cells was probably due to the presence of a scaffold fragment in upper right hand corner. Whereas the decrease in dead cells was likely a result of the initial dead cells disintegrating, resulting in fewer cells with available nuclei to stain.

In the process of scaffold phase transfer, some fragments ($n > 5$) sheared off and were estimated to be composed of 2-6 printed droplets. These fragments were subsequently cultured 6 days without imaging. After culture it was observed that cells had proliferated into a dense cellular mass within the fragment (**Figure 4.10 B**). Live/dead staining showed that the cellular mass was mainly viable and was composed of many smaller budding aggregates (**Figure 4.10 C**). To investigate if the cells of the scaffold fragment had healthy biological activity a sample ($n = 1$) was stained using immunocytochemistry (ICC) (**Figure 4.10 D**).

ICC was performed on the day 6 cellular mass/scaffold fragment by James Nicholson and Dr Sam Olof. The scaffold was stained with DAPI, anti-phospho-histone H3 antibodies and anti-vimentin antibodies (**Figure 4.10 D**). DAPI is a nuclear dye that can pass through cell membranes but is commonly used on fixed samples and is used to stain live cell nuclei. Phospho-histone H3 (PH3) staining, colours the chromatin in cells undergoing chromosome condensation for mitosis. Specifically the antibodies bind to phosphorylated Ser10 residues of the H3 histones that make up the histone octameric nucleosomes. Finally, vimentin, a natural cytoskeletal protein found in HEK-293T and other cells, was stained to check for regular cell function.

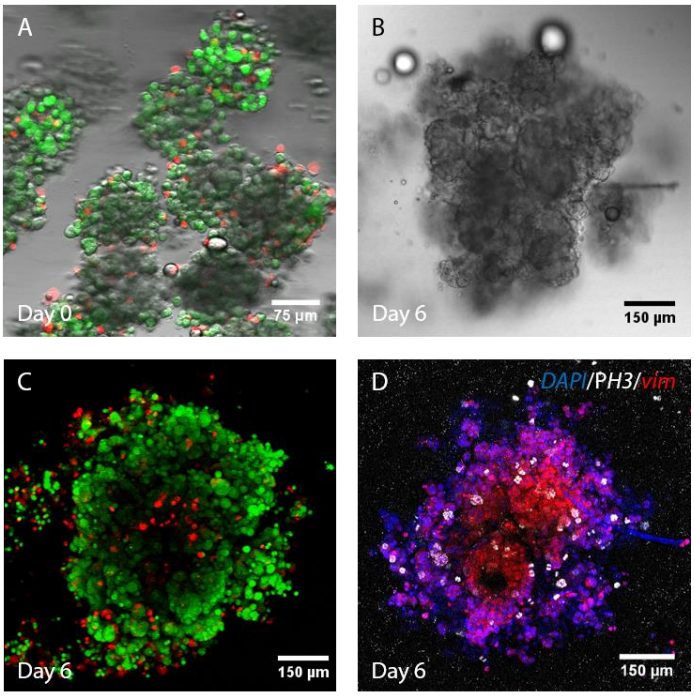

Figure 4.10 HEK-293T morphologies within collagen supplemented scaffolds. **A**-**D** Images of cellular morphologies of HEK-293T within scaffolds supplemented with 300 µg/mL collagen type I over 6 days of culture. **A** Composite bright-field and fluorescence confocal micrographs of cell aggregate laden droplets within scaffold at day 0. **B**-**D** HEK-293T scaffold fragment after 6 days of culture visualised as: **B** bright-field confocal micrograph; **C** 3D projection of live/dead stained cells and; **D** 3D projection of immunostained cells. **D** cells were stained with DAPI (**blue**); anti-phospho-histone 3 antibodies (**white**) and anti-vimentin antibodies (**red**). Over 6 days the scaffold fragment had formed a dense cellular mass showing mitotic cells. ICC staining was performed by James Nicholson and Dr Sam Olof.

The ICC staining showed fluorescent nuclei and vimentin signal throughout, indicating cells were viable with regular cell function and mitosis (**Figure 4.10 D**). PH3 stained

scaffolds were found to contain 28 cells undergoing mitosis by automated object counting. This was calculated to be a 1% proportion of cells within the scaffold fragment that were mitotically active (see *section 4.7.3*). Thus, the tissue mass demonstrated healthy biological activity and it was inferred that the scaffold fragment had proliferated over the 6 days.

Due to healthy proliferation being observed within the cellular fragment, collagen type I was kept as a standard supplement within the bioink. The supplement was reduced to 4-15 μg/mL, attaining practical prints where cells were present homogenously rather than fragmented into cellular bands.

4.6.3 Modified Culture Methodology

4.6.3.1 Repeated Culture

In an attempt to get HEK-293T scaffolds to mature from cellular scaffolds into tissue constructs, scaffolds fabricated from the modified bioink (i.e. **SS8**) were repeatedly cultured using the initial method. It was thought that the combination of high cell density and ECM protein supplementation would enhance viability and proliferation.

Although many HEK-293T scaffold sets (n = 10) were cultured, all attempts showed a decline in cell viability even with ECM proteins present. **Figure 4.11** shows the typical viability trace over 6 days of culture, for scaffolds supplemented with and without collagen type I. Cell-patterned scaffolds could be produced with high average viabilities of 82% (**Figure 4.11 A,E**) which dropped to 50% average after 3 days of culture (**Figure 4.11 B,E**) and then plummeted to 25% average by day 6 (**Figure 4.11 C,E**).

Whereas the scaffold controls of *section 4.5.3* had shown cellular proliferation, but were not repeatedly imaged over the course of culture like printed scaffolds. As such a printed cell-patterned scaffold (n = 1) was intentionally left to culture for 7 days without imaging to see if cellular proliferation could be enhanced (**Figure 4.11 F**). This day 7 scaffold contained cells with high viabilities of 86%, unlike the cellular viability of multiply imaged cell-patterned scaffolds of the same composition (**Figure 4.11 A-C**). This

was a significant discovery as it indicated that the multi-imaging process was far more detrimental to cells than initially speculated. Extended radiant energy exposure is phototoxic to cells through the generation of reactive oxygen species or cell heating[179]. Consequently our cells were damaged during imaging through a combination of extended radiant energy exposure (up to 30 min per construct) and time away from culture conditions (up to 90 min).

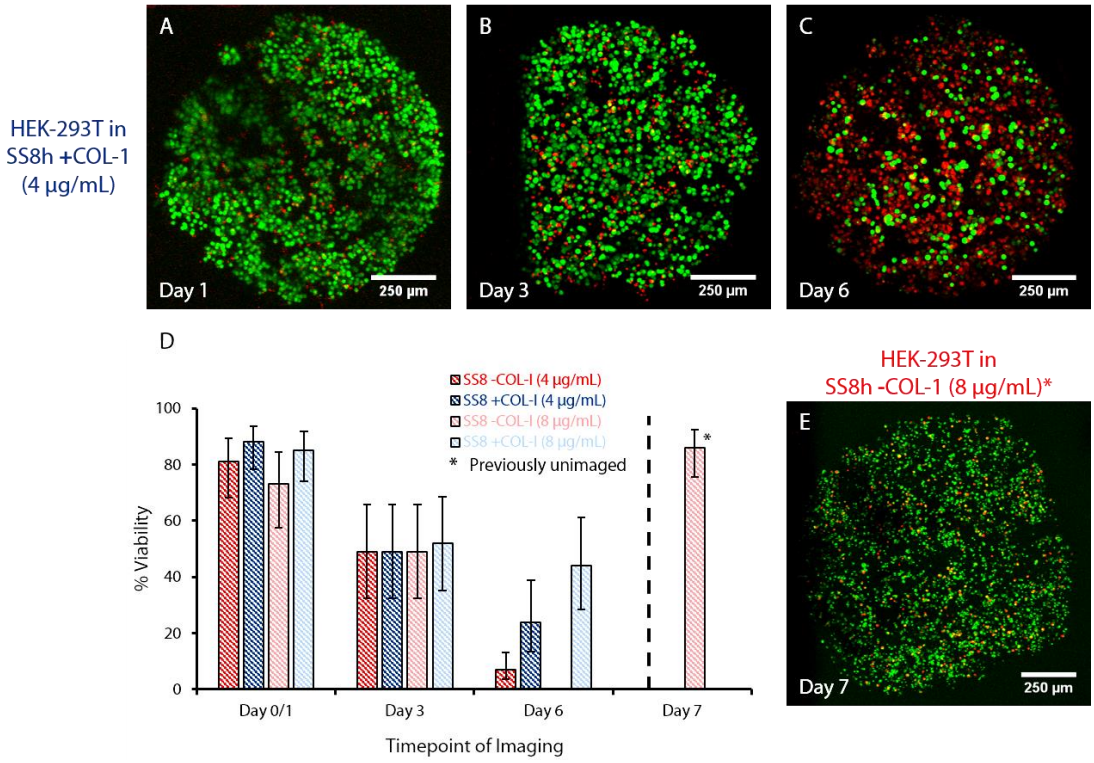

Figure 4.11 Declining viability trends for scaffolds cultured using the initial culture method. **A-C** 3D projections of live/dead cell stained scaffolds composed of HEK-293T at 14×10^6 cell/mL in **SS8h** supplemented with 4 µg/mL collagen type I over 6 days. **D** Column chart of viabilities for four cultured scaffolds composed of HEK-293T in **SS8h** supplemented with either: 4 µg/mL collagen type I (**dark blue**), 8 µg/mL collagen type I (**light blue**) or no collagen (as controls for: 4 µg/mL collagen (**dark red**) and; 8 µg/mL collagen (**pink**) scaffolds). All chart viabilities are calculated from automated cells counts of a single scaffold imaged at different time points, except for the day 7 scaffold, which was previously unimaged. **E** 3D projection of live/dead cell stained scaffold composed of HEK-293T at 15×10^6 cell/mL in **SS8h** supplemented with 8 µg/mL collagen type I on day 7 and previously unimaged.

The unimaged scaffold at day 7 still appeared with discrete single cells and did not show signs of internal cellular proliferation. As this scaffold was cultured in the same microscope chamber as other scaffolds imaged over 7 days, it had experienced the same

environment as its neighbouring scaffolds, but not the microscope's laser irradiation. It was inferred that the irradiation damaged and slowly caused cell death. Additionally, it was also concluded that the time spent outside of an ideal culture environment was detrimental, with cells potentially being damaged by the pH dropping around the scaffold during the imaging duration (0.5-1.5 h). As such, a new optimised culture method was designed which meant scaffolds would only be imaged once.

4.6.3.2 Optimised Culture

The optimised culture method involved limiting the time spent outside ideal culture environments and restricted the scaffold to being imaged once. This was by separating the set of printed cellular scaffolds into different culture chambers, with each chamber corresponding to a single imaging time point for the viability assay. This avoided scaffolds, to be imaged at a later time point, being removed from ideal culture environments during the microscopy duration. The optimised culture also saw the introduction of HEPES, penicillin and streptomycin, and non-essential amino acids to the culture medium, with the final composition referred to as **standard cellular scaffold culture medium**.

To test the optimised culture method, HEK-293T-laden spheres composed of **SS8h** containing different mixes of the ECM proteins, collagen type I, fibronectin and laminin (n = 3 per formulation), were cultured for 7 days (**Figure 4.10**). By day 7, spheres displayed significant cellular proliferation internally, with the scaffold becoming opaque due to the high cell density (**Figure 4.12 A,E**). Live/dead cell staining indicated that the spheres contained viable cells throughout, with dead cells mainly present at the centre of the sphere. As such it can be inferred that the cell aggregates become thicker than the 200 μm diffusion limit, experience low oxygen conditions and become necrotic.

There was some variances in the day 7 cellular topologies, with the scaffold being composed of either, multiple small aggregates (**Figure 4.12 D**) or a few large continuous tissue clumps (**Figure 4.12 H**). As cells cultured within each scaffold solution blend demonstrated high viability and high proliferation, it appeared that none of the ECM

protein supplements were better suited for HEK-293T. Furthermore, the proliferation was so pronounced that cellular outgrowths from the spheres was noticed in all cases, with the migratory cells subsequently forming 2D structures on the chamber's surface. It was concluded that the optimised culture method allowed the proliferation of HEK-293T patterned within scaffolds and should be suitable for future printed cellular scaffolds.

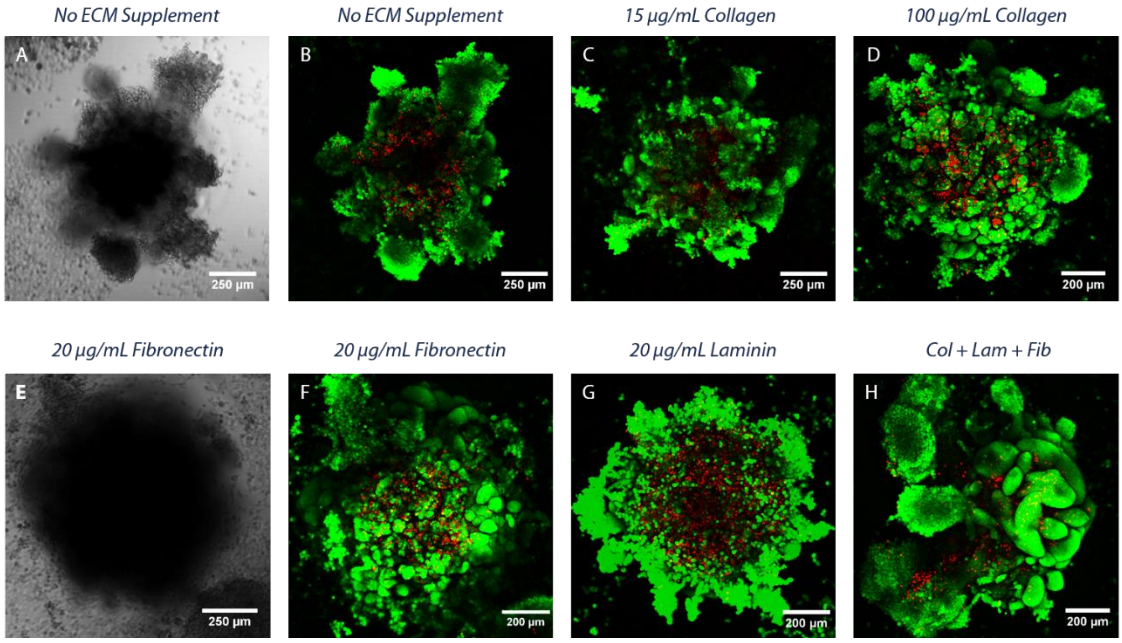

Figure 4.12 Optimised culture of HEK-293T in ECM protein supplemented spheres. **A**-**H** Images of HEK-293T spherical scaffolds after 7 days of culture. **A**,**E** Bright-field confocal micrographs of cultured spherical scaffolds, showing dense cellular masses. **B**-**D**,**F**-**H** 3D projections of live/dead cell stained of cultured scaffolds, showing large viable signals and dense cellular morphologies. Spheres were made with 10×10^6 cells/mL supplemented with different ECM proteins: **A**,**B**; none; **C** 15 µg/mL collagen type I; **D** 100 µg/mL collagen type I, **E**,**F** 20 µg/mL fibronectin, **G** 20 µg/mL laminin and **H** a mix of 15 µg/mL collagen type I, 10 µg/mL laminin and 10 µg/mL fibronectin.

4.7 Proliferation Study

The optimised culture method was employed to investigate the ability of printed HEK-293T scaffolds to develop into tissue constructs over seven days. The proliferation of HEK-293T was investigated by live/dead assays and ICC staining. Additionally the cell counting methodology was modified to give more accurate cell counts for day 0 HEK-293T and oMSC containing scaffolds.

4.7.1 Optimised HEK-293T Scaffold Culture

To confirm that printed HEK-293T patterned scaffolds were compatible with the optimised culture methodology a set of printed scaffolds ($n = 5$) and sphere scaffolds ($n = 4$) were fabricated and cultured for 7 days, with scaffolds imaged on day 7 only (**Figure 4.13**). Here the scaffolds were composed of 15×10^6 cells/mL in **SS8h,** supplemented with 15 μg/mL collagen type I. Additionally, to prove multiple-imaging events were detrimental to printed HEK-293T development, a printed cellular scaffold ($n = 1$) was imaged on day 0 and then day 7.

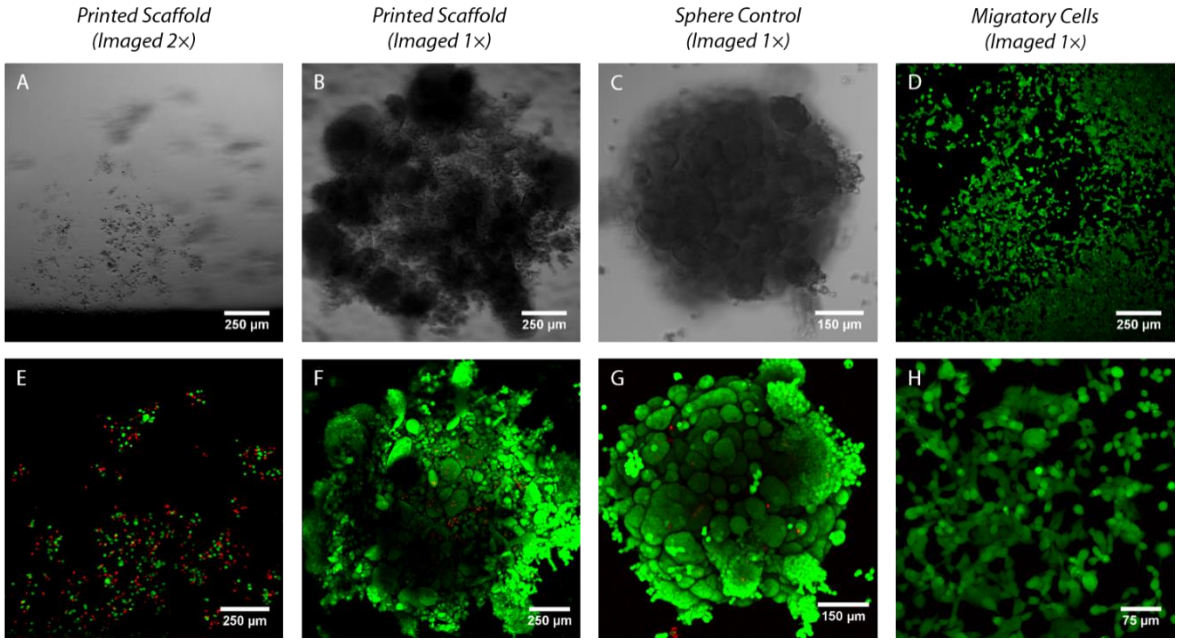

Figure 4.13 Optimised 3D culture of HEK-293T scaffolds on day 7. **A**-**H** Images of HEK-293T scaffolds after 7 days of culture, with each scaffold initially composed of 15×10^6 cells/mL in **SS8h** supplemented with 15 μg/mL collagen type I. **A**,**E** Printed HEK-293T patterned scaffold that was previously imaged on day 0, showed arrested development on day 7. **B**,**F** Printed HEK-293T patterned scaffold previously unimaged, proliferated into a dense cellular mass and showed high viability. **C**,**G** Sphere control scaffold containing HEK-293T, previously unimaged also showed cellular proliferation and high viabilities. **D**,**H** In wells of cultured scaffolds which were previously unimaged, the cells had additionally migrated out of the scaffolds and formed 2D structures on the glass base. Images were: **A**-**C** bright-field confocal micrographs; **D**,**H**, fluorescence confocal micrographs and **E**-**G** 3D projections of live/dead stained cells.

The printed scaffold on day 0 showed a high initial HEK-293T viability of 90% (calculated by the resolved count method, see *section 4.7.4*). After 7 days culture this scaffold had been sheared, resulting in pattern loss (**Figure 4.13 A**,**E**). Regardless, the viability of the

twice imaged scaffold was still assessed, and was found to have dropped to 48% and consequently no cells had proliferated. Whereas the scaffolds, imaged for the first time on day 7, showed large cellular proliferation giving rise to dense cellular masses within the scaffold (**Figure 4.13 B**,**C**). These proliferated scaffolds were live/dead cell stained, revealing very high viabilities with few dead cells (**Figure 4.13 F**,**G**). This observation was found for all once imaged, printed and sphere scaffolds, with each scaffolds composed of multiple large aggregates joined together. These cell morphologies were similar to sphere controls for the ECM protein blends. Cells had also migrated out of the scaffold and formed 2D morphologies on the glass surface of the culture chamber (**Figure 4.13 D**,**H**). Consequently, some scaffolds where difficult to resolve as they were resting on these 2D colonies.

Additionally, a printed HEK-293T patterned scaffolds which was imaged on day 7 was aspirated and transported into a new culture chamber, in which it was cultured till day 13 day (data not shown). By day 13 the structure was a fragment of the original scaffold, and unlike day 7 samples, did not appear as a continuous tissue, but instead as discrete smaller aggregates. ICC staining of the structure revealed 2% of cells were about to enter mitosis, indicating the cells were still biologically active after two weeks culture.

Significantly, the optimised culture of printed scaffolds showed that scaffolds in medium where biologically active, retaining viability and were cultured such that they consumed nutrients and proliferated into dense cellular masses. A control experiment also demonstrated how imaging a scaffold can arrest further cellular development and cause slow cell death. Employing the optimised culture method on printed scaffolds, thus allowed patterned cells to proliferate into tissue like densities. Therefore this method should be compatible with different cell types making it a powerful technique for fabricating a range of tissues.

4.7.2 HEK-293T Proliferation Over 7 Days

To better understand the cellular development within a cultured scaffold, printed HEK-293T laden scaffolds were cultured for a 7 day period and then live/dead assayed on

days 3 (n = 4), and 7 (n = 5). Three to four printed scaffolds were produced for each time point, and once again scaffolds were composed of 15×10^6 cells/mL in **SS8h** supplemented with 15 μg/mL collagen type I.

All cultured cell-laden scaffolds showed cellular proliferation and high viability over their culture period. Scaffolds on day 3 and 7, showed the square cellular patterns had proliferated into a roughly square, dense cellular masses (**Figure 4.14**). These structures showed viable cell signals throughout the structure with only 10s of dead cells present (**Figure 4.14 D-F**). The growth of patterned cells, starts from spherical cells (*size* = ø 15 μm) initially distributed as discrete single entities (**Figure 4.14 G**). Over 3 days culture the cells had proliferated into small spherical aggregates, the majority of which were ~30 μm diameter, but some aggregates had joined to give clusters up to 70 μm wide (**Figure 4.14 H**). Furthermore, cellular scaffolds left to culture for 7 days showed advanced cellular proliferation with the majority of aggregates sized >50 μm wide, and up to 140 μm wide (**Figure 4.14 I**). The development of cells within the scaffolds to these high packing densities is analogous to the formation of tissue morphologies.

The results demonstrate that patterned cells could be cultured over 7 days, with the cells proliferating into dense cellular masses, which still represented the patterned shape. Cells appeared to multiply from their original positions and formed smaller aggregates which became connected with further growth. In one day 7 scaffold, cells had grown outside of the scaffold and the pattern was lost. Such outgrowth may prevented in the future by incorporating an alternative exterior hydrogel which is non-adherent for cells, causing the tissues to retain their patterned cellular structure. Alternatively, culture could be slowed or stopped after seven days so that tissues retain their desired structure.

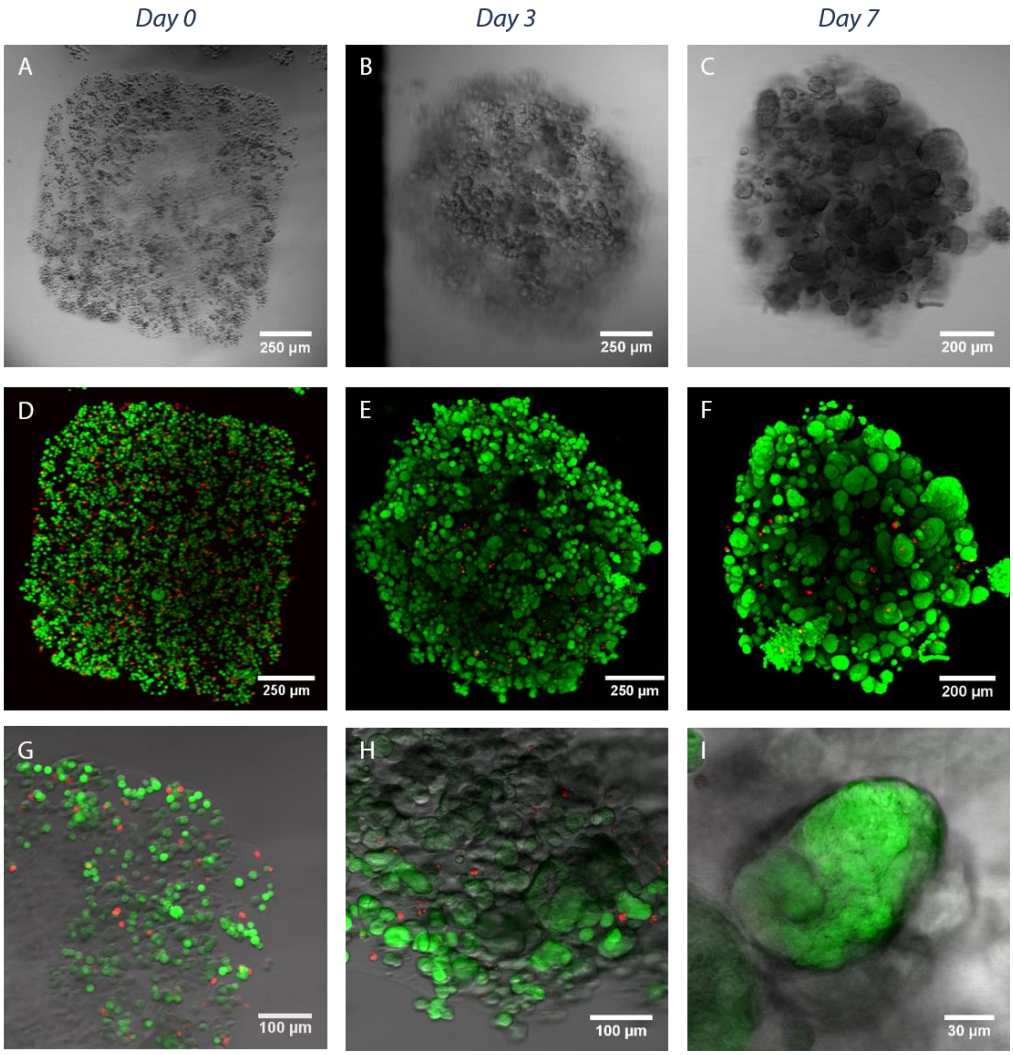

Figure 4.14 Development of HEK-293T printed scaffolds over 7 days. **A-I** Images of individual printed HEK-293T scaffolds over 7 days of cell culture, here scaffolds were printed as 15×10^6 cells/mL in **SS8h** supplemented with 15 µg/mL collagen type I. Scaffolds were imaged on day 0 (left-hand column), day 3 (middle column) and day 7 (right-hand column). **A-C** Bright-field confocal micrographs of scaffolds, here the scaffold becomes dark and opaque over 7 days as the cells proliferated. **D-F** 3D projections of live/dead cell stained scaffolds, indicating a high viability throughout the course of culture. **G-I** Composite bright-field and fluorescence micrographs of scaffolds, showing the cells proliferate from individual entities to dense cell clusters.

4.7.3 Immunostaining of HEK-293T Constructs

To further support the evidence that printed HEK-293T were biologically healthy and showed intrinsic cellular properties after culture, the metabolism of HEK-293T was investigated (**Figure 4.15**). As bulk metabolic assays, such as the colorimetric MTT assay, did not scale well for cell numbers below 50,000 cells, they were unsuitable for analysing printed scaffolds composed of thousands of cells. Consequently we developed our own

metabolic assay involving the ICC staining of printed scaffolds. Here, scaffolds cultured to day 3, and 7 in *section 4.7.2* were ICC stained after live/dead assays by James Nicholson and Dr Sam Olof.

Scaffolds were stained with nuclear dye DAPI and mitotic marker anti-phospho-histone H3 antibodies (see *section 4.6.2.4*). Scaffolds on day 3 (**Figure 4.15 A**) and day 7 (**Figure 4.15 B,C**) showed DAPI signals throughout the structure, indicating cells were healthy throughout. They also showed an even distribution of cells undergoing GII/M transition of mitosis across the structure, indicating the cellular aggregates were still proliferating.

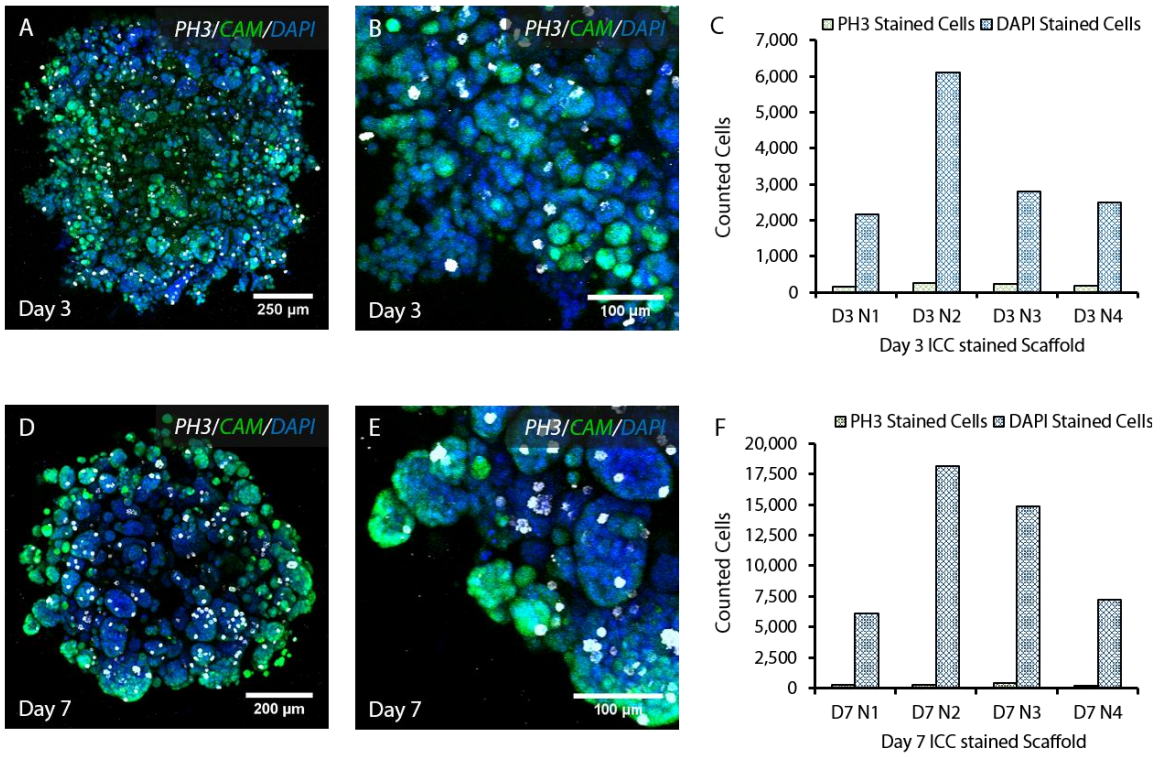

Figure 4.15 Immunostained printed HEK-293T scaffolds after 3D culture. **Left hand and middle column** 3D projections of independent HEK-293T scaffolds immunostained after culture. These scaffolds were printed as 15×10^6 cells/mL in **SS8h** supplemented with 15 µg/mL collagen type I. Cells were stained with DAPI (**blue**); anti-phospho-histone 3 antibodies (**white**) and calcein-AM (**green**). **A**,**D** Images of whole scaffold on: **A** day 3 and; **D** day 7. **B**,**E** Magnified sections of scaffolds showing cellular morphology on: **B** day 3 (scaffold **A**) and; **E** day 7 (scaffold **D**). **Right hand column** Column charts of counted cells within ICC stained scaffolds on: **C** day 3 and; **F** day 7. Plotted here are the resolved counts of DAPI stained cells (**blue**) and the unmodified counts of PH3 stained cells (**green**). ICC staining was performed by James Nicholson and Dr Sam Olof.

The proportion of scaffold cells undergoing mitosis was determined as the fraction of mitotic cells compared to the total number of cells. The mitotic cell number was measured by automated object counting. Whilst the total number of cells was treated as the total number of DAPI stained cells, also counted. Here the DAPI stained cell count was resolved against the average volume of a DAPI stained cell. The measured cell counts and the calculated proportion of mitotic cells in the scaffold can be seen in **Table 6.15** of *section 6.11.6.4*.

Evidence for the proliferation of cells within printed scaffolds can be seen by the increase in the number of counted DAPI cells on day 3 compared to day 7. Scaffolds on day 3 were estimated to contain an average of 3,400±1,600 cells ($\bar{x}$±s.d., n = 4), which rose to 11,600±5,100 cells ($\bar{x}$±s.d., n = 4) cells for day 7 scaffolds (n = 4). This is a 3.4 fold increase, equivalent to almost two HEK-293T doubling events over four days. This may indicate that the average double time of HEK-293T cells in 2D culture (~24 h), has been lengthened due to the scaffold environment.

Scaffolds also showed a healthy proportion of mitotically active cells. It was calculated that in the day 3 scaffolds on average 7.0±1.4% ($\bar{x}$±s.d., n = 4) of scaffold cells were about to undergo mitosis (**Figure 4.15 C**). Whilst for day 7 scaffold this decreased to a 2.6±0.8% ($\bar{x}$±s.d., n = 4) proportion of mitotic cells (**Figure 4.15 F**). As only a low proportion of cells will be undergoing mitosis at any time, it is unsurprising that the day 3 scaffolds exhibit 7% mitotic activity. Whereas the day 7 scaffolds showed a slightly low proportion of mitotically active cells. It could be possible due to the enhanced growth, that the PH3 signals were harder to resolve via microscopy on day 7. Consequently the mitotic proportion may be underestimated. Alternatively the day 7 scaffolds may exhibit a lower proportion of mitotically active cells. This could be the cells adapting to the reduced space for cellular growth caused by the high cellular density.

4.7.4 Initial Viabilities of Scaffolds

The automated object counting methodology employed in previous sections (*4.5.2, 4.5.3.2, 4.6.2.4* and *4.6.3.1*) generally resulted in an underestimate of scaffold cell numbers

giving rise to unrepresentative viabilities. To calculate more accurate viabilities, a method of resolving the automated object counts was devised. Here, each counted object's volume was divided by the size of the average live or dead cell of that scaffold. Using this method the cell viabilities of scaffolds immediately after phase transfer were determined for HEK-293T-laden scaffolds ($n = 5$) and oMSC-laden scaffolds ($n = 5$, see *section 6.11.6.3*). These viabilities can be seen summarised in **Figure 4.16**.

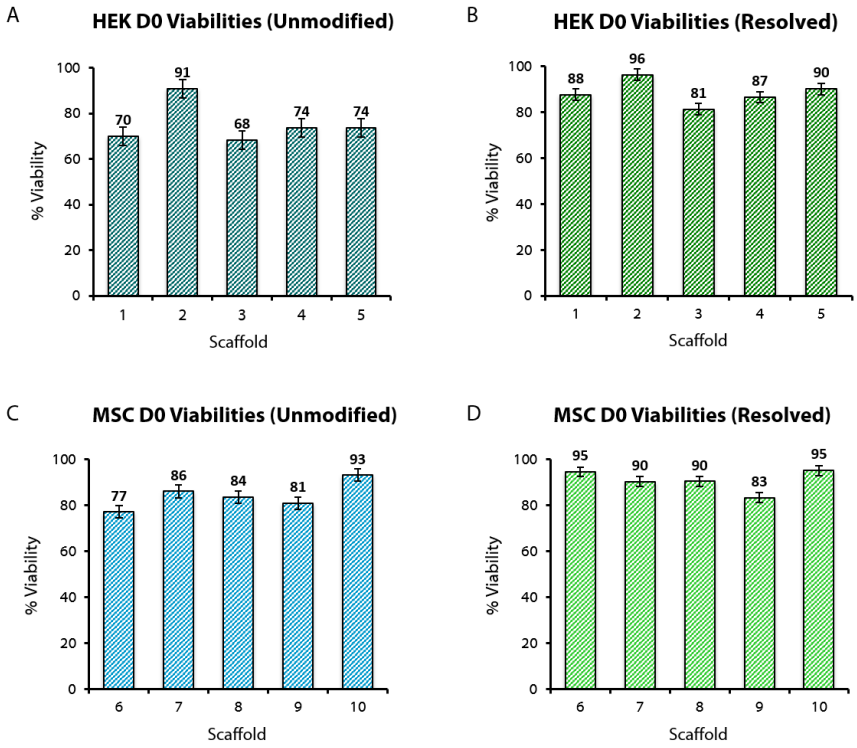

Figure 4.16 Initial viabilities of HEK-293T and oMSC scaffolds. **A**-**D** Calculated viabilities of scaffolds post phase transfer for: **A**-**B** HEK-293T scaffolds **1**-**5** (of **Table 6.13** in *section 6.11.6.3*) and; **C**-**D** oMSC scaffolds **6**-**10** (of **Table 6.14** in *section 6.11.6.3*). **A**,**C** Unmodified viabilities (**blue**) i.e. viabilities calculated using the number of objects counted as the assumed number of cells. **B**,**D** Resolved viabilities (**green**) i.e. viabilities calculated after resolving the number of counted objects, by dividing each object's volume by the average cell size. The group average for day 0 viabilities were calculated for HEK as 78±8% (unmodified) and 89±5% (resolved), and for oMSCs 84±5% (unmodified) and 91±4% (resolved). The viability error bars represent the standard deviation of the calculated viabilities for the cell line under study (*unresolved*: HEK-293T ±8%; oMSC ±5%; *resolved*: HEK-293T ±5%; oMSC ±4%).

Using the unresolved count methodology, scaffolds made with bioinks ≥10×10^6 cells/mL were found to contain between 593 and 2189 cells. When the resolved counting methodology was employed this count range rose to between 1520 and 3447 cells per

scaffold, with the average calculated to be 2968 cells. In most cases the number of counted live cells rose whilst the number of counted dead cells dropped. Here, small dead cell fragments picked up in the unresolved count were no longer being counted as cells, precluding, dead cells that have sheared, being counted multiple times.

Using the resolved cell count data, the average viabilities of scaffolds post phase transfer were calculated to be 89±5% ($\bar{x}$± s.d., n = 5) and 91±4% ($\bar{x}$± s.d., n = 5) for HEK-293T and oMSC scaffolds respectively (**Figure 4.16 B,D**). Thus the overall scaffold viability average was calculated to be 90±5% ($\bar{x}$± s.d., n = 10). Compared with the unmodified count viabilities, i.e. 77±8% ($\bar{x}$ ± s.d., n = 5) for HEK-293T and 84±8% ($\bar{x}$± s.d., n = 5)% for oMSC, the HEK-293T scaffold viability was calculated to be 12% higher. This large increase was due to the resolution of overlapping or joined cells within the HEK-293T scaffolds, which were produced with high bioink cell density and thus contained a high proportion of aggregated cells. The resolved viability for oMSC scaffolds also was higher than the viability calculated from the unmodified count by 7%.

This method could not, however, determine the total number of scaffold bound cells. This was due to the confocal microscope not being able to pick up signals for all the cells within the scaffolds. In particular, cells at high scaffold z heights (i.e. ≥ 200 μm within scaffold sample) appeared at low or with no fluorescence. The counted values are still valid for viability estimates as the proportion of live to dead cells should be even throughout the structure, and thus the counted cells can be representative of the whole structure.

As cellular scaffolds showed high viabilities after phase transfer (90±5%, $\bar{x}$± s.d., n = 10) it was concluded that the fabrication method was not immediately detrimental to cells. As these scaffold subsequently proliferated it can also be concluded that printing did not damage the cells long term either.

4.8 Patterned Scaffold Culture

The functionality of an organ and certain tissues arises through the specific interaction of different cell types. Thus to develop a tissue with intrinsic function from a printed construct, the multiple patterned cell types need to proliferate into high order tissue architectures. As such it was important to study how patterned cells develop within our printed construct and to see if the initial pattern after culture was retained displaying distinct cell regions.

4.8.1 Culture of Layered Sheets

To investigate the pattern development over the culture duration, a set of cellular layered sheets, with distinct cell populations, were fabricated and then imaged on day 3 (n = 2) and 5 (n = 2). To be able to distinguish the different cell populations, HEK-293T cells stained with CellTracker™ were printed. Specifically Deep Red CellTracker™ (DR) and Red CMPTX CellTracker™ (RC) were used. These dyes are retainable within the cell for over 5 days and can be passed onto daughter cells, thus allowing the pattern development to be studied.

The cells were patterned in the same manner as previous layered sheets (*section 3.9.3*). Specifically for a scaffold print, 3 lower square layers of RC stained HEK-293T were initially assembled and then topped by 3 upper square layers of DR stained HEK-293T (**Figure 4.17 A,B**). After wrapping these printed networks, one scaffold was imaged and displayed distinct layers of stained cells (**Figure 4.17 C**). The coated scaffolds were then phase transferred and culture for 5 days.

When the day 3 and 5 scaffolds were initially imaged, the DR stained cell layer were on the glass base and it was difficult to resolve the higher RC stained cells. After flipping the network 180°, such that the RC stained cell layer was in contact with the glass, two distinct layers were observed (**Figure 4.17 D,E**). This showed that the DR stained layer became dense with cells and resulted in poor penetration of fluorescent emissions.

Side on 3D projections of layered sheets show that pattern was retained on day 3 and day 5 (**Figure 4.17 D**,**E**). However, in both cases, the RC stained cell layer was not homogenous as some cell-laden printed droplet were sheared off during phase transfer. The viability of scaffolds were also check by CAM staining. All scaffolds appeared viable with live cells present in both layers (**Figure 4.17 F**).

It was also observed that the DR stained cell's the density of emitted fluorescence increased, whilst the RC stained cells stayed constant. It was inferred that the upper layer (DR) proliferated, whilst the lower RC stained HEK-293T stayed viable but had arrested development. The inhibited proliferation for RC stained cell was likely due to the RC CellTracker™ presence, as the DR and RC stained cells came from the same source but showed different development.

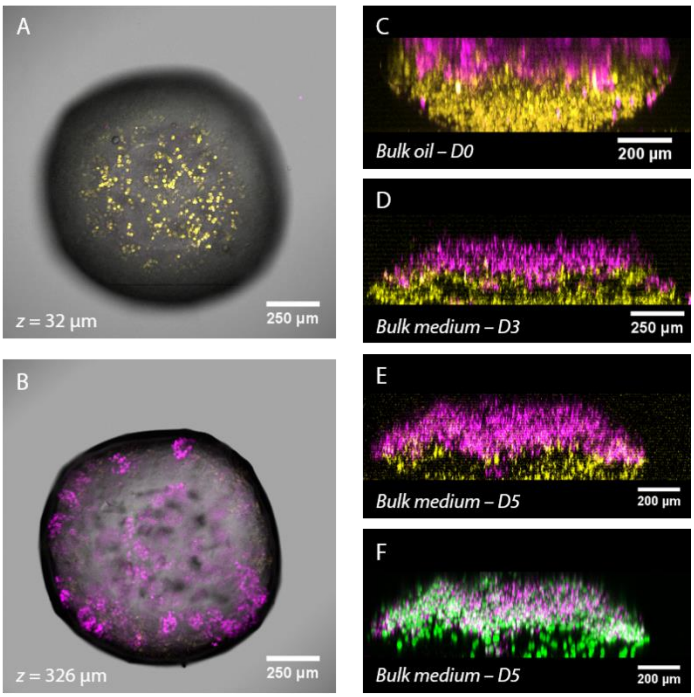

Figure 4.17 Pattern development of printed stained HEK-293T layered sheets over 5 days. **A**-**F** Images of a HEK-293T lamellar networks (lower: 7×8×3 droplets; lower: 6×7×3 droplets) over 5 days culture (n = 6), here RC stained cells (yellow) were patterned below DR stained cells (purple). Cell populations were printed as 12×10^6 to 14×10^6 cells/mL in **SS7h**. **A**-**B** Composite bright-field and fluorescence confocal micrographs of layered sheets at z heights of: **A** 32 µm and **B** 326 µm. **C**-**E** Side-on 3D projections of layered sheets over 5 days of culture, showing the pattern is conserved at time-points: **C** day 0 (post print in bulk oil); **D** day 3 (in bulk culture medium) and; **E** day 5 (in bulk culture medium). **F** 3D projections of live stained cells alongside DR stained cell population, showing that the scaffold is viable throughout.

The results signify that a simple pattern can be conserved throughout culture. As such it is likely, due to low mobility of cells within the scaffolds, that more complex patterns can be conserved over culture. The cells of these complex patterns would then grow and join to neighbouring cells and make the relevant cell-cell contacts. Thus this platform has the potential to be able to fabricate a range of complex tissues due to the ability of high feature resolution patterning and pattern conservation over culture.

4.9 Differentiation Capacity Study

The ability to pattern multipotent or pluripotent stem cells, whose fate can be directed post print, would enable the fabrication of multiple tissues. As such, a patterned construct of stem cells could be induced by biomolecules, for example growth factors, to develop into a specific tissue. Furthermore, if the bioink was engineered to immobilise biomolecules, then cellular scaffolds could be fabricated with defined gradients of these biomolecules which direct stem cell fate[8]. Stem cells within these scaffolds could develop into multiple sub populations of different lineages[8]. A fibrocartilage tissue model was developed in a similar manner, with bioprinted human mesenchymal stem cells grown in growth factors patterned with density gradients[62].

To investigate whether differentiation of patterned cells within printed constructs was possible, multipotent oMSCs containing constructs were fabricated and the cells of which were induced towards a cartilage lineage. This investigation was performed in collaboration with Madeline Burke, Dr James Armstrong, James Nicholson and Dr Sam Olof.

4.9.1 Chondrogenesis

Chondrogenesis is the differentiation of mesenchyme cells into chondrocytes, the singular component of cartilage. Cartilage is a flexible connective tissue present in animals, located in, joints between bones, the ear, bronchial tubes, among other places. The chondrocytes produce high quantities of collagen and proteoglycans. This ECM

gives rise to cartilage's characteristic flexible nature and its ability to respond to compressive forces[180].

Chondrogenesis is also the first step of endochondral ossification, which is the process of developing bones from cartilage tissue[181]. As such, chondrogenesis is not only key to cartilage development, but also foetal development of the mammalian skeletal system. The initiation and steps of chondrogenesis are described below.

The development of cartilage tissues from multipotent mesenchymal cells can be split into two main steps. Firstly, chondrogenesis is induced by environmental growth factors, causing chondrogenic progenitors to form and then condense[181]. These aggregates of progenitor cells, over time, differentiate in chondrocytes and deposit matrix[181].

It has been shown that a number of growth factors are responsible for the initiation and maintenance of chondrogenesis in developing limbs[181]. These include members of the transforming growth factor superfamily (TGF) and fibroblast growth factor (FGF). The induction of chondrogenesis results in the expression of specific genes. These include genes for the transcription factor family, Sry-related high-mobility-group box (Sox), with Sox9, Sox5 and Sox6 all involved in chondrogenesis[182]. Most pivotal is Sox9, which is expressed in all chondrogenic progenitors and chondrocytes except hypertrophic chondrocytes[182]. The presence of Sox9 is required for the cellular commitment to a chondrogenic cell lineage and subsequent cellular condensation[182]. The transcriptional activation of Sox9 has been linked to TGF-β3 whose downstream effector/signalling molecule, Smad3, induces the process[182]. For these reasons, TGF-β3 can be used to induce chondrogenesis, which can be subsequently monitored by the production of Sox9.

Once chondrogenesis is induced, chondrogenic progenitors initially do not proliferate and closely pack into aggregates, increasing the number of cell-cell contacts[183]. The onset of differentiation is marked by a change in expression of ECM proteins. Post cellular condensation, pre-cartilaginous cells express an ECM rich in collagen type I, hyaluronan, tenascin and fibronectin[181]. Differentiated chondrocytes stop this collagen

type I production and start expressing cartilage specific ECM proteins including collagen type II, and aggrecan. Consequently the chondrocytes become wrapped in ECM and acquire a characteristic rounded morphology. Maturation of the chondrocytes leads to unidirectional proliferation, the production of collagen type X and hypertrophic conversion[182]. In endochondral ossification, chondrogenesis ends when the cartilage is vascularised, delivering osteoblasts from the invading blood vessels. These osteoblasts then replace the cartilage with mineralised bone.

4.9.2 Culture of Patterned oMSC Scaffold

In our study we employed TGF-β3 to biochemically induce oMSC chondrogenesis and monitored their differentiation to a chondrogenic lineage by Sox9 expression. Initially, we monitored the cellular development of patterned oMSCs within scaffolds cultured with and without TGF-β3 presence. Printed oMSC scaffolds were cultured in either **MSC differentiation medium** or **MSC control medium** over 10 days (**Figure 4.18**). Here the differentiation culture medium contained a cocktail of chondrogenic differentiation factors: TGF-β3, ascorbic acid and dexamethasone, whilst the control culture medium omitted TGF-β3. In the presence of TGF-β3 chondrogenesis should be induced (see *section 4.9.1*). This will cause the cells to, stop proliferating, condense and slowly differentiate into chondrocytes. Whilst in the absence of TGF-β3 the cells should continue to proliferate as multipotent oMSCs.

Patterned oMSC scaffolds were live stained only on day 3, 7 and 10 ($n = 3$ for each time point and culture condition) (**Figure 4.18**). Here, the dead stain was omitted so that the scaffolds could be Sox9 ICC stained (*section 4.9.4*) without an overlap of the emitted fluorescent signal between the propidium iodide and the anti-body conjugated fluorophore. All patterned oMSC scaffolds showed viable signals across the cellular structures, indicating the oMSCs were mainly viable.

Over 10 days, scaffolds in the presence of TGF-β3 formed spheroidal cell aggregates of 25-60 μm diameter, which were evenly distributed throughout the

structure (**Figure 4.18 A-D**). This aggregation of the oMSC occurred within the first three days, showing that cells were able to migrate to one another and form multiple cell-cell contacts. Scaffolds cultured without TGF-β3 formed fewer but larger aggregates, which were non-uniformly distributed throughout the networks. The average size of the cellular aggregate increased over 10 days, with the largest aggregate present on day 10 at 350 μm length. This indicated that cellular proliferation had been ongoing throughout the culture without TGF-β3 presence (**Figure 4.18 E-H**). As such, the difference in oMSC aggregation was pronounced and indicated an effect of TGF-β3.

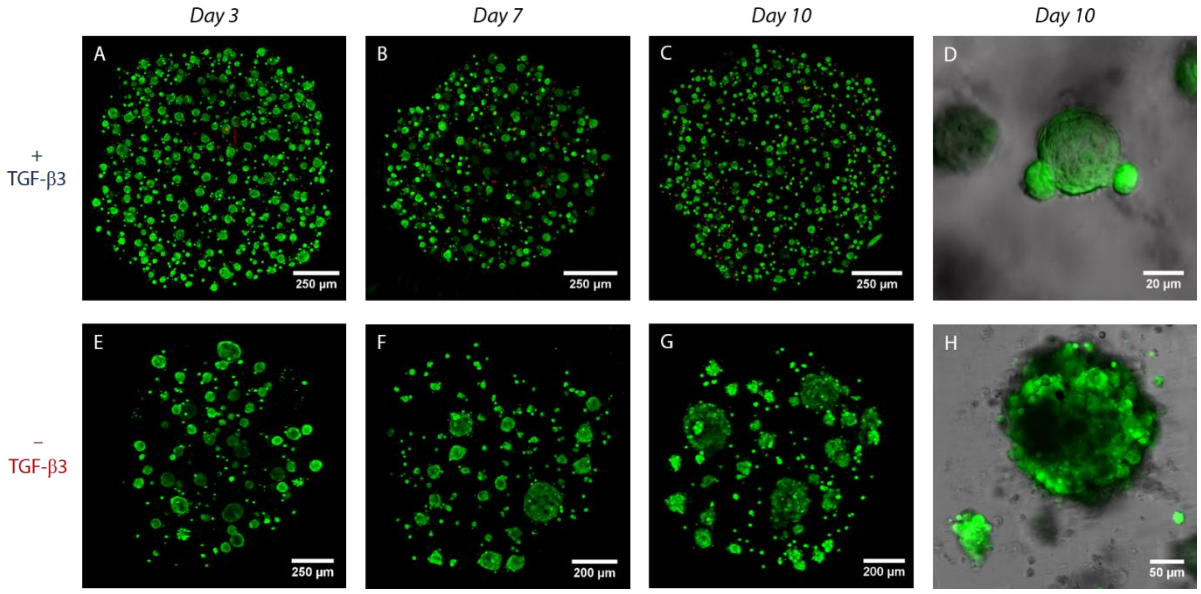

Figure 4.18 Development of printed oMSC scaffolds 3D cultured with and without growth factor. **A-H** Images of printed oMSC scaffolds over 10 days culture with TGF-β3 (top row) or without TGF-β3 (bottom row). Scaffold were composed of 15×10^6 cells/mL in **SS8m** supplemented with 15 μg/mL collagen type I. **A-C**, **E-G** 3D projections of live/dead cell stained scaffolds on: **A**,**E** day 3; **B**,**F** Day 7 and; **C**,**G** day 10. **D**,**H** Composite bright-field and fluorescence confocal micrograph of a zoomed in section of the oMSC scaffold on day 10. It can be seen that in the presence of TGF-β3, spheroidal cell aggregates of 25-60 μm diameter are regularly distributed throughout the scaffold, whereas without TGF-β3 fewer larger aggregates of up to 350 μm are present.

4.9.3 Sox9 Gene Expression

To confirm that the printed scaffolds cultured in TGF-β3 showed chondrogenic commitment, the expression of Sox9 was investigated. Sox9, a transcription factor, is expressed during the development of chondrogenic progenitors and chondrocytes from

mesenchyme cells (see *section 4.9.1*). Mesenchyme cells otherwise express Sox9 at levels below the detection limit of digital polymerase chain reaction. Expression levels of genes, including Sox9, can be measured with techniques such as quantitative polymerase chain reaction (qPCR), which quantify the transcription of gene products, i.e. mRNA, which indicate protein levels. mRNA analysis of Sox9 can therefore be used to distinguish between undifferentiated and chondrogenic lineage committed cells.

Sets of oMSC printed scaffolds (n = 4-6 per set) were created for four sheep replicates for Sox9 analysis of chondrogenic differentiation in scaffolds. Analysis was also performed on pellet controls (n = 24 total), composed of harvested oMSCs centrifuged to formed pellets containing 0.4×10^6 cells. The author fabricated the printed oMSC scaffolds with a **SS8m** based bioink containing 15×10^6 to 17×10^6 cells/mL. Madeline Burke and Dr James Armstrong, cultured all scaffolds with and without the presence TGF-β3 and then analysed gene expression by digital polymerase chain reaction (dPCR). They also formed the pellet controls.

Pellet controls and printed scaffolds (n = 22 total) were assessed by dPCR for the gene expression of beta-actin and Sox9. Analysis was performed after 7 days of culture for both pellet controls and printed scaffolds. On the day of analysis, RNA was extracted, reverse transcribed and then measured using dPCR with is a method for absolute quantification.

The beta-actin gene was studied as it is a reference house-keeping gene that is expressed by oMSCs in viable conditions. Here it was found that beta-actin was expressed by all pellets and printed scaffolds, regardless of TGF-β3 presence. The Sox9 gene expression was then analysed and normalised to the beta-actin level. The results showed that all pellet controls and printed scaffolds cultured in TGF-β3 expressed Sox9 mRNA (**Figure 4.19**). While the scaffolds and pellet controls in the absence of TGF-β3 expressed Sox9 below the detection limit.

It was discovered that Sox9 expression was lower for the printed scaffolds than for the pellet control (**Figure 4.19**). This is unsurprising as the pellet with its reduced intercellular space is an optimised environment for cellular condensation and the

progression of chondrogenesis. Whereas within the scaffold oMSCs are initially distributed homogeneously with negligible cell-cell contact and consequently have to migrate before condensing leading to a slower progression of chondrogenesis.

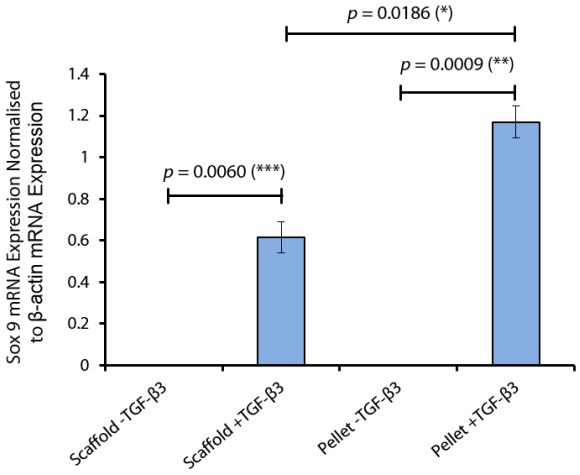

Figure 4.19 Sox9 gene expression normalised to beta-actin mRNA levels for constructs cultured with and without TGF-β3. mRNA expression was measured by dPCR for printed scaffolds (scaffold, $n = 22$) and pellet controls (pellet, $n = 24$) cultured for 7 days. The normalised data is an average of assays performed on the same four sets of oMSC-laden constructs. Each set used oMSCs extracted from separate sheep. Comparison of differences were tested using a paired t-test, with two-tailed p values <0.05 considered significant. Error bars represent the standard deviation of the data. Measurements performed by Madeline Burke and Dr James Armstrong.

4.9.4 Sox9 ICC Staining

To support the Sox9 gene expression for chondrogenic differentiation in oMSC scaffolds, the protein expression of Sox9 was investigated by ICC of printed oMSC scaffolds and a cartilage control. Here a set of printed oMSC scaffolds were cultured over 10 days with and without TGF-β3 by the author. This cultured scaffold set, is the same one as shown in **Figure 4.18**. Here 3 scaffolds were cultured for each combination of time point (day 3, 7 and 10) and culture condition (±TGF-β3). Prior to ICC staining the scaffold set was imaged by live staining on days 3, 7 and 10 by the author and Dr Sam Olof. Scaffolds and a 5 week cartilage control sample were then Sox9 ICC stained by James Nicholson and Dr Sam Olof.

To check the appearance of Sox9 protein in differentiated cartilage tissue, a non-printed cartilage was initially immunostained (**Figure 4.20 A**). Specifically, the non-printed cartilage was engineered using polyglycolic acid scaffolds seeded with oMSCs and then grown in **MSC differentiation medium** over 35 days. Here it can be seen that Sox9 was present in all chondrocytes at varying levels of expression (**Figure 4.20 A**).

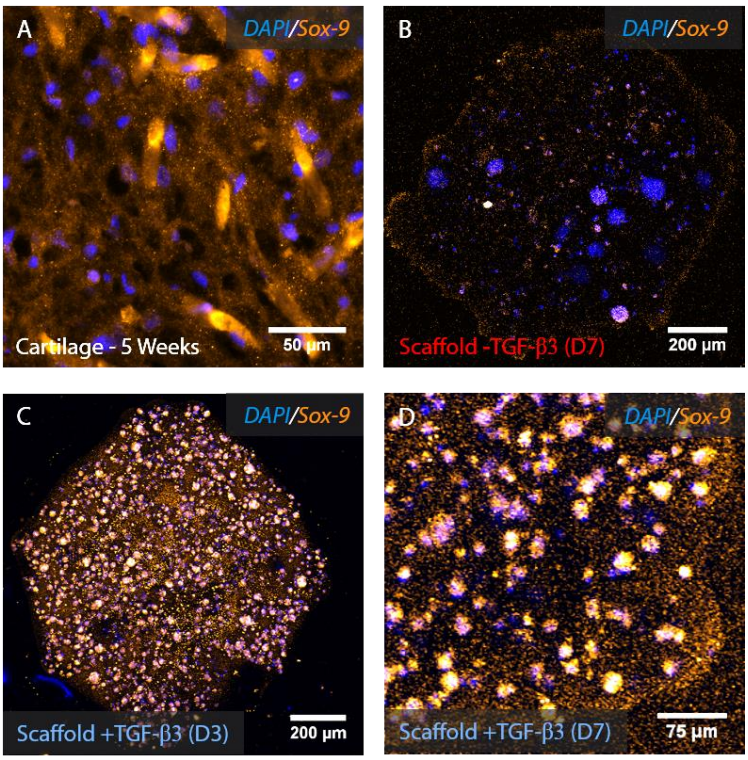

Figure 4.20 Sox9 ICC staining of cartilage sample and printed oMSC scaffolds grown with and without TGF-β3. **A.** 3D projections of cartilage sample grown over 35 days. **B** Fluorescence confocal micrograph of printed oMSC scaffold after 7 days culture without TGF-β3. **C-D** 3D projections of printed oMSC samples cultured with TGF-β3 for: **C** 7 days; and **D** 7 days. Samples were ICC stained with DAPI (blue) and anti-Sox9 antibodies (orange). The cartilage sample prepared by Dr James Armstrong and Madeline Burke, whilst ICC staining was performed by James Nicholson and Dr Sam Olof.

Printed scaffolds cultured without TGF-β3 showed no high intensity signals across the network for Sox9 but showed fluctuating background signals (**Figure 4.20 B**), indicating Sox9 protein was not expressed. Whereas printed scaffolds cultured in TGF-β3 after 3 days displayed Sox9 signals, present as clusters, across the structure (**Figure 4.20 C**). Similar Sox9 signals were also observed across scaffolds cultured with TGF-β3 for 7 days (**Figure 4.20 D**). Although with all printed scaffolds a high fluctuating background signal

of the Sox9 fluorophore conjugated secondary antibody was observed, even with repeated washes. Consequently it was not possible to accurately establish if the Sox9 protein had increased by comparing signal intensities from the different time points.

The results indicate that early stage chondrogenesis was induced in printed oMSC scaffolds exposed to TGF-β3. The oMSC patterned scaffold cultured without TGF-β3 displayed Sox9 mRNA expression was below the detection limit (**Figure 4.19**) and high cellular proliferation rates (**Figure 4.18**). Whereas by culturing with TGF-β3, Sox9 expression was induced in scaffolds by day 3 (**Figure 4.20**) and was still expressed in scaffolds on day 7 and day 10 (**Figure 4.19** and **Figure 4.20**). Within the scaffold, the expression of Sox9 induced oMSC condensation into aggregates which showed inhibited proliferation (**Figure 4.18**). This indicated the scaffold oMSCs were differentiated into chondrogenic progenitor cells which displayed cellular morphologies of early chondrogenesis.

The differentiation observed is only early stage, but, in the future, the process may be extended to engineer cartilage tissue. This would require longer culture periods of the patterned oMSCs (typically 21-35 days) and more sophisticated analysis techniques such as immunohistochemistry, biochemical assays and mechanical testing. Additionally, as the extracted RNA was low, the study of early stage chondrogenesis by dPCR analysis was limited to two genes (beta-actin and Sox9). Ideally the RNA extraction would have been further optimised to provide more material for more extensive genetic analysis.

These results demonstrate that the printing process was non-detrimental to oMSCs which remained, multipotent and responsive to environmental growth factors. This signifies the potential of our platform to print multipotent stem cells which, after printing, can be directed into a specific cell lineage and subsequently develop into a specialised tissue.

4.10 Conclusions

In this chapter we developed a method to culture the 3D printed cell-patterned scaffolds of Chapter 3. Their preliminary culture showed a decline in cell viabilities over a week, consequently the culture method was optimised. To enhance cellular viability and proliferation, the bioink was adapted to contain high cell densities (up to 15×10^6 cells/mL) and supplemented with ECM proteins. However, proliferation was limited using the initial culture method, where the cell-patterned scaffolds away from an ideal culture environment, i.e. the cell incubator, for long durations during scaffold imaging. This was resolved by only culturing scaffolds of the same time point in the same chambers and then imaging the scaffolds only once. This optimised culture method was tested on sphere controls containing different ECM protein blends, which subsequently showed high cellular viability and proliferation after 7 days. Thus this optimised culture method was applied to printed cellular scaffolds.

The biological activity of patterned cells within printed scaffolds, was investigated by culturing HEK-293T-laden scaffolds over 7 days. It was found HEK-293T viabilities started high at 89±5% ($\bar{n}$ ± s.d., n = 5), with cells proliferating into dense cellular masses by day 7. Over 7 days culture, viable cells were visible throughout the structure and there was an increase in cellular aggregate size. ICC of cells within scaffolds after 3 and 7 days of culture, showed healthy DAPI signals throughout and an even distribution of PH3 stained cells at approximately 7% and 3% respectively. Thus the scaffolds employed were proved to be optimal growth environment with cells showing healthy viabilities and proliferations.

This demonstrate the platform's ability to generate complex tissues from patterns composed of two cell types, a printed construct composed of layered sheets was fabricated and cultured over 5 days. Throughout the duration the two cell populations were conserved as distinct layers and remained viable. This signified that the technique had the potential to culture higher order cellular patterns, with cells forming the necessary cell-cell contacts to develop functional tissue.

The ability for printed cells to differentiate was also investigated by introducing chondrogenic growth factors to oMSC patterned scaffolds. oMSCs responded to TGF-β3 presence, by compacting into dense cellular spheroids by day 3 and showed no further proliferation by day 10. The expression of Sox9 mRNA was found to be upregulated in day 7 oMSC laden scaffolds cultured with TGF-β3 as confirmed by dPCR and ICC staining. As the oMSC scaffolds cultured without TGF-β3 showed different cellular development, specifically, continual proliferation and no Sox9 expression, oMSCs were inferred to be biochemically responsive after printing. This Sox9 expression and cellular condensation confirmed that the printed oMSCs in the presence of chondrogenic growth factor committed to a chondrogenic lineage.

Overall, the cellular organisations which developed from printed cells could be defined as tissues because, they contained high cell densities, tightly packed cellular morphologies, high viabilities, mitotically active cells and regular cell functions. The feasibility to develop complex tissues composed of two cell types was also demonstrated by the pattern conservation of cellular layered sheets over 5 days culture. Furthermore, multipotent oMSC patterned scaffolds were fabricated with undifferentiated oMSCs which were biochemically induced to a chondrogenic lineage after printing.

5 Future Work

5.1 Summary of Work

This thesis has presented the design and implementation of a novel bioprinter which could fabricate soft tissue-like materials and cell-patterned scaffolds for tissue generation. The printer was designed around droplet interface bilayers and assembled highly compartmentalised droplet networks from lipid-coated droplets in oil (Chapter 1). Millimetre-scale networks were self-standing and could be printed with two droplet types at very high droplet resolution (~65 pL) and high feature resolution (2- 4 droplet width). Emergent tissue-like behaviour could be programmed into printed networks such as, rapid electrical communication to mimic nervous tissue, and self-folding in a manner similar to muscle contractions.

Latterly, we adapted the printing process to print high resolution cell-laden networks in oil (Chapter 3 and 4). Utilising an agarose-based bioink, HEK-293T cells and oMSCs were printed at high viabilities (~90%), high droplet resolution (~1 nL) and at tissue-like densities (3×10^7 cells/mL). Using two cell populations, scaffolds could be printed with capillary-like and lamellar architectures that contained high resolution cell features (≤ 200 μm). A novel gel-encapsulation method stabilised the scaffolds during transfer to culture medium with networks retaining their printed shape and cellular pattern. Culture of the scaffolds showed that printed cells retained fundamental biological processes such as proliferation and differentiation. Significantly, HEK-293T cells divided into dense cellular masses over 7 days, with 3% of the cells displaying mitotic activity on day 7. Furthermore, oMSCs remained multi-potent and responded to diffusible signals to differentiate into chondrocyte progenitor cells. To show the capability of the approach, a high-resolution osteochondral mimic was printed with adjoining layers of chondrocytes and osteoblasts.

The potential future applications of printed droplet networks and cell-patterned scaffolds is numerous, however, certain critical challenges need to be overcome for many of them to be achieved. These applications and challenges are now discussed.

5.2 3D Printed Droplet Networks

In the future, droplet networks could feasibly be printed with multiple inks composed of a range of materials, to give structures with diverse emergent properties. Chapter 2 demonstrated how printed droplet networks are tissue like, and as such, there is the potential to print a diversity of structures which mimic living tissue functionalities. Such networks may also be interface with living tissues to support their function. These interactions would have to be performed in air, or aqueous solutions, away from the print oil. Thus a method of phase transferring printed networks in bulk oil would need to be developed. Phase transfer of printed networks may be attained by transferring the structure through a planar lipid monolayer at the interface of oil and aqueous phases[152,157]. However, the structure would need to be stabilised towards rupturing with the bulk aqueous phase, possibly by incorporating internal vesicles or by crosslinking the bilayer lipids. Additionally, for an aqueous bound network to interact with living tissues, the system would also need to have gap junctions in the external bilayers complimentary to those of the living tissue.

An application of networks printed in bulk aqueous solution could be vehicles for combinatorial drug delivery or cell delivery, with their inner droplets containing either drugs, prodrugs with their activators or cells[100]. Such cargo could be released gradually by diffusion through pores in the external bilayers or by a triggered release induced by a pH or temperature change[100]. These engineered networks could be injected into a living host in order to delivery drugs or cells to a specific site, with targeted drug release triggered by a physiological stimulus. Challenges to overcome include, the miniaturisation of networks to sizes below the diameters of blood-vessel and the high-throughput production of networks. Such problems could be overcome ejecting micron-size droplets in a confined space and then parallelising the printing process.

In Chapter 2, it was also demonstrated that networks could deform, i.e. fold, into new topologies when an osmotic gradient was present. However, the speed of folding was slow and the network motion was uncontrolled. A future project would be the design of controlled motile networks, which can be triggered to fold on demand, potentially at faster speeds. Furthermore, if reversible network deformation is developed, it would be feasible to fabricate soft robotic like structures which are able to move and potentially cage macroscopic items.

One potential method of achieving controlled network motion would be to incorporate a stimulus responsive osmolytes into selected regions of a network. When the stimulus is applied to such a network, an osmolarity change is triggered along with subsequent network deformation (**Figure 5.1**). Preliminary responsive osmolyte experiments were attempted with poly (*N*-isopropylacrylamide) (PNIPAM) which, when heated above its lower critical solubility temperature (LCST) became insoluble[184]. When responsive PNIPAM containing droplets bound to isotonic salt droplets were heated above the LCST, it was found that PNIPAM collapsed, resulting in the responsive droplet shrinking whilst the salt droplet grew. Thus demonstrating that responsive osmolytes exist and signifying that control network motion may be achieved using response osmolytes.

To aid the fine patterning of future networks, it would be of interest to elucidate conditions that give ideal droplet packing i.e. either hexagonal packing or another packing style that produces minimal oil gaps. These parameters could then be employed to reproducibly pattern different droplet solutions at high resolution. Preliminary work alongside Chapter 2 and Chapter 3 has shown that varying network osmolarity, the network solutes and the oil composition results in varied packing (**Figure 5.2**). Thus different print solutions would need to be printed into optimised lipid-in-oil solutions to ensure optimal packing.

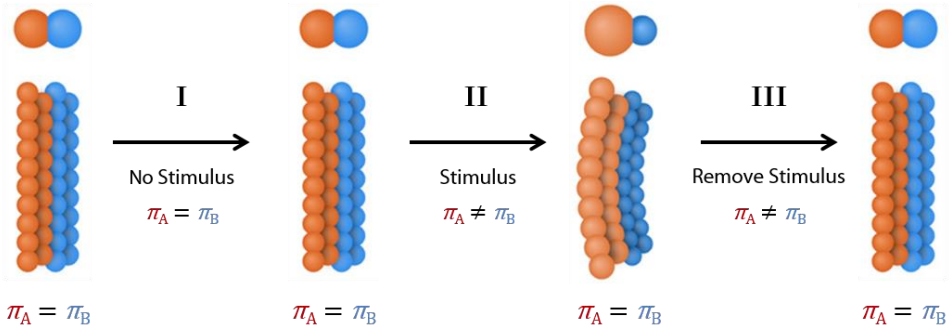

Figure 5.1 Illustration of a droplet pair and droplet network strip that can reversible change volume using responsive osmolytes. Here, either the blue or red droplets would contain a responsive osmolyte, such that upon exposure to the relevant stimulus, the osmolyte changes its osmolarity. **I** Initially the droplets have equal osmotic pressure (π) and are static. **II** Application of the stimulus results in the osmotic pressure becoming unbalanced, causing deviations in droplet volumes and resulting in network folding. Once the osmotic pressure of the network equilibrates it remains static. **III** Removal of the stimulus results in the responsive droplet's osmotic pressure returning to its initial value, causing the network to reversibly fold into its original state

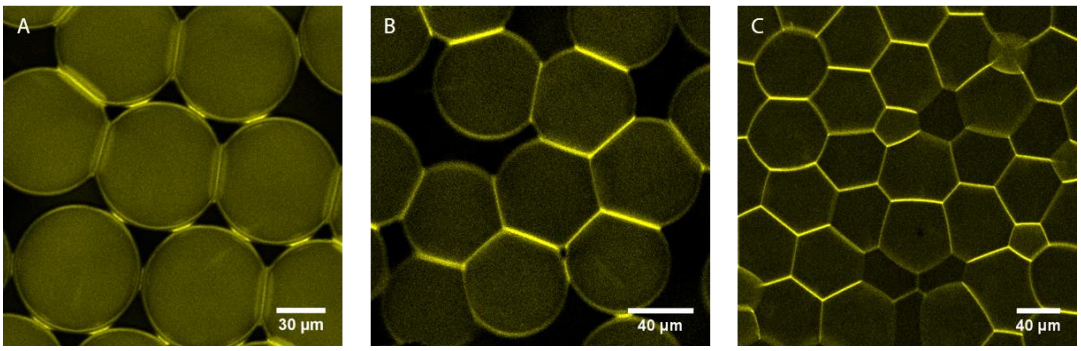

Figure 5.2 Packing of droplet within networks of differing osmolarities. **A-C** Fluorescence confocal micrographs of droplet networks stained with 5 µM sulforhodamine 101. Here, networks were printed in **fluorescent print oil A** and were composed of Tris buffer solution containing KCl at: **A** 0 mM; **B** 145 mM and **C** 1 M. It was observed that as the salt concentration increased so did the bilayer area connecting droplets.

5.3 3D Printed Cell-Laden Constructs

In the future, cell patterned constructs could feasible be printed as droplet networks with multiple cell types, patterned in optimal materials for growth to develop a range of functional tissues. Parallelisation of the tissue fabrication technique could create arrays of tissues. These tissues could subsequently be used as models for healthy or diseased

tissues to screen in high-throughput manners their interactions with drugs, toxins or pathogenic infections. Alternatively printed tissues could be used in regenerative medicine by interfacing with damaged living tissue to restore (wound healing) or support its function. A significant challenge to overcome is the vascularisation of printed tissues, which without, precludes the fabrication of tissues sized beyond the nutrient diffusion limit. Vascularisation of printed tissues may allow the fabrication of large tissues or whole organs, which could be subsequently used for implantation into living hosts.

To develop a diverse range of functional tissues the platform developed in Chapter 3 and Chapter 4 needs to be expanded to other cell types including alternative mammalian cells and bacteria. As HEK-293T and oMSCs were printed and successfully proliferated into tissues within the printed construct, the process should be compatible with other cell lines. Therefore future projects could print specialised natural tissues or unnatural tissue chimeras, which potentially could be engineered to function better than natural tissues, by selecting cells with optimal functions. Additionally cells from different taxon could be printed together, such as bacterial and mammalian cells to serve as host-pathogen infection models.

One set of mammalian cells that preliminary research has started on are neuronal stem cells (NSCs, in collaboration with James Nicholson, Dr Roderick Walker and Dr Sam Olof). These NSCs have the potential to be used in regenerative medicine to replace neurons lost or damaged by neurodegenerative diseases or acute brain trauma[185]. NSC laden scaffolds transplanted into injured mice brains have helped reconstitute lost tissue[186] and even recovered behavioural function[187]. NSCs patterned as 3D printed constructs may enable the recapitulation of in vivo neuroanatomical features thus producing tissue grafts more able to functionally integrate into, and restore function to, the damaged brain. Initial results have shown that neural cells can be patterned in agarose constructs, demonstrating the printer's compatibility with alternative mammalian cell lines. Future work will involve, tailoring the printing material to be a growth environment suited to NSC development and patterning NSCs in cerebral tissue architectures, such as the sub ventricular zone.

Whilst agarose blended with ECM proteins allowed the proliferation and development of HEK-293T cells and oMSCs, it will not be ideal scaffold for the culture of all specialised cells, such as NSCs which need a high laminin content. Consequently, some future bioinks will need to be composed of an alternative hydrogels for 3D mammalian cell culture. Suitable hydrogels such as collagen, decellularised ECM and Matrigel® are thermoresponsive and gel if at room temperature. The printer would not be able to print these without a temperature controller, as the bioink would gel in the nozzle. As such, an alternative project in the Bayley lab performed by Dr Linna Zhou, has been to adapt the printer such that it can print temperature sensitive hydrogels. Using a temperature controller and an amplified piezo driver, initial results have shown cell-laden Matrigel® and collagen type I can be 3D printed as droplet networks. The refinement of this technology will allow the fabrication of cell-laden droplet networks from a range of hydrogels, expanding the platforms compatibility with specialised cells.

To be able to create functional tissues of dimensions beyond the diffusion limit, cell-laden printed constructs will need to contain either natural vasculature or unnatural perfusable microchannels. Such channels need to recapitulate tissue microcirculation by capillaries for effective nutrient exchanged across the scaffold. Blood vessels could be potentially introduced into scaffolds by printing endothelial vein cells alongside the desired tissue cells. The challenge would be to encourage the endothelial vein cells to form hollow vessels within the printed construct, potentially by directing them to grow around hollow printed architectures. Alternatively, blood vessels could be grown into the scaffold from resected tissue, a similar method has been successful for tissues fabricated by cell sheet technology[86]. Perfusable microchannels may be fabricated alongside the printed construct, the Lewis lab have demonstrated this by printing a fugitive ink alongside cells that was dissolved post print[36]. These perfusable microchannels were then seeded with endothelial cells, which lined the channel with vasculature tissue. Overall the combination of expanding the printing to other cells and the successful vascularisation of printed tissues, would enable the fabrication of thick tissues that mimic natural tissues and organs.

6 Material & Methods

This chapter gives a detailed summary of the materials and methods used throughout Chapters 2-4. The contents for each section is briefly described. *Section 6.1* summarises the materials, standard solutions and cell sources used throughout. *Section 6.2* explains the 3D printer setup and the printing process, including the printer software. *Section 6.3* describes the analysis of droplet networks in Chapter 2. *Section 6.4* summarises the cell culture methods of Chapter 3 and 4. *Section 6.5* describes the production of cargo-laden scaffold solutions. *Section 6.6* explains all 3D scaffold printing of Chapter 3 and 4. *Section 6.7* recounts scaffold gelation methods. *Section 6.8* details the phase transfer methods of preliminary scaffolds and printed scaffolds. *Section 6.9* describes the 3D culture of cell-laden scaffolds. *Section 6.10* explains the cellular scaffolds controls. *Section 6.11* details the analysis of cellular scaffolds including microscopy, immunocytochemistry, image analysis and dPCR. Finally, *Section 6.12* describes the fabrication of lab-made items.

6.1 Materials, Standard Solutions & Cells

Each sub-section of this section will mention the source of the specific reagents used and how common solutions were prepared.

6.1.1 Common Solvents

Purified water was used throughout the methods, specifically ultrapure (type 1) Milli-Q® water and pure (type 2) Elix® water which have a resistivity at 25 °C of 18.2 MΩ·cm and 10-15 MΩ·cm, respectively. Water was purified by Milli-Q® Synthesis water purification system using a Q-Gard® 1 purifier (*Merck Millipore*, UK) and Elix® Essential 10 UV water purification System using a Pro-Gard® TS2 purifier (*Merck Millipore*, UK). Solvents such

as ethanol, isopropanol, acetone and pH correcting solutions sodium hydroxide and hydrochloric acid were obtained from *Sigma-Aldrich*.

6.1.2 Oil Solutions

All oils were purchased from *Sigma-Aldrich.* Prior to lipid solubilisation or oil use, oils were initially mixed at the desired volume ratio where relevant, and filtered through a 0.22 μm polyethersulfone membrane (Millex® Syringe Filter Unit, *Merck Millipore*); this sterilised the oil and removed any macroscopic debris.

6.1.2.1 Lipid-in-Oil Solutions

All lipids were all purchased from *Avanti Polar Lipids, Inc.* except cholesterol which, along with chloroform and pentane was obtained from *Sigma-Aldrich*. In every instance oil containing lipid solutions were produced using the following method. Powdered lipid (~25 mg) from airtight ampules, would be dissolved in chloroform or pentane, and subsequently dried by a gentle nitrogen flow and then vacuum (20 mbar, >12 h), and accurately weighed to sub-milligram precision, typically giving 23.0-28.0 mg total weight. From this dried film, a stock solution of 20 mM lipid in chloroform was prepared. Aliquots of this stock solution would be dried by a gentle nitrogen flow and then vacuum (20 mbar, 2 h), to give individual lipid films which would be solubilised in the relevant oil mixtures by vortex mixing. These films could also be stored until needed at -20 °C if placed under argon gas.

6.1.2.2 Standard Oil Solutions

There were many routine oil solutions for different periods of this research. Below, **Table 6.1** lists the most frequently used oils and their compositions including lipid concentrations.

Table 6.1 List of oils commonly used throughout the research, and their typical compositions.

Standard Oil Solutions	Bulk Solvent	Lipid Solubilised	[Lipid] / mM
standard print oil	50:50 v:v hexadecane : silicone oil AR20	DPhPC	0.6-2.4
fluorescent print oil (A)	50:50 v:v hexadecane : silicone oil AR20	8:2 mol:mol DPhPC : DPHPE with 0.1 mol% NBD-DPhPE	1.5
fluorescent print oil (B)	50:50 v:v hexadecane : silicone oil AR20	8:2 mol:mol DPhPC : cholesterol with 0.1 mol% NBD-DPhPE	1.5
bioink print oil	35:65 v:v undecane : silicone oil AR20	DPhPC	1.2
wash oil (gel-encapsulation step)	silicone oil AR20	none	N/A
initial scaffold phase-transfer oil	75:25 v:v hexadecane : mineral oil (M3516)	DOPC	4.8
standard scaffold phase-transfer oil	75:25 v:v hexadecane : mineral oil (M3516)	none	N/A

6.1.3 Droplet Network Solutions

This section goes through the droplet network solutions used in Chapter 2, all reagents of the droplet network solutions were purchased from *Sigma-Aldrich* unless otherwise stated.

6.1.3.1 Standard Droplet Solutions

In Chapter 2 the **standard print solution** consisted of 25 mM Tris·HCl, 1 M KCl, 100 μM EDTA, buffered at pH 8.0 in ultrapure water and were often dyed. Predominantly if networks were coloured, they contained either 0.16-1 mM xylene cyanol FF (blue), 0.8-10 mM orange G (orange) or 10 mM pyranine (green). The internal strip networks (**Figure 2.7**) were the exception as they contained 5 μM fluorescein (green, *Life Technologies*) and 5 μM sulforhodamine 101 (yellow, *Life Technologies*). These print solutions were filtered through a 0.2 μm membrane after being made.

Table 6.2 List of dye concentrations used in Chapter 2. Here, droplets were dyed with either, xylene cyanol-FF (blue), orange-G (orange), pyranine (green), fluorescein (green) or sulforhodamine (yellow).

Figure	Droplet Type	Dye concentration
2.6 A,B,C	printed	1 mM xylene cyanol-FF and 10 mM orange-G
2.7 A	printed	1 mM xylene cyanol-FF and 2.5 mM orange-G
2.7 C,D	printed	5 μM sulforhodamine 101 and 5 μM fluorescein
2.8 B	printed	1 mM xylene cyanol-FF and 10 mM orange-G
2.9 A	syringe-made	1 mM xylene cyanol-FF and 2.5 mM orange-G
2.9 B	syringe-made	1 mM xylene cyanol-FF
2.9 C	printed	1 mM xylene cyanol-FF and 2.5 mM orange-G
2.9 D	printed	0.9 mM xylene cyanol-FF and 10 mM orange-G
2.10 A	printed	1 mM xylene cyanol-FF
2.10 C	printed	10 mM pyranine
2.10 A,C	electrode-droplet	10 mM pyranine
2.11 B,D	printed	10 mM pyranine
2.11 B,D	electrode-droplet	10 mM pyranine
2.13 A	pipette-made	1 mM xylene cyanol-FF and 2.5 mM orange-G
2.14 A	printed	0.32 mM xylene cyanol-FF and 2.5 mM orange-G
2.14 B,D	printed	0.16 mM xylene cyanol-FF and 0.8 mM orange-G

6.1.3.2 Folding Droplet Network Solutions.

Volume changing and self-folding droplet networks of Chapter 2, comprised of diluted **standard print solution**. The dilution was with ultrapure water, at the relevant volumes to obtain the salt concentrations stated in the captions of **Figure 2.13** and **Figure 2.14**.

6.1.3.3 Alpha Hemolysin Solution

Ionically conductive pathway networks were printed with a solution containing alpha hemolysin (αHL) that was diluted a 100-fold in **standard print solution**. The undiluted solution comprised ~2 mg mL^{-1} of heptameric αHL in 20 mM sodium phosphate buffer

with 150 mM NaCl and SDS (0.3% w/v) at pH 8.0. The electrode-impaled-droplets in the electrical recordings also used this diluted αHL solution.

The heptameric αHL solution was produced by a former Bayley research group member, Qiuhong Li (University of Oxford), and stored at -80 ºC until use. This protein solution was formed as described in the reference[188]. In brief, a culture was grown from a single colony of the Wood 46 strain of *Staphylococcus aureus* (*American Type Culture Collection*). Then, spontaneously formed αHL heptamers were precipitated from the culture and resuspended. This solution was dialysed and then purified, first by cation exchange chromatography and then by gel electrophoresis to give a 90% purity homoheptamer (as judged by SDS page).

6.1.3.4 Cell-Lines

Multiple cell-lines were used throughout the experiments in Chapter 3 and Chapter 4 such as HEK-293 derivatives and oMSC derivatives. The HEK-293 derivatives are established cell lines, with HEK-293T cells a gift from the Schofield Lab, University of Oxford, and HEK-293/YFP and HEK-293/CFP purchased from *Cell*. Ovine mesenchymal stem cells (oMSCs) were extracted from the bone marrow of sheep at the Royal Veterinary Collage London. Murine chondrocytes were derived from murine mesenchymal stem cells that were isolated from mouse femurs by Dr Shang Zhang at the University of Bristol. Osteoblasts were formed from oMSCs by Madeline Burke and James Armstrong in Bristol (see *section 6.4.2*).

6.1.4 Cell-Culture Solutions

This section lists the common cell culture solutions use throughout Chapter 3 and Chapter 4.

6.1.4.1 Basic Culture Media

Each cell type has its own specific cell culture medium composition. All culture media were composed of an essential medium with or without the following supplements: 10% v/v FBS (*Sigma-Aldrich*), 2 mM GlutaMAX™ (*Life-Technologies*), 0.1 mM minimum essential medium (MEM) non-essential amino acids (*Sigma-Aldrich*), 10-25 mM HEPES (pH 7.0-7.6, *Sigma-Aldrich*), 100 U/mL penicillin and 100 µg/mL streptomycin (*Life-Technologies*). The ratio of these components can be seen in **Table 6.3**.

Table 6.3 Compositions for standard culture media used to grow the various cell-lines. The 100× concentrated stocks are 200 mM L-alanyl-L-glutamine (GlutaMAX™), 10 mM MEM non-essential amino acids (MEM-NEAA), and 10,000 U/mL penicillin with 10,000 µg/mL streptomycin (PenStrep). Stock 1 M HEPES was supplied at pH 7.0-7.6.

Cell Culture Medium Type	Culture Media Composition						
	Base Culture Medium	FBS (% v/v)	GlutaMAX™ (100×) (% v/v)	100× MEM-NEAA (% v/v)	1 M HEPES (% v/v)	100× PenStrep (% v/v)	Additional Nutrients
HEK-293T culture medium	DMEM D6546	10	1	0	0	0	No
HEK-293/XFP culture medium	DMEM D6546	10	1	1	0	0	No
initial cell scaffold culture medium	DMEM D6546	10	1	0	0	0	No
standard cell scaffold culture medium	DMEM D6546	10	1	1	1	1	No
MSC culture medium	DMEM D5564	10	1	0	0	1	Yes
MSC differentiation medium	DMEM D5671	0	1	0	1-2	1	Yes
MSC control medium	DMEM D5671	0	1	0	1-2	1	Yes
chondrocyte culture medium	DMEM D5564	10	1	0	0	1	Yes
osteoblast culture medium	MEM M4526	10	1	0	0	1	Yes

The base culture medium, was an essential medium. This varied between the different cell lines and was either Dulbecco's modified Eagle's Medium (DMEM) or minimum essential medium (MEM). Specifically three different DMEM culture media were used throughout the culture of most cell lines. DMEM D6546 (*Sigma-Aldrich*) was a high glucose culture medium used for all HEK-293 cell-line derivatives. DMEM D5564 (*Sigma-Aldrich*) was a low glucose culture medium used in the culture of MSCs. Whilst DMEM D5671 (*Sigma-Aldrich*) was a high glucose culture medium with no sodium pyruvate, used to make **DMEM-ITS** base culture medium (see *section 6.1.4.3*). Each DMEM contained either high (4500 mg/L) or low (1000 mg/mL) glucose, alongside sodium bicarbonate, pyridoxine hydrochloride and 10 mg/L sodium pyruvate (unless stated). For osteogenic differentiation of oMSCs and culture of osteoblasts, MEM M4526 (*Sigma-Aldrich*) was used, and contained sodium bicarbonate and increased amino acid concentrations compared to standard MEM. The base medium of each cell-line's culture medium is also described in **Table 6.3**.

Additional nutrients or special antibiotics were also used for all cell-lines apart from the HEK-293T. These are described below for each cell type and **Table 6.4** displays a summary of growth factor supplements for oMSC culture.

6.1.4.2 Fluorescent HEK-293 Culture Medium

The fluorescent protein expressing HEK-293 cells were cultured in **HEK-293/XFP culture medium** (**Table 6.3**). The solution was supplemented with 10 µg/mL blasticidin. Stock blasticidin solution (10 mg/mL) was prepared by dissolving blasticidin powder (50 mg, *Life-Technologies*) in filter sterilised ultrapure water (5 mL) and stored as 10 µL aliquots at -20 °C. The stock solution was added at 1 µL/mL per culture flask.

6.1.4.3 oMSC and Chondrocyte Culture Medium

All oMSC culture media involved additional supplements. **MSC culture medium** (**Table 6.3**), was freshly supplemented (i.e. just before time of use) with 5 ng/mL FGF from stock

solutions (see *section 6.1.4.6*). **Chondrocyte culture medium** (**Table 6.3**) was exactly the same as the **MSC culture medium** (**Table 6.3**).

6.1.4.4 oMSC Differentiation Media

For MSCs differentiation experiments, the cells were cultured in **MSC differentiation medium** or **MSC control medium** (**Table 6.3**), the base culture medium for both was **DMEM-ITS**. This **DMEM-ITS** comprised of DMEM D5671 supplemented with ITS (insulin-transferrin-selenium) at 10.0 mg/mL bovine insulin, 5.5 mg/mL human transferrin and 6.7 µg/mL sodium selenite (with 100× ITS solution from *Life-Technologies*). It also contained 1 mM sodium pyruvate (*Sigma-Aldrich*), 2 mM GlutaMAX™, 100 U/mL penicillin and 100 µg/mL streptomycin. The **MSC differentiation medium** for day 0-7 also contained growth factors (**Table 6.4**). These were 100 nM dexamethasone, 80 µM ascorbic acid-2-phosphate and 10 ng/mL transforming growth factor-β3 (TGF-β3), all freshly supplemented from stock solutions (see *section 6.1.4.6*). After day 7 the **MSC differentiation medium** additionally included 10 ng/mL insulin, also added fresh. Whereas the **MSC control medium** is the same as **MSC differentiation medium** for day 0-7, but omitted the TGF-β3.

Table 6.4 Proportion of additional nutrient supplements added to the MSC media. The nutrients added are from stock solutions which are as follows, 100× concentrated ITS (at 1.00 g/mL bovine insulin, 0.55 g/mL human transferrin and 0.67 mg/mL sodium selenite), 100×concentrate sodium pyruvate (100 mM), 10 µg/mL FGF, 100 µM dexamethasone, 80 mM ascorbic acid-2-phosphate, 10 µg/mL TGF-β3 and 10 mg/mL insulin.

Culture Media Type	Proportion of Additional Nutrient Supplements						
	ITS (% v/v)	Sodium Pyruvate (% v/v)	FGF µL/mL	Ascorbic Acid µL/mL	Dexametha-sone µL/mL	TGF-β3 µL/mL	Insulin µL/mL
chondrocyte / MSC culture medium	0	1	0.5	0.0	0.0	0.0	0.0
MSC differentiation medium (day 0-7)	1	1	0.0	1.0	1.0	1.0	0.0
MSC differentiation medium (day>7)	1	1	0.0	1.0	1.0	1.0	1.0
MSC control medium	1	1	0.0	1.0	1.0	0.0	0.0

6.1.4.5 Osteoblast Culture Medium

For MSC osteogenesis, the **osteoblast culture medium** (**Table 6.3**) also contained 50 µL/mL StemXVivo™ osteogenic supplement (*R&D Systems*), which was added as supplied on the day of use. Osteogenic supplement was stored as aliquots at -20 °C.

6.1.4.6 Growth Factor Stock Solutions

Stock solutions of supplements, FGF, dexamethasone, ascorbic acid, TGF-β3 and insulin, were all prepared were prepared by Madeline Burke and James Armstrong. Powdered reagents were dissolved into solutions, which were vortexed mixed, filter-sterilised and then stored as aliquots at -20 °C. Stock 10 µg/mL FGF solution was made by dissolving recombinant human FGF (50 µg, *PeproTech*) in filter-sterilised 5 mM Tris·HCl solution (5 mL, pH 7.6, *Sigma Aldrich*). The 100 µM dexamethasone stock was prepared by dissolving dexamethasone (3.925 mg, *Sigma-Aldrich*) in ethanol (1 mL) and then diluting to a 0.01% v/v solution in 1 mL **DMEM-ITS** (*section 6.1.4.4*). For ascorbate, the 80 mM

stock was made by dissolving L-ascorbic acid 2-phosphate sesquimagnesium salt hydrate (*Sigma-Aldrich*) in ultrapure water (3 mL). The 10 μg/mL TGF-β3 stock was created by dissolving recombinant human TGF-β3 (*R&D Systems*) in filter sterilised 4 mM hydrochloric acid (*Sigma-Aldrich*) containing 1 mg/mL BSA (*Sigma-Aldrich*). Finally, the 10 mg/mL stock insulin was prepared by dissolving insulin (20 mg, *Sigma-Aldrich*) in ultrapure water diluted acetic acid (2 mL, pH 2.0, *Sigma-Aldrich*).

6.1.5 Scaffold Supplement Preparation

This section describes how the additives of the scaffold solutions were prepared.

6.1.5.1 10 mM Fmoc-IG & 10 mM Fmoc-FF solutions

10 mM solutions of Fmoc-isoleucine-glycine (Fmoc-IG) and Fmoc-phenylalanine-phenyalanine (Fmoc-FF), were prepared from powder aliquots (*Bachem*) stored at -20 °C and allowed to warm to room temperature. Fmoc-IG (16 mg) and Fmoc-FF (12 mg) were separately dissolved in ultrapure water (1.5 mL) with 1 M NaOH (10-20 μL), and left to stir overnight. The partially solubilised Fmoc-dipeptide solution was sonicated (20 min, 37 °C, 40 kHz) in a ultrasonic bath [2800 model, *Branson*, UK], pH corrected with 0.1 mM NaOH to either 8.50 (Fmoc-IG) or 10.50 (Fmoc-FF) and then diluted to 3 mL total volume in ultrapure water. Fmoc-IG and Fmoc-FF were used within a week and pH corrected if necessary before use.

6.1.5.2 10 mM **Fmoc-XX** Solution

An **Fmoc-XX** solution was an equal molar ratio solution of Fmoc-IG and Fmoc FF. For a 10 mM **Fmoc-XX** solution, 10 mM Fmoc-FF and 10 mM Fmoc-IG were mixed as a 1:1 v:v solution and then sonicated (40 kHz, 5 min). Here the molarity of the **Fmoc-XX** is the sum of constituent Fmoc-FF and Fmoc-IG molarities. **Fmoc-XX** was made fresh on the day of use.

6.1.5.3 PEG-X Solutions

All PEG X solutions (where X is either 400, 4,000 or 20,000 molecular weight) were made up as w/v solutions. In brief, the PEG X (*Sigma-Aldrich*) was weighed within a volumetric flask at the required weight (where 10 g/L = 1% w/v solution), and topped up with either ultrapure water or Dulbecco's phosphate buffer solution (PBS, *Sigma-Aldrich*). For **SS4** (see *Section 6.1.6*) the PEG additive was added as an 80% w/v PEG 400 solution.

6.1.5.4 Agarose Solutions

Ultra-low gelling point agarose (ULGT-agarose) powder (A5030, *Sigma Aldrich*) was used to make the 13-15 mg/mL ULGT-agarose solution. Typically ULGT-agarose powder and base culture medium were warmed in a water bath (65 °C). Warmed ULGT-agarose powder (typically ~12 mg) was dissolved in warmed base culture medium (typically ~0.8 mL). To aid solvation, the solution was vortex mixed and may have been, mechanically perturbed by micropipette aspiration or sonicated (40 kHz). The ULGT-agarose solution once made was left in the water bath (65 °C). The base culture medium was either Opti-MEM® (31985-062, *Life Technologies*) for HEK-293 derivative cell lines or **DMEM-ITS** (*section 6.1.4.4*) for oMSC, osteoblasts and chondrocytes.

6.1.5.5 ECM Protein Supplements

The ECM proteins were prepared by diluting stock concentrations into an active gel form i.e. the working solution. Stock solutions of the ECM proteins were 5.0 mg/mL bovine collagen type I (*Life Technologies*), 1.0 mg/mL natural mouse laminin (*Life Technologies*) and 1.0 mg/mL human fibronectin (*Life Technologies)*. They were stored as aliquots at either 4 °C (collagen) or -20 °C (laminin and fibronectin). The collagen type I gel working solution (3.0 mg/mL) was prepared by mixing ice cold reagents in the order: collagen type I stock (50 µL), 10× concentrate Dulbecco's phosphate buffer solution (10× PBS, 8.3 µL, *Sigma-Aldrich*), 1 N NaOH (1.3 µL) and ultrapure water (23.8 µL). Laminin and fibronectin working solutions (0.1 mg/mL) were made by diluting their respective

stock solutions in PBS (typically 10 µL protein stock with 90 µL PBS). All ECM protein working solutions were prepared just before their addition to the bioink, in a laminar flow biological safety cabinet.

6.1.6 Scaffold Solutions

Various scaffold solutions were used in Chapter 3 and Chapter 4. This section goes through the general preparation protocols for making cargo-less/void scaffold solutions. The addition of cells and beads to these solutions is later described in *section 6.5*.

6.1.6.1 Preliminary Scaffold Solution

In section 3.6.3, cells were printed in an initial scaffold solution composed of only **MSC culture medium** (*section 6.1.4*). This scaffold solution was unnamed.

6.1.6.2 Standard Scaffold Solutions

The scaffold solutions were denoted as **scaffold solution 1-8** (**SS1**-**SS8**), and are summarised in **Table 6.4**. These were used and tested in Chapter 3 (**SS1**-**SS6**) and Chapter 4 (**SS6**-**SS8**). They can be broadly split into non-agarose based (**SS1**-**SS4**) and agarose based (**SS5**-**SS8**), which gave oil-bound and phase-transferrable scaffolds respectively. Each scaffold solution was made of a liquid base, generally culture medium, containing a mix of scaffold supplements prepared as described in *section 6.1.5*.

6.1.6.3 Base Culture Medium of **SS1**-**SS8**

For all scaffold solutions, the base culture medium was kept consistent. Solutions to incorporate HEK-293T cells contained base culture medium Opti-MEM® [31985-062, *Life Technologies*]. Whilst solutions intended for oMSCs contained **DMEM-ITS** (*section 6.1.4*). These scaffold solutions were denoted as **SSXh** and **SSXm** for HEK-293T and oMSC intended solutions respectively, here the **X** represents the number of the scaffold solution. For example, the **SS1** for MSC use contained **DMEM-ITS** and was denoted **SS1m**.

Table 6.5 List of standard scaffold solutions and their composition. Here the base culture medium was Opti-MEM® for HEK-293T experiments and **DMEM-ITS** (*section 6.1.4*) for oMSC experiments.

Name	Scaffold Solution Type	Typical Composition
SS1	culture medium only	90% v/v culture medium 10% v/v CAM & PI dye stock in culture medium
SS2	culture medium with **Fmoc-XX**	60% v/v culture medium 30% v/v 1-10 mM **Fmoc-XX** in ultrapure water 10% v/v CAM & PI dye stock in culture medium
SS3 Test	PBS or water with PEG	100% v/v PBS or ultra-pure water 10-40% w/v PEG *X*
SS3 Bead	culture medium with PEG	50% v/v 80% w/v PEG 400 in PBS 50% v/v microsphere solution
SS4	culture medium with **Fmoc-XX** & PEG	55% v/v culture medium 10% v/v 10 mM **Fmoc-XX** in ultrapure water 25% v/v 80% w/v PEG 400 in PBS 10% v/v CAM & PI dye stock in culture medium
SS5	agarose only	13-15 mg/mL agarose in culture medium or PBS
SS6	agarose with **Fmoc-XX** (initial)	89% v/v 13-15 mg/mL agarose in culture medium 11% v/v 10 mM **Fmoc-XX** in ultrapure water
SS7	agarose with **Fmoc-XX** (diluted)	80% v/v 13-15 mg/mL agarose in culture medium 10% v/v 10 mM **Fmoc-XX** in ultrapure water 10% v/v PBS
SS8	agarose, **Fmoc-XX** with ECM protein	80% v/v 13-15 mg/mL agarose in culture medium 10% v/v 10 mM **Fmoc-XX** in ultrapure water 10% v/v ECM protein dissolved in PBS

6.1.6.4 General Conduct

To minimise bacterial infection, different steps were taken to sterilise the scaffold solution, however, each scaffold solution production used aseptic techniques and solution processing where possible was performed in a laminar flow biosafety cabinet.

6.1.6.5 Non-Agarose Based Solutions (**SS1**-**SS4**)

The solutions **SS1** to **SS4** were prepared by vortex mixing the base solvent, of either culture medium, ultra-pure water or Dulbecco's phosphate buffer solution (PBS), with the relevant scaffold supplement at the appropriate volume ratios. Calcein-AM (CAM) and Propidium iodide (PI) were contained in **SS1**, **SS2** and **SS4,** added as a working live/dead dye solution. This working solution comprised of 50 μM CAM and 50 μM PI in culture medium (see *section 6.11.3.3* for preparation). The scaffold solutions are now described.

Scaffold Solution 1 (**SS1**): Culture *medium Only*

SS1 was a culture medium only solution and consisted of a 9:1 v:v mix of culture medium with working live/dead dye solution. The final composition of **scaffold solution 1** was: 5 μM calcein-AM and 5 μM propidium iodide, in 100% v/v base culture medium.

Scaffold Solution 2 (**SS2**): Culture medium with **Fmoc-XX** additive

SS2 was a **Fmoc-XX** supplemented culture medium that comprised of a 6:3:1 v:v:v mix of culture medium with, 1-10 mM **Fmoc-XX** solution and working dye solution. Typically 4 mM **Fmoc-XX** was added at 30% v/v. The final composition of **scaffold solution 1** was: 0.3-3.0 mM **Fmoc-XX**, with 5 μM calcein-AM and 5 μM propidium iodide, in 70% v/v culture medium and 30% v/v ultrapure water.

Scaffold Solution 3 (**SS3**): Water or PBS with PEG additive

SS3 was a solution supplemented with PEG but no **Fmoc-XX**. The base composition varied depending on its use for either test print experiments (**SS3 test**) or bead print

experiments (**SS3 bead**). For the **SS3 test**, PEG X (*section 6.1.5.3*) was diluted in ultra-pure water or PBS to give the required PEG X weight fraction. Whilst **SS3 bead** comprised of 13:5:2 v:v:v culture medium, 80% w/v PEG 400 in PBS. The final composition of **scaffold solution 3 test** was: 10-40% w/v PEG X in 100% v/v PBS or ultra-pure water. The final composition of **scaffold solution 3 bead** was: 0-20% w/v PEG 400, in 50% v/v PBS and 50% v/v 10 μm bead solution (section 6.5.2).

Scaffold Solution 4 (**SS4**): Culture medium with **Fmoc-XX** and PEG additives

SS4 was a solution supplemented with PEG and **Fmoc-XX**. It comprised of 55% v/v culture medium with 10% v/v 4 mM **Fmoc-XX**, 25% v/v PEG 400 in PBS (at 80% w/v concentration) and 10% v/v working live/dead dye solution. The final composition of **scaffold solution 4** was: 20% w/v PEG 400 with 5 μM calcein-AM and 5 μM propidium iodide, in 65% v/v culture medium, 25% v/v PBS and 10% v/v ultra-pure water.

6.1.6.6 Agarose Based Solutions (**SS5-SS8**)

The **scaffold solutions 5-8** consisted of ULGT-agarose solution with or without scaffold supplements, both prepared as described in *section 6.1.5*. These solutions were prepared as a sol and kept above the agarose gel melting temperature (i.e. ~50 °C) until the addition of ECM protein or cells, at which point the solution was kept at 37 °C. If cells were to be added, the solutions were irradiated with UV (15 min, 365 nm) prior to cell addition. Solutions were placed 4.5 cm beneath an UV LED [Eclipse-M365L2-C5, *Nikon*, Japan] controlled by an LED driver [LEDD1B, *Thorlabs*, USA] set to half power. All agarose based scaffold solutions were used on the day of creation and not stored for future use.

Scaffold Solution 5 (**SS5**): Agarose only in culture medium or PBS

SS5 was the preliminary agarose scaffold solution containing 13-15 mg/mL agarose in culture medium or PBS.

Scaffold Solution 6 & 7 (**SS6-7**): Agarose with **Fmoc-XX** additive in culture medium

The Fmoc-dipeptide supplemented agarose solutions, were prepared as an 8:1 v:v mix of 13-15 mg/mL agarose with 10 mM **Fmoc-XX** respectively. This original agarose solution was either left undiluted for **SS6** or for **SS7** was diluted with PBS to a final PBS concentration of 10% v/v. UV treatment was performed after the agarose and Fmoc-dipeptides were mixed. The final composition of **scaffold solution 6** was: 11.6-13.3 mg/mL agarose and 1.1 mM **Fmoc-XX**, in 88.9% v/v culture medium and 11.1% v/v ultrapure water. Whereas the final composition of **scaffold solution 7** was: 10.4-12.0 mg/mL agarose and 1.0 mM **Fmoc-XX**, in 80% v/v culture medium, 10% v/v ultrapure water and 10% v/v PBS.

Scaffold Solution 8 (**SS8**): Agarose with **Fmoc-XX** and ECM additives in culture medium **SS8** was composed of **SS6** supplemented with ECM proteins (either collagen, fibronectin or laminin) dissolved in PBS at varied concentrations. To **SS6**, a working solution of ECM protein in PBS was added followed by PBS to give a 10% v/v PBS fraction. The scaffold solution at this stage would be sonicated (5 min, 40 kHz) in an ultrasonic bath [2800 model, *Branson*, UK]. The ECM proteins were supplemented between the concentration ranges of: 3.5-300 μg/mL for collagen; and 0.5-20 μg/mL for both fibronectin and laminin. A supplement of 15 μg/mL collagen became a standard for microtissue growth.

The final composition for the standard collagen supplemented **scaffold solution 8** was: 10.4-12.0 mg/mL agarose, 1.0 mM **Fmoc-XX** and 15 μg/mL collagen, in 80% v/v culture medium, 10% v/v ultrapure water and 10% v/v PBS.

6.2 Droplet Network 3D Printing

This section explains the setup and functioning of the printer developed in Chapter 2. The printer was also used in the same manner in Chapter 3 and Chapter 4, after some minor modifications (*section 6.6*).

6.2.1 Printer Overview

The printer consisted of one or two static piezoelectric powered droplet generators (section 6.12.1.1), which ejected droplets from their oil-submerged nozzle into a lipid-in-oil bath. The bath rested on a motorised stage [PatchStar 7000, *Scientifica*, UK], which moved in x (left, right), y (front, back), z (up, down) dimensions within a 2 cm^3 confinement. For dual nozzle printing, one piezo remained static, whilst the other was mounted on a micromanipulator, the tips of the two droplet generator's nozzles were then orientated within 200 μm of each other. Printing was monitored by using a side-on stereomicroscope [SMZ660, *Nikon*, Japan], the ocular of which held a web-camera [Lifecam HD-3000, *Microsoft*, USA] to record videos and images or printing.

Droplet ejection was triggered by the application of a square-wave voltage pulse (from custom-electronics) to the piezo element of the droplet generator (*section 6.2.3*). Lab-designed print programs, designed by Dr Gabriel Villar, allowed both user defined droplet ejection (*section 6.2.4*) and automated printing of networks (*section 6.2.5*).

6.2.2 Printing Process

The protocol to automatically print a droplet network is as follows.

6.2.2.1 Droplet Generator Preparation

Prior to printing, the droplet generator was prepared i.e. cleaned, filled with solution and then had the nozzle inserted. The droplet generator was usually cleaned by rinsing the aqueous chamber with ultrapure water and ethanol, and then dried under a gentle flow of nitrogen. The aqueous chamber of the droplet generator was filled through its inlet with ~400 μL of either the print solution or ultrapure water, using a micropipette with a gel-loading tip. When the nozzle was inserted, it spontaneously filled with the chamber solution through capillary action. After nozzle insertion the chamber was topped up with additional solution.

6.2.2.2 Loading a Print Solution

For printing of standard buffered salt solutions, the whole chamber of the droplet generator was filled with the print solution, and no further loading was necessary. Whereas for the αHL solutions and fluorescent buffered salt solutions, the piezo chamber was filled with ultrapure water and then the print solution was loaded into the nozzle at a low volume (~4 μL).

Low volume loading was performed in all instances as follows, hexadecane (~8 μL) and print solution (~10 μL) were loaded into separate wells of a printer loading well array (*section 6.12.1.3*). The nozzle was lowered into the hexadecane and suction was applied to the piezo's inlet by a P20 micropipette, until ~2 μL of hexadecane was drawn into the capillary, after which the nozzle was raised. By the same process, the print solution was loaded into the nozzle below the oil plug at ~4 μL.

6.2.2.3 Tuning Droplets

The loaded piezo's nozzle was lowered into a bath containing lipid-in-oil (~300 μL). The graphical user interface (*section 6.2.4*) was be used to eject droplets by application of different square-wave voltage pulses to the piezo. An ideal pulse was searched for; here, an ideal pulse is one that reproducibly ejected singlet droplets of uniform size. If two droplet generators were used then ideal pulses were determined for each droplet generator. During this tuning stage the size of the droplets (i.e. droplet spacing parameter) and the nozzle offset values were determined. The droplet size was determined as the *x* distance moved by the nozzle to allow ejection of two droplets such that they just kissed. The nozzle offset was deduced by ejecting one droplet from generator II directly onto a droplet ejected from generator I; the offset was the distance moved (in *x*, *y*) to allow this to happen.

6.2.2.4 Automated Printing

The nozzle(s) would be kept in the oil bath whilst print parameters (*section 6.2.6*) were assign in the automated print software (*section 6.2.5*). Automated printing would then be

initialised (*section 6.2.5*), with the layer by layer ejection of droplets, until the print model was finished. Once a network was printed, the software was set for the subsequent network. This process would be repeated until the final network was printed, at which point the nozzle was raised out of the oil and the print container was left to rest for 5 min.

6.2.3 Printer Electronics

The following text (section 6.2.3) was adapted from *A tissue-like printed material* (DOI: 10.1126/science.1229495)[1] and reprinted with permission from AAAS.

The electronic circuit built to drive the droplet generators is shown schematically in **Figure 6.1** and was designed by Dr Gabriel Villar. The circuit interprets instructions from a computer to produce a square voltage pulse of specified duration and amplitude, and applies this voltage to the piezoelectric transducer, in either of two droplet generators. Below is a description of how the circuit generates the voltage pulse.

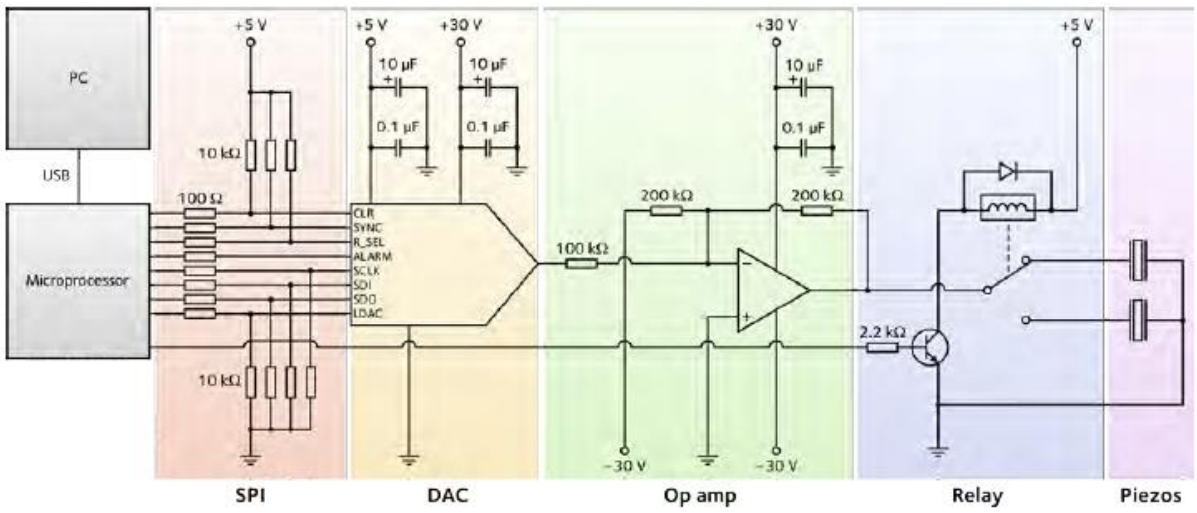

Figure 6.1 Schematic of driving electronics for droplet generators. The electronics allow a computer to apply a voltage in the range -30 V to +30 V, with 12-bit resolution, to one of two piezoelectric transducers. Abbreviations: PC, personal computer; USB, universal serial bus; SPI, serial peripheral interface; DAC, digital-to-analogue converter; op amp, operational amplifier. The figure is from *A tissue-like printed material* (DOI: 10.1126/science.1229495)[1] and reprinted with permission from AAAS.

Piezo selection. First, the computer sends a serial message that represents the desired piezo to a microcontroller board [Arduino Uno, *SmartProjects*, Italy]. The microcontroller interprets this message, and activates a relay [NRP-04, *NCR*, China] through a transistor such that the desired piezo will receive the voltage output of the circuit. Once a piezo is selected in this way, it is held at the maximum negative voltage of -30 V. The piezo terminal that is connected to the voltage output was chosen such that a negative voltage produces compression of the piezo.

Voltage output. The computer then sends a serial message to the microcontroller that represents the instruction to generate a voltage pulse. The duration and amplitude of the pulse can be either specified in the serial message or previously programmed into the microcontroller. The microcontroller interprets this message, and writes a value encoding the amplitude of the voltage pulse to the digital-to-analogue converter (DAC) [AD5504, *Analog Devices*, USA] through a serial peripheral interface (SPI) bus. The DAC outputs a corresponding voltage between 0 V and +30 V with 12-bit resolution. The DAC output enters an operational amplifier [OPA551, *Texas Instruments*, USA] circuit that acts as a current buffer, and also offsets and increases the output voltage range to -30 V to +30 V. The output of this circuit is applied to the piezo previously selected by the relay. After the specified duration of the voltage pulse, the microcontroller again sets the piezo to the maximum negative voltage. Voltage pulses typically had a duration of 100-800 μs and a peak-to-peak amplitude of 20-60 V.

6.2.4 Graphical User Interface

A graphical user interface (**Figure 6.2**) that allowed the printer user to eject droplets and position the oil-bath in real-time was written in the Processing programming language by Dr Gabriel Villar. Here the voltage pulse for the droplet generator could be applied between 50-1000 μs pulse width and between 0-60 V peak-to-peak amplitude. The number of pulses (droplets ejected) and the pulse frequency (delay between droplets) could also be set. The interface was used to tune droplets (*section 6.2.2.3*) and to print networks in bulk aqueous (*section 6.2.8*).

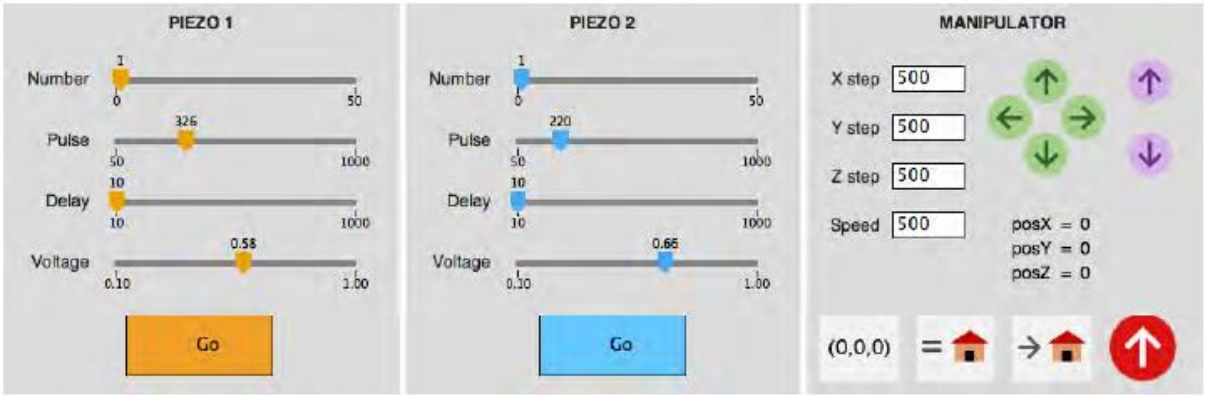

Figure 6.2 Graphical user interface. The left and centre panels allow, for each of the two generators, variation of the duration (in μs) and amplitude (as a proportion of 60 V) of the voltage pulse, the triggering of droplet ejection, variation of the number of droplets to be ejected per trigger, and variation of the delay (in ms) between multiple droplets made per trigger. The right panel allows interactive control of the manipulator, and variation of the manipulator step size and speed. The figure is from *A tissue-like printed material* (DOI: 10.1126/science.1229495)[1] and reprinted with permission from AAAS.

6.2.5 Automated Printing Program

The following text (*section 6.2.5*) is adapted from *A tissue-like printed material* (DOI: 10.1126/science.1229495)[1] and reprinted with permission from AAAS.

Droplet networks were printed according to an algorithm written in the Processing programming language by Dr Gabriel Villar, and executed by the computer that controlled the two droplet generators and the motorized micromanipulator. The general pattern in which networks are printed has already been described in *section 2.6.2*. A description of how the printing algorithm allows networks to be successfully printed is described.

6.2.5.1 Computer Algorithm

The algorithm begins with an initialization phase that is executed once, followed by a printing phase that persists until printing has completed.

Initialization. In the initialization stage, the user first inputs the print parameters (*section 6.2.6*). The program then loads into its memory all the maps that define the network to be printed. A path for the printing nozzles, encoded as a series of goals

according to the pattern detailed above, is established for the first pass of the first layer. Finally, the manipulator is instructed to move to the first goal. Once that goal is reached, the program sets a lower speed for the subsequent motion of the manipulator.

Printing. In the printing phase, the computer synchronizes the motion of the oil bath with the ejection of droplets from the two generators. When each goal is reached, a droplet is ejected only if the goal type corresponds to the current pass. After allowing a delay after ejection, the next goal is determined according to the basic pattern of printing (*section 2.6.2*). If the current goal represents the end of a row, another delay is introduced. Finally, if the **interface reset period** has elapsed upon reaching the current goal, the oil-aqueous interface of the idle generator in the current pass is reset as described in *section 6.2.5.2*.

6.2.5.2 Leakage Prevention

As described in *section 2.6.3.2*, when a nozzle was beginning to leak a high frequency, low amplitude voltage waveform could be applied to the piezo-element of the droplet generator to reset the interface. The voltage waveform used to reset the interface typically consisted of three square pulses, each of 40 μs duration and -12 V amplitude, with a 20 ms interval between them. This could either be applied manually in real-time or automatically during printing. Specifically in each automated print pass, this waveform was applied every *n* goals to the droplet generator not used in that pass, where *n* is the **interface reset period**.

6.2.5.3 Goal Skipping

The print algorithm includes a goal skipping command. This allows the printing path to miss goals representing no droplet production, skipping to the next goal that requires a droplet in the current pass. This command is initialised only when no droplets have been ejected at any of the previous *n* goals in the current pass, where *n* is the **goal skipping threshold**. The goal skipping threshold is chosen to allow recently-ejected droplets

enough time to incorporate into the network, and so be unaffected by the motion of the printing nozzles.

6.2.6 Print Parameters

The user-defined parameters of the automated printing program were related to the droplet network print model and print settings. The print model was defined as cross-sectional maps printed for a set number of layers (*section 2.6.2*). While the print settings were: starting position, spacing between droplets (in *x* and *y*), delay times, piezo voltage pulse, **interface reset period** (*section 6.2.5.2*) and **goal skipping threshold** (*section 6.2.5.3*). The *y* dimension of spacing between droplets was set equal to the *x* spacing for the prints of Chapter 2 and was latterly changed for the prints of Chapter 3 and 4 to 87% of the *x* spacing to attain hexagonal packing. The three delay times correspond to delays used, after each droplet ejection, after finishing each row and after finishing each layer. The other parameters that were user defined are nozzle positioning offsets for: nozzle II relative to nozzle I (*section 6.2.2.3*), alternate droplet rows (in *x*) and alternate droplet layers (in *x* and *y*). In all cases the positioning offsets for alternate rows and layers was set to half the *x* spacing, i.e. half the printed droplet diameter. The typical user settings for a buffered salt solution print (Chapter 2) can be seen in **Table 6.6**.

Table 6.6 Typical user defined print parameters for buffered salt solution prints of Chapter 2.

Parameter	Typical Value
x spacing between droplets	50 μm
y spacing between droplets	50 μm
x offset for alternative rows	25 μm
x and *y* offset for alternative layers	25 μm
delay after ejecting each droplet	200 ms
delay after finishing each row	2 s
delay after finishing each layer	4 s
goal skipping threshold	4 goals
interface reset period	10 goals
manipulator speed during printing	200 μm s^{-1}
amplitude of piezo pulse	30 V
width of piezo pulse	200 μs

6.2.7 Printed Droplet Networks (Ch. 02)

Printed droplet networks of Chapter 2 were fabricated using the droplet printer at ambient temperatures (20-22 ºC). Non functionalised networks were fabricated by printing **standard print solutions** (*section 6.1.3.1*) into a **standard print oil** (*section 6.1.2*). Functionalised networks were also printed in **standard print oil** however, instead of using **standard print solutions,** αHL containing print solutions (*section 6.1.3.3*) or folding network solutions (*section 6.1.3.2*) were printed as appropriate.

6.2.8 Encapsulated Networks (Ch. 02)

A drop of **standard print oil** (*section 6.1.2*) was placed on a polymethyl methacrylate coated silver wire (ø 100 μm, *Sigma-Aldrich*) held within a custom-made cuvette filled with dyed **standard print solution** (*section 6.1.3.1*). The droplet generators' nozzles were suction loaded with **standard print solution** and then an oil plug vertically under (*section 6.2.2.2*). The loaded nozzles were lowered into the suspended oil drop and the oil plug

spontaneously flowed out of the nozzle. Droplets were subsequently ejected in user defined positions using the printer's graphical user interface (*section 6.2.4*). After droplet ejection, the remaining oil of the suspended drop was removed into the nozzle by aspiration.

6.3 Droplet Network Analysis (Ch. 02)

This section goes through the analysis methods used on droplet networks produced in Chapter 2.

6.3.1 Microscopy

The majority of printed droplet network micrographs and time-lapse micrographs were imaged with a SZX10 stereomicroscope [*Olympus*, Japan] and captured with a micropublisher 5.0 RTV camera [*Q-imaging*, Canada]. Micrographs of the electrophysiology networks were taken by a digital camera aligned down the ocular of a SMZ660 stereomicroscope [*Nikon*, Japan]. Whilst the fluorescent networks displayed in **Figure 2.7**, were imaged with a SP5 confocal microscope [*Leica*, Germany], imaging details of which are in *section 6.11.1.1* and *6.11.2*.

6.3.2 Testing Droplet Generation

Droplet ejection of the droplet generator was tested for different applied voltage pulses, as seen in **Figure 2.4**. Here, each pulse combination of amplitudes between 0.24-0.60 V (at 0.06 V increments) and pulse-widths between 50-800 μs (at 50 μs increments) were tested. Micrographs of the nozzle were recorded immediately after application of the voltage pulse to the piezo. Reproducibility of droplet generation was tested by applying each pulse combination five times with an interval of 3 s between droplets. This entire procedure was then repeated. It was found that droplets were generated consistently for each voltage pulse combination for a given nozzle ($n = 10$).

6.3.3 Electrophysiology

The text in this section (*6.3.3*) was adapted from *A tissue-like printed material* (DOI: 10.1126/science.1229495)[1] and reprinted with permission from AAAS.

The Ag/AgCl electrodes were prepared by treating silver wire (ø 100 μm, *Sigma Aldrich*) with 25% v/v sodium hypochlorite solution for ~1 h, and then coating the end of each electrode with 3% w/v agarose gel. Currents were measured with the electrodes by using a patch-clamp amplifier [Axopatch 200B, *Axon Instruments*, USA] and a 16-bit digitizer [1322A, *Molecular Devices*, USA]. Signals were processed with a 5 kHz low-pass Bessel filter and acquired at 20 kHz.

6.3.4 Measurements & Modelling

6.3.4.1 Models of Printed Networks

All models of printed networks in oils were performed using computer simulations designed and performed by Dr Gabriel Villar. The simulations were used to investigate mechanical properties of networks (*section 2.6.5*), model the electrically conductive network with a defined pathway (section 2.7.1) and to model the folding of the flower-shaped network which contained osmotic gradients (**Figure 2.14**). Details of the modelling assumptions and parameters can be found in the supplementary information of *A Tissue-Like Printed Material* (DOI: 10.1126/science.1229495)[1].

6.3.4.2 Droplet Volume Calculation

Dr Gabriel Villar performed the droplet volume experiment and measurements. The volume change of droplet pairs ($n = 3$) was recorded as a micrograph every 10 minutes for >2 h duration as shown in **Figure 2.13**. The pairs comprised of a 1M KCl droplet joined to a 250 mM KCl droplet. The bilayer and droplet diameter were measured from these images using ImageJ[134,135]. Droplet volumes and bilayer area were calculated assuming the droplets' geometries were spherical caps.

6.3.4.3 Water Permeability Across Droplet Interface Bilayer

The water permeability coefficient across droplet interface bilayers was calculated by Dr Gabriel Villar using **Equation 6.1**, the derivation of which is in the supplementary information of our Science publication[1] along with further discussion. The variables involved and the values used were as follows: van't Hoff factor of salt (i) = 2 (for KCl); droplet area (A) = measured value (*section 6.3.4.2*); molar volume of water ($\bar{V}$) = 18.0 mL mol^{-1}; osmotic coefficient ($ø$) = 0.90 (from the literature[189]); salt concentration of droplet at time zero ($C_1(0)$) = KCl concentration; initial water transfer across bilayer = measured volume change. The initial rate of water transfer was calculated independently from the first two volume measurements of *section 6.3.4.2.* Resultantly, the permeability coefficient was calculated to be P = 27±5 μm s^{-1}.

Equation 6.1

$$P = [iA\bar{V}ø(C_1(0) - C_2(0))]^{-1} \cdot \left(\frac{dV_1}{dt}\right)_{t=0}$$

6.4 Cell Culture & Harvesting

6.4.1 Cell Maintenance Fore Note

All cells were cultured in 2D before being harvested for cell scaffold experiments, as cell lines came from within the research group and from collaborators, cell culture was performed at different sites. All HEK cell line derivatives were cultured at the Chemistry Research Laboratory, University of Oxford by myself, Dr Sam Olof and Ellina Mikhailova. oMSCs, osteoblasts and chondrocytes were cultured in the Chemistry Department of the University of Bristol by Madeline Burke and Dr James Armstrong.

6.4.2 Osteogenisis of MSCs

Osteoblasts where created by inducing osteogenesis in oMSCs by Madeline Burke & Dr James Armstrong. In brief, oMSCs were cultured in a minimal volume of **osteoblast culture medium** containing osteogenic supplement (see *section 6.1.4.4* for composition). Progress of the osteogenesis was compared to an undifferentiated control sample, prepared similarly but using **osteoblast culture medium** without osteogenic supplement.

6.4.3 2D Cell Culture

All cell-lines were maintained using standard 2D cell-culture protocols[132]. In brief, primary cells or thawed stocks cells were seeded into a tissue culture flask containing pre-warmed culture medium (37 °C). This flask would be transferred to a cell incubator (37 °C, 5% CO_2), where the cells would be allowed to adhere to the plastic substrate and grow. When the cells were 80-90% confluent, the cells would be passaged i.e. sub-cultured into a new culture flask containing warmed culture medium. This would be by resuspending the confluent cells in fresh culture medium and transferring a low fraction (typically 1/6 or 1/12) of this volume to the new flask. The passaged cells would be returned to the cell incubator (37 °C, 5% CO_2) until the next sub-culture. For highly adherent cell lines i.e. oMSCs, HEK-293/CFP and HEK-293/YFP, cell detachment by enzymes, i.e. trypsin, was necessary prior to passage. Trypsinisation was performed by adding trypsin (*Sigma-Aldrich*), at a minimum volume, to the cells and leaving for 5 min in a cell incubator (37 °C, 5% CO_2), after which the flask was mechanically perturbed by hand. The cellular trypsin solution would subsequently be diluted in warmed culture medium and then centrifuged (400×*g*; 4 min), with the resultant pellet resuspended in warmed culture medium, ready to be sub-cultured. If cells were cultured over a long duration i.e. a week, without sub-culture, then the old culture medium would be replaced with fresh warm culture medium every 2-5 days. All cell handling steps such as cell harvesting, sub-culture and culture medium exchanges, were carried out in a laminar flow class II biosafety cabinet with a HEPA (high-efficiency particulate arrestance) air filter. Below are further details on the culture, use and storage, specific to each cell line.

6.4.3.1 HEK-293 Derivatives

The HEK cell line derivatives were grown in the relevant culture media (see *section 6.1.4*) and were passaged 1-3 times a week. HEK-293T were used between the 16th and 40th passage, while HEK-293/YFP and HEK-293/CFP between the 16th and 35th passage.

6.4.3.2 oMSCs

oMSCs were cultured with **MSC culture medium** (*section 6.1.4.3*) and were slower growing compared to HEK-293T so were passaged less frequently 1-2 times a week. The oMSCs were grown up to the 7th passage, but were used between the 1st-4th passage.

6.4.3.3 Ovine Osteoblasts

Osteogenic differentiated and undifferentiated oMSCs were grown in **osteoblast culture medium** (*section 6.1.4.5*) over three weeks with culture medium changed twice a week. Osteoblasts were grown from oMSCs on their first passage and were not further sub-cultured or frozen as a stock solution before use.

6.4.3.4 Chondrocytes

Chondrocytes were cultured in **chondrocyte culture medium** (*section 6.1.4.3*) and passaged 1-2 times a week. Chondrocytes were used prior to the 7th passage and their stock solutions were stored in liquid nitrogen vapour.

6.4.4 Cryopreservation

All cells were cryopreserved in the same manner as described below.

Freezing of Cells. A culture of cells was harvested (*section 6.4.5*) to give a cell suspension. This was centrifuged (300-500×*g*, 3-5 min) and the resultant pellet was resuspended at 1×10^6 to 4×10^6 cells/mL in freezing solutions (*see next paragraph*). Aliquots (1 mL) of this solution were stored into 1.5 mL cryogenic tubes [*Nunc*™, *Thermo Scientific*, USA], which were slowly frozen over 12-24 h at -80 °C in a Mr Frosty freezing

container [*Thermo Scientific, USA*]. Frozen cell stocks were then transferred to their long term storage. All HEK-293 cell derivatives were stored at -80 °C within an ultra-low temperature freezer. Whilst oMSC cells were stored in the vapour phase of liquid nitrogen at -196 °C within a Biorack 6000 refrigerator [*Statebourne Cryogenics*, USA].

The HEK-293 cell-line freezing solution comprised of 70% v/v DMEM D6546, 20% v/v FBS and 10% v/v sterile dimethyl sulfoxide (DMSO, *Sigma-Aldrich*). Whereas the oMSC freezing solution was: 33.3% v/v **MSC culture medium** (see *section 6.1.4.3*), 60% v/v FBS and 6.7% v/v DMSO.

Thawing of HEK-293T Cells. Frozen HEK-293T cell stock solutions were thawed quickly in a water-bath (37 °C) and then diluted into warmed culture medium (10 mL). This solution was centrifuged (400×*g*; 4 min), with the pellet resuspended in warmed culture medium (1 mL). This cellular suspension was seeded into a T25 culture flask containing warm culture medium (5 mL). The cells were then left undisturbed for 24 h in a cell culture incubator (37 °C, 5% CO_2).

Thawing of oMSCs. The frozen oMSC stock solution was thawed quickly in a water-bath (37 °C) and then transferred immediately into a T175 flask containing warmed expansion medium (20 mL). The cells were left to adhered to the plastic substrate by transferring the container to cell culture incubator (37 °C, 5% CO_2).

6.4.5 Cell Harvesting & Resuspension

All cells were harvested in the same manner, either for subculture (*section 6.4.3*) or for resuspension into scaffold solutions (*section 6.5*). For HEK-293T i.e. non adherent cell-lines, confluent cells of a T25 culture flask would be resuspended in Opti-MEM® (5 mL), and an aliquot of this (typically 1-2 mL) would be pelleted by centrifugation (3-5 min, 300-500×*g*) in a 5702 model centrifuge [*Eppendorf*, Germany]. The resultant pellet would be resuspended in the desired solution at the required cell density. Where-as, for adherent cell lines such as HEK-293/YFP and oMSCs, before an aliquot of suspended cell solution was obtained, the culture would first be trypsinised (s*ection 6.4.3*), and then resuspended in Opti-MEM® after centrifugation. When oMSC, osteoblast or chondrocyte

laden scaffold solutions were prepared, the cells were resuspended in **DMEM-ITS** (*section 6.1.4.4*) instead of Opti-MEM®.

6.4.5.1 Calculating Resuspension Volume

To resuspend cells at the selected density from an aliquot of cell suspension the cell density of the aliquot would be measured (*section 6.4.5.2*) and then the resuspension volume would be calculated using **Equation 6.4.** This equation derives from the cell number (N_{cells}) of a solution being equal to cell number density (n_{cells}, in cells/mL) multiplied by the solution's volume ($V_{aliquots}$, in mL) (**Equation 6.2**). For a resuspension, the number of cells doesn't change, hence the cell number formula can be used to equate the original and final volume of solutions (sol.) as **Equation 6.3**, which can then be rearrange as **Equation 6.4**.

Equation 6.2

$$N_{cells} = n_{cells} \times V_{aliquot}$$

Equation 6.3

$$n_{initial\ cells} \times V_{initial\ sol.} = n_{final\ cells} \times V_{final\ sol.}$$

Equation 6.4

$$\frac{n_{initial\ cells}}{n_{final\ cells}} \times V_{initial\ sol.} = V_{final\ sol.}$$

6.4.5.2 Measuring Cell Densities

The standard way to measure the density of the cell aliquot, was to produce a count solution of a 100 µL cell aliquot to 100 µL trypan blue solution (*Life-Technologies*), which stained dead cells only to dark blue. This solution (2×10 µL) was added to a disposable hemocytometer chip which was read by an automated cell counter [Countess II FL, *Invitrogen*, USA] on each side of the chip to give two sets of live and dead cell density values. Specifically, the counter imaged cells at 5-megapixel resolution in the bright-field

channel at 2.5× optical magnification and analysed the image using advanced counting algorithms. The average of the two live cell density counts was used as the value for the initial cell density, and subsequently used in order to calculate the resuspension/final volume using **Equation 6.4**.

Prior to the acquisition of the automated cell counter, cells were manually counted, i.e. during the period of **scaffold solutions 1-4** i.e. Chapter 3 research**.** Manual counting was performed by, adding count solution (2×10 µL) into a C-Chip disposable hemocytometer [*INCYTO*, Korea] and counting the cells across the eight 1 mm square corners of the two 3×3 grids. Using the average cell count in **Equation 6.5**, the initial cell density was determined and could then in turn be used to calculate the resuspension volume. **Equation 6.5** equates the cell density to the multiplication of the average count per square with the dilution factor and the volume factor. The dilution factor corresponds to how much the cells were diluted by the trypan blue and can be calculated by **Equation 6.6,** where V_{cell} is the cell aliquot volume and V_{TB} is the volume of trypan blue. The volume factor refers to the inverse of, the count square volume, which is 10^{-4} mL, hence the volume factor is 10^{4} mL^{-1}.

Equation 6.5

$$n_{cells} = \overline{count\ per\ square} \times dilution\ factor\ \times volume\ factor$$

Equation 6.6

$$dilution\ factor\ = \frac{V_{cell} + V_{TB}}{V_{TB}}$$

6.4.6 Cartilage Sample for ICC

A cartilage construct was produced by Dr James Armstrong and Madeline Burke (both University of Bristol) for an ICC control (*section 6.11.5.3*).

6.4.6.1 Cartilage Production

A cylindrical scaffold (ø 5 mm by 6 mm thick) of non-woven polyglycocilic acid (PGA, *Biomedical Structures*) were sterilised by ethylene oxide treatment (*Anderson Caledonia*) and then immersed in 100% v/v ethanol. The scaffold was washed with PBS (3μ) and subsequently coated in 100 μg/mL fibronectin in PBS. The coated scaffold was dried overnight and then added to an inner well of a 24 well plate that was coated in agarose (1 mL). **MSC culture medium** (1 mL) was added to the well and any bubbles formed were removed using sterile forceps. After 30 min the medium was aspirated from the scaffold, which was then seeded with oMSCs (90 μL of 1,200,000 oMSCs suspended in **MSC culture medium**). Antifungal water, composed of 100 units/mL penicillin, 100 μg/mL streptomycin and 2.5 μg/mL amphotericin B in autoclaved purified water, was added to the outer well of the 24 well plate. After the scaffold was incubated overnight (37 °C, 5% CO_2) it was turned over and then returned to the incubator for 2 h (37 °C, 5% CO_2). **MSC differentiation medium** was added to the well (1.5 mL) and the scaffold was left to incubate (37 °C, 5% CO_2) on a rotating platform with the medium changed three times a week. After seven days, each medium exchange was with **MSC differentiation medium** supplemented with 10 μg/mL insulin. After thirty five days, the cartilage constructs were harvested and then sectioned for histological analysis.

6.4.6.2 Cartilage Sectioning

The cartilage construct was fixed in 4% w/v paraformaldehyde in PBS (2 mL) and then immersed in 70% v/v ethanol for 2 h. The fixed construct was submitted to the Histology Services Unit (Medical Sciences, University of Bristol), where it was enveloped in paraffin wax and cut into 3 μm sections. The construct was them fixed to a Polysine™ microscope slide (*Thermo Scientific*).

6.5 Cargo-Laden Scaffold Solutions

To create cargo laden scaffold solutions, the scaffold solutions described in *section 6.1.6* were mixed with either cells or beads.

6.5.1 Cell-Laden Scaffold Solutions

The general preparation method of cell-laden scaffold solutions, was by one of two methods.

Resuspension into SS1-SS4. The cell resuspension method used in *section 3.6-3.7* was to suspend cells at a moderate density in cell culture medium and then add scaffold supplements to form the cell-laden scaffold solution. This method was used for **SS1, SS2** and **SS4** of **Table 6.5**. Cells were suspended with a final concentration of 0.1×10^6 to 3×10^6 cells/mL, but typically 2×10^6 cells/mL was used.

Resuspension into SS5-SS8. For cell suspensions of *section 3.8-3.9* and Chapter 4, cells were directly resuspend into the desired scaffold solution at the required density. This was used for **SS5-SS8** of **Table 6.5**.

Typical resuspensions. A confluent T25 flask of cells would be resuspended in culture medium and a 40% v/v aliquot of this centrifuged. The resulting pellet would be resuspended in 100-200 µL of scaffold solution at 5×10^6 to 15×10^6 cells/mL, but routinely 15×10^6 cells/mL was used.

General Conduct. The resuspension followed the cell harvesting protocol outlined in *section 6.4.5*. To minimise bacterial infection, the scaffold solution production employed aseptic techniques and solution processing where possible was performed in a laminar flow biosafety cabinet. Prior to use, the resulting cell-laden bioinks were stored in a cell incubator [Midi 40, *Thermo Scientific*, USA] at 37 °C with 5% CO_2. Bioinks comprising a

cellular scaffold solution were generally printed within 30 min of production, but have been stored up to 4 h prior to use.

6.5.2 Bead-Laden Scaffold Solutions

For some test prints and during phase transfer development, scaffold solutions were mixed with fluorescent beads, either ø 5 μm or ø 10 μm. The ø 5 μm beads were orange superparamagnetic polystyrene micro-particles (*Sigma-Aldrich*). While the ø 10 μm beads were orange polystyrene microspheres (Fluorosphere®, *Life Technologies*). Bead stock solutions were used as supplied i.e. beads in water with 2 mM sodium azide. The concentration of the stock solutions were 1% w/v ø 5 μm beads i.e. ~70×10^6 beads/mL (as determined by hemocytometer count) and for ø 10 μm beads, 3.6×10^6 beads/mL.

For scaffold component test prints, a bead stock solution was added undiluted to the scaffold solution. For the 12 mM Fmoc-IG test print, the ø 5 μm beads were added at 20% v/v, giving ~14×10^6 beads/mL. Whereas for the PEG 400 test prints, the ø 10 μm were diluted to 1.8×10^6 beads/mL by creating a 1:1 v:v mix of bead stock solution to PEG 400 (giving **SS3 bead**).

Bead laden scaffold solutions for either phase transfer or **SS5** bioink testing were prepared as described. An aliquot of ø 5 μm bead stock was centrifuged (2,000×*g*; 1 min) in a mini centrifuge [Spectrafuge™, *Labnet International*, USA]. The bead pellet was then washed in PBS, repelleted from PBS and finally resuspended in the scaffold solution. Phase transfer experiments were performed at ~35×10^6 beads/mL whilst the **SS5** bioink test print was performed at ~18×10^6 beads/mL.

6.6 Scaffold 3D Printing

This section explains the printing process for 3D printed scaffolds either containing cells, beads or no cargo i.e. the printed scaffolds of Chapter 3 and Chapter 4. Information on non-printed, i.e. micropipetted scaffolds can be found in *section 6.10*.

6.6.1 Scaffold 3D Printer

Cell-laden scaffolds and empty scaffolds were printed using the droplet-in-oil 3D printer described in *Section 6.2* at ambient temperatures (20-22 °C).

6.6.1.1 Modified Printer Setup

The printer components were slightly modified during the scaffold printing to improve printing and component longevity. The modifications are described in brief. Firstly, the printer's oil container was changed to a truncated glass cuvette [3.1125/SOG/10, *Starna Scientific Ltd.*, UK] and the machined ledge of the motorised manipulator was adapted to hold it.

To improve the droplet generator longevity, the droplet generator's design was slightly altered, such that the piezo-electric transducer was more covered by the plastic chamber (*section 6.12.1.1*). The droplet generator's microcontroller was replicated by the electronic workshop (*Chemistry Department* at the *University of Oxford*), but with a higher voltage output (±33 V). The piezo's pulse with this microcontroller had peak to a peak amplitude range of 0-66 V.

To reduce vibrational interference during print, the droplet generator and micromanipulator were placed on a vibration isolation system [model 66-501, *Technical Manufacturing Company*, USA]. Finally, the microscope was stabilised by a custom microscope gantry support (mechanical workshop, *Chemistry Department* at the *University of Oxford*).

6.6.1.2 Printer Preparation

Before printing, the droplet generator's aqueous chamber and capillary/nozzle holder, along with the printer cuvette were thoroughly cleaned with ultrapure water and ethanol, and then were dried under a gentle flow of nitrogen On the day of use, capillaries were flushed with ultrapure water, ethanol and isopropanol, and were then dried under a gentle nitrogen flow. Cleaned capillaries were subsequently vacuum sealed in a plasma cleaner [Femto version A, *Diener Electronic*, Germany] and treated with oxygen plasma

(8 min, 5-10 SCCM). With the instrument cleaned, the piezo was filled with ultrapure water and the capillary inserted.

In between each newly loaded print solution, the capillary was cleaned by soaking in virkon (VWR), then 8 M NaOH, and the aqueous chamber was replenished with lost water. For agarose-based bioinks the capillary would also be cleaned by soaking in pure water at 65 °C.

6.6.2 Scaffold Printing Procedure

Scaffolds were printed following a similar procedures outline in *Section 6.2* with some modifications as described below.

6.6.2.1 Print Oil Selection

Biological print solutions, a.k.a. bioinks, were printed into different oil solutions. For **SS1-SS5** (of **Table 6.5**) based bioinks the **initial bioink print oil** (of **Table 6.1**) was selected. Whilst **SS6-SS8** (of **Table 6.5**) based bioinks were printed in the **bioink print oil** (of **Table 6.1**).

6.6.2.2 Standard Bioink Print Protocol

The bioink was vortexed, placed in a well-loading array (10 µL) alongside hexadecane and loaded into the nozzle at ~4 µL *(section 6.2.2.2*). For ULGT-agarose based bioinks, the outside tip of the glass capillary was subsequently wiped with a lens tissue soaked in pure water.

Once the capillary was submerged into the print oil (usually 200 µL), the piezo would be continually fired with varied voltage pulses until conditions were found for the reproducible ejection of singlet droplets, ideally of uniform size. Typically, tuned pulse parameters were 50-350 µs pulse-width for all bioinks with voltages of 25-60 V for non-agarose based bioinks and 40-63 V for agarose based bioinks. In parallel to droplet tuning,

the gelation of ULGT-agarose bioinks was tested by an inverted vial test (*section 6.7.1.3*), if the bioink gelled automated printing would be conducted.

The tuned pulse would be used to automatically print droplet networks a.k.a. scaffolds. However, typically the voltage of this print pulse would be gradually increased throughout a print session of multiple networks to keep consistent droplet production. Generally, multiple networks were successively printed within the same print chamber, with the last network left to stand for 5 min before moving.

Specific information on the bioink print order and print parameters are found in the next section (*6.6.3*) for the different scaffolds types

6.6.3 Printing Cell-Laden Scaffolds

Each cell-laden scaffold was fabricated using the cell-laden scaffold solutions of *section 6.5.1*, following the print procedure of *section 6.6.2*.

6.6.3.1 Single Cell-Type Scaffolds

Cellular scaffolds of a single cell-type were mainly printed as square cuboids for 2-4 layers with horizontal map dimensions of either, 9×11 droplets (for preliminary **SS1** bioink prints), 11×14 droplets (for **SS1-SS5** bioinks), 7×9 droplets (for **SS5-SS8** bioinks) or 7×8 droplets (for **SS7-SS8** bioinks). For scaffolds to be phased transferred, 4 layers was the usual thickness.

6.6.3.2 Layered Sheets (Two Cell-Types)

For all layered sheets scaffolds, a cell-laden **SS7** or **SS8** bioink was printed using a single droplet generator. First cell-type 1 was printed and then, after nozzle cleaning and bioink loading, cell-type 2 was printed. Each layered sheet consisted of a wider lower droplet sheet (cell-type 1), on top of which, was a centrally aligned narrower droplet sheet (cell-type 2), see **Table 6.7** for map dimensions.

In all instances the layered sheet scaffolds were printed as follows, the lower droplet sheet was printed as a full map (i.e. a map where droplets were ejected at each

pixel, **Figure 6.3 A**) for 3-4 layers. Directly after the structures edges would be flattened by printing a hollow map (i.e. a map where droplets were ejected only at the edge of the map, **Figure 6.3 B**) for two further layers on top. The upper layer was printed only as a full map for 3-4 layer for all layered sheets except the HEK-293/YFP below HEK-293/CFP layered sheets (**Figure 4.17**). Here, the upper layer was printed as a full map for 3 layers followed by a hollow map print for 2 layers. The specific map sizes and number of layers printed for each junction are summarised in **Table 6.7**.

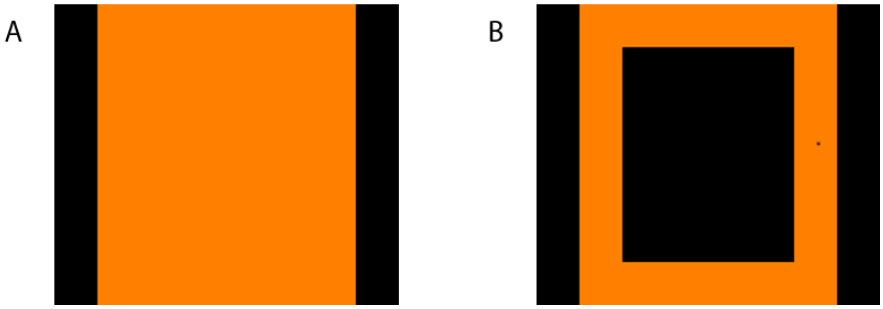

Figure 6.3 Illustration of print maps for layered cell sheets. **A** A full map of 7×8 piezo I droplets (orange pixels). **B** A hollow map of 7×8 piezo I droplets (orange pixel), with the centre of the map void of droplets (black pixels).

Table 6.7 Print details for the layered sheets production. Each print of layered sheets is listed with details on bioink cell density and the map dimensions for the upper and lower layers. The map dimensions are represented as horizontal pixels $x \times y$ by vertical pixels z. Non fluorescent cells were stained with red CMPTX (RC) or deep red (DR) cellTracker™ dye.

Printed Junction	Lower n_{cell} / cells/mL	Upper n_{cell} / cells/mL	Lower Print Dimensions		Upper Print Dimensions	
			Full Map ($(x \times y) \times z$)	Hollow Map ($(x \times y) \times z$)	Full Map ($(x \times y) \times z$)	Hollow Map ($(x \times y) \times z$)
chondrocyte (DR) below osteoblasts (RC) (**Figure 3.29**)	6×10^6	10×10^6	(7×9)×4	(7×8)×2	(6×7)×4	N/A
HEK-293/YFP below HEK-293/CFP (DR) (**Figure 3.28**)	10×10^6	9×10^6	(7×9)×3	(7×9)×2	(6×7)×4	N/A
HEK-293T (RC) below HEK-293T (DR) (**Figure 4.17**)	12×10^6	14×10^6	(7×8)×3	(7×9)×2	(6×7)×3	(6×7)×2

6.6.3.3 Pathway Networks (Two Cell-Types)

For all pathway scaffolds, cell-laden **SS7** or **SS8** bioinks were printed by a single droplet generator. First cell-type 1 were dispensed and then cell-type 2 after nozzle cleaning and bioink loading. Each pathway network consisted of a narrow pathway architecture (cell-type 1), flanked in the same plane and above by structural droplets (cell-type 2).

In all instances pathway networks were printed as follows. The pathway droplets were first printed for 3-7 layers. After which the structural droplets were printed, initially within the pathway plane for 2-6 layers and then above this plan for 2 layers to top the network. The outer map dimension for each of these 3 maps would stay constant throughout the network print (**Table 6.8**). However, the design and dimension of the maps varied between pathway networks (**Table 6.8**).

Table 6.8 Print details for production of pathway scaffolds. Each pathway scaffold print is listed with bioink cell density, map dimensions (horizontal pixels *x*×*y*), no. of layers printed (vertical pixel *z*) and the width of the pathway (pixel width in map). The cells used for each structure were: HEK-293/YFP (path) and HEK-293/CFP (structure) in nested cross 1 (**Figure 3.27 D,E**); HEK-293/CFP (path) and HEK-293/YFP (structure) in nested cross 2 (**Figure 3.27 F**) and; HEK-293T (RC, path) and HEK-293T (DR, structure) in bifurcated pathway (**Figure 3.27 A-C**). Non fluorescent cells were stained with red CMPTX (RC) or deep red (DR) cellTracker™ dye.

Printed Junction	Pathway n_{cell} / cells/mL	Structural n_{cell} / cells/mL	Outer Map Dimensions (*x*×*y*)	Printed Layers			Pathway Width / pixel
				Pathway (*z*)	Sides (*z*)	Top (*z*)	
nested cross 1 (**Figure 3.27 D,E**)	14×10^6	14×10^6	13×13	5	5	0	3
nested cross 2 (**Figure 3.27 F**)	14×10^6	14×10^6	10×12	5 or 7	6 or 5	2	2
bifurcated pathway (**Figure 3.27 A-C**)	10×10^6	13×10^6	8×9	3 or 4	2	2	1

6.6.4 Printing Cell-Free Scaffolds

Each empty scaffolds and bead-laden scaffolds were fabricated following the print procedure of *section 6.6.2*. The bioinks used were plain scaffold solutions (*section 6.1.6*), test print solutions as stated below, and bead-laden scaffolds (*section 6.5.2*). The test print solutions were composed of scaffold supplements as prepared in *section 6.1.5*.

Empty scaffolds, i.e. test printed scaffolds of Chapter 3, were printed with various print solutions, print oils and droplet network dimensions. **Table 6.9** lists the details for the empty scaffold prints. While bead laden scaffolds of Chapter 3 and Chapter 4 were also printed with varied conditions as listed in **Table 6.10**.

Table 6.9 List of empty printed scaffolds including print details of print solution, print oil and map dimensions. Here SR101 is an abbreviation of sulforhodamine 101 (section 6.11.2).

Printed Scaffold	**Figure**	**Print Solution**	**Print oil**	**Map Size / Pixels**		
				x	**y**	**z**
DMEM only	**3.4A**	DMEM (D5564)	**initial bioink print oil**	9	10	7
DMEM + 10% v/v FBS	**3.4B**	MSC culture medium	**initial bioink print oil**	9	10	7
Opti-MEM® (standard)	**3.4C**	Opti-MEM® + 0.5% v/v FBS	**initial bioink print oil**	9	10	7
0 mM **Fmoc-XX** in Opti-MEM®	**3.10A**	30:70 v:v 0 mM **Fmoc-XX** : Opti-MEM® with 0.5% v/v FBS. Plus 5 µM SR101	**initial bioink print oil**	11	14	7
0.6 mM **Fmoc-XX** in Opti-MEM®	**3.10B**	30:70 v:v 2 mM **Fmoc-XX** : Opti-MEM® with 0.5% v/v FBS. Plus 5 µM SR101	**initial bioink print oil**	11	14	7
1.8 mM **Fmoc-XX** in Opti-MEM®	**3.10C**	30:70 v:v 6 mM **Fmoc-XX** : Opti-MEM® with 0.5% v/v FBS. Plus 5 µM SR101	**initial bioink print oil**	11	14	7
3 mM **Fmoc-XX** in Opti-MEM®	**3.10D**	30:70 v:v 10 mM **Fmoc-XX** : Opti-MEM® with 0.5% v/v FBS. Plus 5 µM SR101	**initial bioink print oil**	11	14	7
11 mg/mL agarose test print	**3.18C**	**SS5** with 11 mg/mL ULGT agarose and 5 µM SR101	**initial bioink print oil**	11	14	7
Salt Solution Packing	**3.24B**	145 mM KCl, 10 mM Tris.HCl and 5 µM SR101 in ultra-pure water at pH 8.0	**fluorescent print oil (A)**	9	11	5
SS5 packing	**3.24B**	**SS5** with 5 µM SR101	**bioink print oil**	9	11	5
SS6 packing	**3.24C**	**SS6** with 5 µM SR101	**bioink print oil**	9	11	5

Table 6.10 List of bead-laden printed scaffolds including print details of print solution, print oil and map dimensions.

Printed Scaffold	Figure	Print Solution	Print oil	Map Size / Pixels		
				x	y	z
ø 5 µm beads in Fmoc-IG sol.	**3.9**	12 mM Fmoc-IG in ultra-pure water, with 14×10^6 beads/mL	**fluorescent print oil (B)**	11	14	3
ø 10 µm beads in 0% PEG 400 (**SS3** Test)	**3.12A**	**SS3** bead with 0% w/v PEG400 and 1.8×10^6 beads/mL	**initial bioink print oil**	11	14	2
ø 10 µm beads in (**SS3** Test)	**3.12B**	**SS3** bead with 10% w/v PEG400 and 1.8×10^6 beads/mL	**initial bioink print oil**	11	14	1
ø 10 µm beads in (**SS3** Test)	**3.12C**	**SS3** bead with 20% w/v PEG400 and 1.8×10^6 beads/mL	**initial bioink print oil**	11	14	2
ø 5 µm beads in **SS5**	**3.18D**	**SS5** with 12 mg/mL ULGT agarose and 18×10^6 beads/mL	**42:58 v:v undecane : silicone oil containing 1.3 mM DPhPC**	11	14	5
ø 5 µm beads in **SS5**	**3.19C**	**SS5** with 12 mg/mL ULGT agarose and 18×10^6 beads/mL	**bioink print oil**	11	14	5

6.6.5 Print Oil Optimisation

During the print oil optimisation period, the lipid (1.3 mM DPhPC) was kept constant whilst the v:v ratio of oil components, undecane to silicone oil was varied: 50:50, 40:60, 35:65 and 30:70, with 35:65 was selected as the optimum ratio.

6.7 Scaffold Gelation

Gelation of the scaffolds and scaffold solutions was performed regularly as outlined below. The composition of the oils and scaffold solutions used here can be found in *section 6.1.2* and *6.1.6* respectively. ULGT-agarose was prepared as stated in *section 6.1.5.4*.

6.7.1 Inverted Vial Tests

All inverted vial tests were performed as described. A small volume of pre-gel solution was stored in either a glass vial (1.5 mL) or a microcentrifuge tube (0.75 mL or 1.5 mL) and then gelled. After gelation, the vessel was inverted. The sample was judged as gelled if the sample remained free standing at the base of the vial. Gelation was tested for different solutions as described below.

6.7.1.1 ULGT-Agarose only

The preliminary gel tests of ULGT-agarose in Opti-MEM® were by gelling ULGT-agarose solutions (50 µL) at concentrations of 10, 20, 30 and 40 mg/mL in individual glass vials. Gelation was by cooling to 4 °C for 1 h.

6.7.1.2 ULGT-Agarose with ECM Proteins

The preliminary gel tests of ULGT-agarose with ECM proteins were by gelling (4 °C, 45 min) supplemented solutions (~50 µL) in individual glass vials. The solutions tested were **SS8** containing a single ECM protein supplement of either collagen type I, laminin or fibronectin. Collagen solutions were concentrated at 300, 60, 30, and 15 µg/mL. Whilst laminin and fibronectin were concentrated to 10, 2, 1 and 0.5 µg/mL. An **SS7** solution was also gelled as a control.

6.7.1.3 Gelation Tests of Bioink

The gelation of bioinks was tested for bioinks composed of ULGT-agarose (**SS5**-**SS8**). This was typically tested at the beginning of the print. Commonly ~35 µL of bioink was placed into a microcentrifuge tube and was gelled (4 °C, 20-30 min). If the solution failed to gel, the print was discontinued.

6.7.2 Printed Scaffold Gelation

6.7.2.1 Oil Optimisation for Gelation

Printed scaffolds composed of **SS6** with cargo were gelled in **initial bioink print oil** and **bioink print oil**. The scaffolds were gelled by cooling (4 °C, 1 h) and then imaged at ambient temperature (20-22 °C, *section 6.11.1*).

6.7.2.2 Standard Scaffold Gelation

Printed scaffolds comprised of either **SS7** or **SS8** bound in **bioink print oil** were left to rest (5 min) post print. The scaffolds were then gelled (4 °C, 20-25 min). Gelled networks were either used straight away or stored in a hydration chamber at ambient temperature (20-22 °C).

6.7.3 Droplet Scaffold Gelation

6.7.3.1 Gelled Droplet for Phase Transfer

Gelled droplet scaffolds were composed of 13 mg/mL ULGT-agarose in OptiMEM® with 35×10^6 beads/mL. The droplet scaffolds were made by micropipetting ~2 μL droplets into well arrays filled with **initial bioink print oil**. Scaffolds were gelled (4 °C, 1 h) and were then left to warm to ambient temperature (20-22 °C).

6.8 Phase Transfer of Scaffolds

This section goes through the different methods of phase transfer discussed in Chapter 3, and summarises the standard protocol for printed scaffold phase transfer.

6.8.1 Attempted Liquid Droplet Phase Transfer

A variety of liquid droplet phase transfer experiments were attempted prior to printed scaffold work. All involved creating a two phase system of lipid-in-oil above an aqueous solution, and then micropipetting droplets (~0.5-4.0 μL) into the upper phase in attempt to transfer mediated through gravity. In brief, the two phase systems were created in a custom made glass transfer container with a chamber volume of ~4mm×30 mm×20 mm; this container allowed user visualisation from side-on and below. Typically, the droplet solution was 0.75-1.50 M sucrose (*Sigma-Aldrich*) doped with 10 μM fluorescein (*Life-Technologies*) whilst the bottom aqueous phase was 0.5 M glucose (*Sigma-Aldrich*). Many oil phases were attempted. Lipids, either, 4.8-6.0 mM DOPC, 6.0 mM DPhPC or 1.0 mM mix of DPhPC with cholesterol at 8:2 mol:mol, were dissolved in a base oil. The base oil was either, a 3:1 or 1:1 v:v mix of hexadecane to silicone oil, or alternatively mineral oil alone. All two-phase columns were incubated for at least 30 min and up to 4 h, before attempted phase transfer. Phase transfer was observed either side-on with a transmission microscope [SMZ660, *Nikon*, Japan] or bottom up with an inverted microscope [eclipse TE2000-S, *Nikon*, Japan].

6.8.2 Droplet Scaffold Phase Transfer

The preliminary phase transfer experiments involved phase transferring μL-scale gelled droplet scaffolds (*section 6.7.3.1*) as described herein.

6.8.2.1 Centrifugation of Single Droplets

Two phase columns of lipid in oil (50 μL) above PBS (25 μL) in 0.75 mL microcentrifuge tubes were incubated (2 h) at ambient temperature (20-22 ºC). A single gelled droplet scaffold was relocated by micropipette into each of the columns' upper phases. The tubes were centrifuged twice in a centrifuge [model 5415 D, *Eppendorf*, Germany], first at 100×*g* (1 min) then at 200×*g* (1 min). Phase transferred structures were micropipetted

into PBS contained within individual wells of a microscope chamber slide [Lab-Tek™ 154534K, *Nunc*™, *Thermo Scientific*, USA].

Six lipid-in-oil solutions were attempted, containing either 2.6 mM DOPC or 2.6 mM POPC in base oil. The base oil was either, a 3:1 v:v mix of hexadecane to mineral oil, a 3:1 v:v mix of hexadecane to silicone oil or mineral oil alone.

6.8.2.2 Centrifugation of Conjoined Droplets

The conjoined droplets were formed by coalescing 2-3 gelled droplet scaffolds with a pre-gel droplet (4 μL) composed of 13 mg/mL ULGT-agarose in OptiMEM®. These structures were gelled (4 °C, 1 h) and then left to warm to ambient temperature (20-22 °C). Conjoined droplets were phase transferred through the interface of lipid-in-oil above PBS, using the same protocol as the centrifugation of single droplets (*Section 6.8.2.1*). Here the lipid in oil was 3:1 v:v mix of hexadecane to silicone oil containing 2.6 mM POPC.

6.8.3 Initial Printed Scaffold Phase Transfer

Printed scaffolds were initially phase transferred by centrifugation methods and then gravity mediated protocols.

6.8.3.1 Centrifugation of Printed Scaffolds

Four scaffolds were printed composed of **SS5** at 13 mg/mL ULGT-agarose containing cargo of either 18×10^6 beads/mL ($n = 2$) or 8×10^6 HEK-293T cells/mL ($n = 2$). These were gelled (4 °C, 1 h) and then warmed to room temperature. One of each gelled scaffold type were set aside. The remaining two gelled scaffolds had a ~1 μL droplet of 13 mg/mL ULGT-agarose in OptiMEM® micropipetted onto their upper horizontal surface and with micropipette tip perturbation of the droplet and scaffold the structure partially coalesced. The printer cuvette was subsequently cooled (4 °C, 1 h) and then warmed to ambient temperature (20-22 °C). The gelled coated scaffolds and the uncoated scaffolds were relocated by micropipette into the upper phase of separate two phase columns, which

were subsequently centrifuged (300×*g*, 2 min). Phase transferred structures were micropipetted into PBS contained within individual wells of a microscope chamber slide [Lab-Tek™ 154534K, *Nunc*™, *Thermo Scientific*, USA].

The two phase column was 2.6 mM DOPC in a 3:1 v:v mix of hexadecane to mineral oil (50 μL) above PBS (25 μL) incubator at ambient temperature (20-22 ºC) for 2 h.

6.8.3.2 Gravity Mediated Transfer (Initial)

Cell-laden printed scaffolds were phase transferred similarly to the centrifugation of printed scaffolds (*Section 6.8.3.1*), but with some modifications. As before the printed scaffolds were gelled (4 ºC, 30 min). At this point the **bioink print oil** was exchanged for hexadecane as follows: the printer cuvette's oil volume was reduced to ~150 μL, then 100 μL of hexadecane was gently added, and 100 μL of mixed oil was carefully removed. The hexadecane addition, mixed oil removal step was repeated 8 times further. The network was gel-wrapped by micro-pipetting a ~0.5-1.0 μL agarose solution onto the network which wetted onto the network surface. The resulting scaffold was then gelled (4 ºC, 30 min). Phase transfer was by aspirating the scaffold into a two phase column made in a microscope chamber slide [Lab-Tek™ 154534K, *Nunc*™, *Thermo Scientific*, USA]. with a well containing 200 μL of **initial scaffold phase-transfer oil** above 300 μL of culture medium, previously warmed in a Midi 40 cell incubator [*Thermo Scientific, USA*] at 37 ºC with 5% CO_2 for 60 min. The oil was removed and culture medium (~ 200 μL) was added, after which the scaffolds were stored in the cell incubator (37 ºC, 5% CO_2) until use. These steps were performed next to a blue butane flame.

6.8.3.3 Gravity Mediated Transfer (Modified)

The gravity mediated phase transfer method was gradually optimised with changes to the method now listed. For the coating step, silicone oil instead of hexadecane was exchanged with the print oil. For a short while the two phase columns were created in an alternate microscope chamber slide [Lab-Tek™, catalogue number 734-2122, *VWR*, USA] this was stopped as the chambers would leak within a week of scaffold culture. Also, the scaffold's

time at 4 °C for gelation was reduced to 15-20 min. Finally, the creation of the two phase column, the oil removal step and the culture medium addition step were performed in a laminar flow biological safety cabinet.

6.8.4 Standard Printed Scaffold Phase Transfer

The optimised phase transfer of printed scaffolds method is shown below. Control scaffold droplets (0.2-0.4 μL) can also be phase transferred by this method with or without the gel coating step.

6.8.4.1 Gel Coating of Scaffold

The printed networks were initially gelled (*section 6.7.2.2*). The oil surrounding the gelled networks was reduced to ~100-150 μL. Silicone oil (200 μL) was gently added to the corner of the cuvette, and then mixed oil (200 μL) was removed from the diagonally opposite corner. This silicone oil addition, mixed oil removal step was repeated 3 more times. 13-15 mg/mL ULGT-agarose (0.2-0.4 μL) was micropipetted once onto each network. If the gel drop did not wet the scaffold's surface, then silver wire (⌀ 0.1 mm, *Sigma-Aldrich*) was used to manipulate the droplet onto the scaffold, inducing wetting. The coated scaffolds were then gelled (4 °C, 20-25 min) and then warmed to ambient temperature (20-22 °C). Coated scaffolds were either phase transferred straight away or stored in a hydration chamber. The agarose coalescence step was performed next to a blue butane flame.

6.8.4.2 Phase Transfer of Coated Scaffolds

Two phase columns were made in microscope chamber slides [Lab-Tek™ 154534K, *Nunc*™, *Thermo Scientific*, USA] and then place in a cell incubator (15-60 min, 37 °C, 5% CO_2). The column was composed of ~180 μL of **standard scaffold phase-transfer oil** (**Table 6.1**) above ~300 μL of culture medium. Here the selected culture medium was matched to the cell-line to be cultured (*section 6.9.1*).

The coated scaffolds were transferred by micropipette into the upper phase of the incubated column, typically one scaffold per column. If the coated scaffold did not spontaneously phase transfer, the chamber slide was mechanically perturbed by hand in a circular motion. With all scaffolds phase transferred, the upper oil phase was removed and 300 μL additional culture medium was added. The chamber was then stored in the cell incubator (37 °C, 5% CO_2) until use.

The column creation, oil removal, and culture medium addition steps were performed in a laminar flow biological safety cabinet whilst the phase transfer was performed next to a blue butane flame.

6.9 Cellular Scaffold Culture

The culture of 3D cellular scaffolds is described below.

6.9.1 Standard 3D-Cell Culture

The phase transferred scaffolds were cultured for up to 14 days in microscope chamber slides [Lab-Tek™ 154534K, *Nunc*™, *Thermo Scientific*, USA], which contained ~600 μL of culture medium per sample well. Scaffolds were stored between culture medium exchanges and experimentation in a Midi 40 cell incubator [*Thermo Scientific*, USA] set at 37 °C with 5% CO_2. Every 2-3 days the scaffold's culture medium would be exchanged. The exchange for a single well was as follows: ~200-300 μL of culture medium would be carefully removed close to the air-culture medium interface of the well and then 300 μL fresh culture medium would be added slowly at corner of the well. This old-culture medium removal, fresh-culture medium addition step was repeated 1-2 more time(s). In all instances the culture medium was added at low flow rate using a 100 μL micropipette to avoid disrupting the scaffolds. Culture medium exchanges were performed in a laminar flow biological safety cabinet. The culture media used are now described, their composition can be found in **Table 6.3**.

The majority of HEK-293T and fluorescent HEK-293 scaffolds were cultured in fully supplemented **standard cell scaffold culture medium**. However, initial HEK-293T scaffolds were cultured without antibiotics, HEPES and MEM non-essential amino acids (i.e. in **initial cell scaffold culture medium**)

The oMSC scaffolds were cultured in **MSC culture medium** for standard viability assessment, and for differentiation experiments **MSC differentiation** or **MSC control medium** was used.

6.10 Non-Printed Scaffold Controls

In Chapter 4, control culture experiments of non-printed cell-laden scaffold were performed with μL hydrogel-spheres (droplets) and μL hydrogel-blocks (bulk hydrogel phase). A HEK-293T laden scaffold solutions were also printed directly into culture medium and cultured as a control. These were all cultured in microscope chamber slides [Lab-Tek™ 154534K, *Nunc*™, *Thermo Scientific*, USA] using the 3D cell culture protocol (see *section 6.9.1*). The preparation of these control scaffolds are now described, compositions of reagents can be found previously for culture media (**Table 6.3**), oil (**Table 6.1**) and scaffold solutions (**Table 6.5**).

6.10.1 Hydrogel-Spheres

Cell-laden scaffold solutions were micropipetted as single droplets (0.2-0.4 μL) into individual wells of a well array (made in-house) containing **bioink print oil** (~200 μL). They were subsequently gelled (4 °C, 20 min) and then warmed to ambient temperatures (20-22 °C). In some instances droplets were coated in 0.2-0.4 μL agarose solution (13-15 mg/mL in Opti-MEM®) using the scaffold gel coating protocol in *Section 6.8.4.1*. Coated and uncoated sphere scaffolds were phase transferred using the phase transfer of coated scaffolds protocol in *Section 6.8.4.2*. Scaffold droplets were made and phase transferred next to a blue butane flame.

6.10.1.1 HEK-293T Control Droplets

There were two HEK-293T laden solutions used for control droplets. The first was **SS6** with 5×10^6 cells/mL (*section 4.5.3.2*). The second was in *section 4.6.3.2*, here **SS8** contained 15×10^6 cells/mL and ECM proteins. The ECM supplements were: no supplement, collagen type I (15 or 100 μg/mL), laminin (20 μg/mL), fibronectin (20 μg/mL) or a mix of these ECM proteins (15 μg/mL collagen type I; 20 μg/mL laminin; 20 μg/mL fibronectin). The **SS6** based scaffold controls were culture in **initial cell scaffold culture medium** whilst the **SS8** based controls were cultured in **standard cell scaffold culture medium**.

6.10.1.2 Bioink Control Droplets

For certain scaffold printing experiments, droplet sphere controls were made using the same bioink and then cultured in **standard cell scaffold culture medium**.

6.10.2 Hydrogel-Blocks

Cell-laden scaffold solutions were micropipetted as single droplets (5.0 μL) and slightly spread onto the glass surface of individual wells in a microscope chamber slide. Blocks were gelled (4 °C, 20 min), warmed to ambient temperature (20-22 °C) and then culture medium (~400 μL) was added to each sample well. Non gelling steps were performed in a laminar flow biological safety cabinet.

Blocks containing HEK-293T cells were fabricated with a solution of **SS6** containing 5×10^6 cells/mL and were cultured in **initial cell scaffold culture medium**. The oMSC differentiation control blocks (for ICC) were made with **SS8** containing 15×10^6 cells/mL and 15 μg/mL collagen type I. These oMSC blocks were culture in **MSC differentiation** and **MSC control medium**.

6.10.3 Cells Printed Directly into Medium

A bioink of **SS6** containing 5×10^6 HEK-293T cells/mL, was loaded into the droplet generator's nozzle. Droplets were ejected through air into **initial cell scaffold culture medium** (~300 μL) contained within a printer cuvette. This solution was divided across 4 wells of a microscope chamber slide each already containing 300 μL of **initial cell scaffold culture medium**. Samples were monitored by live-dead staining for 2 days.

6.11 Cellular Scaffold Analysis

Scaffolds solutions, scaffolds and grown tissues of Chapter 3 and Chapter 4 were analysed by fluorescence microscopy and digital PCR. This section goes through the analysis methods used and how data was processed.

6.11.1 Microscopy

6.11.1.1 Confocal Microscopy

Cellular scaffolds were primarily imaged using a confocal microscope [SP5, *Leica,* Germany] with a HC PL FLUOTAR 10× objective lens (0.3 N.A.) in both transmitted light and fluorescent modes. To improve contrast, the transmitted light mode used a scanning polarising differential interference contrast setting. Both images and *z*-stack optical sections were recorded of the cellular scaffolds, using image resolutions of either 512×512, 1024×1024, 2048×2048 or 4096×4096 pixel^2 and frame averaging between 1 and 6 frames. Cell scaffolds typically were not flat on the microscope base, and an optical section of one would usually be ~500 μm thick, with the *z*-stack recording using spacing of 2-10 μm between each slice, commonly 5 μm.

For all fluorescent networks, scaffolds or cell samples the PMT emission-band and laser wavelength were kept constant for a specific dye, however, the laser power and gain varied from sample to sample due to the effective concentration of the dye at the time of

imaging. Furthermore the confocal pin-hole was set to 70.78 for all samples. **Table 6.11** summarise the imaging settings applied for all commonly used fluorescent dyes.

Table 6.11: Imaging settings for confocal microscopy of fluorescent samples. Samples were stained with a fluorescent dye at the concentration indicated; the fluorophores excitation and emission wavelength maxima are also stated. The laser wavelength and emission range observed by the PMT were kept constant between samples for a fluorophore, whilst, the laser power and PMT gain stated were typical values used, however, these did vary from sample to sample.

Fluorescent Dye	**[Dye] /µM**	**λ Ex_{max} / nm**	**λ Em_{max} / nm**	**λ Laser / nm**	**PMT range / nm**	**% Laser power**	**PMT gain / V**
fluorescein	5	494	521	488	500-550	10	800
sulforhodamine 101	5	586	605	543	570-665	35	900
POPO™-3 iodide	1	534	570	543	600-650	50	1100
calcein-AM	5	490	515	488	500-550	10	500
propidium iodide	5	535	615	543	580-660	20	900
HEK-293/YFP	N/A	514	527	514	525-575	30	550
HEK-293/GFP	N/A	488	509	488	500-600	35	400
Red CMPTX CellTracker™	5	577	602	633	645-700	30	750
Deep Red CellTracker™	1	630	660	543	550-615	40	1000
DPhPC-NBD	1.2	460	535	488	500-550	15	900
5 µm beads	N/A	525	544	543	555-650	10	500
10 µm beads	N/A	540	560	543	570-665	10	500

6.11.1.2 Wide-field Microscopy

The arborised pathway network was imaged using a wide-field microscope [DMi8, *Leica*, Germany] in both transmitted light and fluorescent modes. The objectives used were: N Plan 5× lens (0.12 N.A.), HC PL FLUOTAR 10× lens (0.3 N.A.) and HC PL FLUOTAR L 20× lens (0.60 N.A.).

6.11.2 Droplet Network Bulk Staining

Fluorescent droplet networks were fabricated using a print solution that contained either fluorescein, sulforhodamine 101 (SR101) or POPO-3 iodide. Each fluorophore was supplied from *Life Technologies* as a 1 mM solution in either DMSO (fluorescein & SR101) or DMF (POPO-3 iodide). Stock 1 mM solutions were diluted 100-200 fold in print solution and vortexed to give 5-10 μM final dye concentrations.

6.11.3 Live/Dead Assays

Visual cell viability assessment of scaffolds was conducted using a calcein-AM (CAM) and propidium (PI) live/dead stain protocol. This protocol varied depending whether the scaffold was in oil or in culture medium. In all instances networks were imaged by confocal microscopy (*section 6.11.1.1*).

6.11.3.1 Scaffolds in Oil (**SS1**, **SS2 and SS4**)

For scaffolds composed of **SS1**, **SS2** and **SS4**, cellular viability was assessed after scaffold production, with the scaffold in the oil. The working live/dead solution was incorporated as part of the scaffold solution at 5 μM absolute dye concentrations. Networks were imaged after printing immediately and at later time-points of 1-4 days. Cells were then counted in the image (section 6.11.6.2) and viabilities calculated (*section 6.11.7.1*).

6.11.3.2 Scaffolds in Culture Medium (**SS5**-**SS8**)

For scaffolds in culture medium, i.e. those composed of **SS5**-**SS8**, cellular viability was assessed after culture. Prior to imaging, working live/dead solution were added to the culture medium to give 5 μM absolute dye concentrations. Samples were left to incubate for ≥10 min, but unlike typical live/dead staining protocol the dye solution was not washed away post staining.

For the **un-optimised culture** of scaffolds, a single scaffold would be repeatedly live/dead imaged over its culture, typically on days 0, 3 and 6. For **optimised culture** a

single scaffold would only be live/dead imaged once over its culture, either of day 0, 3 or 7. Cells on day 0 were counted (*section 6.11.6.3*) and viabilities calculated (*section 6.11.7.1*).

6.11.3.3 Live/Dead Working Solution

Stock solutions of dyes were prepared from powder and then stored as aliquots at -20 °C. 5 mM CAM stock was prepared by dissolving CAM (1 mg, *Cambridge Biosciences Ltd*) in sterile DMSO (201 µL, *Sigma-Aldrich*). Whilst 5 mM PI stock was made by solvating PI (10 mg, *Sigma-Aldrich*) in sterile DMSO (2.99 mL). A live/dead working solution (with 0.05 mM of each dye) was made by mixing 196 µL of the relevant culture medium with 2 µL of each dye stock.

6.11.4 CellTracker™ Staining

CellTracker™ dyes (*Life-Technologies*), Red CMPTX (RC) and Deep Red (DR), were used to fluorescently stain cells to visualise their printed pattern over time. Stock solutions of CellTracker™ were supplied as 10 mM RC in DMSO and 1 mM DR in DMSO. Both stocks were diluted into serum-free culture medium (OptiMEM® for HEK-293 cell derivatives and **DMEM-ITS** for chondrocytes and osteoblast) to give working solutions: 5 µM RC (by dilution of 0.5 µL dye per 1 mL) and 1 µM DR (by dilution of 1.0 µL dye per 1 mL).

In most instances staining was performed as follows, a flask of confluent cells was washed with PBS, with care taken not to delaminate the cells, and then one working dye solution was added (2 mL for a T25 flask). The flask was placed in a cell incubator (37 °C, CO_2) for 15-45 min. After incubation, the cells would be suspended in serum-free culture medium and centrifuged (400×*g*, 4 min). The pellet was washed with PBS and then resuspended in the cell scaffold solution.

In a few cases, staining followed a similar protocol, but, initially the washed cells (of a T25 flask) were resuspended in culture medium, which was centrifuged (400×*g*, 4 min) as two solutions. The pellets were then resuspended in different working dye

solutions and then added to new culture flasks. The cells were then placed in the cell incubator and processed as before, eventually being resuspended in bioink.

For pattern visualisation experiments osteoblasts and HEK-293T cells were stained with CellTracker™ RC, whilst chondrocytes, HEK-293/CFP and HEK-293T were stained with CellTracker™ DR.

6.11.5 Immunocytochemistry

Immunocytochemistry (ICC) of cell containing printed constructs and their subsequent imaging was performed by James Nicholson and Dr Sam Olof. Scaffold production, culture and imaging prior to ICC was performed by the author aided by Dr Sam Olof for HEK-293T printed construct and for oMSC printed constructs, printing was additionally assisted by Madeline Burke.

6.11.5.1 Sample Handling Prior to ICC

Prior to ICC, printed cellular scaffolds were cultured as appropriate (*section 6.9.1*) and were imaged after live/dead staining for HEK-293T samples and live-only staining for oMSC samples (*section 6.11.3.2*). Printed constructs were fixed on day 3 and 7 for HEK-293T scaffolds and day 7 for oMSC scaffolds. Whilst cartilage samples were prepared as described in *section 6.4.6*.

6.11.5.2 Immunocytochemistry of Printed Scaffolds

Immunocytochemistry of cellular scaffolds was performed within their culture vessel i.e. the microscope chamber slides. Scaffolds were first fixed in 4% v/v paraformaldehyde (*Sigma*) then quenched in 50 mM glycine (*Sigma*). Samples were washed in PBS then blocked for 1 h at room temperature in **blocking solution** consisting of PBS supplemented with 10% v/v donkey serum (*Bio-Rad*) & 0.1% v/v Triton-X 100 (*Fisher Scientific*). Primary antibodies solubilized in **blocking solution** were added to the scaffold which were then left to incubate (2 h, 37 °C). Samples were subsequently washed in PBS and then

incubated (2 h, 37 °C) in **blocking solution** containing Alexa-fluorophore bound secondary antibodies. Finally, samples were washed in PBS, incubated at room temperature (15 min) with PBS containing 2.9 μM DAPI (*Sigma*) and washed again.

One to two of the following primary antibodies were used per immunostaining: 0.25% v/v rabbit anti-phospho-histone 3 (*Merck Millipore*), 0.67% v/v rabbit anti-Sox9 (*Merck Millipore*) and 1.0% v/v mouse IgM anti-vimentin (*DSHB*). Secondary donkey antibodies conjugated to Alexa Fluor 568 or 647 (*Invitrogen*) were used with Sox-9 and phospho-histone 3 respectively. While the goat secondary antibody IgM Alexa Fluor 568 (*Invitrogen*) was paired with vimentin. For all experiments aberrant secondary antibody staining was checked by omitting the primary antibody and was not observed.

Sox9 staining was optimised on control block scaffolds composed of **SS8** with 15 μg/mL collagen type I and containing 15×10^6 oMSC/mL (*section 6.10.2*). These scaffolds were cultured in **MSC differentiation** and **MSC control media** for 7 days (*section 6.9.1*).

6.11.5.3 Immunocytochemistry of Cartilage

The wax-coated cartilage section was washed by immersion for two minutes in the following solvents: (a) xylene; (b) 100% v/v ethanol; (c) 90% v/v ethanol; (d) 70% v/v ethanol; and (e) deionised water. A hydrophobic circle was drawn around the cartilage section with a hydrophobic pen (PAP), creating a hydrophobic enclosure for the staining solution. The cartilage was then placed in a humidified chamber. Enzymatic antigen retrieval was then performed as follows: the cartilage was incubated in hyluronidase dissolved in PBS (200 μL) for 30 min at 37 °C. The excess solution was removed and the cartilage was in washed in PBS at a low speed rotation. The cartilage was then incubated in pronase dissolved in PBS (200 μL) for 30 min at 37 °C, after which the cartilage was in washed in PBS at a low speed rotation. The endogenous peroxidase activity of the cartilage was then quenched by incubated in 3% v/v hydrogen peroxide solution (200 μL) for 5 min at room temperature, after which the cartilage was in washed in PBS at a low speed rotation.

ICC was then performed in the same manner as printed constructs, excluding the paraformaldehyde fixing and glycine quench step. Here the cartilage was stained for Sox9 and with DAPI.

6.11.5.4 Imaging of Immunocytochemistry Samples

Samples were imaged using a fluorescence confocal microscope [LSM 710, *Zeiss*, Germany] using either 10× and 20× lenses. Throughout the experiments the pin-hole was kept constant.

6.11.6 Image Analysis

Images were processed and analysed with ImageJ[134,135]. Cell counts were performed on live/dead stained scaffolds (*section 6.11.3*) as described below.

6.11.6.1 3D Projections

3D projections of *z*-stack image series were formed using the 3D projection function of ImageJ[134,135]. The *z*-stack was initially converted into a sub-stack of the fluorescence channels. The projection method selected was "brightest point" and the image series was interpolated, a function which uses z-scaling to eliminate gaps between the image slices

6.11.6.2 Cell Counting of Oil-Bound Droplet Networks

For cell-laden droplet networks, cells were counted manually using the Cell Counter Plug-In[133] for ImageJ[134,135]. Either one frame of a *z*-stack (typically at 30-60 μm height) or a single image was used to represent the network. For network viability measurements of Chapter 3 (*section 3.6*), three counters were used to count the live cells, dead cells and droplets within the field of view (**Table 6.12**). In Chapter 4, for the scaffold cell density experiments (performed at different bioink cell densities, see *section 4.6.1*), the total number of cells within droplets (n = 25) was measured using a counter for each droplet.

Table 6.12 Summary of cells counted in **SS2h** and **SS4m** based cellular scaffolds. The table lists the bioink composition (cells and solution), counted cell values (live and dead) and the calculated total cell no. and cell viability. The networks which were analysed are displayed in previous figures which are referenced in the scaffold figure column. Live and dead cells were manually counted within these networks using a Cell Counter Plug-In[133] for ImageJ[134,135]. Viabilities were calculated as the percentage of live cells out of total cells.

Bioink	Scaffold Figure	$N_{\text{live cells}}$	$N_{\text{dead cells}}$	$N_{\text{total cells}}$	% Viability
HEK-293T in **SS2h**	**3. 11 A**	907	84	991	92
HEK-293T in **SS2h**	**3.11 B**	614	91	705	87
HEK-293T in **SS2h**	**3.11 C**	273	51	324	84
oMSCs in **SS4m**	**3.13 A**	1419	405	1824	78
oMSCs in **SS4m**	**3.13 B**	780	71	851	92
oMSCs in **SS4m**	**3.13 C**	946	73	1019	93

6.11.6.3 Viable Cell & Bead Counting of Phase Transferred Scaffolds

Count Methodology. In Chapter 4, cell counts of phase transferred scaffolds were performed with an automated 3D Object Counter[174,175] for ImageJ[134,135]. A *z*-stack was selected to represent the network. This was split into individual channels (at 8-bit resolution), with the live and dead channel usually selected for counting (or the DAPI and PH3 channel for ICC samples, see *section 6.11.6.4*). The best threshold value which counted the majority of cells was selected. Objects were counted with a size filter typically set to a range of 15-8000 voxels. Except in *section 4.6.3* where the filter was set to a range of 40-8000 or 100-8000 voxels for 512×512 and 1024×1024 pixel^2 sized images, respectively. Data was exported as "*statistics*" (i.e. the number of objects, object coordinates and object size) and a map of counted objects.

Unresolved Count. In the unresolved count, the number of scaffold cells was assumed to be the same as the number of counted object. Consequently, cellular aggregates where always under counted, giving rise to inaccurate viabilities. To account for this error, the

plots of the viabilities determined with the unresolved counts in *section 4.5-4.6*, included error bars which represent viabilities determined with twice and half as many live cells as counted. This gave positive and negative error bars of ~15% viability.

Resolved Count. For proliferation studies (section 4.7), the number of objects counted within the *z*-stack was resolved to give a more accurate number of cells imaged. This was by dividing the volume of each object counted (V_{object} in voxels) by the average cell size ($\bar{V}_{cell}$ in voxels) and then rounding the quotient to the nearest whole number. The summation of these quotients gave the total cell number (**Equation 6.7**). The average size in voxels for a live and dead cell was determined for each *z*-stack by averaging the volume (in voxels) of single cells ($n = 12$).

Equation 6.7

$$\sum \frac{V_{object}}{\bar{V}_{cell}} = N_{total\ cells}$$

10 μm beads within the PEG scaffolds (*section 3.7.4.2*) were counted and resolved by the same manner, except each counted object's volume in **Equation 6.7** was divided by the average bead volume ($\bar{V}_{bead}$ in voxels) to give the number of beads (N_{beads}).

Count Data. In section 4.7.4, the viabilities of scaffolds immediately after phase transfer (i.e. the day 0 time-point) were determined from counted cell values. A list of the scaffolds selected for counting and their counted cell values is displayed in **Table 6.13** for HEK-293T scaffolds and in **Table 6.14** for OMSC scaffolds

Table 6.13 List of HEK-293T laden scaffolds analysed by object counting and subsequently used for viability calculations. The *Bioink* column describes the scaffold solution used, including the amount of supplemented collagen type I, with the collagen concentration (in μg/mL) being the number preceding **C**. The number of live (N_{live}) and dead (N_{dead}) cells, and their total number (N_{total}), were determined by the unresolved object count and the resolved object count methodologies. The *Figure* column refers to the figure in which the scaffold analysed is displayed in, with N/A corresponding to scaffolds analysed but not displayed in any figures.

Label	Bioink	$n_{bioink\ cells}$ (cells/mL)	Figure	unresolved cell count			resolved cell count		
				N_{live}	N_{dead}	N_{total}	N_{live}	N_{dead}	N_{total}
1	**SS8h**+15**C**	10×10^6	N/A	645	277	922	2548	360	2908
2	**SS8h**+4**C**	14×10^6	**Figure 4.11 A**	539	54	593	1463	57	1520
3	**SS7h**	15×10^6	N/A	1498	691	2189	2474	571	3045
4	**SS8h**+8**C**	15×10^6	N/A	1489	530	2019	3392	527	3919
5	**SS8h**+15**C**	15×10^6	**Figure 3.26 C**	1145	409	1554	3106	341	3447

Table 6.14 List of oMSC laden scaffolds analysed by object counting and subsequently used for viability calculations. Data was analysed and presented in the same manner as **Table 6.13**.

Label	Bioink	$n_{bioink\ cells}$ (cells/mL)	Figure	unresolved cell count			resolved cell count		
				N_{live}	N_{dead}	N_{total}	N_{live}	N_{dead}	N_{total}
6	**SS6m**	5×10^6	**Figure 4.2 E**	398	118	516	2156	123	2279
7	**SS6m**	5×10^6	N/A	861	139	1000	1652	176	1828
8	**SS6m**	5×10^6	N/A	817	160	977	1391	147	1538
9	**SS6m**	5×10^6	N/A	841	199	1040	863	173	1036
10	**SS8m**+15**C**	8×10^6	**Figure 3.26 C**	1055	78	1133	1716	87	1803

6.11.6.4 Counting of DAPI and PH3 Stained Cells

Scaffolds containing DAPI stained HEK-293T were automated object counted (see *section 6.11.6.3*) and then resolved. The parameters used for object counting were: a

minimum size-filter of 80 voxels and no upper size filter. Additionally, objects on the edge of image were included in the count. Thresholding was performed such that most of the cellular mass was counted, resulting in low object number counts (due to object overlaps).

The object count was resolved by dividing every counted object's volume by the average DAPI stained cell volume. As DAPI stained HEK-293T laden scaffolds were recorded at different digital magnifications, average DAPI stained cell volumes were calculated for each magnification (from $n = 6$ measurements). Whilst PH3 stained cells were automated object counted and due to the cells being discrete across the scaffold, each counted object was treated as one cell. Object counting was performing with a size filter range of 80 to 8000 voxels and a low threshold to enable the count of all PH3 stained cells. A summary of the cell counts and mitotic cell proportion can be seen in **Table 6.15**.

Table 6.15 List of immunostained HEK-293T scaffolds analysed by automated object counting and their calculated proportion of mitotic cells. The *Bioink* column describes the scaffold solution used, including the amount of supplemented collagen type I, with the collagen concentration (in μg/mL) being the number preceding **C**. The DAPI stained cell count ($N_{\text{DAPI cells}}$) was resolved whilst the PH3 stained cell count ($N_{\text{PH cells}}$) was left unmodified. The *Figure* column refers to the figure in which the scaffold analysed is displayed in, with N/A corresponding to scaffolds analysed but not displayed in any figures.

Scaffold	Bioink	$n_{\text{bioink cells}}$ (cells/mL)	Figure	$N_{DAPI\,\text{cells}}$	$N_{PH3\,\text{cells}}$	% Mitotic Cells
D3 N1	**SS8h**+15**C**	15×10^6	N/A	2171	166	8
D3 N2	**SS8h**+15**C**	15×10^6	N/A	6105	272	4
D3 N3	**SS8h**+15**C**	15×10^6	**4.15**	2810	230	8
D3 N4	**SS8h**+15**C**	15×10^6	N/A	2496	188	8
D7 N1	**SS8h**+15**C**	15×10^6	**4.15**	6096	230	4
D7 N2	**SS8h**+15**C**	15×10^6	N/A	18130	272	2
D7 N3	**SS8h**+15**C**	15×10^6	N/A	14882	394	3
D7 N4	**SS8h**+15**C**	15×10^6	N/A	7248	187	3
D13 N1	**SS8h**+15**C**	15×10^6	N/A	4691	93	2
D6 N1	**SS8h**+300**C**	15×10^6	**4.10**	3032	27	1

6.11.6.5 Droplet Diameter of Cellular Droplet Networks

The droplet diameters for networks in Chapter 3 were measured in ImageJ[134,135] by fitting circles to the droplets within the networks (n = 52) and recording the diameter (μm). The mean and standard deviation were determined from the recorded values.

6.11.6.6 Scaffold Outer Dimension Measurements

Outer dimensions of aqueous-bound scaffolds in Chapter 3 and Chapter 4 were measured in ImageJ[134,135] by fitting a line across the centre of the scaffolds and recording the length or width (μm).

6.11.6.7 Scaffold Feature Measurements

The features of scaffolds were measured from *z*-stack confocal micrographs using imageJ[134,135]. For the arborised pathway and the nested cross, the width of the droplet pathways were averaged over 12 measurements. For the layered sheets scaffolds, the lower cell sheet height was recorded as the *z*-stack height when cells first appeared in the centre of the scaffold. The second layer height was recorded as the vertical distance between when upper cells first appeared to the upper limit of the *z*-stack.

6.11.7 Scaffold Calculations

6.11.7.1 Scaffold Cell Viabilities

The cell viability of a scaffold was calculated as the proportion of live cells to the total number of cells (**Equation 6.8**). The total number of cells is the summation of counted live and dead cells (**Equation 6.9**).

Equation 6.8

$$\%\ viability = \left(\frac{N_{live\ cells}}{N_{total\ cells}}\right) \times 100$$

Equation 6.9

$$N_{total\ cells} = N_{live\ cells} + N_{dead\ cells}$$

6.11.7.2 Effective Cell Densities of Scaffolds

The effective cell densities of scaffolds in *section 3.6* were calculated as the volume number density ($n_{scaffold\ cells}$ in cells/mL) using **Equation 6.10**. It was assumed the effective scaffold density was proportional to the mean size printed droplet ($\bar{V}_{droplet}$ in mL) containing the mean cell occupancy ($\bar{N}_{droplet\ cells}$). The mean number of cells per droplet was calculated as the quotient of total cells counted divided by the number of droplets the cells were counted within (**Equation 6.11**).

Equation 6.10

$$n_{scaffold\ cells} = \frac{\bar{N}_{droplet\ cells}}{\bar{V}_{droplet}}$$

Equation 6.11

$$\bar{N}_{droplet\ cells} = \frac{N_{total\ cells}}{N_{droplets}}$$

The average cell number per droplet of **SS7** scaffolds printed at different cell densities (*section 4.6.1*) was determined by averaging the measured cell per droplet values (n = 25) (see *section 6.11.6.2*).

6.11.7.3 Mitotic Cell Proportion Calculation

For ICC stained HEK-293T scaffolds, the percentage of scaffold cells undergoing mitosis was calculated as described. The mitotic cell count ($N_{PH3\ cells}$) was divided by the resolved DAPI cell count ($N_{DAPI\ cells}$, *section 6.11.6.4*) and multiplied by 100, as seen in **Equation 6.12**.

Equation 6.12

$$\%N_{PH3\ Cells} = \frac{N_{PH3\ Cells}}{N_{DAPI\ Cells}} \times 100$$

6.11.8 Digital PCR

oMSC scaffolds for dPCR analysis were fabricated by the author aided by Dr Sam Olof and Madeline Burke. The subsequent steps were performed by Madeline Burke and Dr James Armstrong, these were as follows. Scaffolds were transported to Bristol, cultured and on day 7, RNA extraction and cDNA synthesis of cellular scaffolds was performed followed by dPCR Analysis. A similar process was also performed by Madeline Burke and Dr James Armstrong as a control on oMSC pellets.

6.11.8.1 Printed Scaffold Samples

A bioink ink composed of 15×10^6 to 17×10^6 oMSC/mL in **SS8** was printed as 7×8 horizontal droplets for 4 layers and the resulting scaffolds were phase transferred. The oMSC scaffolds were cultured in either **MSC control medium** or **MSC differentiation medium** over 7 days. Printed scaffolds were produced for four sheep replicates, referred to as patient numbers (PN): 345 (n = 6), 419 (n = 6), 342 (n = 6), and 394 (n = 4), with half the scaffolds cultured in **MSC differentiation medium**.

6.11.8.2 Scaffold RNA extraction and cDNA synthesis

Cell lysis was performed using a standard RNA extraction kit (RNeasy Mini Kit, *QIAGEN*). Briefly, to samples within the microscope chamber slide, 300 µL culture medium was removed from every sample well and each construct was left to incubate (10 min) in 200 µL of lysis solution. All constructs were subsequently disrupted with a 20-gauge needle and then 200 µL of 70% v/v ethanol was added and mixed by pipette trituration. Each scaffold was then transferred to an individual RNeasy Mini spin column and centrifuged (8000×*g*, 15 s). The column sample was twice washed with buffer before the sample was eluted in RNase-free water and stored at -80 °C. The RNA concentration

was determined using a spectrophotometer (Beckman Coulter DU530, *Life Science*) before cDNA was synthesized using a PrimeScript RT Reagent Kit (*Takara*) and a PCR cycler [MJ Mini™ personal thermal cycler, *Bio-Rad,* USA]. Here, the input sample volume was 40 µL and the program employed was as follows: 37 °C for 15 min, 85 °C for 5 s and a 4 °C cooling period.

6.11.8.3 oMSC Laden Scaffold dPCR Analysis

Absolute gene analysis was performed using a QuantStudio™ 3D Digital PCR 20k Chip Kit (*Thermo Scientific*). Briefly, samples were prepared by mixing 5 µL cDNA in RNase free water with 7.3 µL QuantStudio™ 3D Digital PCR Master Mix, 1.5 µL RNase free water (*QIAGEN*) and 0.7 µL of primer solution (Taqman® Gene Expression Assay: Sox9 Hs01001343_g1 and β-Actin Hs01060665). The sample was then transferred to a dPCR chip using a 3D Digital PCR Chip Loader [QuantStudio™, *Applied Biosystems®*, *Thermo Scientific*, USA], which was then covered in immersion fluid and sealed using UV glue. Amplification was performed using a thermal cycler [Proflex PCR System™, *Applied Biosystems®*, *Thermo Scientific*, USA] with the default sequence: 96 °C for 10 min, 60 °C for 2 min followed by 98 °C for 30 s (for 39×), 60 °C for 2 min and a 10 °C cooling period. Finally, chips were removed from the thermal cycler, allowed to warm to room temperature and analysed using by a QuantStudio™ 3D Chip Reader [*Applied Biosystems®*, *Thermo Scientific*, USA]. A non-template digital PCR control was performed and showed no signal expression of beta-actin or Sox9 mRNA.

6.11.8.4 Pellet Control Samples

oMSCs were harvested and pelleted by centrifugation at 1.2×10^6 or 1.6×10^6 cells (*section 6.4.5*). The pellets were resuspended in 1.5 or 2 mL of either **MSC differentiation medium** or **MSC control medium**. Cell suspensions were aliquoted (0.5 mL, equivalent to 0.4×10^6 cells) into separate falcon tubes and were centrifuged (500×*g*, 5 min). Pellets under culture medium were cultured in cell incubators (37 °C, 5% CO_2) for 7 days, with

culture medium exchanges 3 times a week. Here the falcon cap was loosened to allow gas exchange. Three pellet was cultured for each condition under study.

Pellet RNA extraction was performed in the same manner as the printed scaffolds (*section 6.11.8.2*) and then were analysed by dPCR. It should be noted, that here, the initial extraction steps, i.e. lysis buffer addition and needle trituration, were performed in the pellet's falcon tube.

6.12 Fabricated Items

This section includes the description, design and fabrication method of the lab-manufactured items commonly used.

6.12.1 Fabrication Overview

The majority of fabricated items (printer parts and containers) were made by subtractive manufacture of clear cast PMMA (poly (methyl methacrylate)) sheets (*Plastics Online LTD*). The machining was performed with a CNC (computer numerically controlled) machine [MDX-40A, *Roland*, Japan] using milling cutters of diameter 0.2-3.0 mm (*Fenn Tool*). All machining models were created on 3D computer aided design software (SolidWorks®, v.2005) and saved as STL files, which were uploaded to CNC controller software (Modela 4, *Roland*). These items were designed by myself, but some of the printer parts were modified designs of Dr Gabriel Villar's models. Items which were glued used either an epoxy resin (Araldite, *RS Components*) or a UV curing adhesive (#81 or #61, *Norland Optical Adhesive*). For containers, glass coverslips were also used and had either 0.1 or 1.0 mm thickness.

6.12.1.1 Droplet Generator

The droplet generator (**Figure 2.2**) is the printer component that ejects pL to nL droplets in the lipid-in-oil bath. It consisted of a machined chamber (PMMA) which was sealed by a piezo electric transducer [7BB-20-6L0, *Murata*, Japan] glued on by epoxy resin.

Protruding out of this chamber, was a nozzle (*section 6.12.1.2*) supported by a rubber adapter [capillary holder, *Drummond*, USA]. The chamber had a tiny inlet at the top through which water could be added using a pipette with a gel-loading tip (200 μL). The design was modified after Chapter 2, with the PMMA support widened to cover the piezoelectric disc more.

6.12.1.2 Droplet Generator Nozzle

The nozzle for each droplet generator was custom made from a glass capillary [100 μL microcap, *Drummond*, USA] with internal and external diameters of 1.0 mm and 1.4 mm respectively. Initially, the capillary was vertically pulled using a PC-10 puller [*Narishige*, Japan] set at 65.0-72.0 relative heat with 3 weights. The capillary's pulled end was trimmed by lightly brushing another pulled capillary tip against it[190], typically giving a tip of 60-120 μm external diameter. The pulled capillary was then bent 90 degrees 15 mm from the pulled end in a blue butane flame. Finally the angled capillary was truncated 35 mm from the pulled end using a silicon wafer.

6.12.1.3 Well Array for Printer Loading

The well array for printer loading is a container for solutions to be loaded into the droplet generator's nozzle i.e. it held the hexadecane plug and print solution which are suction loaded into the capillary. The well array is a machined 3×3 array of wells with 2 mm diameter and 2 mm depth. Each well can contain up to 8 μL of oil or 10 μL of print solution.

6.12.1.4 Original Bulk Oil Print Containers

Prior to the acquisition of truncated glass cuvettes, bulk oil droplet networks were printed within machined containers with a side-on glass observation window. The maximum oil filled volume was 15×10 mm^2 by 5 mm deep. Folding networks were printed on the container's PMMA surface, while all other droplet networks were printed on a truncated glass coverslip placed at the container's base.

6.12.1.5 Standard Well Array

3×3 and 4×4 well arrays are machined containers that could hold individual μL volume droplets or μL-scale droplet networks that would remain in isolated wells, hence multiple conditions could be studied in parallel. The structures had shallow wells (~1.5 mm deep) at their base, above which was an open chamber with tall walls that would be filled with the lipid-in-oil solution (~150 μL). The design allowed clear top-down visualisation of the well's content, as the high curvature of the oil meniscus was to the sides of the well. Each array would have a uniform well diameter of either 1.5 mm or 2.0 mm diameter.

6.12.1.6 Modified Well Array with Glass Base

The glass base well arrays were made to allow multiple droplets to be studied in parallel with clear bottom-up visualisation, making the well array compatible with confocal microscopy. These arrays were of the same design as the standard well arrays, except the wells were machined through the whole structure and a glass coverslip was glued (epoxy resin or UV curing) to the underside.

6.12.1.7 Hydration Chamber

Hydration chambers were designed to keep droplet networks in a humid environment such that the networks would not dehydrate or dehydrate slower, to give a longer sample lifetime. A hydration chamber consisted of a machined holder of either the printer cuvette or droplet well array, which was glued (epoxy resin) to a polystyrene tissue culture dish [ø 10 mm, *Corning*, USA]. The sides of this dish were then filled with water and the chamber was sealed by the lid to create an environment with a high relative humidity.

Bibliography

1. Villar, G., Graham, A. D. & Bayley, H. A tissue-like printed material. *Science* **340,** 48–52 (2013).

2. Malone, E. & Lipson, H. Fab@Home: the personal desktop fabricator kit. *Rapid Prototyp. J.* **13,** 245–255 (2007).

3. Symes, M. D. *et al.* Integrated 3D-printed reactionware for chemical synthesis and analysis. *Nat. Chem.* **4,** 349–354 (2012).

4. Jones, N. Science in three dimensions: The print revolution. *Nature* **487,** 22–23 (2012).

5. Sun, J., Zhou, W., Huang, D., Fuh, J. Y. H. & Hong, G. S. An overview of 3D printing technologies for food fabrication. *Food Bioprocess Technol.* **8,** 1605–1615 (2015).

6. Hull, C. W. Apparatus for production of threedimensional objects by stereolithography. *Patent* US 4575330 A (1986).

7. Ringeisen, B. R. *et al.* Cell and organ printing turns 15: diverse research to commercial transitions. *MRS Bull.* **38,** 834–843 (2013).

8. Tasoglu, S. & Demirci, U. Bioprinting for stem cell research. *Trends Biotechnol.* **31,** 10–19 (2013).

9. Murphy, S. V & Atala, A. 3D bioprinting of tissues and organs. *Nat. Biotechnol.* **32,** 773–785 (2014).

10. Xu, T. *et al.* Complex heterogeneous tissue constructs containing multiple cell types prepared by inkjet printing technology. *Biomaterials* **34,** 130–139 (2013).

11. De Coppi, P. *et al.* Isolation of amniotic stem cell lines with potential for therapy. *Nat. Biotechnol.* **25,** 100–106 (2007).

12. Duan, B., Hockaday, L. A., Kang, K. H. & Butcher, J. T. 3D bioprinting of heterogeneous aortic valve conduits with alginate/gelatin hydrogels. *J. Biomed. Mater. Res. - Part A* **101 A,** 1255–1264 (2013).

13. Koch, L. *et al.* Skin tissue generation by laser cell printing. *Biotechnol. Bioeng.* **109,** 1855–1863 (2012).

14. Ozbolat, I. T. & Yu, Y. Bioprinting toward organ fabrication: challenges and future trends. *IEEE Trans. Biomed. Eng.* **60,** 691–699 (2013).

15. Langer, R. & Vacanti, J. P. Tissue Engineering. *Science* **260,** 920–926 (1993).

16. Lancaster, M. A. & Knoblich, J. A. Organogenesis in a dish: modeling development and disease using organoid technologies. *Science* **345,** 1247125 1–9 (2014).

17. Luni, C., Serena, E. & Elvassore, N. Human-on-chip for therapy development and fundamental science. *Curr. Opin. Biotechnol.* **25,** 45–50 (2014).

18. Castellanos-Gonzalez, A., Cabada, M. M., Nichols, J., Gomez, G. & Clinton White, A. Human primary intestinal epithelial cells as an improved in vitro model for cryptosporidium parvum infection. *Infect. Immun.* **81,** 1996–2001 (2013).

19. Finkbeiner, S. R. *et al.* Stem cell-derived human intestinal organoids as an infection model for rotaviruses. *MBio* **3,** e00159–12 1–6 (2012).

20. Yeung, T. M., Gandhi, S. C., Wilding, J. L., Muschel, R. & Bodmer, W. F. Cancer stem cells from colorectal cancer-derived cell lines. *Proc. Natl. Acad. Sci. U. S. A.* **107,** 3722–3727 (2010).

21. Onuma, K. *et al.* Genetic reconstitution of tumorigenesis in primary intestinal cells. *Proc. Natl. Acad. Sci. U. S. A.* **110,** 11127–11132 (2013).

22. Lancaster, M. A. *et al.* Cerebral organoids model human brain development and microcephaly. *Nature* **501,** 373–379 (2014).

23. Kelm, J. M. *et al.* A novel concept for scaffold-free vessel tissue engineering: Self-assembly of microtissue building blocks. *J. Biotechnol.* **148,** 46–55 (2010).

24. Fennema, E., Rivron, N., Rouwkema, J., Blitterswijk, C. Van & Boer, J. de. Spheroid culture as a tool for creating 3D complex tissues. *Trends Biotechnol.* **31,** 108–115 (2013).

25. Tortora, G. J. & Grabowski, S. R. *Principles of Anatomy & Physiology (10th ed.).* (John Wiley & Sons, Inc., 2003).

26. Alberts, B. *et al. Molecular Biology of the Cell (5th ed.).* (Garland Science, Taylor & Francis Group, 2008).

27. Hynes, R. O. & Naba, A. Overview of the matrisome-An inventory of extracellular matrix constituents and functions. *Cold Spring Harb. Perspect. Biol.* **4,** a004903 (2012).

28. Hynes, R. O. The extracellular matrix: not just pretty fibrils. *Science* **326,** 1216–1219 (2009).

29. Chan, B. P. & Leong, K. W. Scaffolding in tissue engineering: General approaches and tissue-specific considerations. *Eur. Spine J.* **17,** S467–S479 (2008).

30. Discher, D. E., Mooney, D. J. & Zandstra, P. W. Growth factors, matrices, and forces combine and control stem cells. *Science* **324,** 1673–1677 (2009).

31. Thiele, J., Ma, Y., Bruekers, S. M. C., Ma, S. & Huck, W. T. S. 25th anniversary article: designer hydrogels for cell cultures: a materials selection guide. *Adv. Mater.* 1–24 (2013). doi:10.1002/adma.201302958

32. Engler, A. J., Sen, S., Sweeney, H. L. & Discher, D. E. Matrix elasticity directs stem cell lineage specification. *Cell* **126,** 677–689 (2006).

33. Chang, R., Nam, J. & Sun, W. Effects of dispensing pressure and nozzle diameter on cell survival from solid freeform fabrication-based direct cell writing. *Tissue Eng: Part A* **14,** 41–48 (2008).

34. Forgacs, G. Tissue engineering: Perfusable vascular networks. *Nat. Mater.* **11,** 746–747 (2012).

35. Miller, J. S. *et al.* Rapid casting of patterned vascular networks for perfusable engineered three-dimensional tissues. *Nat. Mater.* **11,** 768–774 (2012).

36. Kolesky, D. B. *et al.* 3D bioprinting of vascularized, heterogeneous cell-laden tissue constructs. *Adv. Mater.* **26,** 3124–3130 (2014).

37. Place, E. S., Evans, N. D. & Stevens, M. M. Complexity in biomaterials for tissue engineering. *Nat. Mater.* **8,** 457–470 (2009).

38. Pati, F. *et al.* Printing three-dimensional tissue analogues with decellularized extracellular matrix bioink. *Nat. Commun.* **5,** 3935 1–11 (2014).

39. Lutolf, M. P., Raeber, G. P., Zisch, A. H., Tirelli, N. & Hubbell, J. a. Cell-responsive synthetic hydrogels. *Adv. Mater.* **15,** 888–892 (2003).

40. Lutolf, M. P. *et al.* Synthetic matrix metalloproteinase-sensitive hydrogels for the conduction of tissue regeneration: engineering cell-invasion characteristics. *Proc. Natl.*

Acad. Sci. U. S. A. **100,** 5413–5418 (2003).

41. Li, C. *et al.* Rapid formation of a supramolecular polypeptide-DNA hydrogel for in situ three-dimensional multilayer bioprinting. *Angew. Chemie Int. Ed.* **54,** 1–6 (2015).

42. Boland, T., Xu, T., Damon, B. & Cui, X. Application of inkjet printing to tissue engineering. *Biotechnol. J.* **1,** 910–917 (2006).

43. Takahashi, K. & Yamanaka, S. Induction of pluripotent stem cells from mouse embryonic and adult fibroblast cultures by defined factors. *Cell* **126,** 663–676 (2006).

44. Robinton, D. a & Daley, G. Q. The promise of induced pluripotent stem cells in research and therapy. *Nature* **481,** 295–305 (2012).

45. Lumelsky, N. *et al.* Differentiation of embryonic stem cells to insulin-secreting structures similar to pancreatic islets. *Science* **292,** 1389–1394 (2001).

46. Kehat, I. & Kenyagin-Karsenti, D. Human embryonic stem cells can differentiate into myocytes with structural and functional properties of cardiomyocytes. *J. Clin. Invest.* **108,** 363–364 (2001).

47. Asthana, A. & Kisaalita, W. S. Microtissue size and hypoxia in HTS with 3D cultures. *Drug Discov. Today* **17,** 810–817 (2012).

48. Chen, Y.-C., Lou, X., Zhang, Z., Ingram, P. & Yoon, E. High-throughput cancer cell sphere formation for characterizing the efficacy of photo dynamic therapy in 3D cell cultures. *Sci. Rep.* **5,** 12175 (2015).

49. Yui, S. *et al.* Technical reports functional engraftment of colon epithelium expanded in vitro from a single adult Lgr5 + stem cell. *Nat. Med.* **18,** 618–623 (2012).

50. Xia, Y. *et al.* Directed differentiation of human pluripotent cells to ureteric bud kidney progenitor-like cells. *Nat. Cell Biol.* **15,** 1507–1515 (2013).

51. Eiraku, M. *et al.* Self-organizing optic-cup morphogenesis in three-dimensional culture. *Nature* **472,** 51–56 (2011).

52. Dekkers, J. F. *et al.* WS14.5 A functional CFTR assay using primary cystic fibrosis intestinal organoids. *J. Cyst. Fibros.* **11,** S32 (2012).

53. Roth, E. a. *et al.* Inkjet printing for high-throughput cell patterning. *Biomaterials* **25,** 3707–3715 (2004).

54. Xu, T., Jin, J., Gregory, C., Hickman, J. J. & Boland, T. Inkjet printing of viable mammalian cells. *Biomaterials* **26,** 93–99 (2005).

55. Xu, T. *et al.* Hybrid printing of mechanically and biologically improved constructs for cartilage tissue engineering applications. *Biofabrication* **5,** 015001 (2013).

56. Cui, X., Dean, D., Ruggeri, Z. M. & Boland, T. Cell damage evaluation of thermal inkjet printed chinese hamster ovary cells. *Biotechnol. Bioeng.* **106,** 963–969 (2010).

57. Saunders, R. E., Gough, J. E. & Derby, B. Delivery of human fibroblast cells by piezoelectric drop-on-demand inkjet printing. *Biomaterials* **29,** 193–203 (2008).

58. Xu, T. *et al.* Characterization of Cell Constructs Generated With Inkjet Printing Technology Using In Vivo Magnetic Resonance Imaging. *J. Manuf. Sci. Eng.* **130,** 021013 (2008).

59. Demirci, U. & Montesano, G. Cell encapsulating droplet vitrification. *Lab Chip* **7,** 1428–1433 (2007).

60. Faulkner-Jones, A. *et al.* Development of a valve-based cell printer for the formation of human embryonic stem cell spheroid aggregates. *Biofabrication* **5,** 015013 (2013).

61. Moon, S. *et al.* Drop-on-demand single cell isolation and total RNA analysis. *PLoS One* **6,** e17455 (2011).

62. Gurkan, U. a *et al.* Engineering anisotropic biomimetic fibrocartilage microenvironment by bioprinting mesenchymal stem cells in nanoliter gel droplets. *Mol. Pharm.* **11,** 2151–2159 (2014).

63. Moon, S. *et al.* Layer by layer three-dimensional tissue epitaxy by cell-laden hydrogel droplets. *Tissue Eng. Part C. Methods* **16,** 157–166 (2010).

64. Demirci, U. & Montesano, G. Single cell epitaxy by acoustic picolitre droplets. *Lab Chip* **7,** 1139–1145 (2007).

65. Demirci, U. Acoustic picoliter droplets for emerging applications in semiconductor industry and biotechnology. *J. Microelectromechanical Syst.* **15,** 957–966 (2006).

66. Patterning, T. E., Raghavan, S. & Sabahi-kaviani, R. Rapid Generation of Multiplexed Cell Cocultures Using Acoustic Droplet Ejection Followed by Aqueous. *Tissue Eng. Part C. Methods* **18,** 647–657 (2012).

67. Mannoor, M. S. *et al.* 3D printed bionic ears. *Nano Lett.* **13,** 2634–2639 (2013).

68. Mironov, V. *et al.* Organ printing: tissue spheroids building blocks. *Biomaterials* **30,** 2164–2174 (2009).

69. Norotte, C., Marga, F. S., Niklason, L. E. & Forgacs, G. Scaffold-free vascular tissue engineering using bioprinting. *Biomaterials* **30,** 5910–5917 (2009).

70. Jakab, K. *et al.* Tissue engineering by self-assembly of cells printed into topologically defined structures. *Tissue Eng. Part A* **14,** 413–421 (2008).

71. Schiele, N. R. *et al.* Laser-based direct-write techniques for cell printing. *Biofabrication* **2,** 032001 (2010).

72. Guillotin, B. *et al.* Laser assisted bioprinting of engineered tissue with high cell density and microscale organization. *Biomaterials* **31,** 7250–7256 (2010).

73. Koch, L. *et al.* Laser printing of skin cells and human stem cells. *Tissue Eng. Part C Methods* **16,** 847–54 (2010).

74. Hribar, K. C., Soman, P., Warner, J., Chung, P. & Chen, S. Light-assisted direct-write of 3D functional biomaterials. *Lab Chip* **14,** 268–275 (2014).

75. Michael, S. *et al.* Tissue engineered skin substitutes created by laser-assisted bioprinting form skin-like structures in the dorsal skin fold chamber in mice. *PLoS One* **8,** e57741 (2013).

76. Liu, J. S. & Gartner, Z. J. Directing the assembly of spatially organized multicomponent tissues from the bottom up. *Trends Cell Biol.* **22,** 683–691 (2012).

77. Du, Y., Lo, E., Ali, S. & Khademhosseini, A. Directed assembly of cell-laden microgels for fabrication of 3D tissue constructs. *Proc. Natl. Acad. Sci. U. S. A.* **105,** 9522–9527 (2008).

78. Li, C. Y., Wood, D. K., Hsu, C. M. & Bhatia, S. N. DNA-templated assembly of droplet-derived PEG microtissues. *Lab Chip* **11,** 2967–2975 (2011).

79. Onoe, H. & Takeuchi, S. Cell-laden microfibers for bottom-up tissue engineering. *Drug Discov. Today* **20,** 236–246 (2015).

80. Onoe, H. *et al.* Metre-long cell-laden microfibres exhibit tissue morphologies and functions. *Nat. Mater.* **12,** 584–590 (2013).

81. Derby, B. Printing and prototyping of tissues and scaffolds. *Science* **338,** 921–926 (2012).

82. Melchels, F. P. W. *et al.* Mathematically defined tissue engineering scaffold architectures prepared by stereolithography. *Biomaterials* **31,** 6909–6916 (2010).

83. Rivron, N. C. *et al.* Tissue deformation spatially modulates VEGF signaling and angiogenesis. *Proc. Natl. Acad. Sci.* **109,** 6886–6891 (2012).

84. Haraguchi, Y., Shimizu, T., Yamato, M. & Okano, T. Scaffold-free tissue engineering using cell sheet technology. *RSC Adv.* **2,** 2184 (2012).

85. Haraguchi, Y. *et al.* Fabrication of functional three-dimensional tissues by stacking cell sheets in vitro. *Nat. Protoc.* **7,** 850–8 (2012).

86. Sekine, H. *et al.* In vitro fabrication of functional three-dimensional tissues with perfusable blood vessels. *Nat. Commun.* **4,** 1399 (2013).

87. Gilkes, D. M., Semenza, G. L. & Wirtz, D. Hypoxia and the extracellular matrix: drivers of tumour metastasis. *Nat. Rev. Cancer* **14,** 430–439 (2014).

88. Bertassoni, L. E. *et al.* Hydrogel bioprinted microchannel networks for vascularization of tissue engineering constructs. *Lab Chip* **14,** 2202–2211 (2014).

89. Bayley, H. *et al.* Droplet interface bilayers. *Mol. Biosyst.* **4,** 1191–1208 (2008).

90. Leptihn, S. *et al.* Constructing droplet interface bilayers from the contact of aqueous droplets in oil. *Nat. Protoc.* **8,** 1048–1057 (2013).

91. Holden, M. A., Needham, D. & Bayley, H. Functional bionetworks from nanoliter water droplets. *J. Am. Chem. Soc.* **129,** 8650–8655 (2007).

92. Maglia, G. *et al.* Droplet networks with incorporated protein diodes show collective properties. *Nat. Nanotechnol.* **4,** 437–440 (2009).

93. Woolfson, D. N. Synthetic Biology. *Biochem. Soc.* 19–25 (2011).

94. Elani, Y., deMello, A. J., Niu, X. & Ces, O. Novel technologies for the formation of 2-D and 3-D droplet interface bilayer networks. *Lab Chip* **12,** 3514–20 (2012).

95. Funakoshi, K., Suzuki, H. & Takeuchi, S. Lipid bilayer formation by contacting monolayers in a microfluidic device for membrane protein analysis. *Anal. Chem.* **78,** 8169–8174 (2006).

96. Punnamaraju, S., You, H. & Steckl, A. J. Triggered release of molecules across droplet interface bilayer lipid membranes using photopolymerizable lipids. *Langmuir* **28,** 7657–7664 (2012).

97. Syeda, R., Holden, M. A., Hwang, W. L. & Bayley, H. Screening blockers against a potassium channel with a droplet interface bilayer array. *J. Am. Chem. Soc.* **130,** 15543–15548 (2008).

98. Villar, G. Minimal tissues. *DPhil Thesis, Univ. Oxford, UK* 1–110 (2013).

99. Hwang, W. L., Holden, M. A., White, S. & Bayley, H. Electrical behavior of droplet interface bilayer networks: experimental analysis and modeling. *J. Am. Chem. Soc.* **129,** 11854–11864 (2007).

100. Villar, G., Heron, A. J. & Bayley, H. Formation of droplet networks that function in aqueous environments. *Nat. Nanotechnol.* **6,** 803–808 (2011).

101. Poulin, P. & Bibette, J. Adhesion of water droplets in organic solvent. *Langmuir* **14,** 6341–6343 (1998).

102. Hwang, W. L., Chen, M., Cronin, B., Holden, M. A. & Bayley, H. Asymmetric droplet interface bilayers. *J. Am. Chem. Soc.* **130,** 5878–5879 (2008).

103. Gross, L. C. M., Heron, A. J., Baca, S. C. & Wallace, M. I. Determining membrane capacitance by dynamic control of droplet interface bilayer area. *Langmuir* **27,** 14335–14342 (2011).

104. Boreyko, J. B., Polizos, G., Datskos, P. G., Sarles, S. a & Collier, C. P. Air-stable droplet interface bilayers on oil-infused surfaces. *Proc. Natl. Acad. Sci. U. S. A.* **111,** 7588–7593 (2014).

105. Mruetusatorn, P. *et al.* Control of membrane permeability in air-stable droplet interface bilayers. *Langmuir* **31,** 4224–4231 (2015).

106. Heron, A. J., Thompson, J. R., Mason, A. E. & Wallace, M. I. Direct detection of membrane channels from gels using water-in-oil droplet bilayers. *J. Am. Chem. Soc.* **129,** 16042–16047 (2007).

107. Heron, A. J., Thompson, J. R., Cronin, B., Bayley, H. & Wallace, M. I. Simultaneous measurement of ionic current and fluorescence from single protein pores. *J. Am. Chem. Soc.* **131,** 1652–3 (2009).

108. Huang, S., Romero-Ruiz, M., Castell, O. K., Bayley, H. & Wallace, M. I. High-throughput optical sensing of nucleic acids in a nanopore array. *Nat. Nanotechnol.* 1–7 (2015).

doi:10.1038/nnano.2015.189

109. Acharya, S. A., Portman, A., Salazar, C. S. & Schmidt, J. J. Hydrogel-stabilized droplet bilayers for high speed solution exchange. *Sci. Rep.* **3,** 3139 (2013).

110. Sapra, K. T. & Bayley, H. Lipid-coated hydrogel shapes as components of electrical circuits and mechanical devices. *Sci. Rep.* **2,** 848 (2012).

111. Sarles, S. A., Stiltner, L. J., Williams, C. B. & Leo, D. J. Bilayer formation between lipid-encased hydrogels contained in solid substrates. *ACS Appl. Mater. Interfaces* **2,** 3654–3663 (2010).

112. Sarles, S. A. & Leo, D. J. Regulated attachment method for reconstituting lipid bilayers of prescribed size within flexible substrates. *Anal. Chem.* **82,** 959–966 (2010).

113. Aghdaei, S., Sandison, M. E., Zagnoni, M., Green, N. G. & Morgan, H. Formation of artificial lipid bilayers using droplet dielectrophoresis. *Lab Chip* **8,** 1617–1620 (2008).

114. Wauer, T. *et al.* Construction and manipulation of functional three-dimensional droplet networks. *ACS Nano* **8,** 771–779 (2014).

115. Guzowski, J., Jakiela, S., Korczyk, P. M. & Garstecki, P. Custom tailoring multiple droplets one-by-one. *Lab Chip* **13,** 4308–4311 (2013).

116. Stanley, C. E. *et al.* A microfluidic approach for high-throughput droplet interface bilayer (DIB) formation. *Chem. Commun.* **46,** 1620–1622 (2010).

117. Thutupalli, S., Herminghaus, S. & Seemann, R. Bilayer membranes in micro-fluidics: from gel emulsions to soft functional devices. *Soft Matter* **7,** 1312–1320 (2011).

118. Baret, J.-C., Kleinschmidt, F., El Harrak, A. & Griffiths, A. D. Kinetic aspects of emulsion stabilization by surfactants: a microfluidic analysis. *Langmuir* **25,** 6088–6093 (2009).

119. Kankare, J. & Vinokurov, I. A. Kinetics of langmuirian adsorption onto planar, spherical, and cylindrical surfaces. *Langmuir* **15,** 5591–5599 (1999).

120. Markert, C. D. *et al.* Characterizing the micro-scale elastic modulus of hydrogels for use in regenerative medicine. *J. Mech. Behav. Biomed. Mater.* **27,** 115–127 (2013).

121. Menestrina, G. Ionic channels formed by Staphylococcus aureus alpha-toxin: voltage-dependent inhibition by divalent and trivalent cations. *J. Membr. Biol.* **90,** 177–190 (1986).

122. Thiam, A. R., Bremond, N. & Bibette, J. From stability to permeability of adhesive emulsion

bilayers. *Langmuir* **28,** 6291–6298 (2012).

123. Dixit, S. S., Pincus, A., Guo, B. & Faris, G. W. Droplet shape analysis and permeability studies in droplet lipid bilayers. *Langmuir* **28,** 7442–7451 (2012).

124. Boroske, E., Elwenspoek, M. & Helfrich, W. Osmotic shrinkage of giant egg-lecithin vesicles. *Biophys. J.* **34,** 95–109 (1981).

125. Vunjak-Novakovic, G. & Scadden, D. T. Biomimetic platforms for human stem cell research. *Cell Stem Cell* **8,** 252–261 (2011).

126. Saez, J. C., Berthoud, V. M., Branes, M. C., Martinez, A. D. & Beyer, E. C. Plasma membrane channels formed by connexins: their regulation and functions. *Physiol. Rev.* **83,** 1359–1400 (2003).

127. Thomas, P. & Smart, T. G. HEK293 cell line: A vehicle for the expression of recombinant proteins. *J. Pharmacol. Toxicol. Methods* **51,** 187–200 (2005).

128. Pear, W. S., Nolan, G. P., Scott, M. L. & Baltimore, D. Production of high-titer helper-free retroviruses by transient transfection. *Proc. Natl. Acad. Sci. U. S. A.* **90,** 8392–8396 (1993).

129. Chamberlain, G., Fox, J., Ashton, B. & Middleton, J. Concise review: mesenchymal stem cells: their phenotype, differentiation capacity, immunological features, and potential for homing. *Stem Cells* **25,** 2739–2749 (2007).

130. ThermoFisher Scientific. Calcein, AM, cell-permeant dye. (2015). at <https://www.thermofisher.com/order/catalog/product/C3100MP>

131. ThermoFisher Scientific. Propidium Iodide. (2015). at <https://www.thermofisher.com/uk/en/home/life-science/cell-analysis/fluorophores/propidium-iodide.html>

132. McAteer, J. A. & Davis, J. M. *Basic Cell Culture: A Practical Approach (Practical Approach Series)*. (Oxford University Press, 2002).

133. De Vos, K. Cell Counter [ImageJ Plug-in Software, Version 2.0]. (2001).

134. Schneider, C. A., Rasband, W. S. & Eliceiri, K. W. NIH Image to ImageJ: 25 years of image analysis. *Nat. Methods* **9,** 671–675 (2012).

135. Rasband, W. S. ImageJ [Software, Version 1.49]. (1997).

136. Basu, S., Campbell, H. M., Dittel, B. N. & Ray, A. Purification of specific cell population by

fluorescence activated cell sorting (FACS). *J. Vis. Exp.* e1546 (2010). doi:10.3791/1546

137. Adams, D. J. Dipeptide and tripeptide conjugates as low-molecular-weight hydrogelators. *Macromol. Biosci.* **11,** 160–173 (2011).

138. Jayawarna, V. *et al.* Nanostructured hydrogels for three-dimensional cell culture through self-assembly of fluorenylmethoxycarbonyl-dipeptides. *Adv. Mater.* **18,** 611–614 (2006).

139. Jayawarna, V. *et al.* Introducing chemical functionality in Fmoc-peptide gels for cell culture. *Acta Biomater.* **5,** 934–943 (2009).

140. Liebmann, T., Rydholm, S., Akpe, V. & Brismar, H. Self-assembling Fmoc dipeptide hydrogel for in situ 3D cell culturing. *BMC Biotechnol.* **7,** 88 (2007).

141. Liyanage, W., Vats, K., Rajbhandary, A., Benoit, D. S. W. & Nilsson, B. L. Multicomponent dipeptide hydrogels as extracellular matrix-mimetic scaffolds for cell culture applications. *Chem. Commun.* **51,** 11260–11263 (2015).

142. Zhou, M. *et al.* Self-assembled peptide-based hydrogels as scaffolds for anchorage-dependent cells. *Biomaterials* **30,** 2523–2530 (2009).

143. Adams, D. J., Mullen, L. M., Berta, M., Chen, L. & Frith, W. J. Relationship between molecular structure, gelation behaviour and gel properties of Fmoc-dipeptides. *Soft Matter* **6,** 1971 (2010).

144. Pertoft, H. Fractionation of cells and subcellular particles with Percoll. *J. Biochem. Biophys. Methods* **44,** 1–30 (2000).

145. Skardal, A., Zhang, J. & Prestwich, G. D. Bioprinting vessel-like constructs using hyaluronan hydrogels crosslinked with tetrahedral polyethylene glycol tetracrylates. *Biomaterials* **31,** 6173–6181 (2010).

146. Zieris, A. *et al.* FGF-2 and VEGF functionalization of starPEG-heparin hydrogels to modulate biomolecular and physical cues of angiogenesis. *Biomaterials* **31,** 7985–7994 (2010).

147. Freudenberg, U. *et al.* A star-PEG-heparin hydrogel platform to aid cell replacement therapies for neurodegenerative diseases. *Biomaterials* **30,** 5049–5060 (2009).

148. Bencherif, S. A. *et al.* Injectable preformed scaffolds with shape-memory properties. *Proc. Natl. Acad. Sci. U. S. A.* **109,** 19590–19565 (2012).

149. Nicodemus, G. D. & Bryant, S. J. Cell encapsulation in biodegradable hydrogels for tissue engineering applications. *Tissue Eng. Part B. Rev.* **14,** 149–165 (2008).

150. Eliassi, A., Modarress, H. & Mansoori, G. A. Densities of poly(ethylene glycol) + water mixtures in the 298.15-328.15 K temperature range. *J. Chem. Eng. Data* **9568,** 719–721 (1998).

151. Pautot, S., Frisken, B. J. & Weitz, D. A. Engineering asymmetric vesicles. *Proc. Natl. Acad. Sci. U. S. A.* **100,** 10718–10721 (2003).

152. Pautot, S., Frisken, B. J. & Weitz, D. A. Production of unilamellar vesicles using an inverted emulsion. *Langmuir* 2870–2879 (2003).

153. Yamada, A. *et al.* Spontaneous transfer of phospholipid-coated oil-in-oil and water-in-oil micro-droplets through an oil/water interface. *Langmuir* **22,** 9824–9828 (2006).

154. Yanagisawa, M., Iwamoto, M., Kato, A., Yoshikawa, K. & Oiki, S. Oriented reconstitution of a membrane protein in a giant unilamellar vesicle: experimental verification with the potassium channel KcsA. *J. Am. Chem. Soc.* **133,** 11774–11779 (2011).

155. Hu, P. C., Li, S. & Malmstadt, N. Microfluidic fabrication of asymmetric giant lipid vesicles. *ACS Appl. Mater. Interfaces* **3,** 1434–1440 (2011).

156. Abkarian, M., Loiseau, E. & Massiera, G. Continuous droplet interface crossing encapsulation (cDICE) for high throughput monodisperse vesicle design. *Soft Matter* **7,** 4610–4614 (2011).

157. Ito, H. *et al.* Dynamical formation of lipid bilayer vesicles from lipid-coated droplets across a planar monolayer at an oil/water interface. *Soft Matter* **9,** 9539–9547 (2013).

158. Elani, Y., Gee, A., Law, R. V. & Ces, O. Engineering multi-compartment vesicle networks. *Chem. Sci.* **4,** 3332–3338 (2013).

159. Elani, Y., Law, R. V & Ces, O. Vesicle-based artificial cells as chemical microreactors with spatially segregated reaction pathways. *Nat. Commun.* **5,** 5305 (2014).

160. Shum, H. C., Zhao, Y., Kim, S.-H. & Weitz, D. A. Multicompartment polymersomes from double emulsions. *Angew. Chemie Int. Ed.* **50,** 1648–1651 (2011).

161. Awad, H. a., Wickham, M. Q., Leddy, H. A., Gimble, J. M. & Guilak, F. Chondrogenic differentiation of adipose-derived adult stem cells in agarose, alginate, and gelatin

scaffolds. *Biomaterials* **25,** 3211–3222 (2004).

162. Connelly, J. T., García, A. J. & Levenston, M. E. Interactions between integrin ligand density and cytoskeletal integrity regulate BMSC chondrogenesis. *J. Cell. Physiol.* **217,** 145–154 (2008).

163. Lima, E. G. *et al.* The effect of devitalized trabecular bone on the formation of osteochondral tissue-engineered constructs. *Biomaterials* **29,** 4292–4299 (2008).

164. Schuh, E. *et al.* Chondrocyte redifferentiation in 3D: The effect of adhesion site density and substrate elasticity. *J. Biomed. Mater. Res. - Part A* **100 A,** 38–47 (2012).

165. Ulrich, T. A., Jain, A., Tanner, K., MacKay, J. L. & Kumar, S. Probing cellular mechanobiology in three-dimensional culture with collagen-agarose matrices. *Biomaterials* **31,** 1875–1884 (2010).

166. Yamada, Y. *et al.* Laminin active peptide/agarose matrices as multifunctional biomaterials for tissue engineering. *Biomaterials* **33,** 4118–4125 (2012).

167. Rees, D. A. Shapely polysaccharides. *Biochem. J.* **126,** 257–271 (1972).

168. Arnott, S. *et al.* The agarose double helix and its function in agarose gel structure. *J. Mol. Biol.* **90,** 269–284 (1974).

169. Normand, V., Lootens, D. L., Amici, E., Plucknett, K. P. & Aymard, P. New insight into agarose gel mechanical properties. *Biomacromolecules* **1,** 730–738 (2000).

170. Balgude, A. P., Yu, X., Szymanski, A. & Bellamkonda, R. V. Agarose gel stiffness determines rate of DRG neurite extension in 3D cultures. *Biomaterials* **22,** 1077–1084 (2001).

171. Tien, H. T., Carbone, S. & Dawidowicz, E. A. Formation of 'black' lipid membranes by oxidation products of cholesterol. *Nature* **212,** 718–719 (1966).

172. Choi, D. *et al.* Spontaneous electrical charging of droplets by conventional pipetting. *Sci. Rep.* **3,** 2037 (2013).

173. Jain, R. K., Au, P., Tam, J., Duda, D. G. & Fukumura, D. Engineering vascularized tissue. *Nat. Biotechnol.* **23,** 821–823 (2005).

174. Bolte, S. & Cordelieres, F. P. 3D Object Counter [Image J Plug-in Software, Version 2.0]. (2006).

175. Bolte, S. & Cordelieres, F. P. A guided tour into subcellular colocalisation analysis in light

microscopy. *J. Microsc.* **224,** 213–232 (2006).

176. Lange, W. Cell number and cell density in the cerebellar cortex of man and some other mammals. *Cell Tissue Res.* **157,** 115–124 (1975).

177. Radisic, M. *et al.* High-density seeding of myocyte cells for cardiac tissue engineering. *Biotechnol. Bioeng.* **82,** 403–414 (2003).

178. Kleinman, H. K., Luckenbill-Edds, L., Cannon, F. W. & Sephel, G. C. Use of extracellular matrix components for cell culture. *Anal. Biochem.* **166,** 1–13 (1987).

179. Dixit, R. & Cyr, R. Cell damage and reactive oxygen species production induced by fluorescence microscopy: effect on mitosis and guidelines for non-invasive fluorescence microscopy. *Plant J.* **36,** 280–290 (2003).

180. Asanbaeva, A. *et al.* Articular cartilage tensile integrity: Modulation by matrix depletion is maturation-dependent. *Arch. Biochem. Biophys.* **474,** 175–182 (2008).

181. DeLise, A. M., Fischer, L. & Tuan, R. S. Cellular interactions and signaling in cartilage development. *Osteoarthr. Cartil.* **8,** 309–334 (2000).

182. Akiyama, H. Control of chondrogenesis by the transcription factor Sox9. *Mod. Rheumatol.* **18,** 213–219 (2008).

183. Tacchetti, C. *et al.* Cell condensation in chondrogenic differentiation. *Exp. Cell Res.* **200,** 26–33 (1992).

184. Ramos, J., Imaz, A. & Forcada, J. Temperature-sensitive nanogels: poly(N-vinylcaprolactam) versus poly(N-isopropylacrylamide). *Polym. Chem.* **3,** 852 (2012).

185. Orive, G., Anitua, E., Pedraz, J. L. & Emerich, D. F. Biomaterials for promoting brain protection, repair and regeneration. *Nat. Rev. Neurosci.* **10,** 682–692 (2009).

186. Kim, S. H., Turnbull, J. & Guimond, S. Extracellular matrix and cell signalling: The dynamic cooperation of integrin, proteoglycan and growth factor receptor. *J. Endocrinol.* **209,** 139–151 (2011).

187. Park, K. I., Teng, Y. D. & Snyder, E. Y. The injured brain interacts reciprocally with neural stem cells supported by scaffolds to reconstitute lost tissue. *Nat. Biotechnol.* **20,** 1111–1117 (2002).

188. Maglia, G. *et al.* DNA strands from denatured duplexes are translocated through

engineered protein nanopores at alkaline pH. *Nano Lett.* **9,** 3831–3836 (2009).

189. Hamer, W. J. & Wu, Y.-C. Osmotic coefficients and mean activity coefficients of uni-univalent electrolytes in water at 25 °C. *J. Phys. Chem. Ref. Data* **1,** 1047–1099 (1972).

190. Oesterle, A. *Pipette Cookbook 2015, P-97 & P-1000 Micropipette Pullers*. (Sutter Instrument Company, 2015). at <http://www.sutter.com/PDFs/pipette_cookbook.pdf>